From Defined Polymer Architectures to Structure-Property Relationships *in vivo*

Dissertation zur Erlangung des Grades eines "Doktor rerum naturalium (Dr. rer. nat.)" der Fachbereiche:

08 – Physik, Mathematik und Informatik

09 – Chemie, Pharmazie und Geowissenschaften

10 – Biologie

Universitätsmedizin

der Johannes Gutenberg-Universität Mainz

Mareli Allmeroth

Max Planck Graduate Center

mit der Johannes Gutenberg-Universität Mainz

Mainz, August 2012

Max Planck Graduate Center
mit der Johannes Gutenberg-Universität Mainz

Die vorliegende Arbeit wurde unter der Betreuung von [redacted] in der Zeit von August 2009 bis August 2012 am Institut für Organische Chemie der Johannes Gutenberg-Universität Mainz angefertigt.

„I hereby declare that I wrote the dissertation submitted without any unauthorized external assistance and used only sources acknowledged in the work. All textual passages which are appropriated verbatim or paraphrased from published and unpublished texts as well as information obtained from oral sources are duly indicated and listed in accordance with bibliographical rules. In carrying out this research, I complied with the rules of standard scientific practice as formulated in the statutes of Johannes Gutenberg-University Mainz to insure standard scientific practice."

……

Dekan: [redacted]

Erster Berichterstatter: [redacted]

Zweiter Berichterstatter: [redacted]

Tag der mündlichen Prüfung: 22.10.2012

Table of Contents

^{64}Cu	copper-64
^{18}F	fluorine-18
^{124}I	iodine-124
^{131}I	iodine-131
^{99m}Tc	technetium-99m
^{201}Tl	thalium-201
ABC	accelerated blood clearance
ACE	angiotensin-converting enzyme
AIBN	2,2'-azoisobutyronitrile
ALL	acute lymphoblastic leukaemia
approx.	approximately
ASGPR	asiaglycoprotein receptor
AT-II	angiotensin-II
ATRP	atom transfer radical polymerization
BA	butyl acrylate
BGO	bismuth-germanate
BPO	benzoyl peroxide
CMC	critical micelle concentration
CT	computed tomography
CTA	chain transfer agent
DMF	dimethylformamide
DMSO	dimethylsulfoxide
DNA	deoxyribonucleic acid
DOTA	1,4,7,10-tetraazacyclododecanetetraacetic acid
Dox	doxorubicin
e^+	positron
e.g.	for example

EPR	enhanced permeability and retention
FDA	food and drug administration
FDG	2-[^{18}F]-fluoro-deoxy-*D*-glucose
Gd	gadolinium
Gd-DTPA-BMA	gadolinium-diethylenetriaminepentaacetic-acid-bis-methylamide
GFLG	Gly-Phe-Leu-Gly peptidyl sequence
h	hour/hours
H+E	hematoxylin and eosin
HPMA	*N*-(2-hydroxypropyl)methacrylamide
HPLC	high performance liquid chromatography
ID	injected dose
IgM	immunoglobuline M
i.v.	intravenous
L-Dopa	*L*–3,4-dihydroxyphenylalanine
LMA	lauryl methacrylate
LOR	line of response
LSO	lutetium-oxyorthosilicate
ν_e	neutrino
max.	maximum
MIP	maximum intensity projection
MR	magnetic resonance
MRI	magnetic resonance imaging
MTD	maximum tolerated dose
M_w	weight average molecular weight
n	neutron
NaI	sodium-iodine

NAS	*N*-acryloxysuccinimide
NHS	*N*-hydroxysuccinimide
NMAS	*N*-methacryloxysuccinimide
NO	nitric oxide
p	proton
PAsp	poly(aspartamide)
Pb	plumbum
PDI	polydispersity index
PEG	poly(ethylene glycol)
PEI	poly(ethyleneimine)
PET	positron emission tomography
PGA	poly(glutamic acid)
P(Glu)	poly(glutamic acid)
p.i.	post injection
PICM	polyion complex micelles
PK1	Prague-Keele1 (HPMA copolymer-Gly-Phe-Leu-Gly-doxorubicin)
PK2	Prague-Keele2 (HPMA copolymer-GFLG-dox and galactosamine)
PLL	poly(*L*-lysine)
PMASI	poly(*N*-methacryloxysuccinimide)
PMMA	poly(methyl methacrylate)
PPFA	poly(pentafluoroacrylate)
PPFMA	poly(pentafluoro methacrylate)
PR	partial response
PVP	poly(vinylpyrrolidone)
RAFT	reversible addition-fragmentation chain transfer
RES	reticuloendothelial system
ROI	region of interest

SCID	severe combined immunodeficiency disease
SEM	scanning electron microscopy
SMANCS	styrene maleic anhydride neocarzinostatin
SPECT	single photon emission computed tomography
TI	therapeutic index
VEGF	vascular endothelial growth factor
VPF	vascular permeability factor

1. Introduction

1.1 The rationale behind designing Polymer Therapeutics

One major obstacle concerning the application of pharmacologically active drugs relies on their low therapeutic index (TI). This term describes the ratio of toxic to therapeutic dose of a drug and plays an essential role for the success of novel therapeutic approaches. Nowadays main issues of clinically established drugs - based on their low molecular weight - are short plasma-half life, high overall clearance rate as well as undesirable side effects. Due to their small sizes, they are rapidly distributed within the entire body and only low amounts are actually reaching the desired target site [1]. In this regard, macromolecular based delivery systems are demonstrating a promising tool to improve the pharmacokinetics of therapeutic agents. The idea of using polymers as drug carriers is not new; it has evolved over the last hundred years. Beginning with the "magic bullet" of Ehrlich in 1906 [2] and following De Duve [3], Ringsdorf laid the foundation of the main principle of "Polymer Therapeutics" in the 1970s. The concept comprised the application of a macromolecular drug delivery vehicle for active as well as passive targeting, helping to improve the therapeutic action. On its part, the term "Polymer Therapeutics" was coined by Duncan and Ringsdorf and is used to describe polymeric drugs, polymer-drug conjugates, polymer-protein conjugates, polymeric micelles as well as polyplexes [4]. An overall scheme of the named structures is illustrated in figure 1.

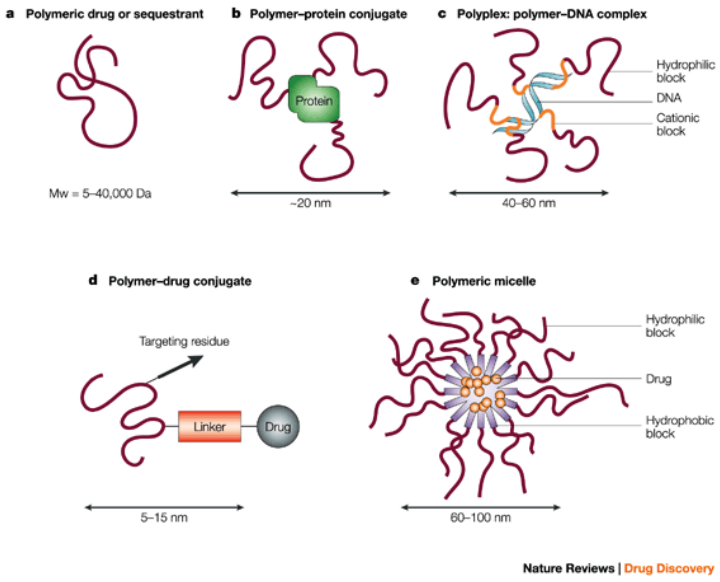

Figure 1: Schematic representation of "Polymer Therapeutics" [4].

Regarding the therapeutic effects, macromolecular carriers have to fulfill essential requirements. They have to be water-soluble, non-toxic as well as non-immunogenic. Furthermore they need to exhibit either biodegradability or biocompatibility with final excretion characteristics. By conjugating a polymer to a low molecular weight drug or protein, several macromolecular properties can be transferred. One advantage is the prolongation of the blood half-life of therapeutically active agents - attributed to an increase in their hydrodynamic volume – and consequential reduced kidney clearance [5]. Furthermore, the polymer (particularly polyethylene glycol (PEG)) protects the linked molecules toward degrading enzymes or enhanced uptake by the reticuloendothelial system (RES), based on a steric hindrance of the polymer strands [6]. Especially considering water-insoluble anticancer drugs, the augmentation of solubility due to the macromolecular delivery vehicle constitutes another major benefit. Concluding, the avoidance of immunogenicity of heterologous proteins as well as increased tumor accumulation are further rationales for the application of polymer based conjugates.

The success of the above mentioned concept could be already confirmed by the market approval of the first polymer-protein conjugates for anticancer treatment in the early 1990s. Among these is for example SMANCS (Zinostatin, Stimalmer), a conjugate consisting out of the antitumor protein neocarzinostatin and poly(styrene-co-maleic acid), used for the treatment of hepatocellular carcinoma [7]. Furthermore, polyethylene glycol based conjugates were emerging, with PEG representing the best polymer candidate for protein modification [8]. In this regard, PEG-adenosine deaminase (Adagen®) [9] as well as PEG-asparaginase (Oncaspar®) [10] were milestones of a consequent series of polymer-protein conjugates [11, 12]. Adagen® is used for the treatment of SCID (severe combined immunodeficiency disease) syndrome and Oncaspar® against acute lymphoblastic leukaemia (ALL). Due to the special characteristics of PEG - the absence of toxicity, immuno- and antigenicity, high water-solubility as well as chain-flexibility - polyethylene glycol derivatized therapeutics are still holding the leading position on the market today. Nevertheless, there are of course other synthetic (e.g. HPMA, PEI, PVP), natural (e.g. dextran, dextrin, chitosans) as well as pseudosynthetic polymers (PGA, PLL, PAsp) intensively investigated to evaluate their potential as macromolecular carrier systems *in vivo* [5]. From the above mentioned examples one promising synthetic candidate is *N*-(2-

hydroxypropyl)methacrylamide, confirmed by six HPMA-anticancer conjugates already progressed into clinical trials [13, 14].

1.2 *N*-(2-hydroxypropyl)methacrylamide copolymers

Poly(*N*-(2-hydroxypropyl)methacrylamide) belongs to the class of synthetic polymers and regarding its therapeutic action, poly(HPMA) is holding required features like biocompatibility, lack of immunogenicity and toxicity as well as water solubility. Originally, HPMA homopolymers were designed as plasma expanders [15, 16] but intensive research on HPMA-drug conjugates concerning their clinical applicability was accomplished by a collaboration between Kopecek and Duncan in the early 1980s. The first HPMA-anticancer conjugate entering clinical trials was based on a conjugation with doxorubicin, an anthracycline, and is widely known under the name PK1 [17]. As seen in figure 2a, it is exhibiting the main characteristics of Ringsdorfs' postulated model of "Polymer Therapeutics".

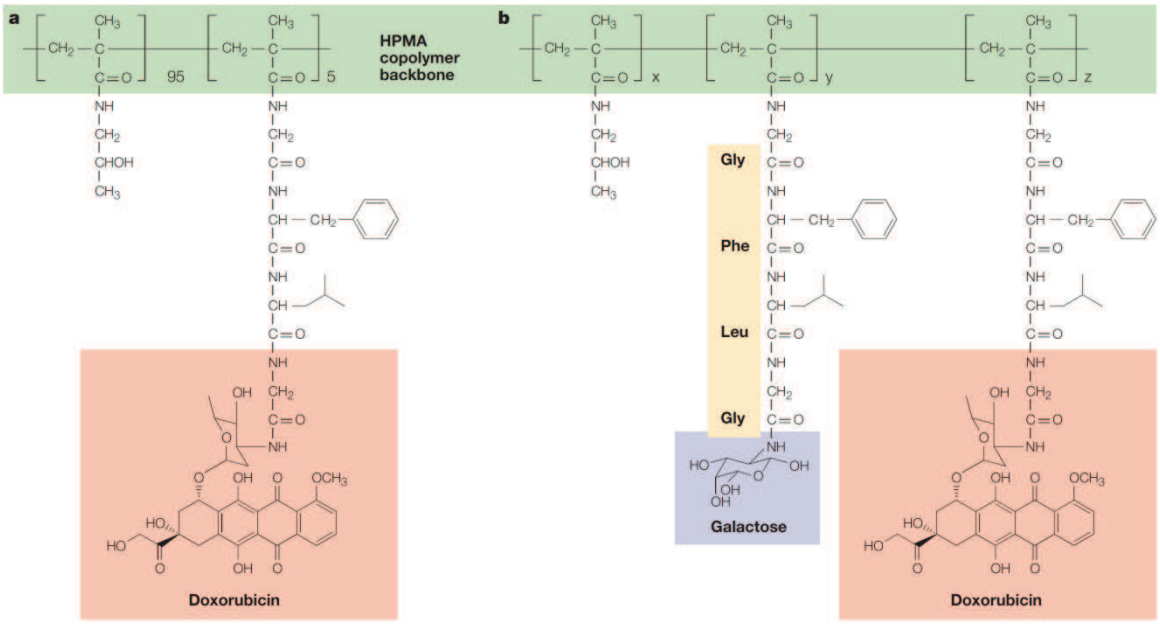

Figure 2: The first two HPMA copolymer drug conjugates entering clinical trials. a) N-(2-hydroxypropyl)methacrylamide copolymer-doxorubicin (PK1; FCE28068) and b) HPMA copolymer-doxorubicin with galactosamine coupled via peptidyl linker (PK2; FCE28069). Green = HPMA copolymer backbone; yellow = peptidyl linker (Gly-Phe-Leu-Gly); blue = galactosamine and red = doxorubicin [4].

The HPMA copolymer backbone displays the soluble as well as biocompatible element, linked via a cleavable peptidyl spacer (Gly-Phe-Leu-Gly; GFLG) to the anticancer drug doxorubicin. Based on earlier studies which concentrated on the dependence of molecular weight on endocytic processes [18] as well as biodistribution patterns [19, 20], the M_w of PK1 was chosen to be ~ 30000 g/mol to ensure renal excretion of the non-biodegradable HPMA backbone after reaching the aimed target site. During phase I evaluations, the doxorubicin content was ~ 8 wt% and compared to the safe dose of the free drug, a four to fivefold increase could be obtained for the intravenously infused polymer-bound chemotherapeutic agent [17]. Clinical pharmacokinetics indicated a prolonged plasma circulation as well as fast renal elimination [21, 22].

In contrast, the first targeted polymer entering clinical trials was PK2 (see figure 2b), designed to improve multivalent targeting of the hepatocyte asiaglycoprotein receptor (ASGPR) for the treatment of primary hepatocellular cancer [23, 24]. It could increase the hepatoma-associated drug to a 12-50 fold higher extent than its free doxorubicin counterpart, thereby highlighting the tremendous impact of the polymer carrier vehicle.

In general, there are some major demands on HPMA copolymers regarding their pharmacokinetic profile. Studies of Seymour et al. [19] revealed a significant effect of molecular weight (M_w) on the subsequent biodistribution pattern of HPMA based copolymers. In their experiment molecular weights were ranging between 12 and 778 kDa (3 - 30 nm in diameter) and a molecular weight threshold limiting glomerular filtration was identified at approx. 45 kDa. Copolymers greater than this threshold were only slowly lost from the bloodstream by means of extravasation. Since a renal excretion cut-off size of ~ 5.5 nm in diameter could be determined for a diversity of macromolecules [25], the observed findings on HPMA copolymers are in good agreement. Nevertheless it has to be mentioned that molecules with molecular weights above the renal threshold were determined to be still able to pass through the glomerular pore as long as they exhibit a flexible structure (also shown for HPMA) [26, 27]. Thus HPMA based copolymer with less than 60 kDa were still exhibiting rapid urinary excretion [19]. Seymour et al. additionally found that with increasing M_w a significant enrichment of HPMA copolymers in the liver, spleen as well as small intestine could be detected. This trend was also observed by Lammers et al. who concentrated on the biodistribution of ^{131}I-

labeled HPMA copolymers varying in molecular weight [28]. Generally it has been suggested that nanoparticles have to be smaller than 100 nm in diameter to achieve low hepatic as well as spleenic uptake [29, 30].

Besides the aforementioned PK1 and PK2, a variety of other HPMA copolymer-anticancer conjugates are still under closer investigation concerning their therapeutic potential [31-33] but overall it can be concluded that the strategy of polymer conjugation demonstrates a versatile route to improve drug-related pharmacokinetics and especially antitumor activity. In regard to the last-mentioned, the discovery of the "EPR effect" (Enhanced Permeability and Retention) by Maeda and coworkers in 1986 [7] was a milestone for the concept of polymer therapeutics.

1.3 The Enhanced Permeability and Retention effect (EPR)

The EPR-effect describes a phenomenon of enhanced extravasation of macromolecules from tumor blood vessels - attributed to their defective vasculature ("Enhanced Permeability") - as well as the retention of the polymeric system in the tumor tissue due to the absence or suppression of lymphatic drainage ("Retention") [7, 34]. These unique anatomical-pathophysiological characteristics are not occurring in normal tissue, thereby enabling a selective tumor targeting by macromolecular anticancer drugs. Furthermore it has to be noted that the EPR-effect is not just a temporary phenomenon of passive targeting to the tumor site but in particular prolonged therapeutic / drug retention for more than several weeks or longer can be realized. The overall concept of the EPR-effect is given in figure 3.

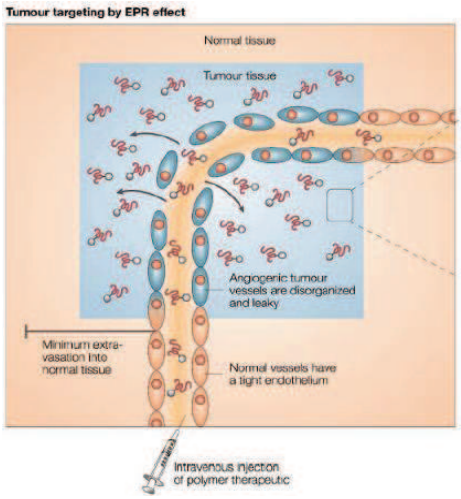

Figure 3: The principle of the "Enhanced Permeability and Retention" effect [4].

The EPR-effect is additionally characterized by a molecular weight dependency. In order to exhibit features of the EPR-effect, a macromolecule must exhibit a higher molecular weight than the renal excretion threshold (typically > 40 kDa) [35]. Noteworthy, this phenomenon was not only observed regarding proteins but also for polymer-drug conjugates, liposomes, micelles and other nanoparticulate systems [7, 34]. Initiative studies were carried out with HPMA copolymers varying in M_w (between 22 and 778 kDa) and demonstrated increased tumor uptake with higher molecular weight [20]. The abnormality of tumor blood vasculature compared to the uniform network and orientation of blood vessels in normal tissue is illustrated by SEM images in figure 4.

Besides molecular weight, there are also other determinants of the EPR-effect. Factors like surface charge as well as *in vivo* surveillance systems for macromolecules (e.g. scavenger receptors of the RES) play quite important roles. Exhaustive studies of Maeda and coworkers also revealed a diverse library of vascular mediators facilitating the effect [34, 35]. These include for example: (a) bradykinin / [hydroxyprolyl^3]bradykinin; (b) nitric oxide (NO) and its derivatives; (c) prostaglandins; (d) angiotensin-converting enzyme (ACE) inhibitors or (e) the vascular endothelial growth factor (VEGF / VPF).

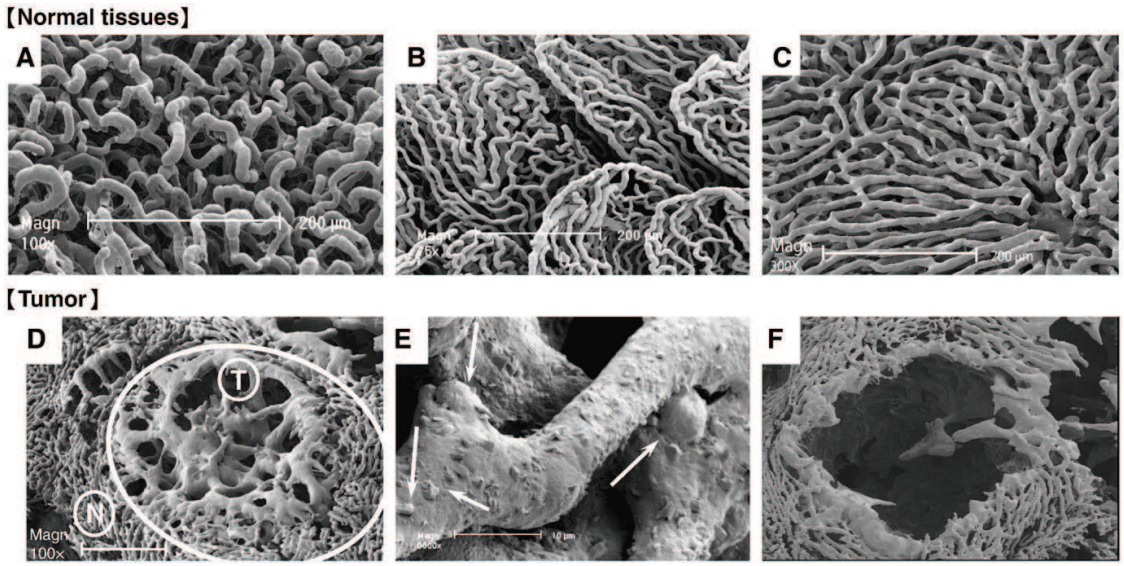

Figure 4: SEM images of blood vessels in normal tissues (A-C) as well as metastatic liver tumors (D-F). Normal capillaries of the pancreas (A), colon (B) and liver (C); metastatic tumor nodule in the liver (D); tumor vessels at the capillary level (E) and empty void (F) [35].

To improve the therapeutic efficacy of macromolecular anticancer drugs, the accession of the EPR-effect was also taken into considerations. In this regard, they first examined

angiotensin-II (AT-II), inducing systemic hypertension and hence pushing the macromolecular agent into the interstitial space or matrix of the tumor tissue. A second method was based on the application of nitric oxide (NO) or NO-releasing compounds and resulted in an elevated blood flow in tumor tissue, leading to an increased drug delivery to the tumor [35]. In summary, it can be concluded that the discovery of the EPR-effect was a breakthrough for cancer chemotherapy, triggering the replacement of the so far applied low molecular weight anticancer drugs with macromolecular linked therapeutic agents. By means of this unique phenomenon, therapeutic efficacy can be enhanced and toxic side effects of the chemotherapeutic reduced. It opened the field in terms of selective macromolecular anticancer drug design and hence initiated the discussion about definition of polymer carrier systems in cancer therapy.

1.4 Synthesis of polymer carrier systems by the RAFT-process

Regarding pharmaceutical development, heterogeneity of polymer-drug conjugates is probably one of the major challenges. Thus well-defined and narrowly distributed polymer carrier systems constitute a main goal to ensure acceptable homogeneity of the final conjugates. Due to these demands, the synthetic route of polymer production is already path-breaking for their subsequent application area. With the introduction of controlled radical polymerization techniques, well-defined polymer structures became accessible, either by using ATRP or RAFT polymerization [36-38]. In respect to the desired therapeutic application, important advantages of the “reversible addition-fragmentation chain transfer (RAFT) polymerization” compared to the “atom transfer radical polymerization” (ATRP) are its high solvent and functionality tolerance as well as the absence of metal ions causing unwanted cytotoxicity. Further benefits are the utilization of conventional radical initiators and the low toxicity of some RAFT agents [39]. The RAFT technique was discovered by Thang et al. in 1998 [37] and its potential for biomedical applications has been further exploited over the last decade [39, 40]. The involved mechanisms are illustrated in the reaction scheme in figure 5.

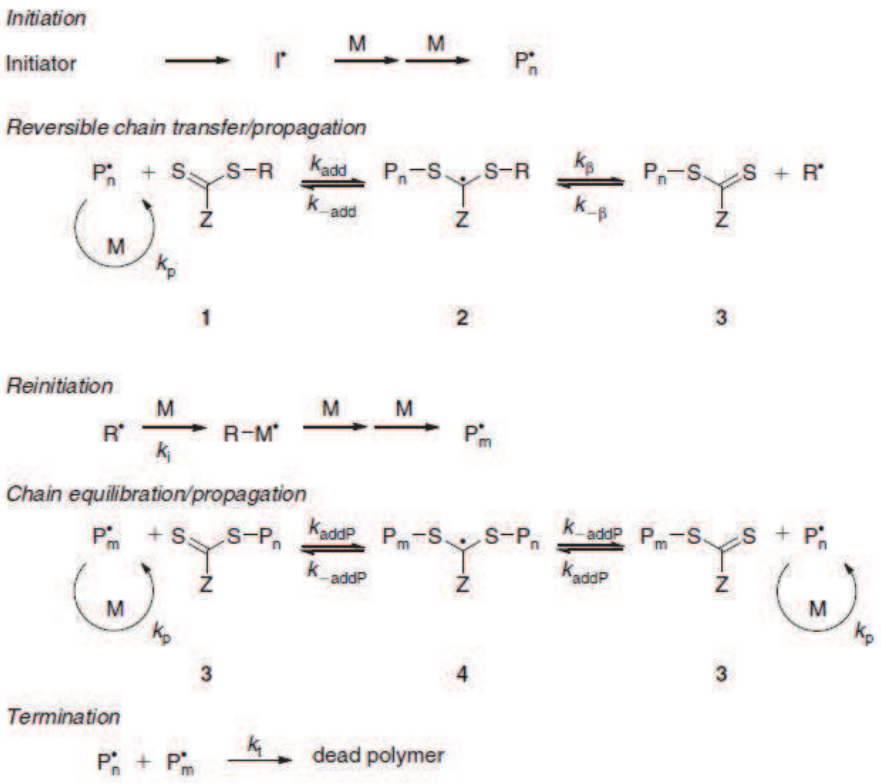

Figure 5: Reaction scheme of the RAFT polymerization process [41].

The characteristic feature of the RAFT polymerization with thiocarbonylthio compounds is based on a sequence of addition-fragmentation equilibria [41]. Initiation is accomplished by conventional initiators like 2,2'-azoisobutyronitrile (AIBN) or benzoyl peroxide (BPO). Radical-radical recombination leads to the termination of the growing polymer chain - similar to conventional radical polymerization. At first, the addition of a propagating radical ($P_n^{\bullet}$) to the thiocarbonylthio fragment [RSC(Z)=S (1)] induces a radical intermediate (2) which is afterwards transferred to a polymeric thiocarbonylthio compound [$P_nS(Z)C=S$ (3)] and a radical $R^{\bullet}$. Reinitiation is achieved by the reaction of the radical $R^{\bullet}$ with further monomers, forming a new propagating radical $P_m^{\bullet}$. Chain equilibration / propagation is based on a fast equilibrium between the growing radical polymer chains ($P_n^{\bullet}$ and $P_m^{\bullet}$) and the dormant polymer thiocarbonylthio species (3). Due to this mechanism there is an equal probability for all polymer chains to grow, resulting in narrowly distributed polymer systems (PDI predominantly < 1.2 and in some cases even < 1.1). After completion or stopping of the polymerization, the majority of polymer chains maintain the thiocarbonylthio end group and subsequent isolation of stable product is possible [41].

It has to be noted that the efficiency of the thiocarbonylthio RAFT agent is strongly influenced by the monomer to be polymerized as well as by the characteristics of the free-radical leaving group R and group Z. Considering a successful RAFT polymerization, some essential requirements have to be fulfilled. The RAFT agents 1 and 3 (figure 5) should have a reactive C=S bond, the intermediate radicals 2 and 4 should fragment rapidly (without any side reactions) and the radicals R˙ have to efficiently re-initiate the polymerization [38].

Besides the already mentioned advantage of narrow molecular weight distributions, the RAFT technique is furthermore characterized by its compatibility with a multitude of monomers (e.g. styrene derivatives, acrylate and acrylamides, methacrylates and methacrylamides as well as vinyl esters) and reaction media (also comprising protic solvents such as alcohols and water). Due to its further modifiable CTA (Chain Transfer Agent) end group, a variety of polymeric architectures - including block copolymers, stars, dendritic polymer structures or microgels – can be created. The above mentioned features emphasize the potential of the RAFT methodology (and its resulting polymer structures) in regard to the growing field of polymer based anticancer treatment. Especially the combination with reactive ester chemistry represents a useful tool to access diverse polymer architectures and various functional moieties.

1.5 Reactive ester chemistry and post-polymerization modification

Activated ester monomers exhibit an outstanding class of bioapplicable compounds. Among them, *N*-methacryloxysuccinimide (NMAS) and *N*-acryloxysuccinimide (NAS) are the most commonly used monomers, being precursors of the side-chain *N*-hydroxysuccinimide (NHS) polymer esters [42]. Their polymerization to polymeric reactive esters was first discussed by Ringsdorf [43] and Ferruti [44], leading the way of pharmacologically active polymers into the field of “Polymer Therapeutics”. Nevertheless they possess a major drawback due to the restricted solubility of poly(NMAS) and poly(NAS) in either dimethylsulfoxide (DMSO) or dimethylformamide (DMF).
In contrast, the reactive ester polymers poly(pentafluoroacrylate) poly(PFA) and poly(pentafluoro methacrylate) poly(PFMA) benefit from an improved solubility as well as increased reactivity compared to the classical NHS-based polymers [45]. Including all of

the here presented polymeric active esters (also see figure 6), nucleophilic substitution is the most frequently applied method to achieve post-polymerization modification [46].

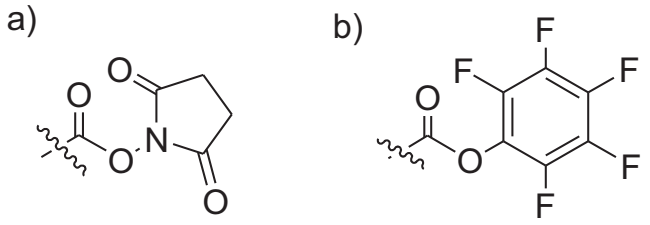

Figure 6: Functional groups of reactive ester precursor monomers for post-polymerization modification. a) NAS, NMSA; b) PFA, PFMA.

In this regard, amines are preferentially reacted with active esters, attributed to their good nucleophilicity compared to other functional groups (e.g. hydroxylic groups of alcohols). This characteristic enables the selectivity of the reaction without the necessity of introducing protecting groups. Besides this advantage, post-polymerization modification facilitates the access to functional polymers which cannot be synthesized via the route of direct polymerization as well as the possibility of introducing multiple functional groups into the polymer side-chains (e.g. fluorescent markers, radiolabels, active targeting moieties etc.). Furthermore, since the reactive ester precursor monomer is generating polymer structures with identical average chain lengths and distributions, the application of polymeranalogous reactions allows a deepening knowledge about structure-property relationships [46]. Regarding this correlation, polymer architecture is also playing a major role and will be further discussed in the upcoming chapter.

1.6 Polymeric micelles and their application in drug delivery

Over the last decades, emerging interest considering the application of polymeric micelles for controlled drug delivery has evolved [47-50]. They can be subdivided into at least three main classes, depending on the type of intermolecular driving forces: 1) amphiphilic block copolymer micelles (caused by hydrophobic interactions); 2) polyion complex micelles (PICM; formed by electrostatic interactions) and 3) polymer-metal complex micelles (induced by metal complexation) [49]. With special focus on block copolymer micelles - consisting of a hydrophilic and a hydrophobic block - their self-assembly in aqueous solution is attributed to non-polar as well as hydrophobic interactions among the lipophilic polymer chains. This process is furthermore driven by a gain of entropy of the

surrounding solvent molecules caused by the withdrawal of the hydrophobic segments [51]. The formation and drug loading of a block copolymer micelle is exemplary illustrated in figure 7.

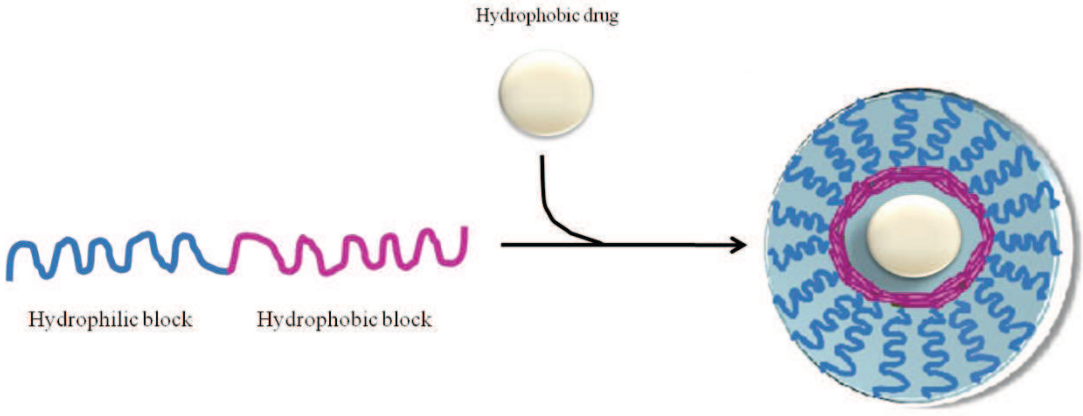

Figure 7: Self-assembly and drug loading of the hydrophilic-hydrophobic block copolymer into a polymeric micelle in aqueous solution.

Their favored suitability as drug delivery vehicles is based on the core-shell morphology – initiated by the exceeding of the critical micelle concentration (CMC). The hydrophobic chains form the core structure and leaves the hydrophilic block as surrounding corona [52]. The inner core is sterically stabilized by the outer shell hence enabling to serve as storage for pharmacologically active drugs which are either entrapped by chemical, physical or electrostatic interactions. According to the chemical nature and molecular weight of the hydrophobic block, important properties of the polymeric micelles (e.g. stability, drug loading capacity or drug release profile) can be influenced [50]. The hydrophilic shell on its part is responsible for the pharmacokinetic characteristics of the block copolymer micelle, ensuring colloidal stability as well as prolonged *in vivo* circulation times. The enhanced plasma-half life was already intensively studied for PEG-based block copolymer micelles [6, 47, 48, 53], underlining the feasibility of the shell to prevent protein adsorption as well as opsonization during the circulation process. In addition to these features, the small size of polymeric micelles in the nanometer range (10 nm to 200 nm [50]) protects them toward RES-uptake and allows extravasation at leaky sites of capillaries. This results in their passive accumulation at certain biological sites with vasculature abnormalities (e.g. tumors or inflamed tissue) and can be described by the “enhanced permeability and retention” effect (see chapter 1.3).

Especially in comparison to other drug delivery platforms, like low molecular weight amphiphiles, polymeric micelles are holding favorable benefits concerning their tendency for micellization and thermodynamic stability. These characteristics are due to low CMC values in the µmolar range, staying in contrast to millimolar CMC levels obtained for low molecular weight tensides [48]. Furthermore, the tuning of the core and shell-forming block, the incorporation of stimuli-responsive moieties or cross-linkable functionality as well as the control over size and shape render polymeric micelles unique nanocarrier systems.

The majority of block copolymer micelles comprise polyethylene glycol as hydrophilic shell, the so called "golden standard" for polymer coating. Relevant examples involve studies about the anticancer efficacy of Dox-coupled PEG-*b*-p(Asp) [54] or cisplatin-carrying PEG-*b*-p(Glu) [55] block copolymers by Kataoka et al. as well as the closer investigation of Pluronics® by Kabanov and coworkers [56, 57]. A diversity of other PEG based polymeric micelles can be found in the literature, too [48, 58-60]. Nevertheless there is a need for alternative water-soluble polymer systems since it was demonstrated several times that PEG-liposomes were rapidly cleared at low lipid doses as well as after repeated administration. This observation is called "ABC" phenomenon (Accelerated Blood Clearance) [61, 62] and probably attributed to the presence of anti-PEG IgM induced by the first dose of PEGylated liposomes [63].

In this regard, poly(HPMA) can be considered as an attractive candidate, being biocompatible, non-toxic as well as non-immunogenic and furthermore possessing the benefit of multifunctionality. So far, only HPMA-anticancer conjugates have been extensively studied during the past years. The application of poly(HPMA) as part of polymeric micelles is fairly new and already obtained promising results. Regarding the use of HPMA as hydrophilic shell, Konak et al. observed the formation of small (size < 50 nm) and dense micellar structures of HPMA-*b*-BA copolymers [64] in water. Comparable results could be achieved by Barz et al. [65] who focused on the synthesis and self-assembly of HPMA-LMA block copolymers with varying block length. In aqueous solution, polymeric micelles with diameters of 100-200 nm were determined, not showing any cell toxicity up to a concentration of 2 mg/mL.

In addition, poly(HPMA) was introduced as a hydrophilic coating for polyion complex micelles in the field of gene delivery [66, 67] and micelle-like structures (around 300 nm) could be proven after DNA complexation. HPMA based polymeric micelles were also formed out of triblock copolymers with poly(ε-caprolactone) [68], star-shaped [69] or stimuli-responsive block copolymers [70]. It can be concluded that pHPMA is an encouraging polymer system regarding the improvement of drug delivery vehicles and a closer look on the *in vivo* fate of HPMA composed polymeric micelles is a special need for future research.

1.7 HPMA based copolymers as polymeric nanomedicine for anticancer therapy *in vivo*

The motivation of HPMA based copolymers for anticancer treatment was already arising in the 1970s [15, 71, 72] and aimed to optimize the obstacles of conventional intravenously injected antitumor agents. The limiting factors of chemotherapeutic drugs can be subdivided into four different classes: chemical, biological, physical as well as clinical barriers [73]. From the chemical point of view anticancer agents suffer from their low solubility, stability, molecular weight as well as their large volume of distribution which leads to an increased accumulation in healthy tissues. Furthermore they undergo rapid renal clearance and hepatic degradation (biological barrier). Taking the clinical challenges into consideration, chemotherapeutic drugs are not accumulating well at the tumor site thereby leading to low efficacy as well as high toxicity issues. Frequent administration and their low cost-effectiveness render them unfavorable concerning the clinical setting and alternative concepts were developed.

In the past decades a diversity of passively tumor-targeted drug delivery vehicles were created, involving liposomes [74], polymers [22], polymeric micelles [47] or nanospheres [60]. Considering their therapeutic action, they are confronted with severe demands. With special focus on HPMA based copolymers and their lack of biodegradability, narrowly distributed nanocarriers with high renal excretion rates have to be guaranteed. In this regard, Seymour et al. [19] intensively studied the effect of M_w of HPMA copolymers on their biodistribution and renal elimination pattern. They identified a molecular-weight threshold limiting glomerular filtration at around 45 kDa but nevertheless molecules with molecular weights above the renal threshold were determined to be still able to pass

through the glomerular pore as long as they exhibit a flexible structure (also shown for HPMA) [26, 27].

Besides, a further requirement is the introduction of a bioresponsive polymer-drug linker, ensuring stability of the agent during bloodstream transport but enabling an optimal drug release at the target site. One example would be the incorporation of acid-labile linkers, profiting from the pH-change in subcellular vesicles like lysosomes [75, 76]. On the other hand, oligopeptide sequences are representing another promising approach for drug-attachment and subsequent enzymatically triggered release [77, 78]. Early studies of Kopecek et al. revealed that length and structure of the oligopeptide sequences, drug architecture as well as steric hindrance were the major determinants of oligopeptide-dependent drug release [79, 80]. Lysosomal degradation - with special emphasis on the lysosomal cysteine proteinase cathepsin B - could be proven [81] hence introducing the glycylphenylalanyl-leucylglycine (GFLG) moiety for polymer-drug conjugates [82].

PK1 (pHPMA-GLFG-Doxorubicin) was the first polymeric prodrug i.v. applied for passive tumor-targeting in clinical trials [17]. Phase I studies demonstrated a significant enhancement of the therapeutic index of doxorubicin-based chemotherapy with a MTD of conjugates four-fivefold higher than the free drug. These promising results lead to a phase II trial of PK1 in breast, lung and colorectal cancer - showing tolerable toxicities as well as 6/62 partial responses (PR) with limited side effects [83]. To achieve deepening knowledge about the pharmacokinetics of the polymer-drug conjugate, a ^{123}I-labeled polymer-Dox analog was i.v. injected and time-dependently monitored via γ-scintigraphy (illustrated in figure 8).

After 4 hours, radioactivity was still concentrated in the bloodstream as clearly indicated by the heart and major blood vessels. Tumor accumulation of the radiolabeled conjugate could also be seen. Significant iodine-123 signal was further observed for kidneys and bladder, demonstrating renal excretion of the compound. After 24 hours, detection of radioactivity in the blood pool was still evident but to a considerably lower extent.

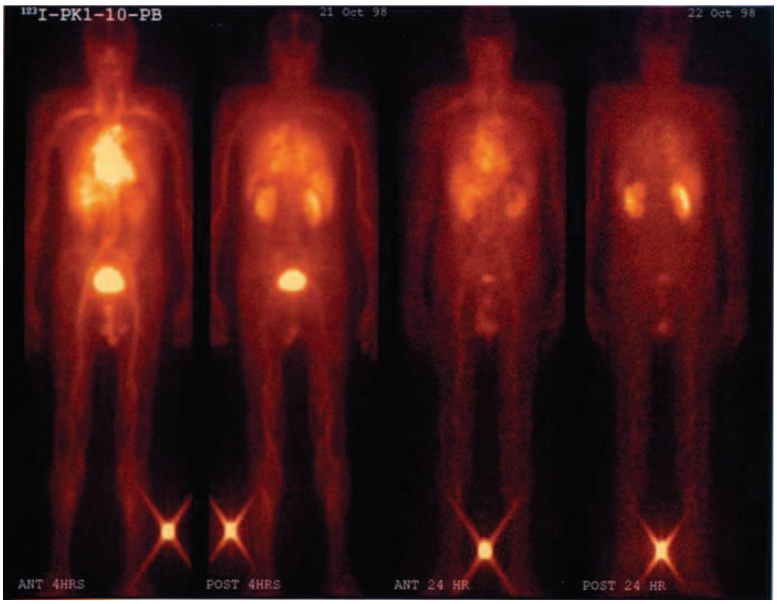

Figure 8: Planar γ-camera imaging of patient 4, 24 and 48 h after i.v. administration of PK1 (FCE28068). Images were calibrated with an external standard (placed between the patient's feet). Patient is affected by large cell lung carcinoma [83].

Blood clearance kinetics of the ^{123}I-PK1 analog were consistent with studies on unlabeled polymer-conjugate [17], suggesting the transferability of this approach. In fact, it emphasized the usefulness of this non-invasive technique to monitor the biodistribution and tumor accumulation pattern of the polymer-bound drug. Based on these investigations, it can be assumed that the anticancer activity of PK1-doxorubicin is mostly defined by its kinetics and biodistribution. Compared to free doxorubicin, it is benefiting from prolonged plasma circulation, subsequent passive tumor accumulation and a low volume of distribution (visible in figure 8).

Only a couple of years after phase I studies of PK1, PK2 entered clinical trials. In addition to PK1, this polymer-drug conjugate possesses a covalently linked galactosamine residue (see figure 2b) thus being the first actively targeted polymer-drug conjugate evaluated in patients to date. The incorporation of galactosamine was aimed to improve the treatment of liver cancer by selectively targeting the highly expressed hepatocyte asialoglycoprotein receptor [23, 24]. Biodistribution of PK2 was monitored via γ-scintigraphy and SPECT (Single Photon Emission Computed Tomography) / CT (Computed Tomography) demonstrated enhanced accumulation of the compound in kidney and liver (SPECT/CT images are illustrated in figure 9).

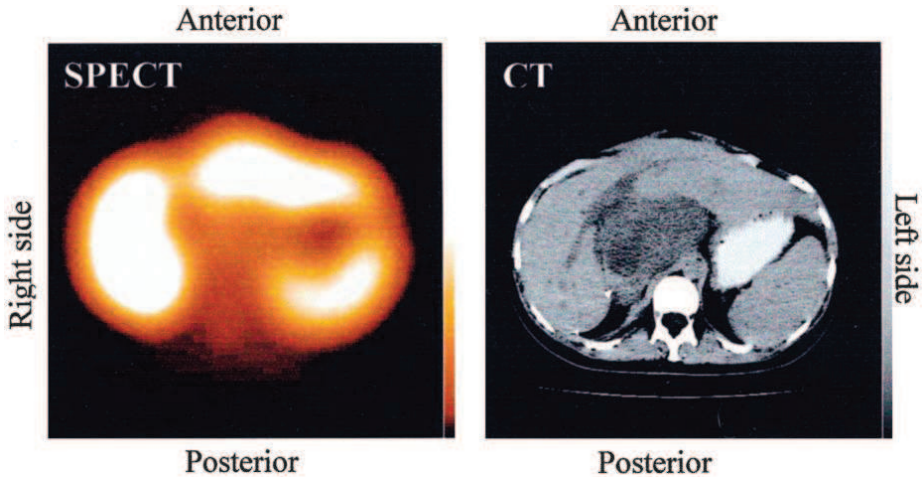

Figure 9: SPECT (left) and CT (right) images after administration of PK2 [24].

Somehow disappointing, the majority of radioactivity was associated with areas of healthy liver tissue (17±4 %). Liver tumors – seen as dark mass in the center of the CT scan - indicated a pronounced lower conjugate uptake (3±6 %). This investigation may be attributed to a known decreased level of ASGPR expression in hepatoma *versus* normal liver, particularly occurring in poorly differentiated disease [24]. Furthermore, liver tumors incline to less perfusion as well as less vascularization [73]. Noteworthy, the maximum tolerated dose of PK1 was considerably higher (320 mg/m^2 compared to 160 mg/m^2) thereby highlighting the influence of the active galactosamine targeting moiety.

Besides the two herein presented HPMA-doxorubicin conjugates, there have been some more HPMA based compositions entering clinical trials. These include for example PNU166945 - a paclitaxel-conjugate [32] - or AP5280 (polymer-bound cisplatin derivative) [33] as well as AP5346 (HPMA-oxaliplatin), the most promising candidate among the ones here listed [84]. The multitude of HPMA based polymeric drugs evaluated in phase I and II studies demonstrate their great suitability for tumor targeted therapy. They markedly improve the pharmacokinetics as well as biodistribution characteristics of attached pharmacologically active drugs and encourage their use in the field of nanotheranostics.

Regarding the clinical application of polymeric nanomedicine, there is a need for appropriate preclinical screening techniques. By means of contrast agents like radionuclides or MRI (Magnetic Resonance Imaging) probes - additionally introduced into the polymeric carrier system – information on biodistribution and target site accumulation of the polymer-drug conjugate can be already generated at early stages.

Main advantages of radio- or MRI probes toward fluorescent dyes consist in their non-invasive nature, allowing longitudinal studies in the same animal in real-time, as well as the quantitative determination of information (e.g. ID/g tissue in %) [85]. Due to the named benefits, studies of Lammers et al. coined the concept of image-guided drug delivery, the combination of (cancer) diagnosis and therapy. This approach enables e.g. monitoring of the biodistribution of chemically attached or physically entrapped therapeutic agents, the detection of their tumor accumulation profile as well as the estimation of their medical efficacy.

To achieve a better understanding and optimize drug targeting to tumors, Lammers et al. applied HPMA based copolymers for γ-scintigraphy and MRI. A detailed biodistribution study with gadolinium-labeled HPMA copolymers (molecular weight of 25 kDa) was carried out by means of magnetic resonance, γ-camera imaging as well as HPLC [86]. As seen in the MR angiography scans in figure 10A, the gadolinium-labeled polymer exhibited an enhanced accumulation to the vascular compartment 0.5 h post i.v. injection. Using the color-coded maximum intensity projection (MIP), prolonged blood circulation properties of the copolymer could be proven, too. Furthermore, the projection indicated that the high molecular weight Gd-pHPMA was even in the tumors predominantly found within the vasculature 0.5 h p.i.. Comparative studies between 25 kDa-sized Gd-pHPMA and Gd-DTPA-BMA (gadolinium-diethylenetriaminepentaacetic-acid-bis-methylamide 0.5 kDa) revealed a polymer-dependent decrease in kidney accumulation as well as an EPR-mediated enrichment of Gd-pHPMA in the tumor over time. Significant liver accumulation was additionally detected (see figure 10B and 10C).

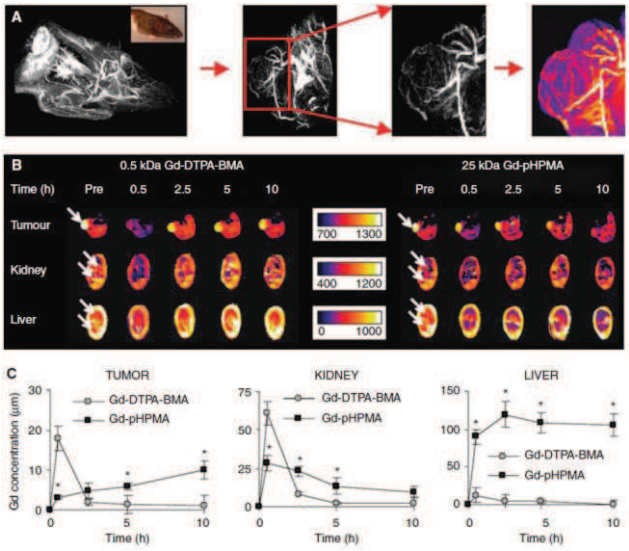

Figure 10: MRI-based biodistribution studies of Gd-labeled HPMA copolymer. (A) from left to right: MR angiography scans of the chest and head region of a rat; a tumor bearing paw; an AT1 tumor and MIP of the polymer-monitored perfusion of the tumor. (B) Dynamic color-coded MRI T1 determination for AT1 tumor, kidney and liver at different time points of injection (0.5 kDa Gd-DTPA-BMA vs. 25 kDa Gd-pHPMA). (C) Quantification of Gd-concentrations [86].

To generate an overall picture of the *in vivo* fate of the polymeric carrier system – in particular regarding its long-term disposition – Lammers and coworkers introduced an iodine-131 radiolabel to two differing, tyrosinamide-containing HPMA copolymers. The copolymers varied in molecular weight (31 and 65 kDa) and visualization of their biodistribution pattern was accomplished scintigraphically (as shown in figure 11A).

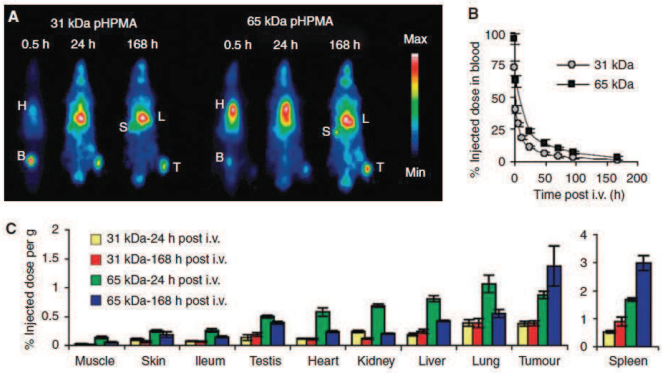

Figure 11: Biodistribution studies of ^{131}*I-labeled HPMA copolymers differing in molecular weight (31 kDa vs. 65 kDa). (A) γ-scintigraphy images of radiolabeled compounds 0.5, 24 and 168 h post injection in AT1 tumor-bearing Copenhagen rats. (B) Blood concentrations of* ^{131}*I-labeled HPMA copolymers. (C) Quantitative biodistribution studies of copolymers in selected organs (muscle, skin, ileum, testis, heart, kidney, liver, lung, tumor and spleen) 24 and 168 h p.i.* [86].

These results stay in good correlation with the MR angiography (figure 10A), illustrating prolonged blood pool concentration of the ^{131}I-labeled HPMA copolymers with additional quantification by the % of injected does in the blood (figure 11B). Particularly the high molecular weight HPMA copolymer showed increased plasma-half life over a time period of 24 hours as indicated by strong heart localization. Besides, the polymeric carriers exhibit a low volume of distribution, mainly in organs of the RES (lung, liver and spleen) hence reflecting known mechanisms of polymer clearance [22, 74]. Considering tumor accumulation, the molecular weight difference of pHPMA (31 kDa to 65 kDa) plays a major role, demonstrating higher tumor levels with increasing size and time (as seen in figure 11C). These findings can be explained by the EPR-effect in combination with high blood pool retention of the large HPMA copolymer. In conclusion, the presented studies strongly emphasize the versatility of HPMA copolymers for chemotherapy based on their improved tumor-targeted transport of low molecular weight anticancer agents. It has to be noted that the obtained results are based on the incorporation of a MRI or radioactive probe, enabling the facile and fast *in vivo* tracking of the polymers. In this regard, the term "Personalized Therapy" is more and more emerging in the field of polymeric nanomedicine. It is raising the question of adequate preclinical screening tools required for the development of suitable therapies to the individual patient needs. Besides the so far introduced techniques, Positron Emission Tomography (PET) demonstrates a more versatile and refined method to augment tumor diagnostics.

1.8 Diagnostic imaging techniques – with special focus on PET

Nuclear medicine constitutes an essential branch of diagnostic radiology, providing specific information about disease status. Among the established applications in this field, scintigraphy is an important diagnostic technique which uses the emission of γ-irradiation of administered radiopharmaceuticals in the body. The detection of emitted radiation by a γ-camera and subsequent transformation enables the production of two-dimensional images of internal body tissue. In this regard, there are three major shortcomings to be named [87]. First, since the obtained images are projection images, issues of masking the organ of interest can occur. Furthermore, photons which were emerged in the organ of interest can be attenuated by overlying tissue. The second problem is attributed to the applied radiopharmaceuticals, including the incorporation of relatively heavy isotopes (e.g. ^{201}Tl or ^{99m}Tc) which do not naturally occur in biological active molecules.

Modifications needed for nuclide incorporation often alter the effectiveness *in vivo* and therefore limit the amount of potent radiopharmaceuticals. Finally, the issue of sensitivity has to be addressed. Due to the high absorbance of photons by the lead collimator, the sensitivity of the camera is markedly reduced. Taken all these issues into account, it emphasizes the necessity of progressive methodology.

To this effect, Positron Emission Tomography (PET) as well as Single Photon Emission Computed Tomography (SPECT) have to be named. Even though they are based on the same principles of conventional scintigraphy, they are classified as separate techniques. Since PET and SPECT are both tomographic methods, they benefit from the three-dimensional visualization of spatial as well as temporal distribution of radioactive labeled compounds *in vivo*.

Single photon emission computed tomography can be explained by the following fundamental principles. The administered tracer (comprising a single photon emitting nuclide) is emitting γ-irradiation during its stay in the organism, subsequently detected by multiple rotating gamma-cameras (mainly equipped with sodium-iodine (NaI) scintillation detectors). During this process only photons that pass through the holes of the collimator – a plumbum plate connected ahead of the γ-camera – will be detected. The majority of photons (> 99%) will be absorbed by the present Pb. By means of the rotating camera, projections from different spatial directions can be generated. These will be afterwards converted by the so called “Radon-Transformation” thereby allowing the determination of the position of the radiopharmaceutical in the organism. In comparison, PET is profiting from the decay of two γ-photons which are traveling at 180° from each other with energy E(γ) of 511 keV per photon. Only the coincident arrival of the γ-photons at opposing detectors (within a few nanoseconds) will be detected. Thus Positron Emission Tomography (PET) is enabling higher spatial resolution compared to SPECT.
In general PET is based upon the application of positron-emitting radionuclides which are incorporated into the molecular probes. SPECT on its part is using γ-irradiation-emitting tracers. The unique properties of positron emission tomography are accredited to the nature of its radionuclides, possessing unstable neutron deficient nuclei. As a consequence positrons are emitted for stabilization purposes.

The decay mechanism is described as follows:

$$^{1}_{1}\mathrm{p} \rightarrow {}^{1}_{0}\mathrm{n} + \mathrm{e}^{+} + \nu_{e}$$

The decay involves the conversion of a proton (p) into a neutron (n) combined with the emission of a positron (e^{+}) for charge equalization and a neutrino (ν_e) for spin maintenance. Depending on its energy, the emitted positron is traveling a finite distance (so called positron range: 0.22-1.6 mm [87]) in the tissue, loosing its kinetic energy in terms of elastic collisions toward the surrounding. This process is named thermalization. The following recombination of the positron with an electron of an adjacent atom is denoted as annihilation reaction and responsible for the actual detection of this transformation mechanism. The mass of the two particles is converted to two photons which are traveling at 180° from each other with energy E(γ) of 511 keV. The registration of the γ-photons is accomplished by their coincident arrival at opposing radiation detectors within a few nanoseconds (the coincidence timing window). Due to the high energy of the annihilation radiation (511 keV) tissue penetration is enhanced which results in a better detectability as compared to SPECT. These characteristics favor PET toward SPECT since the latter is mostly using low energy γ-photons such as 140 keV of technetium-99m in nuclear medicine imaging. A general overview of the main principles of Positron Emission Tomography is illustrated in figure 12.

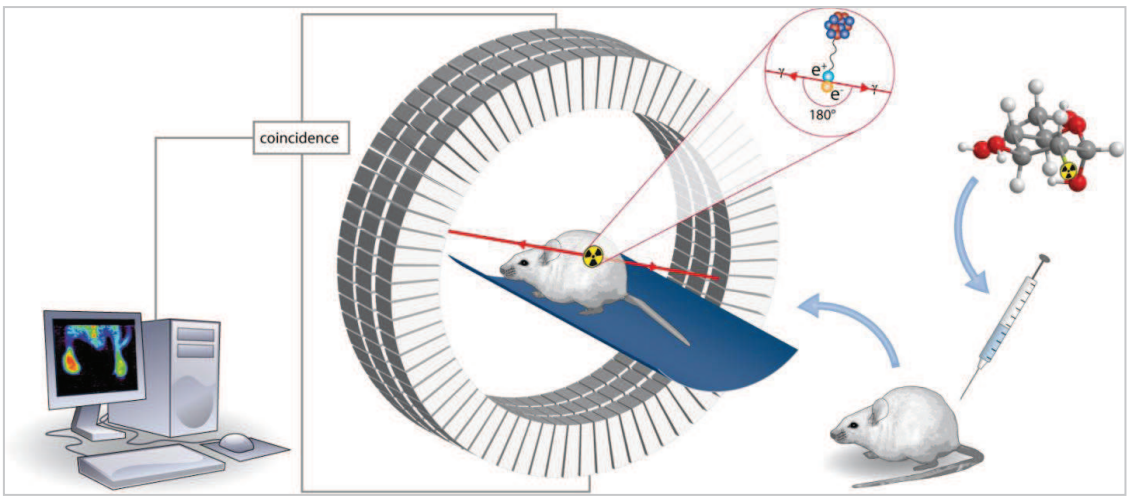

Figure 12: The principle of Positron Emission Tomography exemplified by animal μPET.

Both techniques detect emitted γ-irradiation of radiotracers via gamma-cameras. The main advantage of PET in respect to SPECT- its high spatial resolution – is based on the coincident registration of the two γ-photons, leading to localize the annihilation event along the line connecting the two detectors. This line is sometimes referred to as line-of-response (LOR). Due to a multitude of singe annihilation processes and subsequent overlay of the lines-of-responses, the position of annihilation and hence the localization of the radioactive tracer can be precisely determined. The application of modern PET-scanners which are partially equipped with more than thirty detector rings (predominantly bismuth-germanate (BGO) or lutetium-oxyorthosilicate (LSO) block detectors) enables a spatial resolution of 4-6 mm for clinical PET scanners and up to 1 mm in the case of preclinical μPET imaging scanners [88]. Furthermore, the absence of a collimator - collimation is done electronically – is leading to a relatively high sensitivity [87]. These two main features of PET, high spatial resolution and sensitivity, emphasize its particular progress compared to SPECT. The combination of high sensitivity and the generation of fast exposure sequences (with intervals in the seconds range) facilitate the determination of dynamic alterations of the radiopharmaceutical in the organ of interest [89]. It permits the detection of radioactive tracers *in vivo* in a truly regional and quantitative manner. Thus a diversity of metabolic, biochemical and physiological questions can be explored. In this regard, its wide application in oncology (tumor and metastasis imaging) and inflammation processes as well as neuroimaging and cardiology has to be addressed. Nevertheless it has to be noted that SPECT – due to its minor electronic expenses – is more cost-effective and furthermore the possibility of simultaneously using several radionuclides with differing γ-energies allows the parallel investigation of distributions and kinetics of radiolabeled substrates [89].

1.9 Radionuclides and applications of Positron Emission Tomography

Positron emission tomography is mostly using ^{18}F as well as ^{68}Ga and ^{124}I as positron emitters. Besides the already named characteristics of improved sensitivity and spatial resolution of the PET technique, the size of PET-nuclides is another important benefit. Due to the small size of e.g. fluorine-18 and the absence of voluminous chelators, the chemical structure and physicochemical properties of the labeled compound can be preserved. Especially regarding the investigation of structure-property relationships *in vivo*, the aspect of molecular alteration by introducing radioactive markers is playing a

fundamental role. Furthermore, the short half life of positron emitters significantly reduces the dose of radiation to the subject and facilitates the handling of the radionuclides.

The key role of ^{18}F in PET diagnostic is attributed to its favorable physical and nuclear characteristics. Due to a half-life of ~ 110 minutes, synthesis, purification as well as clinical application can be secured. Nucleophilic radiofluorination via ^{18}F-fluoride is the favored technique for radiolabeling, also including the prime example ^{18}F-FDG (2-[^{18}F]-fluoro-deoxy-*D*-glucose) [90]. It is an analog of glucose – exchange of the hydroxyl group toward ^{18}F at position 2 – and by far the best clinically known and most successful PET radiopharmaceutical. ^{18}F-FDG is FDA approved and routinely used for clinical applications, e.g. assessment of glucose metabolism in heart, lungs and brain. It is further established for tumor imaging in the field of oncology. Another important ^{18}F-derivative is [^{18}F]Fluorodopa (6-[^{18}F]-fluoro-3-4-dihydroxyphenylalanine) - an analogue of *L*-Dopa – being the first visualizing the intracerebral disposition of the neurotransmitter dopamine as well as the dopaminergic signaling pathway [91].

Reflecting positron emission tomography from another point of view, this technique is further a promising methodology for the monitoring of macromolecular radio-pharmaceuticals. By means of PET and suitable radionuclides, tumor accumulation as well as biodistribution of a polymer carrier system can be easily visualized in the living organism. The group of Hawker was one of the first applying the positron emitter ^{64}Cu combined with PET for tracking polymeric nanoparticles *in vivo* [92]. Even though ^{64}Cu is the most frequently used radionuclide for PET imaging of nanoparticles so far, it possesses some major obstacles. Due to the necessity of chelating agents for complexation, the molecular structure of the polymeric system can be significantly influenced and hence altering its biodistribution pattern. Thus small radioisotopes like ^{18}F might be interesting alternatives, also providing increased image resolution. In this regard, studies of Devaraj et al. demonstrated the successful synthesis and *in vivo* characterization of ^{18}F-labeled nanoparticles (^{18}F-CLIO) [93].

The above mentioned examples clearly emphasize the versatility of PET-nuclides for *in vivo* tracking of macromolecular carrier systems. Due to the favorable characteristics of

fluorine-18, pre-clinical screening of polymer drug delivery vehicles can be easily accomplished, placing the focus on individualized patient therapy in the future.

1.10 Polymeric carrier systems and the tumor model

With discovery of the enhanced permeability and retention effect in solid tumors (see chapter 1.3), a variety of polymer based drug carrier systems were studied for their ability to passively accumulate in tumors [22, 30, 34, 94]. Because of the multitude of papers out on polymer enrichment in different tumor models, in this chapter we are only concentrating on two tumor models which were intensively investigated during the herein presented PhD project: the AT1 Dunning prostate carcinoma R3327 as well as the Walker 256 mammary carcinoma.

Beginning with the Dunning tumor R3327, it was described as a most useful model system in studies of human prostatic cancer by Lubaroff and Reynolds in 1980 [95]. This statement was attributed to its predominant resemblance to the human disease related to histology, ultrastructure as well as most metastatic abilities. As already investigated for human prostate cancer, the Dunning tumor is developing multiple sublines which differ in their histologic pictures, growth rate as well as androgen dependence. Due to the promising transferability to human cancer, intensive effort has been carried out to understand tumor-related processes. In this regard research on oncogene expression [96], influence of hyperthermia [97], tumor angiogenesis [98], tumor oxygenation [99, 100] or in general tumor imaging [101, 102] are only some examples for selective investigations on the AT1 Dunning prostate carcinoma R3327 subline.

Since tumor characteristics like tumor vascularity and perfusion, vascular permeability or metabolic parameters (e.g. oxygenation, pH or bioenergetic status) can possess major impact on the *in vivo* fate of macromolecular nanocarrier systems [103, 104], it is crucial to understand the correlation between tumor properties and polymer features (e.g. architecture, size, molecular weight or amphiphilicity) in the living organism. From this point of view, Kissel et al. for example aimed to gain further knowledge concerning the biodistribution and cellular localization of biotinylated poly(HPMA) in the AT1 tumor model [105]. They applied scintigraphy, autoradiography as well as dissection analysis to determine the *in vivo* disposition of polymers with and without biotin – both exhibiting

the same molecular weight of ~ 27 kDa. Biodistribution studies revealed a tremendous influence of biotin on the polymer uptake in the kidney, represented by a 33-fold higher uptake for biotin-pHPMA compared to the homopolymer. Their findings demonstrated the necessity of combining different imaging techniques to generate an overall picture of the macromolecular carrier system *in vivo* and in particular the awareness of changing the pharmacokinetics of polymeric nanocarriers dramatically by only introducing small probes.

Another study of Lammers and coworkers closely investigated the correlation between differing Dunning tumors and their impact on passive drug targeting - also including treatments like radiotherapy and hyperthermia [106]. They first evaluated biodistribution as well as tumor accumulation properties of two differently sized HPMA copolymers (31 kDa *vs.* 65 kDa) in three tumor models: AT1-sc, AT1-im and H-sc. As seen in figure 13A, H-sc tumors grow much slower compared to AT1-sc tumors hence exhibiting a well-differentiated vasculature with diminished leakiness toward macromolecules. Furthermore, radiolabeling of the HPMA homopolymers with iodine-131 and subsequent scintigraphic analysis showed highest tumor accumulation in AT1-sc tumors (50 % lower levels in AT1-im and H-sc) as well as increasing tumor concentrations with higher molecular weight (see figure 13B and C).

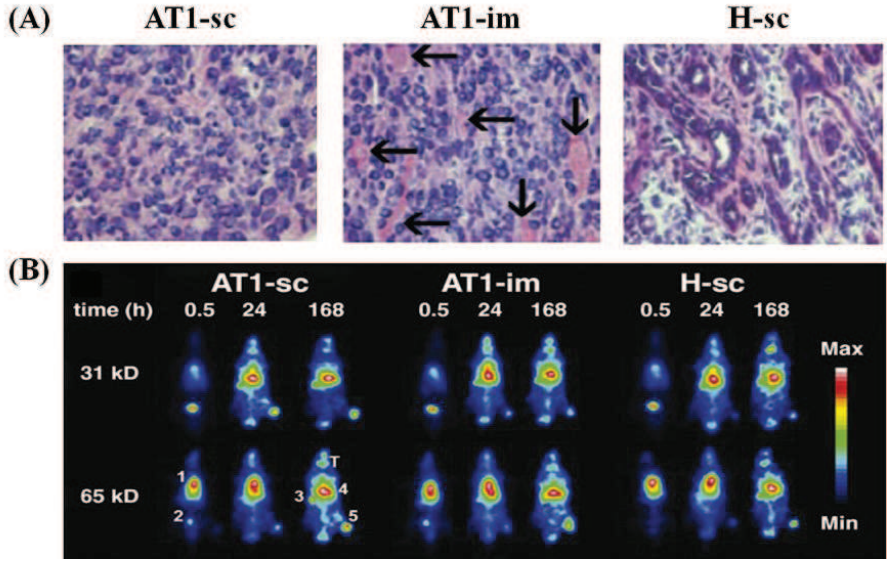

Figure 13: (A) Histological images (H+E staining) of subcutaneously transplanted Dunning AT1 tumors (AT1-sc; left), intramuscularly inoculated AT1 tumors (AT1-im; middle) and subcutaneously transplanted Dunning H tumors (H-sc, left). (B) Scintigraphic analysis of the biodistribution and tumor accumulation of 31 kDa vs. 65 kDa ^{131}I-poly(HPMA) in AT1-sc, AT1-im and H-sc tumor bearing rats. (1 = circulation; 2 = bladder; 3 = spleen; 4 = liver and 5 = tumor) [106].

Besides the so far presented examples of HPMA based copolymers in the AT1 Dunning prostate carcinoma, research studies on polymeric carrier systems in the Walker 256 carcinoma model are holding emerging interest, too.

Cassidy et al. were the first investigating the activity of HPMA copolymers containing daunomycin against the Walker 256 mammary carcinoma model [107]. The pharmacokinetic behavior of the anthracycline could be significantly enhanced by polymer-linkage, demonstrating greater concentrations in the tumor compared to the free drug. They presumed the fenestrated capillaries of the Walker 256 carcinoma [108] to be responsible for the observed increased tumor uptake – facilitating a preferential "leakage" of the HPMA based copolymer in the tumor vascular bed. Further studies on this tumor model were accomplished using MR contrast agents of various molecular weights (0.57, 30 and 50 kDa) to closely examine the relation between tumor growth rate and vascular permeability [109]. In comparison to another tumor model (R3230 AC tumor), they found greater vascular permeability for the faster-growing Walker 256 carcinoma. This result was based on the observation that the macromolecular MRI agents entered the interstitial space of the Walker 256 tumor more rapidly and in higher concentrations than the slowly growing tumor. Besides the above mentioned examples, a variety of other macromolecule-drug conjugates have been explored regarding their antitumor effects in the Walker 256 model – including polysaccharides [110], methotrexate – albumin conjugates [111] or liposomes [112].

In conclusion, both tumor models - the AT1 Dunning prostate carcinoma R3327 and the Walker 256 carcinoma - are widely established in the field of polymer based therapeutics but nevertheless fundamental research concerning their tumor-dependent polymer uptake mechanisms is still remaining in the future.

1.11 References

1. Haag, R.; Kratz, F., Polymer Therapeutics: Concepts and Applications. *Angewandte Chemie International Edition* **2006,** 45, (8), 1198-1215.
2. Ehrlich, P., Die Behandlung der Syphilis mit dem Ehrlichschen Präparat 606. *Deutsche medizinische Wochenschrift* **1910**, 1893-1896.
3. de Duve, C.; Wattiaux, R., Functions of Lysosomes. *Annual Review of Physiology* **1966,** 28, (1), 435-492.
4. Duncan, R., The dawning era of polymer therapeutics. *Nat Rev Drug Discov* **2003,** 2, (5), 347-360.
5. Pasut, G.; Veronese, F. M., Polymer-drug conjugation, recent achievements and general strategies. *Progress in Polymer Science* **2007,** 32, (8-9), 933-961.
6. Pasut, G.; Veronese, F. M., PEG conjugates in clinical development or use as anticancer agents: An overview. *Advanced Drug Delivery Reviews* **2009,** 61, (13), 1177-1188.
7. Matsumura, Y.; Maeda, H., A New Concept for Macromolecular Therapeutics in Cancer Chemotherapy: Mechanism of Tumoritropic Accumulation of Proteins and the Antitumor Agent Smancs. *Cancer Research* **1986,** 46, (12 Part 1), 6387-6392.
8. Abuchowski, A.; van Es, T.; Palczuk, N. C.; Davis, F. F., Alteration of immunological properties of bovine serum albumin by covalent attachment of polyethylene glycol. *Journal of Biological Chemistry* **1977,** 252, (11), 3578-81.
9. Levy, Y.; Hershfield, M. S.; Fernandez-Mejia, C.; Polmar, S. H.; Scudiery, D.; Berger, M.; Sorensen, R. U., Adenosine deaminase deficiency with late onset of recurrent infections: Response to treatment with polyethylene glycol-modified adenosine deaminase. *The Journal of Pediatrics* **1988,** 113, (2), 312-317.
10. Graham, M. L., Pegaspargase: a review of clinical studies. *Advanced Drug Delivery Reviews* **2003,** 55, (10), 1293-1302.
11. Wang, Y.-S.; Youngster, S.; Grace, M.; Bausch, J.; Bordens, R.; Wyss, D. F., Structural and biological characterization of pegylated recombinant interferon alpha-2b and its therapeutic implications. *Advanced Drug Delivery Reviews* **2002,** 54, (4), 547-570.
12. Bailon, P.; Palleroni, A.; Schaffer, C. A.; Spence, C. L.; Fung, W.-J.; Porter, J. E.; Ehrlich, G. K.; Pan, W.; Xu, Z.-X.; Modi, M. W.; Farid, A.; Berthold, W.; Graves, M., Rational Design of a Potent, Long-Lasting Form of Interferon: A 40 kDa Branched Polyethylene Glycol-Conjugated Interferon alpha-2a for the Treatment of Hepatitis C. *Bioconjugate Chemistry* **2001,** 12, (2), 195-202.
13. Duncan, R., Development of HPMA copolymer-anticancer conjugates: Clinical experience and lessons learnt. *Advanced Drug Delivery Reviews* **2009,** 61, (13), 1131-1148.
14. Duncan, R.; Vicent, M. J., Do HPMA copolymer conjugates have a future as clinically useful nanomedicines? A critical overview of current status and future opportunities. *Advanced Drug Delivery Reviews* **2010,** 62, (2), 272-282.
15. Kopecek, J.; Bazilová, H., Poly[N-(2-hydroxypropyl)methacrylamide]--I. Radical polymerization and copolymerization. *European Polymer Journal* **1973,** 9, (1), 7-14.
16. Šprincl, L.; Exner, J.; Štěrba, O.; Kopeček, J., New types of synthetic infusion solutions. III. Elimination and retention of poly-[N-(2-hydroxypropyl)methacrylamide] in a test organism. *Journal of Biomedical Materials Research* **1976,** 10, (6), 953-963.
17. Vasey, P. A.; Kaye, S. B.; Morrison, R.; Twelves, C.; Wilson, P.; Duncan, R.; Thomson, A. H.; Murray, L. S.; Hilditch, T. E.; Murray, T.; Burtles, S.; Fraier, D.; Frigerio, E.; Cassidy, J., Phase I Clinical and Pharmacokinetic Study of PK1 [N-(2-Hydroxypropyl)methacrylamide Copolymer Doxorubicin]: First Member of a New Class of Chemotherapeutic Agents-Drug-Polymer Conjugates. *Clinical Cancer Research* **1999,** 5, (1), 83-94.
18. Duncan, R., Pratten, M.K., Cable, H.C., Ringsdorf, H. & Lloyd, J.B., Effect of molecular size of ^{125}I-labelled poly(vinylpyrrolidone) on its pinocytosis by rat visceral yolk sacs and rat peritoneal macrophages. *Biochem. J.* **1980,** 196, 49-55.
19. Seymour, L. W.; Duncan, R.; Strohalm, J.; Kopeček, J., Effect of molecular weight (Mw) of N-(2-hydroxypropyl)methacrylamide copolymers on body distribution and rate of excretion after subcutaneous, intraperitoneal, and intravenous administration to rats. *Journal of Biomedical Materials Research* **1987,** 21, (11), 1341-1358.
20. Seymour, L. W.; Miyamoto, Y.; Maeda, H.; Brereton, M.; Strohalm, J.; Ulbrich, K.; Duncan, R., Influence of molecular weight on passive tumour accumulation of a soluble macromolecular drug carrier. *European Journal of Cancer* **1995,** 31, (5), 766-770.

21. Thomson, A. H.; Vasey, P. A.; Murray, L. S.; Cassidy, J.; Fraier, D.; Frigerio, E.; Twelves, C., Population pharmacokinetics in phase I drug development: a phase I study of PK1 in patients with solid tumours. *Br J Cancer* **1999,** 81, (1), 99-107.
22. Duncan, R., Polymer conjugates as anticancer nanomedicines. *Nat Rev Cancer* **2006,** 6, (9), 688-701.
23. Julyan, P. J.; Seymour, L. W.; Ferry, D. R.; Daryani, S.; Boivin, C. M.; Doran, J.; David, M.; Anderson, D.; Christodoulou, C.; Young, A. M.; Hesslewood, S.; Kerr, D. J., Preliminary clinical study of the distribution of HPMA copolymers bearing doxorubicin and galactosamine. *Journal of Controlled Release* **1999,** 57, (3), 281-290.
24. Seymour, L. W.; Ferry, D. R.; Anderson, D.; Hesslewood, S.; Julyan, P. J.; Poyner, R.; Doran, J.; Young, A. M.; Burtles, S.; Kerr, D. J., Hepatic Drug Targeting: Phase I Evaluation of Polymer-Bound Doxorubicin. *Journal of Clinical Oncology* **2002,** 20, (6), 1668-1676.
25. Alexis, F.; Pridgen, E.; Molnar, L. K.; Farokhzad, O. C., Factors Affecting the Clearance and Biodistribution of Polymeric Nanoparticles. *Molecular Pharmaceutics* **2008,** 5, (4), 505-515.
26. Renkin, E. M.; Gilmore, J. P., Renal Physiology. *Handbook of Physiology (VIII)* **1973,** J. Orloff and R.W. Berliner (Eds.).
27. Rennke, H. G.; Venkatachalam, M. A., Glomerular permeability of macromolecules. Effect of molecular configuration on the fractional clearance of uncharged dextran and neutral horseradish peroxidase in the rat. *The Journal of Clinical Investigation* **1979,** 63, (4), 713-717.
28. Lammers, T.; Kühnlein, R.; Kissel, M.; Subr, V.; Etrych, T.; Pola, R.; Pechar, M.; Ulbrich, K.; Storm, G.; Huber, P.; Peschke, P., Effect of physicochemical modification on the biodistribution and tumor accumulation of HPMA copolymers. *Journal of Controlled Release* **2005,** 110, (1), 103-118.
29. Barreto, J. A.; O'Malley, W.; Kubeil, M.; Graham, B.; Stephan, H.; Spiccia, L., Nanomaterials: Applications in Cancer Imaging and Therapy. *Advanced Materials* 23, (12), H18-H40.
30. Davis, M. E.; Chen, Z.; Shin, D. M., Nanoparticle therapeutics: an emerging treatment modality for cancer. *Nat Rev Drug Discov* **2008,** 7, (9), 771-782.
31. Schoemaker, N. E.; van Kesteren, C.; Rosing, H.; Jansen, S.; Swart, M.; Lieverst, J.; Fraier, D.; Breda, M.; Pellizzoni, C.; Spinelli, R.; Porro, M. G.; Beijnen, J. H.; Schellens, J. H. M.; ten Bokkel Huinink, W. W., A phase I and pharmacokinetic study of MAG-CPT, a water-soluble polymer conjugate of camptothecin. *Br J Cancer* 87, (6), 608-614.
32. Meerum Terwogt, J. M.; ten Bokkel Huinink, W. W.; Schellens, J. H.; Schot, M.; Mandjes, I. A.; Zurlo, M. G.; Rocchetti, M.; Rosing, H.; Koopman, F. J.; Beijnen, J. H., Phase I clinical and pharmacokinetic study of PNU166945, a novel water-soluble polymer-conjugated prodrug of paclitaxel. *Anti-Cancer Drugs* **2001,** 12, (4), 315-323.
33. Rademaker-Lakhai, J. M.; Terret, C.; Howell, S. B.; Baud, C. M.; de Boer, R. F.; Pluim, D.; Beijnen, J. H.; Schellens, J. H. M.; Droz, J.-P., A Phase I and Pharmacological Study of the Platinum Polymer AP5280 Given as an Intravenous Infusion Once Every 3 Weeks in Patients with Solid Tumors. *Clinical Cancer Research* **2004,** 10, (10), 3386-3395.
34. Maeda, H.; Bharate, G. Y.; Daruwalla, J., Polymeric drugs for efficient tumor-targeted drug delivery based on EPR-effect. *European Journal of Pharmaceutics and Biopharmaceutics* **2009,** 71, (3), 409-419.
35. Fang, J.; Nakamura, H.; Maeda, H., The EPR effect: Unique features of tumor blood vessels for drug delivery, factors involved, and limitations and augmentation of the effect. *Advanced Drug Delivery Reviews* **2011,** 63, (3), 136-151.
36. Matyjaszewski, K.; Xia, J., Atom Transfer Radical Polymerization. *Chemical Reviews* **2001,** 101, (9), 2921-2990.
37. Chiefari, J.; Chong, Y. K.; Ercole, F.; Krstina, J.; Jeffery, J.; Le, T. P. T.; Mayadunne, R. T. A.; Meijs, G. F.; Moad, C. L.; Moad, G.; Rizzardo, E.; Thang, S. H., Living Free-Radical Polymerization by Reversible Addition-Fragmentation Chain Transfer: The RAFT Process. *Macromolecules* **1998,** 31, (16), 5559-5562.
38. Moad, G. R., E.; Thang, S.H., Living Radical Polymerization by the RAFT process. *Aust. J. Chem.* **2005,** 58, (6), 379-410.
39. Boyer, C.; Bulmus, V.; Davis, T. P.; Ladmiral, V.; Liu, J.; Perrier, S. b., Bioapplications of RAFT Polymerization. *Chemical Reviews* **2009,** 109, (11), 5402-5436.
40. Pissuwan, D.; Boyer, C.; Gunasekaran, K.; Davis, T. P.; Bulmus, V., In Vitro Cytotoxicity of RAFT Polymers. *Biomacromolecules* **2010,** 11, (2), 412-420.
41. Moad, G.; Rizzardo, E.; Thang, S. H., Living Radical Polymerization by the RAFT Process- A Second Update. *Australian Journal of Chemistry* **2009,** 62, (11), 1402-1472.

42. Eberhardt, M.; Théato, P., RAFT Polymerization of Pentafluorophenyl Methacrylate: Preparation of Reactive Linear Diblock Copolymers. *Macromolecular Rapid Communications* **2005,** 26, (18), 1488-1493.
43. Batz, H.-G.; Franzmann, G.; Ringsdorf, H., Model Reactions for Synthesis of Pharmacologically Active Polymers by Way of Monomeric and Polymeric Reactive Esters. *Angewandte Chemie International Edition in English* **1972,** 11, (12), 1103-1104.
44. Ferruti, P.; Bettelli, A.; Feré, A., High polymers of acrylic and methacrylic esters of N-hydroxysuccinimide as polyacrylamide and polymethacrylamide precursors. *Polymer* **1972,** 13, (10), 462-464.
45. Eberhardt, M.; Mruk, R.; Zentel, R.; Théato, P., Synthesis of pentafluorophenyl(meth)acrylate polymers: New precursor polymers for the synthesis of multifunctional materials. *European Polymer Journal* **2005,** 41, (7), 1569-1575.
46. Gauthier, M. A.; Gibson, M. I.; Klok, H.-A., Synthesis of Functional Polymers by Post-Polymerization Modification. *Angewandte Chemie International Edition* **2009,** 48, (1), 48-58.
47. Kataoka, K.; Harada, A.; Nagasaki, Y., Block copolymer micelles for drug delivery: design, characterization and biological significance. *Advanced Drug Delivery Reviews* **2001,** 47, (1), 113-131.
48. Lavasanifar, A.; Samuel, J.; Kwon, G. S., Poly(ethylene oxide)-block-poly(l-amino acid) micelles for drug delivery. *Advanced Drug Delivery Reviews* **2002,** 54, (2), 169-190.
49. Gaucher, G.; Dufresne, M.-H.; Sant, V. P.; Kang, N.; Maysinger, D.; Leroux, J.-C., Block copolymer micelles: preparation, characterization and application in drug delivery. *Journal of Controlled Release* **2005,** 109, (1-3), 169-188.
50. Talelli, M.; Rijcken, C. J. F.; van Nostrum, C. F.; Storm, G.; Hennink, W. E., Micelles based on HPMA copolymers. *Advanced Drug Delivery Reviews* **2010,** 62, (2), 231-239.
51. M.H. Dufresne, E. F., M.-C. Jones, M. Ranger, J.C. Leroux, Block copolymer micelles-engineering versatile carriers for drugs and biomacromolecules. *R. Gurny (Ed.)* **2003,** 96, 87-102.
52. Joralemon, M. J.; McRae, S.; Emrick, T., PEGylated polymers for medicine: from conjugation to self-assembled systems. *Chemical Communications* **2010,** 46, (9), 1377-1393.
53. Gref, R.; Domb, A.; Quellec, P.; Blunk, T.; Müller, R. H.; Verbavatz, J. M.; Langer, R., The controlled intravenous delivery of drugs using PEG-coated sterically stabilized nanospheres. *Advanced Drug Delivery Reviews* **1995,** 16, (2-3), 215-233.
54. Nakanishi, T.; Fukushima, S.; Okamoto, K.; Suzuki, M.; Matsumura, Y.; Yokoyama, M.; Okano, T.; Sakurai, Y.; Kataoka, K., Development of the polymer micelle carrier system for doxorubicin. *Journal of Controlled Release* **2001,** 74, (1-3), 295-302.
55. Nishiyama, N.; Okazaki, S.; Cabral, H.; Miyamoto, M.; Kato, Y.; Sugiyama, Y.; Nishio, K.; Matsumura, Y.; Kataoka, K., Novel Cisplatin-Incorporated Polymeric Micelles Can Eradicate Solid Tumors in Mice. *Cancer Research* **2003,** 63, (24), 8977-8983.
56. Kabanov, A. V.; Batrakova, E. V.; Alakhov, V. Y., Pluronic® block copolymers as novel polymer therapeutics for drug and gene delivery. *Journal of Controlled Release* **2002,** 82, (2-3), 189-212.
57. Kabanov, A. V.; Lemieux, P.; Vinogradov, S.; Alakhov, V., Pluronic® block copolymers: novel functional molecules for gene therapy. *Advanced Drug Delivery Reviews* **2002,** 54, (2), 223-233.
58. Savic, R.; Luo, L.; Eisenberg, A.; Maysinger, D., Micellar Nanocontainers Distribute to Defined Cytoplasmic Organelles. *Science* **2003,** 300, (5619), 615-618.
59. Liggins, R. T.; Burt, H. M., Polyether-polyester diblock copolymers for the preparation of paclitaxel loaded polymeric micelle formulations. *Advanced Drug Delivery Reviews* **2002,** 54, (2), 191-202.
60. Gref, R.; Minamitake, Y.; Peracchia, M.; Trubetskoy, V.; Torchilin, V.; Langer, R., Biodegradable long-circulating polymeric nanospheres. *Science* **1994,** 263, (5153), 1600-1603.
61. Ishida, T.; Kiwada, H., Accelerated blood clearance (ABC) phenomenon upon repeated injection of PEGylated liposomes. *International Journal of Pharmaceutics* **2008,** 354, (1-2), 56-62.
62. Carstens, M. G.; Romberg, B.; Laverman, P.; Boerman, O. C.; Oussoren, C.; Storm, G., Observations on the disappearance of the stealth property of PEGylated liposomes, effects of lipid dose and dosing frequency. *Liposome Technology* **2006,** 3rd ed, 79-93.
63. Ishida, T.; Wang, X.; Shimizu, T.; Nawata, K.; Kiwada, H., PEGylated liposomes elicit an anti-PEG IgM response in a T cell-independent manner. *Journal of Controlled Release* **2007,** 122, (3), 349-355.
64. Konak, C.; Ganchev, B.; Teodorescu, M.; Matyjaszewski, K.; Kopeckova, P.; Kopecek, J., Poly[N-(2-hydroxypropyl)methacrylamide-block-n-butyl acrylate] micelles in water/DMF mixed solvents. *Polymer* **2002,** 43, (13), 3735-3741.

65. Barz, M.; Tarantola, M.; Fischer, K.; Schmidt, M.; Luxenhofer, R.; Janshoff, A.; Theato, P.; Zentel, R., From Defined Reactive Diblock Copolymers to Functional HPMA-Based Self-Assembled Nanoaggregates. *Biomacromolecules* **2008,** 9, (11), 3114-3118.
66. Konak, C.; Mrkvickova, L.; Nazarova, O.; Ulbrich, K.; Seymour, L. W., Formation of DNA complexes with diblock copolymers of poly(N-(2-hydroxypropyl) methacrylamide) and polycations. *Supramolecular Science* **1998,** 5, (1-2), 67-74.
67. Oupický, D.; Konak, C.; Ulbrich, K., Preparation of DNA complexes with diblock copolymers of poly[N(2-hydroxypropyl)methacrylamide] and polycations. *Materials Science and Engineering: C* **1999,** 7, (1), 59-65.
68. Lele, B. S.; Leroux, J. C., Synthesis and Micellar Characterization of Novel Amphiphilic A-B-A Triblock Copolymers of N-(2-Hydroxypropyl)methacrylamide or N-Vinyl-2-pyrrolidone with Poly(e-caprolactone). *Macromolecules* **2002,** 35, (17), 6714-6723.
69. Kang, N.; Leroux, J.-C., Triblock and star-block copolymers of N-(2-hydroxypropyl)methacrylamide or N-vinyl-2-pyrrolidone and d,l-lactide: synthesis and self-assembling properties in water. *Polymer* **2004,** 45, (26), 8967-8980.
70. Hong, C.-Y.; Pan, C.-Y., Direct Synthesis of Biotinylated Stimuli-Responsive Polymer and Diblock Copolymer by RAFT Polymerization Using Biotinylated Trithiocarbonate as RAFT Agent. *Macromolecules* **2006,** 39, (10), 3517-3524.
71. Ringsdorf, H., Structure and properties of pharmacologically active polymers. *Journal of Polymer Science: Polymer Symposia* **1975,** 51, (1), 135-153.
72. Kopecek, J., Soluble biomedical polymers. *Polim. Med.* **1977,** 7, 191-221.
73. Lammers, T., Improving the efficacy of combined modality anticancer therapy using HPMA copolymer-based nanomedicine formulations. *Advanced Drug Delivery Reviews* **2010,** 62, (2), 203-230.
74. Torchilin, V. P., Recent advances with liposomes as pharmaceutical carriers. *Nat Rev Drug Discov* **2005,** 4, (2), 145-160.
75. Choi, W.-M.; Kopeckova, P.; Minko, T.; Kopecek, J., Synthesis of HPMA Copolymer Containing Adriamycin Bound via an Acid-Labile Spacer and its Activity toward Human Ovarian Carcinoma Cells. *Journal of Bioactive and Compatible Polymers* **1999,** 14, (6), 447-456.
76. Etrych, T.; Chytil, P.; Jelínková, M.; Říhová, B.; Ulbrich, K., Synthesis of HPMA Copolymers Containing Doxorubicin Bound via a Hydrazone Linkage. Effect of Spacer on Drug Release and in vitro Cytotoxicity. *Macromolecular Bioscience* **2002,** 2, (1), 43-52.
77. Rejmanová, P.; Kopeček, J.; Pohl, J.; Baudyš, M.; Kostka, V., Polymers containing enzymatically degradable bonds, 8. Degradation of oligopeptide sequences in N-(2-hydroxypropyl)methacrylamide copolymers by bovine spleen cathepsin B. *Die Makromolekulare Chemie* **1983,** 184, (10), 2009-2020.
78. Kopecek, J.; Kopecková, P.; Minko, T.; Lu, Z.-R., HPMA copolymer-anticancer drug conjugates: design, activity, and mechanism of action. *European Journal of Pharmaceutics and Biopharmaceutics* **2000,** 50, (1), 61-81.
79. Kopecek, J., Controlled biodegradability of polymers- a key to drug delivery systems. *Biomaterials* **1984,** 5, (1), 19-25.
80. Kopeček, J.; Rejmanová, P.; Chytrý, V., Polymers containing enzymatically degradable bonds, 1. Chymotrypsin catalyzed hydrolysis of p-nitroanilides of phenylalanine and tyrosine attached to side-chains of copolymers of N-(2-hydroxypropyl)methacrylamide. *Die Makromolekulare Chemie* **1981,** 182, (3), 799-809.
81. Rejmanova, P.; Kopecek, J.; Duncan, R.; Lloyd, J. B., Stability in rat plasma and serum of lysosomally degradable oligopeptide sequences in N-(2-hydroxypropyl) methacrylamide copolymers. *Biomaterials* **1985,** 6, (1), 45-48.
82. Kopecek, J.; Rejmanova, P.; Strohalm, J.; Ulbrich, K.; Rihova, B.; Chytrý, V.; Lloyd, J. B.; Duncan, R., Synthetic polymeric drugs. *US Patent* **1991,** 5,037,883.
83. L. W. Seymour, D. R. F., D. J. Kerr, D. Rea, M. Whitlock, R. Poyner, C. Boivin, S. Hesslewood, C. Twelves, R. Blackie, A. Schatzlein, D. Jodrell, D. Bissett, H. Calvert, M. Lind, A. Robbins, S. Burtles, R. Duncan, J. Cassidy, Phase II studies of polymer-doxorubicin (PK1, FCE28068) in the treatment of breast, lung and colorectal cancer. *Int. J. Oncol.* **2009,** 34, 1629-1636.
84. Nowotnik, D. P.; Cvitkovic, E., ProLindac(TM) (AP5346): A review of the development of an HPMA DACH platinum Polymer Therapeutic. *Advanced Drug Delivery Reviews* **2009,** 61, (13), 1214-1219.
85. Lammers, T.; Subr, V.; Ulbrich, K.; Hennink, W. E.; Storm, G.; Kiessling, F., Polymeric nanomedicines for image-guided drug delivery and tumor-targeted combination therapy. *Nano Today* **2010,** 5, (3), 197-212.

86. Lammers, T.; Subr, V.; Peschke, P.; Kuhnlein, R.; Hennink, W. E.; Ulbrich, K.; Kiessling, F.; Heilmann, M.; Debus, J.; Huber, P. E.; Storm, G., Image-guided and passively tumour-targeted polymeric nanomedicines for radiochemotherapy. *Br J Cancer* **2008,** 99, (6), 900-910.
87. Ollinger, J. M.; Fessler, J. A., Positron Emission Tomography. *IEEE Signal Processing Magazine* **1997,** 14, (1), 43-55.
88. Khalil, M. M.; Tremoleda, J. L.; Bayomy, T. B.; Gsell, W., Molecular SPECT Imaging: An Overview. *International journal of molecular imaging* **2011,** 2011, 796025.
89. Herzog, H.; Rösch, F., PET- und SPECT-Technik: Chemie und Physik der Bildgebung. *Pharmazie in unserer Zeit* **2005,** 34, (6), 468-473.
90. Alauddin, M. M., Positron emission tomography (PET) imaging with 18F-based radiotracers. *Am J Nucl Med Mol Imaging* **2012,** 2, (1), 55-76.
91. Garnett, E. S.; Firnau, G.; Nahmias, C., Dopamine visualized in the basal ganglia of living man. *Nature* **1983,** 305, (5930), 137-138.
92. Pressly, E. D.; Rossin, R.; Hagooly, A.; Fukukawa, K.-i.; Messmore, B. W.; Welch, M. J.; Wooley, K. L.; Lamm, M. S.; Hule, R. A.; Pochan, D. J.; Hawker, C. J., Structural Effects on the Biodistribution and Positron Emission Tomography (PET) Imaging of Well-Defined 64Cu-Labeled Nanoparticles Comprised of Amphiphilic Block Graft Copolymers. *Biomacromolecules* **2007,** 8, (10), 3126-3134.
93. Devaraj, N. K.; Keliher, E. J.; Thurber, G. M.; Nahrendorf, M.; Weissleder, R., 18F Labeled Nanoparticles for in Vivo PET-CT Imaging. *Bioconjugate Chemistry* **2009,** 20, (2), 397-401.
94. Peer, D.; Karp, J. M.; Hong, S.; Farokhzad, O. C.; Margalit, R.; Langer, R., Nanocarriers as an emerging platform for cancer therapy. *Nat Nano* **2007,** 2, (12), 751-760.
95. Lubaroff, D. M.; Canfield, L.; Reynolds, C. W., The Dunning tumors. *Progress in clinical and biological research* **1980,** 37, 243-63.
96. Cooke, D. B.; Quarmby, V. E.; Mickey, D. D.; Isaacs, J. T.; French, F. S., Oncogene expression in prostate cancer: Dunning R3327 rat dorsal prostatic adenocarcinoma system. *The Prostate* **1988,** 13, (4), 263-272.
97. Huber, P.; Peschke, P.; Brix, G.; Hahn, E. W.; Lorenz, A.; Tiefenbacher, U.; Wannenmacher, M.; Debus, J., Synergistic interaction of ultrasonic shock waves and hyperthermia in the dunning prostate tumor r3327-at1. *International Journal of Cancer* **1999,** 82, (1), 84-91.
98. Häggström, S.; Bergh, A.; Damber, J.-E., Vascular endothelial growth factor content in metastasizing and nonmetastasizing dunning prostatic adenocarcinoma. *The Prostate* **2000,** 45, (1), 42-50.
99. Hunjan, S.; Zhao, D.; Constantinescu, A.; Hahn, E. W.; Antich, P. P.; Mason, R. P., Tumor oximetry: demonstration of an enhanced dynamic mapping procedure using fluorine-19 echo planar magnetic resonance imaging in the Dunning prostate R3327-AT1 rat tumor. *International Journal of Radiation Oncology*Biology*Physics* **2001,** 49, (4), 1097-1108.
100. Zhao, D.; Ran, S.; Constantinescu, A.; Hahn, E. W.; Mason, R. P., Tumor Oxygen Dynamics: Correlation of In Vivo MRI with Histological Findings. *Neoplasia* **2003,** 5, (4), 308-318.
101. Heckl, S.; Pipkorn, R. d.; Waldeck, W.; Spring, H.; Jenne, J. r.; von der Lieth, C.-W.; Corban-Wilhelm, H.; Debus, J. r.; Braun, K., Intracellular Visualization of Prostate Cancer Using Magnetic Resonance Imaging. *Cancer Research* **2003,** 63, (16), 4766-4772.
102. Cho, H. J.; Ackerstaff, E.; Carlin, S.; Lupu, M. E.; Wang, Y.; Rizwan, A.; O'Donoghue, J.; Ling, C. C.; Humm, J. L.; Zanzonico, P. B.; A., K. J., Noninvasive Multimodality Imaging of the Tumor Microenvironment : Registered Dynamic Magnetic Resonance Imaging and Positron Emission Tomography Studies of a Preclinical Tumor Model of Tumor Hypoxia. *Neoplasia* **2009,** 11, (3), 247-259.
103. Heuser, L. S.; Miller, F. N., Differential macromolecular leakage from the vasculature of tumors. *Cancer* **1986,** 57, (3), 461-464.
104. Yuan, F.; Dellian, M.; Fukumura, D.; Leunig, M.; Berk, D. A.; Torchilin, V. P.; Jain, R. K., Vascular Permeability in a Human Tumor Xenograft: Molecular Size Dependence and Cutoff Size. *Cancer Research* **1995,** 55, (17), 3752-3756.
105. Kissel, M.; Peschke, P.; Subr, V.; Ulbrich, K.; Strunz, A.; Kühnlein, R.; Debus, J.; Friedrich, E., Detection and cellular localisation of the synthetic soluble macromolecular drug carrier pHPMA. *European Journal of Nuclear Medicine and Molecular Imaging* **2002,** 29, (8), 1055-1062.
106. Lammers, T.; Peschke, P.; Kühnlein, R.; Subr, V.; Ulbrich, K.; Debus, J.; Huber, P.; Hennink, W.; Storm, G., Effect of radiotherapy and hyperthermia on the tumor accumulation of HPMA copolymer-based drug delivery systems. *Journal of Controlled Release* **2007,** 117, (3), 333-341.

107. Cassidy, J.; Duncan, R.; Morrison, G. J.; Strohalm, J.; Plocova, D.; Kopecek, J.; Kaye, S. B., Activity of N-(2-hydroxypropyl)methacrylamide copolymers containing daunomycin against a rat tumour model. *Biochem Pharmacol.* **1989,** 38, (6), 875-879.
108. Warren, B. A., The ultrastructure of the microcirculation at the advancing edge of Walker 256 carcinoma. *Microvascular Research* **1970,** 2, (4), 443-453.
109. Su, M.-Y.; Mühler, A.; Lao, X.; Nalcioglu, O., Tumor characterization with dynamic contrast–enhanced MRI using mr contrast agents of various molecular weights. *Magnetic Resonance in Medicine* **1998,** 39, (2), 259-269.
110. S. Sugahara, S. O., T. Yano, H. Hamana and K. Inoue, Characteristics of Tissue Distribution of Various Polysaccharides as Drug Carriers: Influences of Molecular Weight and Anionic Charge on Tumor Targeting. *Biol. Pharm. Bull.* **2001,** 24, (5), 535-543
111. Wunder, A.; Stehle, G.; Schrenk, H. H.; Hartung, G.; Heene, D. L.; Maier-Borst, W.; Sinn, H., Antitumor activity of methotrexate-albumin conjugates in rats bearing a Walker-256 carcinoma. *International Journal of Cancer* **1998,** 76, (6), 884-890.
112. Takeuchi, H.; Kojima, H.; Yamamoto, H.; Kawashima, Y., Passive Targeting of Doxorubicin with Polymer Coated Liposomes in Tumor Bearing Rats. *Biological & Pharmaceutical Bulletin* **2001,** 24, (7), 795-799.

2. Aims and Objectives

The scope of this dissertation was highly influenced by the idea of Paul Ehrlichs' magic bullet as well as the concept of Helmut Ringsdorf and Ruth Duncan to create polymer based therapeutics. Both approaches involve the interaction between different research areas and thus open the field to interdisciplinary projects profiting from diverse expertise.

With special emphasis on macromolecular based drug delivery vehicles, each variation in polymer structure is aiming for an alteration in body distribution. In this respect, it is fundamental to determine the appearing changes and furthermore to gain deepening knowledge about structure-property relationships *in vivo*.

Considering the aforementioned challenges, well-defined and narrowly distributed polymer systems are major requirements for the successful realization. Besides – with special focus on structure-property relationships – it is essential to modify characteristic features of the macromolecule in order to investigate the impact on the consequential pharmacokinetic profile. In this regard, we altered parameters such as polymer architecture (homopolymers, random as well as block copolymers) and molecular weight which resulted in different polymer sizes and superstructure formation. Furthermore, we varied the hydrophilic / lipophilic balance as well as the hydrophilic group, thereby changing the surface properties of the respective polymer system.

The modified polymer structures were then combined with radioactive labeling and Positron Emission Tomography (PET), constituting suitable diagnostic tools for the quantification of pharmacokinetics and biodistribution of the herein presented systems at an early stage. Deepening knowledge about the correlation of polymer-dependent characteristics and their influence on the *in vivo* fate can be obtained, hence efficiently determining the suitability of particular polymer structures in the field of polymer based (chemo) therapy.

To conclude, one focus of the present work was laid on the controlled synthesis of the aforementioned polymer architectures. Radioactive labeling was accomplished by Dorothea Moderegger from the Institute of Nuclear Chemistry and following *in vivo* evaluation of the polymeric compounds was carried out in collaboration.

It was aimed to gain further insights regarding the effect of structural modifications of the investigated polymers (particularly in terms of molecular weight, amphiphilicity, size and surface properties) on organ distribution as well as tumor accumulation in the living organism.

3. Results and Discussion

In the following, a general overview about the different research approaches – including the variation in polymer architecture, radioactive labeling procedures as well as animal models – is given. The herein presented research work can be divided into five different chapters as schematically depicted in Figure 1.

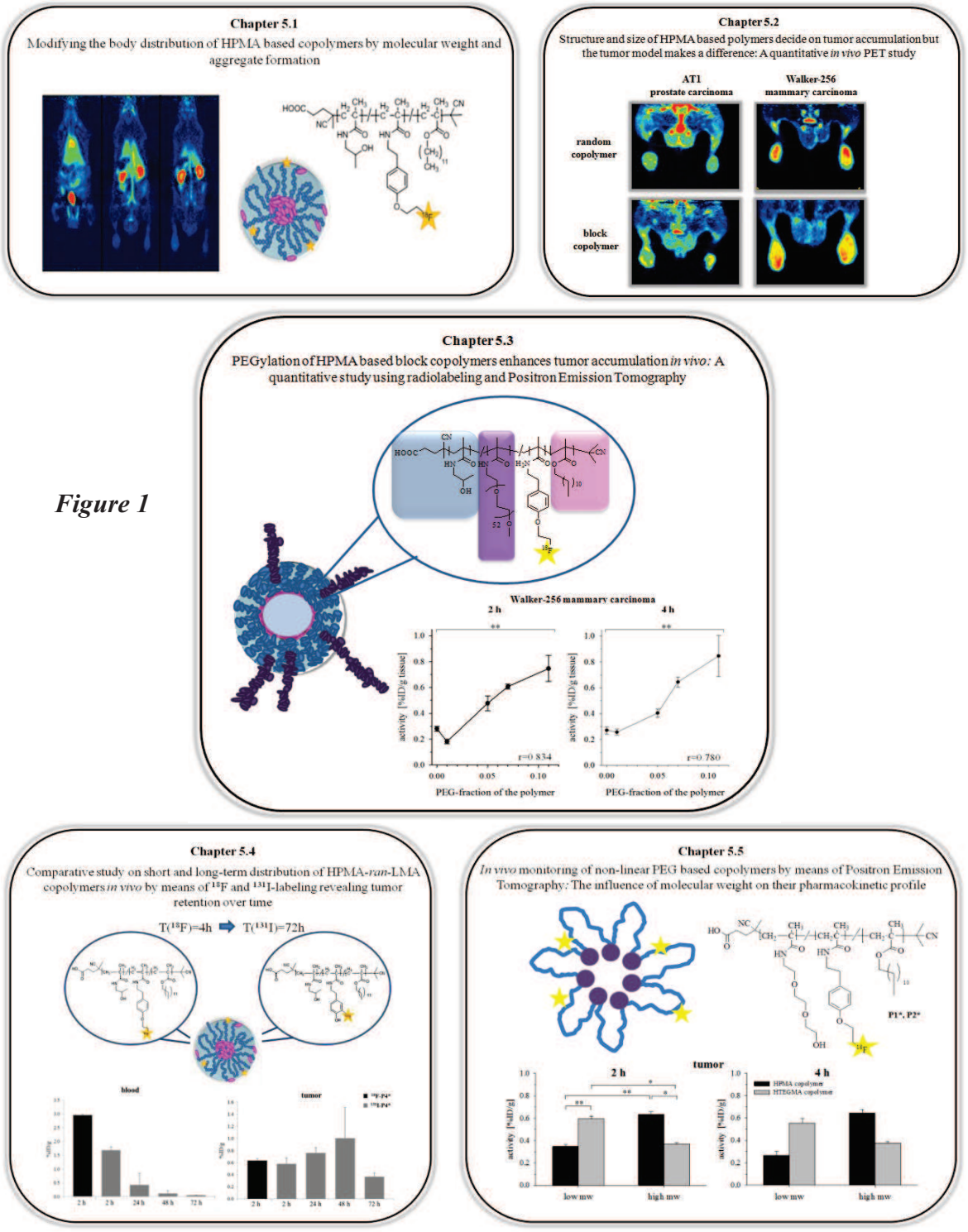

Figure 1

Previous studies in our group revealed the successful radioactive labeling of HPMA based polymer systems by means of positron emitting isotopes such as F-18 or As-72/74 [1, 2]. Based on these promising results, the motivation of the present work was concentrating on a systematic *in vivo* evaluation of different HPMA and PEG based polymer structures by means of Positron Emission Tomography as well as *ex vivo* biodistribution studies.

In this regard, first we created a library of different HPMA based polymer architectures (homopolymers, random as well as block copolymers) with lauryl methacrylate as hydrophobic group and varied their molecular weights below and above the renal threshold (see chapter 5.1 and 5.2). The diversity of polymer structures could be accomplished by the combination of the controlled radical polymerization technique RAFT as well as reactive ester chemistry. Well-defined and narrowly distributed reactive ester precursor polymers were created – due to their overall hydrophobic nature – facilitating a precise characterization via gel permeation chromatography as well as ^{1}H-NMR spectroscopy. Conversion to HPMA based polymer systems was accomplished by means of polymeranalogous reaction; furthermore enabling the introduction of imaging moieties such as fluorescent dyes or radioactive probes. An overall reaction scheme is depicted in Fig. 2, analytical data of the investigated compounds can be found in table 1.

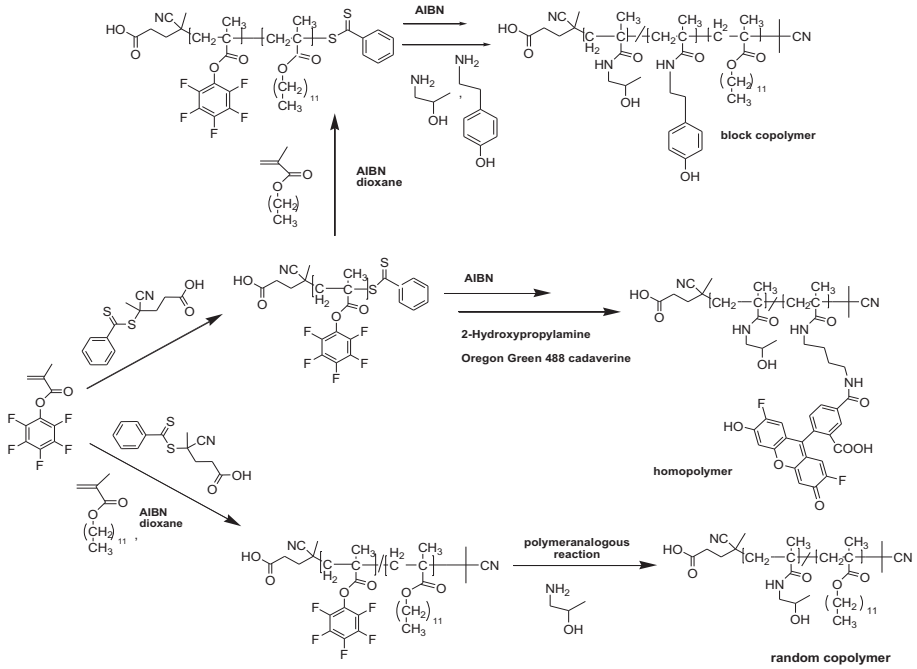

***Figure 2**: Synthetic route of reactive ester precursor systems as well as their polymeranalogous reaction to final HPMA based polymer structures*

Table 1**: Analytical data of reactive ester homopolymers (**P1*-R** and **P2*-R**), random copolymers (**P3*-R** and **P4*-R**) and block copolymers (**P5*-R** and **P6*-R**) as well as the final polymers **P1*-P6

Nomen-clature	Polymeric structure	Monomer ratio	M_n in g/mol	M_w in g/mol	PDI[2]	R_h[5] in nm
P1*-R	Homopolymer	100%[1]	18000[2]	23000[2]	1.29	n.d.
P2*-R	Homopolymer	100%[1]	87000[2]	130000[2]	1.49	n.d.
P3*-R	Random copolymer	80:20%[1]	17000[2]	21000[2]	1.26	n.d.
P4*-R	Random copolymer	80:20%[1]	57000[2]	80000[2]	1.41	n.d.
P5*-R	Block copolymer	60:40%[1]	14000[2]	18000[2]	1.26	n.d.
P6*-R	Block copolymer	60:40%[1]	25000[2]	31000[2]	1.25	n.d.
P1*	Homopolymer	100%[3]	9000[4]	12000[4]	1.29	1.1
P2*	Homopolymer	100%[3]	52000[4]	77000[4]	1.49	3.0
P3*	Random copolymer	82:18[3]	11000[4]	14000[4]	1.26	33.4
P4*	Random copolymer	75:25[3]	39000[4]	55000[4]	1.41	39.9
P5*	Block copolymer	79:21[3]	9000[4]	12000[4]	1.24	58.7
P6*	Block copolymer	75:25[3]	17000[4]	21000[4]	1.24	112.8

*[1] = Calculated monomer ratio; [2] = Determination by GPC in THF as solvent; [3] = Monomer ratio determined by ^{1}H-NMR spectroscopy after polymeranalogous reaction with 2-hydroxypropylamine; [4] = Calculated from the molecular weights of the reactive ester polymers **P1*-R to P6*-R** as determined by GPC in THF as solvent; [5] = Hydrodynamic radii determined by Fluorescence Correlation spectroscopy (FCS)*

As clearly seen from table 1, the hydrophobically modified polymers form aggregates in aqueous solution (e.g. buffer) and thus polymer size can be varied between some nm (size of individual hydrophilic polymer coil depending on the molecular weight) and up to 100 nm in radius for block copolymers. Due to these polymer-dependent characteristics, different pharmacokinetic profiles in terms of organ distribution, tumor accumulation, circulation time as well as excretion properties were expected. To study the behavior of the varying polymeric architectures *in vivo*, the positron emitter fluorine-18 ($t_{1/2}$ = 110 min) was incorporated via a prosthetic labeling procedure using [^{18}F]FETos. Organ / tumor uptake was followed by *ex vivo* biodistribution and *in vivo* μPET imaging in two different tumor models – the AT1 Dunning prostate and the Walker 256 mammary carcinoma. Vascular permeability was measured by dextran extravasation and *in vitro* cellular studies accomplished using Oregon Green 488 labeled polymers.

In direct comparison between the aforementioned polymer architectures (see table 1), some major differences in body distribution could be seen. In general, the low molecular weight polymer systems (**P1***, **P3*** and **P5***) were predominantly found in the kidney whereas the high molecular weight analogs (**P2***, **P4*** and **P6***) were found to a greater

extent in liver and spleen (see section 5.1 and 5.2). Furthermore, studies revealed that the HPMA-*ran*-LMA copolymers **P3*** and **P4*** stayed much longer in the blood compartment, probably attributed to an appropriate polymer size (< 100 nm in diameter) and an adequate balance of hydrophilicity / lipophilicity. The last-mentioned was assumedly also responsible for the low liver accumulation of the high molecular weight random copolymer **P4*** (lauryl methacrylate content = 25 %). The observed trends for the varying HPMA based polymer architectures are illustrated in Fig. 3.

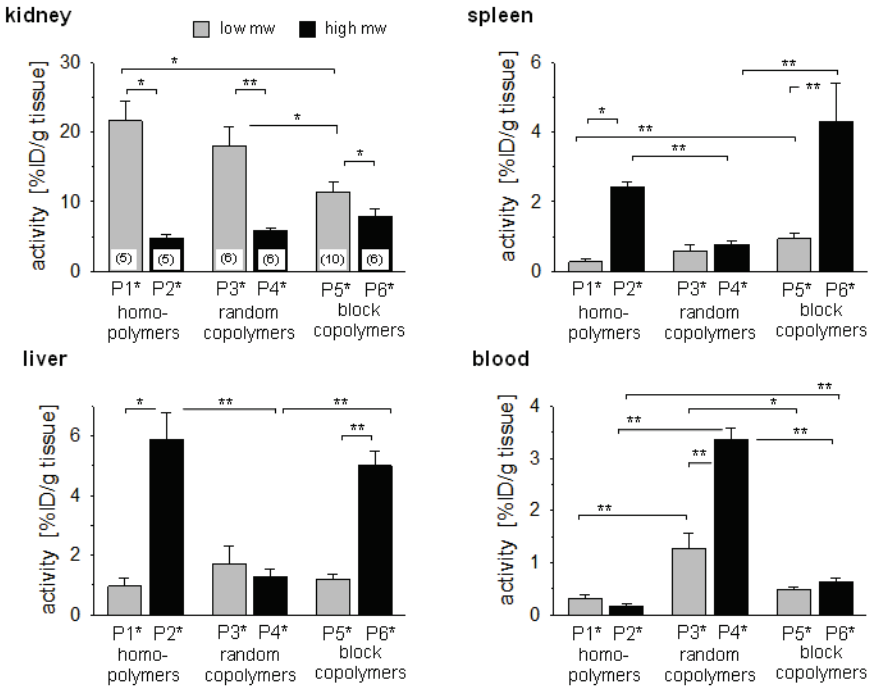

***Figure 3**: Quantification of the polymer uptake in different tissues. Uptake is expressed by the fraction of the injected dose (ID) of the polymer per gram tissue 2 h after i.v. injection. n= 5-10, (*) p<0.05, (**) p<0.01*

With special focus on polymer based anticancer treatment, body distribution of the macromolecular (chemo) therapeutic may not only be affected by specific characteristics of the polymer system (e.g. molecular weight, architecture, lipophilicity or superstructure formation) but also biological and physiological properties of the specific tumor can hold an important effect. In this regard, the differing polymer systems were investigated concerning their tumor targeting ability in dependency of the specific tumor model in the living organism (see section 5.2). Notably, the analysis of the varying polymer architectures in the two carcinoma lines of the rat showed pronounced disparities in tumor

accumulation, depending on the respective tumor line. Regarding the AT1 Dunning prostate carcinoma, all polymers were accumulating equally to a very low extent. In contrast, Walker 256 tumors displayed an approximately 5-fold higher tumor uptake for the HPMA based random copolymer structures (see Fig. 4). Since both tumor lines demonstrated comparable sites of tumor growth, proliferation rates as well as histological and vascular properties, other tumor specific characteristics have to be taken into account concerning the disparities in polymer accumulation.

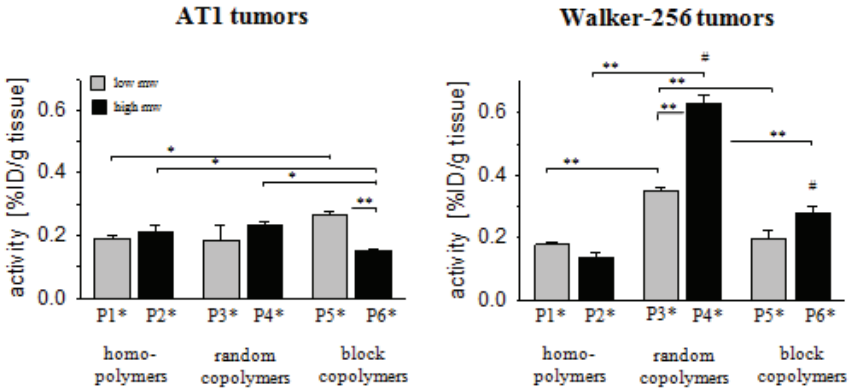

Figure 4: *Tumor uptake of the varying polymer architectures (homopolymers **P1*** and **P2***, random copolymers **P3*** and **P4*** as well as block copolymers **P5*** and **P6***) in AT1 prostate and Walker 256 mammary carcinomas determined by biodistribution measurements 2 hours p.i.. n=5-6; (*) p <0.05, (**) p<0.01; (#) p<0.01 Walker 256 vs. AT1 tumors.*

Cellular uptake studies clearly revealed that polymer uptake was also markedly varying between the two cell lines *in vitro* and thus polymer-cell specific interactions have to play a major role, too. In conclusion it can be summarized that the variation of polymer architectures (with special focus on amphiphilicity) and size of HPMA based polymers had a tremendous influence on a prolonged presence in blood circulation as well as on the tumor accumulation *in vivo*. Furthermore, it could be demonstrated that the efficacy of polymer based drug vehicles regarding anticancer treatment is strongly affected by each individual tumor. Thus a precise polymer characterization combined with its pre-clinical screening is essential to design polymer therapeutics in terms of individual patient therapy. This approach can be realized by means of radiolabeling and monitoring of the pharmacokinetic profile of polymeric nanocarriers by means of PET.

Based on the findings of the high molecular weight HPMA-*ran*-LMA copolymer **P4*** showing favorable *in vivo* characteristics (prolonged blood circulation times combined

with highest tumor accumulation as well as minor hepatic and spleenic elimination) the question was arising whether the observed pharmacokinetic profile was attributed to the high incorporation ratio of lauryl methacrylate (25 %) as hydrophobic group. Thus comparative studies with lower amounts of hydrophobic moiety – HPMA-*ran*-LMA copolymers with 16 % and 20 % LMA content respectively – were accomplished. Biodistribution studies revealed that all random copolymer structures possessed prolonged blood circulation times, lower hepatic and spleenic uptake as well as higher tumor accumulation (Walker 256 carcinoma) compared to the HPMA homopolymer **P2***. Nevertheless - among the investigated polymer structures - **P4*** (25 % LMA) was the one exhibiting the most favorable pharmacokinetic profile regarding the therapeutic application. It can be assumed that the hydrophilic / lipophilic balance has a major influence on the recognition of the investigated nanoparticles by the MPS and thus the incorporation ratio of 25 % hydrophobic groups seems to be a reasonable approach for HPMA based polymer therapeutics. The protection toward opsonization is also leading to prolonged blood circulation times of the random copolymer **P4*** - fundamental for the well-known EPR-effect.

In direct correlation to the aforementioned investigated random copolymer structures, it has to be noted that their dynamic nature can also be an obstacle regarding an efficient and particularly controlled drug release in the field of polymer based (chemo) therapy. Thus amphiphilic block copolymers illustrate more defined structures and due to their core-shell morphology, the hydrophobic inner core enables the storage of pharmacologically active drugs. Furthermore – attributed to a comparative lower critical micelle concentration – the micellar structure can be also retained at high levels of dilution (e.g. in the blood compartment) and based on their sizes above the renal excretion cut-off size (~ 5.5 nm [3]) they profit from a reduced renal clearance. Nevertheless, an effective application of block copolymers in cancer therapy is related to an appropriate polymer size, suggesting that nanoparticles have to be between 10 and 100 nm in diameter to exhibit desired *in vivo* properties [4]. In this regard, the HPMA-*b*-LMA copolymers synthesized in our lab possess a major drawback since their diameters above 200 nm induce an enhanced recognition by the mononuclear phagocyte system, resulting in an increased hepatic and spleenic uptake (see section 5.2). Based on these findings, we wanted to improve the pharmacokinetic profile (in terms of blood circulation time, tumor

accumulation as well as decreased MPS uptake) of HPMA based block copolymers by reducing their polymer size (see section 5.3). Thus we incorporated PEG_{2000} groups into the hydrophilic block to increase on one hand its hydrophilicity and hence inducing a decrease in polymer size. On the other hand poly(ethylene glycol) is widely known for its shielding efficacy toward the MPS [5, 6]. Due to this concept, we synthesized five different HPMA-*b*-LMA copolymers – varying in their degree of PEGylation – listed in table 2 below.

Table 2: *Analytical data of reactive ester precursor polymer (**P*-R**) and final polymer structures (**$P_{0\%}$** to **$P_{11\%}$**)*

Nomen clature	Polymer structure	Monomer ratio	PEG_{2000} incorp.[5]	M_n in g/mol	M_w in g/mol	PDI[2]	R_h[6] in nm
P*-R	Block copolymer	60:40%[1]	-	25.000[2]	31000[2]	1.25	n.d.
$P_{0\%}$	Block copolymer	75:25%[3]	0%	17000[4]	21000[4]	1.25	112.8 +/- 5.7
$P_{1\%}$	Block copolymer	75:25%[3]	1%	20000[4]	24000[4]	1.25	55.4 +/- 2.9
$P_{5\%}$	Block copolymer	75:25%[3]	5%	26000[4]	33000[4]	1.25	38.0 +/- 2.1
$P_{7\%}$	Block copolymer	75:25%[3]	7%	30000[4]	38000[4]	1.25	38.1 +/- 2.1
$P_{11\%}$	Block copolymer	75:25%[3]	11%	39000[4]	47000[4]	1.25	53.0 +/- 2.8

*[1] = Calculated monomer ratio; [2] = Determination by GPC in THF as solvent; [3] = Monomer ratio determined by ^{1}H-NMR spectroscopy after polymeranalogous reaction with 2-hydroxypropylamine; [4] = Calculated from the molecular weight of the reactive ester polymer **P*-R** as determined by GPC in THF as solvent; [5] = PEG_{2000} incorporation (incorp.) ratio determined by ^{1}H-NMR spectroscopy after polymeranalogous reaction; [6] = Hydrodynamic radii of the aggregates determined by Fluorescence Correlation Spectroscopy (FCS)*

Block copolymers were ranging from 0 % PEG to 11 % PEG incorporation efficiency and radiolabeling was carried out by means of [^{18}F]fluoroethylation. Organ / tumor uptake was quantified by *ex vivo* biodistribution as well as *in vivo* μPET imaging in Walker 256 mammary carcinoma bearing rats. A tremendous impact of the respective polymer architecture on the pharmacokinetic profile could be observed. Most strikingly, the *in vivo* results revealed a linear trend in tumor accumulation, exhibiting highest tumor levels for the block copolymer with 11 % PEG side chains. Whereas block copolymers with lower PEG content and highest hydrodynamic radii demonstrated increased renal clearance as

well as predominant hepatic and spleenic uptake, an increase in PEGylation resulted in prolonged blood circulation times, reduction of MPS uptake and particularly higher tumor concentration of the HPMA-*b*-LMA copolymers (see Fig. 5A/B) .

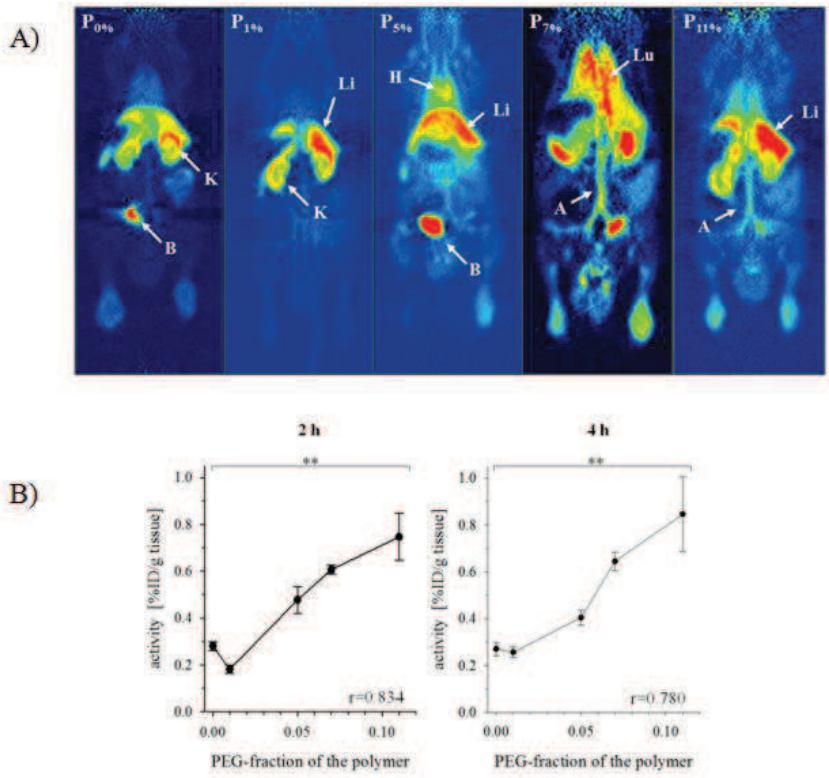

Figure 5A/B: *(A) Whole body µPET image sections obtained 120-135 min after administration of* ^{18}*F-polymers showing renal clearance (kidney (K), bladder (B)), distribution in liver (Li) and lung (Lu) as well as enhanced blood retention (heart (H), aorta (A)) of PEGylated polymers.(B) Tumor accumulation of polymers as a function of the incorporated amount of* PEG_{2000}*. n=4-6, (**) p<0.01.*

Additional *in vitro* studies in the Walker 256 mammary carcinoma cell line revealed an inverse accumulation pattern, illustrating enhanced cellular uptake of block copolymers with lowest degree of PEGylation. Furthermore, cellular experiments in another breast carcinoma cell line (MCF-7 cells) stayed in accordance with the herein observed *in vitro* findings and former studies in our group [7]. FACS measurements demonstrated major cellular uptake of the non-PEGylated block copolymer and lowest internalization for HPMA-*b*-LMA copolymers $\mathbf{P_{5\%}}$ and $\mathbf{P_{7\%}}$. Live-cell confocal fluorescence microscopy at different time points (4, 5 and 24 hours) revealed that the pure and the block copolymer with highest PEG content were predominantly found in the endoplasmic reticulum but not co-localizing with lysosomes. Experiments with peroxisomal marker are ongoing.

Additional inhibitor studies suggested that the non-PEGylated block copolymer is internalized via a clathrin- and caveolae independent pathway but these results have to be further evaluated with endocytosis markers as positive controls. In general it can be concluded that the combination of *in vivo* and *in vitro* studies is essential to tailor polymer based therapeutics for the patient needs. Not only can the effect of polymer architecture on the pharmacokinetic profile be determined by means of non-invasive *in vivo* imaging techniques such as PET but furthermore *in vitro* studies deepen the knowledge of intracellular trafficking of the polymeric compounds.

All so far presented results of structural variation and their resulting impact on the biodistribution pattern in the living organism underline the potential of using [^{18}F]fluoroethylation combined with Positron Emission Tomography as pre-clinical screening techniques to determine suitable polymeric drug delivery candidates in the clinical setting. Nevertheless - as already mentioned earlier - polymer based nanocarriers are particularly holding a great advantage compared to the low molecular weight anticancer agent due to the well-known EPR effect. The enhanced permeability of tumor tissue coupled with the absence of lymphatic drainage - leading to the retention of macromolecules within the tumor site – enables passive accumulation and sustained drug release over days / weeks. In this regard, the short half-life of fluorine-18 is limiting the application of this radionuclide in terms of monitoring the herein presented polymer architectures over a longer time span. Particularly focusing on the high molecular weight HPMA-*ran*-LMA copolymer (see chapter 5.1 and 5.2) which exhibited favorable *in vivo* characteristics over a time window of 4 hours, we wanted to further investigate its potential of EPR-mediated tumor retention in the long term. Thus radiolabeling using longer-lived radioisotopes such as iodine-131 ($t_{1/2}$ = 8 days) demonstrates a versatile tool, already exploited for HPMA based copolymers in the literature [8]. In a proof-of-principle study, HPMA based homopolymers as well as HPMA-*ran*-LMA copolymers were labeled by means of ^{131}I (see chapter 5.4). Special focus was laid on the high molecular weight random copolymer **P4*** and organ / tumor uptake was followed in Walker 256 tumor bearing rats over a time span of 3 days. Most remarkable, even though a continuous blood clearance of the polymer could be observed (total blood clearance within 3 days) enhanced tumor uptake over 48 hours could still be proven. This inverse accumulation profile can be attributed to an EPR-mediated retention of the random

copolymer in the tumor tissue and hence is underlining the potential of HPMA-*ran*-LMA copolymers in the field of continuous drug release.

Finally, we want to shortly present the results of chapter 5.5 which concentrated on the synthesis and *in vivo* evaluation of non-linear PEG analogs and their feasibility as polymer based therapeutics. Based on the overall concept of combining the RAFT process with reactive ester chemistry, the hydrophilic group can be easily varied by means of post-polymerization modification and particularly the same polymeric precursor can be applied for comparative investigation. Thus the aim of the present study was focused on the influence of the hydrophilic group (HTEGMA *vs.* HPMA) and molecular weight on the pharmacokinetic profile of random copolymers *in vivo*. Radioactive labeling was accomplished using fluorine-18 and monitoring via PET enabled their precise tracking *in vivo*. Whereas the HTEGMA-*ran*-LMA copolymers (**P1*** and **P2***) exhibited hydrodynamic radii of < 10 nm thus assuming intrachain micellation, the HPMA-*ran*-LMA copolymers **P3*** and **P4*** formed larger aggregates (R_h ~ 40 nm) in isotonic solution. Studies revealed that molecular weight had a major impact on the biodistribution characteristics of HTEGMA based random copolymers since the high molecular HTEGMA-*ran*-LMA copolymer was directly taken up by the MPS and showed comparatively low tumor uptake. In contrast, its low molecular weight HTEGMA counterpart demonstrated pronounced renal clearance combined with nearly two-fold higher tumor accumulation in the Walker 256 mammary carcinoma. These findings were in accordance to the high M_w HPMA based polymer structure which exhibited a concurrent tumor concentration. The observed results emphasize the potential of non-linear PEG analogs in the field of polymer based anticancer treatment but nevertheless there is still the necessity of improving their plasma-half life in the long run. In this respect, the elongation of the methacrylamide based PEG side chains might be a suitable approach for future studies.

In conclusion, the present work is explicitly underlining that molecular weight, size and polymer architecture are major determinants for the pharmacokinetic pattern of polymer drug delivery vehicles and precisely adjusting these parameters is essential for designing efficient polymer based (chemo) therapy in the future. In this regard, non-invasive imaging techniques such as Positron Emission Tomography in combination with short-

lived radionuclides constitute a versatile tool for their fast pre-clinical screening and thus might be useful to individualize anticancer treatment to the patients' needs.

References

1. Herth, M. M.; Barz, M.; Moderegger, D.; Allmeroth, M.; Jahn, M.; Thews, O.; Zentel, R.; Rösch, F., Radioactive Labeling of Defined HPMA-Based Polymeric Structures Using [18F]FETos for In Vivo Imaging by Positron Emission Tomography. *Biomacromolecules* **2009,** 10, (7), 1697-1703.
2. Herth, M. M.; Barz, M.; Jahn, M.; Zentel, R.; Rösch, F., 72/74As-labeling of HPMA based polymers for long-term in vivo PET imaging. *Bioorganic & Medicinal Chemistry Letters* **2010,** 20, (18), 5454-5458.
3. Alexis, F.; Pridgen, E.; Molnar, L. K.; Farokhzad, O. C., Factors Affecting the Clearance and Biodistribution of Polymeric Nanoparticles. *Molecular Pharmaceutics* **2008,** 5, (4), 505-515.
4. Gullotti, E.; Yeo, Y., Extracellularly Activated Nanocarriers: A New Paradigm of Tumor Targeted Drug Delivery. *Molecular Pharmaceutics* **2009,** 6, (4), 1041-1051.
5. Gref, R.; Lück, M.; Quellec, P.; Marchand, M.; Dellacherie, E.; Harnisch, S.; Blunk, T.; Müller, R. H., "Stealth" corona-core nanoparticles surface modified by polyethylene glycol (PEG): influences of the corona (PEG chain length and surface density) and of the core composition on phagocytic uptake and plasma protein adsorption. *Colloids and Surfaces B: Biointerfaces* **2000,** 18, (3-4), 301-313.
6. Veronese, F. M.; Pasut, G., PEGylation, successful approach to drug delivery. *Drug Discovery Today* **2005,** 10, (21), 1451-1458.
7. Barz, M.; Luxenhofer, R.; Zentel, R.; Kabanov, A. V., The uptake of N-(2-hydroxypropyl)-methacrylamide based homo, random and block copolymers by human multi-drug resistant breast adenocarcinoma cells. *Biomaterials* **2009,** 30, (29), 5682-5690.
8. Lammers, T.; Kühnlein, R.; Kissel, M.; Subr, V.; Etrych, T.; Pola, R.; Pechar, M.; Ulbrich, K.; Storm, G.; Huber, P.; Peschke, P., Effect of physicochemical modification on the biodistribution and tumor accumulation of HPMA copolymers. *Journal of Controlled Release* **2005,** 110, (1), 103-118.

4. Summary

Macromolecular based drug delivery systems are of emerging interest regarding the clinical administration of (chemo) therapeutic agents. In order to investigate their clinical potential, it is crucial to determine the pharmacokinetic profile *in vivo*. Each alteration in polymer structure is influencing the body distribution of the respective macromolecule and thus deepening knowledge about structure-property relationships in the living organism is needed to adjust the nanocarrier system for future applications. In this regard, pre-clinical screening via radiolabeling combined with Positron Emission Tomography (PET) constitutes a useful tool for fast and quantitative monitoring of drug delivery candidates *in vivo*. Particularly poly(HPMA) and PEG are widely exploited in the field of polymer based therapeutics and thus derivatized structures might provide new generations in this research area.

This work describes the successful synthesis of diverse HPMA and PEG based polymer architectures - including homopolymers, random and block copolymers – accomplished via RAFT polymerization and reactive ester chemistry. Furthermore, their radioactively labeling and biological evaluation was carried out by means of ^{18}F and ^{131}I combined with μPET imaging and *ex vivo* biodistribution in tumor bearing rats.

The variation in polymer architecture and subsequent analysis *in vivo* resulted in some major conclusions. First, the hydrophilic / lipophilic balance had a major influence on the pharmacokinetic profile, demonstrating most favorable *in vivo* characteristics (low hepatic and spleenic uptake as well as prolonged blood circulation times) for HPMA-*ran*-LMA copolymers with increasing content of hydrophobic moiety. Second, long term biodistribution studies with iodine-131 demonstrated enhanced retention in the tumor tissue for high molecular weight HPMA based random copolymers thus proofing the well-known EPR-effect. Third, superstructure formation and hence polymer size are key factors for efficient tumor targeting since polymer structures above 200 nm in diameter are rapidly recognized by the MPS and cleared from the bloodstream. In this regard, the herein synthesized HPMA block copolymers were chemically modified with PEG side chains to induce a decrease in size as well as reduced blood clearance, yielding enhanced tumor accumulation in the Walker 256 mammary carcinoma model. Forth, the overall polymer architecture as well as molecular weight are strongly influencing the body distribution of HPMA / PEG based polymers and their efficacy of tumor treatment is significantly depending on the properties of each individual tumor. Due to this

observation, the present work is underlining the necessity of a precise polymer characterization in combination with pre-clinical screening to tailor polymeric carrier systems for individualized patients' (chemo) therapy in the future.

5. Manuscripts

The publications contributed to this PhD thesis are summarized below:

5.1 *"Modifying the Body Distribution of HPMA-Based Copolymers by Molecular Weight and Aggregate Formation"*

Mareli Allmeroth[#], [redacted], *Biomacromolecules* **2011**, *12*, 2841

5.2 *"Structure and Size of HPMA-Based Polymers decide on Tumor Accumulation but the Tumor Model makes a Difference: A quantitative In Vivo PET Study"*

Mareli Allmeroth*, [redacted], *Angewandte Chemie, in preparation*

5.3 "*PEGylation of HPMA-based block copolymers enhances tumor accumulation in vivo: A quantitative study using radiolabeling and Positron Emission Tomography"*

Mareli Allmeroth*, [redacted], *Journal of Controlled Release, in preparation*

5.4 "*Comparative study on short and long-term distribution of HPMA-ran-LMA copolymers in vivo by means of* ^{18}F *and* ^{131}I*-labeling revealing tumor retention over time"*

[redacted], **Mareli Allmeroth**, [redacted], *Macromolecular Rapid Communications, in preparation*

5.5 "*In vivo monitoring of non-linear PEG based copolymers by means of Positron Emission Tomography: The influence of molecular weight on their pharmacokinetic profile"*

Mareli Allmeroth[§], [redacted][§], *Manuscript in preparation*

5.1 Modifying the Body Distribution of HPMA-Based Copolymers by Molecular Weight and Aggregate Formation

Mareli Allmeroth[1,§], [redacted]

§ *Institute of Organic Chemistry, Johannes Gutenberg University, Duesbergweg 10-14, 55099 Mainz, Germany;* [redacted]

* [redacted]

Biomacromolecules, **2011**, *12*, 2841-2849

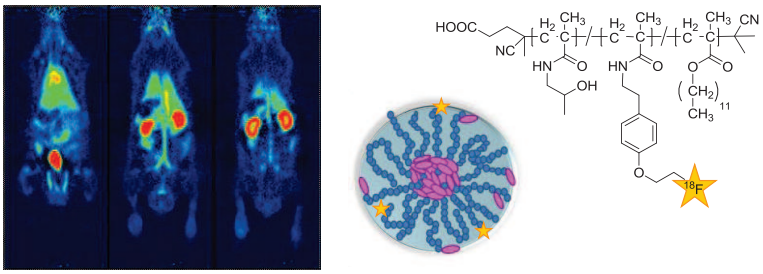

In vivo pharmacology (using positron emission tomography PET) allows to analyze non-invasively the biodistribution of aggregate forming copolymers which can combine long blood circulation, low liver accumulation and renal clearance.

Abstract

There is a recognized need to create well-defined polymer probes for *in vivo* and clinical positron emission tomography (PET) imaging to guide the development of new generation polymer therapeutics. Using the RAFT polymerization technique in combination with the reactive ester approach, here we have synthesized well-defined and narrowly distributed *N*-(2-hydroxypropyl)methacrylamide homopolymers (pHPMA) (**P1*** and **P2***) and random HPMA copolymers consisting of hydrophilic HPMA and hydrophobic lauryl methacrylate comonomers (**P3*** and **P4***). The polymers had molecular weights below (**P1*** and **P3***) and above the renal threshold (**P2*** and **P4***). Whereas the homopolymers dissolve in isotonic solution as individual coils, the random copolymers form larger aggregates above their critical micelle concentration (around 40 nm) as determined by Fluorescence Correlation Spectroscopy. Structure-property relationships of the pharmacokinetics and biodistribution of the different polymer architectures were monitored in the living organism following radiolabeling with the positron emitter ^{18}F via fluoroethylation within a few hours. *Ex vivo* organ biodistribution and *in vivo* μPET imaging studies in male Copenhagen rats revealed that both size and the nature of the aggregate formation (hydrophobically modified copolymers) played a major role in blood clearance and biodistribution, especially concerning liver and kidney accumulation. The high molecular weight random copolymer **P4*** (hydrophobically modified) in particular combines low liver uptake with enhanced blood circulation properties, showing the potential of hydrophobic interactions - as seen for the represented model system- that are valuable for future drug carrier design.

Keywords: HPMA, RAFT polymerization, Structure-property relationships, Drug delivery, Fluorine-18 labeling, PET

1. Introduction

"Polymer therapeutics" - a term describing polymeric drugs, polymer-drug conjugates, polymer-protein conjugates, polymeric micelles and polyplexes - became an emerging field of interest in both chemical and medical sciences over the last four decades [1]. Their diversity regarding loading capacity with multiple pharmaceutics, reduction of usually occurring toxic side effects as well as an inherent tendency to accumulate in tumor tissue due to the EPR (enhanced permeability and retention) effect [2, 3], constitutes them as an attractive tool for clinical applications. Based on the first concept of Ringsdorf in the 1970's [4] concerning a macromolecular-based drug delivery vehicle for active and passive targeting for improving the therapeutic action, fundamental research in this discipline has evolved. Intensive studies on polymer-drug conjugates [5-9], micelle forming polymers [10-13] or newly established polymer-enzyme combination therapy [14-16] have been carried out, demonstrating the great potential of the route pursued. Altogether only poly(ethylene glycol) (PEG), poly-*N*-(2-hydroxypropyl)methacrylamide (HPMA) copolymers, dextran derivatives as well as polyglutamic acid based drug conjugates have progressed into clinical trials, six among them being HPMA anticancer conjugates [1, 9, 17].

Regarding the clinical application of polymer based therapeutics, there is a need for appropriate preclinical screening methodologies to select a suitable therapy for the individual patient [18, 19]. In this respect introducing small radioactive probes into the polymeric system and using nuclear medicine imaging techniques such as positron emission tomography (PET), pharmaco-kinetics and distribution of the polymer therapeutic can be easily monitored. Depending on the biological time-frame to be monitored, PET-nuclide and labeling strategy need to be adjusted. Based on the short-lived positron emitter fluorine-18 ($t_{1/2}$ = 110 min), we have recently developed PET based HPMA copolymers for short-term *in vivo* visualization, thereby being time-efficient and enabling minimal radiation exposure concerning a clinical application [20]. In contrast, also new labeling approaches for HPMA based polymers using PET-nuclides of longer half-lives, e.g. $^{72/74}$As ($t_{1/2}(^{72}As)$ = 26 h), $t_{1/2}(74)$ = 17.8 d) were established, offering the possibility for long-term

PET-imaging with time-frames of weeks to months [21].

By introducing fluorine-18 as PET nuclide, initial excretion pathways and organ uptake can be identified and measured quantitatively. Due to its excellent physical and nuclear characteristics, fluorine-18 is considered the ideal radioisotope for PET imaging probes, providing visualization of high spatial resolution and because of its size not influencing the polymeric structure. In contrast to radionuclides for SPECT (Single Photon Emission Computed Tomography) (e.g. ^{123}I, ^{131}I and ^{99m}Tc) - so far used to image HPMA-based polymers [22, 23] - fluorine-18 as short-lived isotope combines the requirements for fast and detailed screening of potential drug carrier systems giving insight into individual early phase accumulations and clearance mechanisms.

Regarding the therapeutic effects of a polymer based drug carrier system its backbone plays a crucial role. Essential requirements are mainly either biodegradability or biocompatibility with final excretion properties. Being water soluble, non-toxic and non-immunogenic, poly-*N*-(2-hydroxypropyl) methacrylamide, has evolved as promising biocompatible artificial polymer, already intensively studied *in vitro* and *in vivo* [9, 24-26]. Compared to PEG it possesses the advantage of multifunctionality whereas PEG only has two functional end groups. That enables covalent conjugation of a higher drug payload, attachment of recognition units for receptor-mediated targeting or combination therapy [15].

When being developed as a polymer therapeutic, it is important that a polymer should be as well-defined as possible [27]. The first HPMA-based polymers were, however, originally made by free radical polymerization [28-31] and required lengthy as well as laborious fractionation processes to reduce their polydispersity [32]. With the introduction of living radical polymerization techniques, well-defined polymer structures became available, either by ATRP or by RAFT techniques [33-36]. Especially in combination with the reactive ester approach[12, 20, 37], RAFT offers an elegant access to different polymer architectures and various functional groups, e.g. imaging moieties or therapeutics can be attached. By applying this route, HPMA random as well as block copolymers of specific composition can be easily prepared, exhibiting the tendency to aggregate in solution due to hydrophobic lauryl methacrylate side chains [12].

To be effective as an antitumor agent, a polymer drug conjugate must be able to localize to the tumor tissue by the EPR-effect [2, 38] (resulting from leaky tumor blood vessels and a lack of lymphatic drainage) and prevent the drug from localizing to normal tissues that are potential sites of toxicity. Furthermore long circulation properties in the blood pool might be beneficial for a controlled and continuous drug release.

Lammers et al. [39] applied radiolabeling with SPECT isotope iodine-131 to investigate the influence of the incorporation of various functional groups into HPMA (copolymers) on the body distribution and accumulation in the tumor. This work included polymer therapeutics like PK1 polymers but focused on functional groups which interact by H-bonding or ionic charges like carboxylate, amine groups or peptides. The authors found that the copolymer units mostly reduced the circulation time in the body but did not change the relative accumulation in different tissues as well as the tumor. Classical polymeric therapeutics like PK1 or PK2 [40, 41] often carry hydrophobic pharmaceutics. Based on these characteristics they are – in a physico-chemical sense - hydrophobically modified copolymers. This underlines the importance to focus also on the aspect of intra- and intermolecular aggregate formation due to hydrophobic interactions in model systems. In this respect, the synthesis of HPMA-based hydrophilic / hydrophobic copolymers and their aggregate formation makes model systems available in which it is easy to vary the size and the hydrophilic / hydrophobic balance. Experiments with cell cultures already demonstrated the tremendous influence of the variation of these segments on the cellular uptake of HPMA based polymers [12] and recent studies underline their potential to transport pharmaceutics across the blood-brain-barrier [42].

Consequently, the aim of the present study focused on the determination of correlations between size and aggregate formation due to hydrophobic interactions and resulting biological properties (body and organ distribution) of well-defined HPMA based polymers in living animals.

Applying fast and versatile radiolabeling techniques for noninvasive high resolution PET imaging helps to understand how the *in vivo* fate of a polymer model system can be affected by structural modification thus speeding up the time consuming evaluation

process necessary for the design of potential drug carrier candidates.

2. Materials and Methods

2.1 Materials

All solvents were of analytical grade, as obtained by Sigma Aldrich and Acros Organics. Dioxane was distilled over a sodium/potassium composition. Lauryl methacrylate was distilled to remove the stabilizer and stored at -18 °C. 2,2'-azoisobutyronitrile (AIBN) was recrystallized from diethyl ether and stored at -18 °C as well.

2.2 Characterization

^{1}H-NMR spectra were obtained by a Bruker AC 300 spectrometer at 300 MHz, ^{19}F-NMR analysis was carried out with a Bruker DRX-400 at 400 MHz. All measurements were accomplished at room temperature and spectroscopic data were analyzed using ACDLabs 9.0 1D NMR Manager. The synthesized polymers were dried at 40 °C under vacuum over night, followed by Gel Permeation Chromatography (GPC). GPC was performed in tetrahydrofuran (THF) as solvent, using following equipment: pump PU 1580, autosampler AS 1555, UV detector UV 1575 and RI detector RI 1530 from Jasco as well as a miniDAWN Tristar light scattering detector from Wyatt. Columns were used from MZ Analysentechnik, 300x8.0 mm: MZ-Gel SDplus 10^{6} Å 5 µm, MZ-Gel SDplus 10^{4} Å 5 µm and MZ-Gel SDplus 10^{2} Å 5 µm. GPC data were evaluated by using the software PSS WinGPC Unity from Polymer Standard Service Mainz. The flow rate was set to 1 mL/min with a temperature of 25 °C.

For synthesis of 2-[^{18}F]fluoroethyl-1-tosylate ([^{18}F]FETos), a Sykam S 1100 pump and a Knauer UV-detector (K-2501) HPLC system were used. Size Exclusion Chromatography (SEC) of ^{18}F-labeled polymers was performed using HiTrap™ Desalting Column, Sephadex G-25 Superfine and a waters pump (1500 series), a Waters UV-detector (2487 λ absorbance detector) and a Berthold LB 509 radiodetector.

In *ex vivo* studies, fluorine-18 activities were determined using a Perkin Elmer 2470 Wizard^{2} γ- counter.

2.3 Synthesis of the polymers

The polymers **P1*** to **P4*** were prepared in analogy to reference [12, 20]. The details are added as supplementary information.

2.4 Characterization of the polymers

The amphiphilic character of the hydrophobically modified HPMA copolymers (**P3*** and **P4***) was characterized by a "du Noüy" ring tensiometer used to determine the cmc (critical micelle concentration) in isotonic sodium chloride solution. The protocol can be found as supplementary data.

The hydrodynamic radii of the polymeric systems were determined by Fluorescence Correlation Spectroscopy (FCS) using a commercial FCS setup. This method proves the aggregate formation of the copolymers. The details can be found in the supplementary information.

2.5 Radiolabeling and purification for *ex vivo* and *in vivo* experiments

Synthesis of [^{18}F]FETos, labeling of polymers **P1*** - **P4*** as well as purification of labeled polymers for *ex vivo* and *in vivo* experiments was accomplished according to literature [20].

For metabolic studies, blood samples were taken 140 min p.i., centrifuged and blood plasma was analyzed using SEC. Details are provided as supplementary information.

2.6 Animal experiments

2.6.1 Tumor and animal model

Tumor experiments were performed with the subline AT1 R3327 Dunning prostate carcinoma of the rat. Tumors were used when they reached a volume of 1 to 2 ml approximately 10 to 14 days after tumor cell injection. At this time point tumors were in the exponential growing phase and did not show signs of necrosis (confirmed by histology; data not shown). All experiments had previously been approved by the regional animal ethics committee and were conducted in accordance with the German Law for Animal Protection and the UKCCCR Guidelines [43]. Details are provided as supplementary information.

2.6.2 Biodistribution measurements

In order to assess the distribution of the radiolabeled polymers in different organs of the animals, the polymer (concentration of 1 mg in 1 mL sodium chloride solution) was injected i.v. in anaesthetized tumor-bearing rats via the tail vein with a mean activity of 18.7 ± 5.8 MBq. After 120 or 240 min, the animals were sacrificed and different organ (kidney, liver, lung, spleen, heart, skeletal muscle, small intestine, testis, blood) and tumor samples were taken. The tissue samples were weighed and

minced. Finally, the ^{18}F-activity in the organs was measured in a γ-counter.

2.6.3 Small animal PET studies

In addition the uptake of the different polymers in tumors and organs was imaged using PET. Details of the imaging procedure are described as supplementary information.

3. Results and Discussion

3.1 Synthetic concept of HPMA based homo- and random copolymers

To study the *in vivo* behavior of different polymeric architectures in dependence of their molecular weight and the effect of aggregate formation due to the presence of hydrophobic segments, diverse HPMA-based polymeric systems were synthesized applying the RAFT polymerization technique [33, 34, 44]. Barz et al. already found that especially the aggregate formation significantly influences the cellular entry into MCF7/ADR cells *in vitro* [12]. Here we aimed to gain more knowledge about structure-property relationships not only on the cellular level but in the living organism. First results emphasized a successful radioactive labeling of such polymers [20]. For further systematic studies, a series of HPMA homo-polymers and HPMA-*ran*-LMA copolymers were prepared, with molecular weights chosen to be below and above the renal threshold (limit of renal clearance of HPMA copolymers M_w < 40000 g/mol [45]). The incorporation of the hydrophobic lauryl methacrylate constitutes the basis for aggregate formation. Due to differences in size and aggregate formation we expected different pharmacological behavior in terms of organ accumulation, circulation time as well as excretion characteristics. The synthetic route to these polymers (**P1* - P4***) is depicted in scheme 1. Starting with the pentafluorophenyl methacrylate monomer, the precursor homopolymers **P1*-R** and **P2*-R** were synthesized and by simultaneous addition of lauryl methacrylate, the statistical copolymers **P3*-R** and **P4*-R**. The polymerization was achieved according to literature [12, 46, 47]. These reactive polymers can afterwards be converted to HPMA based polymers by a clean conversion. A main advantage of this synthetic route to HPMA-*ran*-LMA copolymers lies in the statistical copolymerization of two methacrylate-based monomers (both esters). Due to the comparable copolymerization parameters, a random integration of both monomers is reasonable (copolymer-ization parameters were determined with r_1 and r_2 both < 1). This provides an

important advantage compared to the copolymerization of amides with esters [48]. In addition the primarily formed reactive polymers **P1*-R** to **P4*-R** are well soluble and do not form aggregates as all monomer units are hydrophobic. The dithioester endgroup was cleaved by an excess of 2, 2'-azoisobutyronitrile, a method first presented by Perrier et al. [49], possessing the benefit of avoiding side reactions during the post-polymerization step. The polymeric precursors were functionalized by aminolysis via tyramine groups, necessary for further radioactive labeling. The incorporation efficiency was calculated to be 2 - 4 % for each polymer chain. 2-hydroxypropylamine was finally added, resulting in the polymeric structures **P1*** - **P4***. Full conversion of the reactive ester side groups could be proven by means of ^{19}F-NMR spectroscopy, demonstrating complete disappearance of the ^{19}F-signals at the polymeric backbone.

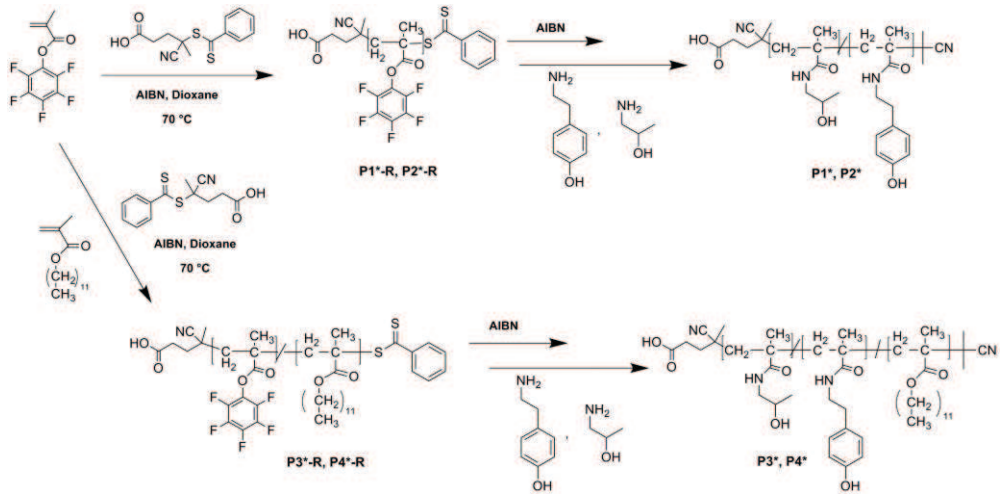

Scheme 1: *Reaction scheme of polymeric precursor systems based on the reactive ester approach and their polymer-analogous conversion for further radioactive labeling*

3.2 Molecular weights and incorporation ratios of polymeric architectures

Overall, four different polymeric systems were synthesized (all hydrophilic polymers **P1*** and **P2*** for reference and hydrophilic / hydrophobic copolymers **P3*** and **P4***), each architecture exhibiting a low and high molecular weight sample. Characterization of the precursor structures **P1*-R** – **P4*-R** was carried out using gel permeation chromatography. The results are summarized in table 1.

Table 1: *Analytical data of reactive ester homopolymers (**P1*-R**, **P2*-R**) and random copolymers (**P3*-R**, **P4*-R**) as well as the final polymeric structures **P1* - P4*** (see scheme 1)*

Nomenclature	Polymeric structure	Monomer ratio	M_n in g/mol	M_w in g/mol	PDI[2]
P1*-R	Homopolymer	100%[1]	18000[2]	23000[2]	1.29
P2*-R	Homopolymer	100%[1]	87000[2]	130000[2]	1.49
P3*-R	Random copolymer	80:20[1]	17000[2]	21000[2]	1.26
P4*-R	Random copolymer	80:20[1]	57000[2]	80000[2]	1.41
P1*	Homopolymer	100%[3]	9000[4]	12000[4]	1.29
P2*	Homopolymer	100%[3]	52000[4]	77000[4]	1.49
P3*	Random copolymer	82:18[3]	11000[4]	14000[4]	1.26
P4*	Random copolymer	75:25[3]	39000[4]	55000[4]	1.41

*[1] = Calculated monomer ratio; [2] = Determination by GPC in THF as solvent; [3] = Monomer ratio determined by ^{1}H-NMR spectroscopy after polymeranalogous reaction with 2-hydroxypropylamine (**P1*-P4***); [4] = calculated from the molecular weights of the reactive ester polymers **P1*-R to P4*-R** as determined by GPC in THF as solvent*

As indicated, well-defined polymeric systems with relatively narrow molecular weight distribution have been achieved by the RAFT polymerization process [PDI= 1.26-1.49].

3.3 Aggregation parameter

The major distinction between homo- and copolymers relies in the formation of micelle-like structures due to the incorporation of hydrophobic groups, in our case lauryl methacrylate. To determine the concentration-dependant aggregation behavior of the copolymers **P3*** and **P4***, the critical micelle concentration (cmc) was determined by surface tension measurements with a "du Noüy" ring tensiometer. Stock solutions of 0.1 mg/mL in 0.9 % NaCl solution were prepared and the measurement was performed at 37 °C to mimic *in vivo* conditions. For the low molecular weight copolymer **P3*** a cmc value of 4.6 x 10^{-3} mg/mL was obtained. Copolymer **P4*** exhibited a lower cmc of 1.6 x 10^{-3} mg/mL which is reasonable due to the increased LMA ratio. Based on these data it can be assumed that the polymeric aggregates are also present in the bloodstream of the rat (blood volume of the rat ~ 16 mL [50], corresponding to a concentration of 6.3 x 10^{-2} mg/mL polymer in the blood after i.v. injection of 1 mL of a 1 mg/mL isotonic solution). Even after renal clearance of more than 50 % of the polymer injected, the micellar-like structure should be retained. The cmc values are additionally summarized in table 2.

Table 2: *Critical micelle concentration of random copolymers (**P3***, **P4***) in isotonic NaCl solution at 37°C*

Nomenclature	Polymeric structure	cmc in mg/mL[5]	cmc in mol/L
P3*	Random copolymer	4.6×10^{-3}	4.2×10^{-7}
P4*	Random copolymer	1.6×10^{-3}	4.2×10^{-8}

[5] = *As determined by surface tension vs. concentration applying the ring method of the "du Noüy" ring tensiometer*

To facilitate size determination of the aggregates formed from the amphiphilic copolymers in water, we additionally attached fluorescent Oregon Green 488 cadaverine onto the polymer chains. Fluorescence Correlation Spectroscopy was used to determine the diffusion constants of the individual polymer chains as well as of the aggregates and hence their hydrodynamic radii. The homopolymer **P1*** exhibited a hydrodynamic radius of 1.1 nm and the higher molecular weight polymer **P2*** a size of 3 nm (NaCl solution). Both values are a bit smaller than expected (for **P4*** in methanol, as non aggregating solvent, we observed a hydrodynamic radius of 6 nm) and are just taken as proof for the existence of individual random coils. The random copolymers **P3*** and **P4*** showed a different behavior and superstructure formation.

Copolymer **P3*** possessed a hydrodynamic radius of 33 nm and the random copolymer **P4*** an R_h of ~ 40 nm. Both values are much too large for individual chains, but also for classical micelles in which the size should not be much larger than two times the size of the individual chain. These data are consistent with earlier observations from our group [12]. They may be explained by the formation of "compound micelles" [51]. Also Haag and coworkers reported the formation of unexpectedly large supramolecular assemblies for nonionic dendritic amphiphiles being composed of hydrophilic polyglycerol dendrons and hydrophobic C_{11} or C_{16} alkyl chains [52]. The formation of more complex hydrophobic / hydrophilic super-structures can be the reason for the hydrodynamic radii of the random copolymer superstructures. A collection of the sizes for polymers **P1*-P4*** is given in table 3.

Table 3: *Size of homopolymers (**P1***, **P2***) and random copolymers (**P3***, **P4***) in isotonic NaCl solution by FCS at RT.*

Nomenclature	Concentration in mg/mL	R_h in nm	Δ R_h in nm
P1*	0.1 mg	1.1	+/- 0.1
P2*	0.1 mg	3.0	+/- 0.2
P3*	0.1 mg	33.4	+/- 1.7
P4*	0.1 mg	39.9	+/- 2.2

3.4 Radioactive labeling with [^{18}F]fluorine

To study the behavior of the different polymeric architectures *in vivo*, the positron emitter fluorine-18 ($t_{1/2}$= 109.7 min) was introduced for both *ex vivo* organ distribution measurements as well as µPET imaging via a prosthetic labeling procedure using [^{18}F]FETos. Compared to γ-imaging using SPECT nuclides (e.g. ^{99m}Tc or ^{123}I), PET provides images of much higher spatial resolution due to the nuclear characteristics of fluorine-18.

For labeling purposes the polymeric backbone had been derivatized with 2 - 4 % of tyramine groups (these groups were present during the experiments described above), thus offering a reactive site for the regio-selective incorporation of the [^{18}F]fluoroethyl moiety [20]. The applied indirect labeling method is shown in scheme 2. In a first step fluorine-18 is incorporated via nucleophilic substitution yielding [^{18}F]FETos and subsequently transferred to a solution of the tyramine derivatized polymer which is deprotonated using a small amount of base.

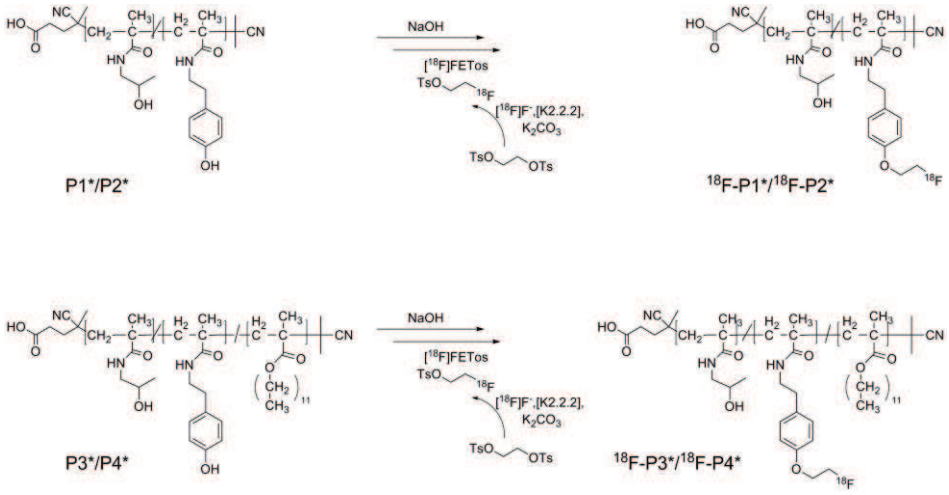

Scheme 2: *Radioactive labeling of homopolymers (**P1***, **P2***) and random copolymers (**P3***, **P4***) via prosthetic labeling procedure using [^{18}F]FETos*

Table 4: *Decay-corrected radiochemical labeling yields of homopolymers (**^{18}F-P1***, **^{18}F-P2***) and random copolymers (**^{18}F-P3***, **^{18}F-P4***) after 15 min at 120 °C using 3 mg of each polymer precursor in DMSO*

Nomenclature	Polymeric structure	Monomer ratio[3]	M_w in g/mol[4]	RCY in %
^{18}F-P1*	Homopolymer	100%	12.000	37± 6
^{18}F-P2*	Homopolymer	100%	77.000	24 ±2
^{18}F-P3*	Random copolymer	82:18	14.000	26 ±1
^{18}F-P4*	Random copolymer	75:25	55.000	10 ±2

[3], [4] = cf. table 1

Decay-corrected radiochemical yields (RCY) were determined by SEC and are summarized in table 4. RCYs were found to be dependent on the molecular weight and the lauryl methacrylate ratio at constant temperature. RCYs for the low molecular weight HPMA based polymers were higher compared to the high molecular weight counterpart. We assume that this is the result of the lower accessibility of phenolic groups in the interior of the polymer coils. Likewise minor RCYs were observed for the lauryl methacrylate derivatives under the same conditions probably due to the formation of hydrophobic pockets leading to less accessible tyramine moieties.

For biological experiments, the radiolabeled polymer systems were freed from low molecular weight by-products using SEC leading to a pure, ^{18}F-labeled polymer solution ready for *ex vivo* and *in vivo* experiments in an overall synthesis of less than 90 min beginning at the start of [^{18}F]FETos synthesis.

Altogether we were able to successfully apply the [^{18}F]fluoroethylation labeling method to a new series of HPMA homopolymers and HPMA-*ran*-LMA copolymers using optimized labeling conditions thus enabling *in vivo* imaging of different polymeric architectures.

3.5 Biodistribution studies

Fig. 1A shows the impact of the molecular weight of the HPMA-homopolymers **^{18}F-P1*** and **^{18}F-P2*** on the biodistribution in different tissues *ex vivo*. The smaller polymer (**^{18}F-P1***, 12 kDa) showed highest concentrations in the kidneys (15.2±3.1 % ID/g tissue) and the liver (1.6±0.1 % ID/g tissue) 2 h after i.v. injection. These results correlate to already published data on the molecular weight dependence of HPMA copolymers [45], ensuring that the non-biodegradable HPMA based polymer is

cleared from the blood stream by renal filtration if the molecular weight is low enough. In other organs only marginal accumulation of the polymer was found.

In contrast, the high molecular weight homopolymer **^{18}F-P2*** (77 kDa) was found less pronounced in the kidneys (6.0±0.1 % ID/g tissue, Fig. 1A) whereas in the liver the concentration was 4-times higher (8.0±1.0 % ID/g tissue) as compared to the **^{18}F-P1*** polymer. In addition, the accumulation in the spleen was also much higher (2.8±0.2 % ID/g tissue). These results indicate that the majority of i.v. injected radiolabeled high molecular weight polymer **^{18}F-P2*** cannot be filtered by the renal system and is presumably taken up by the macrophages of the MPS (mononuclear phagocyte system) [53] or excreted by the liver and bile. This indicates that the molecular weight is an important factor for the route of elimination of well-defined polymeric architectures, as already demonstrated for ^{125}I-labeled HPMA copolymers by Seymour et al. [45]. In comparison, the differences between the two polymers in other organs are marginal. In summary, most of the data received by the presented biodistribution study on HPMA-based homopolymers are comparable to the results of Lammers et al. who could demonstrate that different radioiodinated molecular weight poly(HPMA) showed significant disparities in body distribution [39]. Nevertheless the polymers differed slightly in molecular weight and the incorporation of the labeling group may also influence the *in vivo* behavior. By applying [^{18}F]fluoroethylation labeling, accumulation tendencies consistent with the above mentioned results could be obtained, accomplished in a shorter time span and enabling the benefit of non-invasive high resolution PET imaging - both favorable for patient selection concerning clinical therapies in the future [19].

Similar experiments were performed with the well-defined HPMA-*ran*-LMA copolymers **^{18}F-P3*** and **^{18}F-P4*** which differed in molecular weight (14 kDa *vs.* 55 kDa). These substances are different from the so far studied HPMA-based copolymer systems for drug delivery [13, 17, 54] because the copolymerization of two methacrylate-based monomers (penta-fluorophenyl- and lauryl methacrylate) allows the preparation of randomly distributed copolymers. The incorporation efficiency of the hydrophobic fatty acid segment was calculated to be 18 % for the low molecular weight copolymer **^{18}F-P3*** and 25 % for the high molecular weight

copolymer **^{18}F-P4*,** respectively. When the body distribution of these probes was studied (Fig. 1B) the low molecular weight polymer **^{18}F-P3*** was preferentially localized in kidney (12.6± 1.7 % ID/g tissue), liver (3.0±0.4 % ID/g tissue) and blood (2.0±0.3 % ID/g tissue). In contrast, the high molecular weight polymer **^{18}F-P4*** showed higher levels in the blood (3.7±0.5 % ID/g tissue) and levels were lower in kidney (6.4±1.2 % ID/g tissue) and liver (1.8±0.3 % ID/g tissue). Both polymers were also found at low concentration in other organs such as lung, spleen and heart (Fig. 1B).

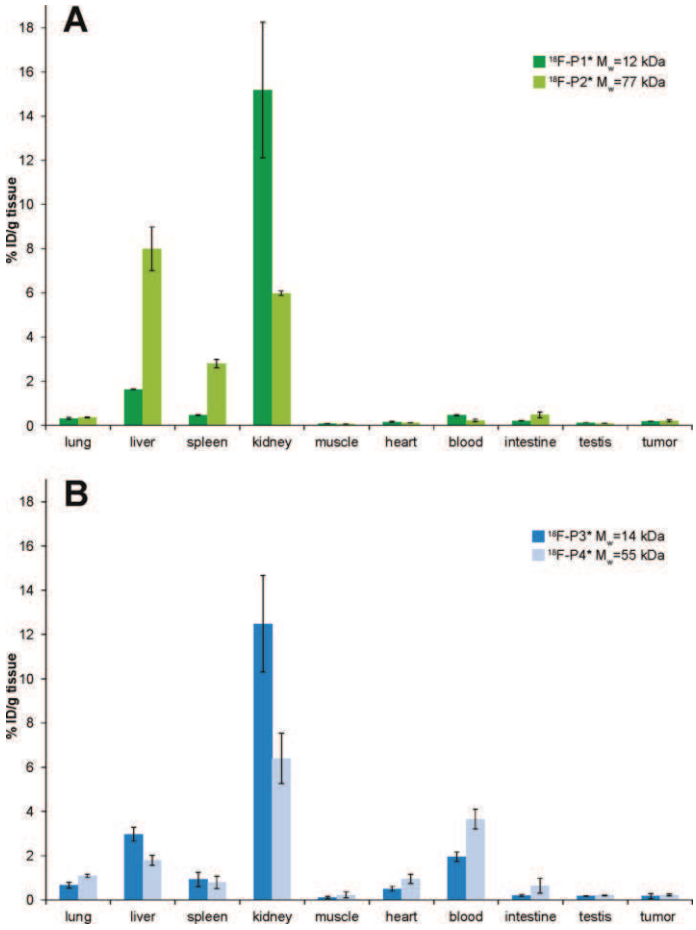

Figure 1: *Influence of low and high molecular weight HPMA based homopolymers and random HPMA-LMA copolymers on their biodistribution in male Copenhagen rats bearing AT1 R3327 Dunning prostate carcinoma 2 h post i.v. injection. (A) Recovered dose of injected* ***^{18}F-P1**** *(M_w = 12 kDa) versus* ***^{18}F-P2**** *(M_w = 77 kDa) in % ID/g tissue in organs of interest. (B) Recovered dose of molecular weight average 14 kDa (****^{18}F- P3***)** *and 55 kDa (****^{18}F- P4***)** *HPMA ran-LMA copolymers (n=3)*

When comparing the corresponding polymers of the different types (homopolymer *vs.* copolymer) of the approximately same sizes (**^{18}F-P1*** *vs.* **^{18}F-P3*** and **^{18}F-P2*** *vs.* **^{18}F-P4***) several pronounced differences can be seen. The most striking difference between the homo- and the copolymers is, that independently from the molecular weight, the HPMA-*ran*-LMA copolymer stays longer in the blood compartment. The small homopolymer was excreted rapidly by the kidneys and the large one by the liver, both leading to a negligible polymer concentration in the blood. The copolymers were excreted in the same principal manner, however, much slower leading to marked sustained blood concentration. With an assumed blood volume of the rat of 16 mL [50] the % ID/g blood values found for the copolymers translate into values of about 30 % (**^{18}F-P3***) and 60 % (**^{18}F-P4***) of the injected dose being still present in the blood compartment 2 h p.i., illustrating significant retention of the copolymeric systems in the blood stream. Especially the uptake of the larger copolymer **^{18}F-P4*** by the liver was much lower than for the comparable homopolymer (as indicated by a 4-times lower accumulation in the liver, illustrated in Fig. 2). Since the blood within the liver has not been washed out completely before taking the tissue samples, the measured signal might be slightly influenced by the tracer concentration in the blood. The question of specific liver uptake could be addressed in further experiments by using tracers with longer-lived isotopes for measuring late-stage accumulation after complete blood clearance.

In addition, the accumulation in the spleen (e.g. by uptake in macrophages) was less pronounced in the case of the copolymer **^{18}F-P4***. These results are indicating that the incorporation of the hydrophobic lauryl methacrylate segment holds a considerable impact on the biodistribution and especially on recognition mechanisms of the reticuloendothelial system (RES). By avoiding an increased uptake of the polymers by the cells of the MPS or by minimizing the renal filtration processes, the presence in the blood stream can be significantly enhanced. The feature of a high long-lasting blood concentration is of high importance as a long-term uptake into a tumor or other organs of interest depends mainly on the plasma concentration of the drug.

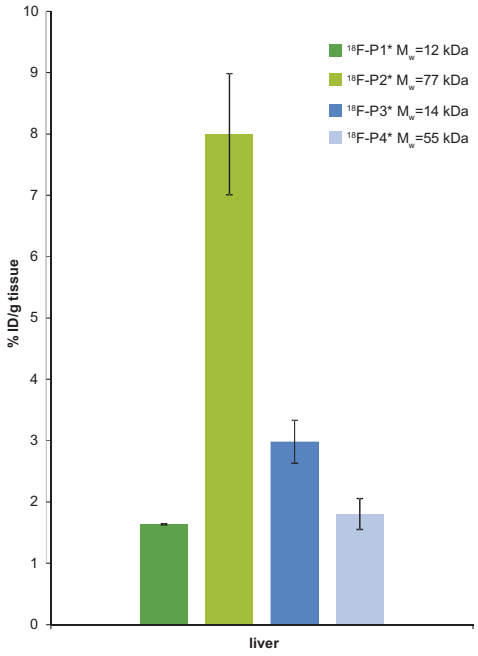

Figure 2: *Liver uptake of* ***^{18}F-P1* - ^{18}F-P4*** *in dependency of their molecular weight and polymer architecture 2 h p.i. expressed as % ID/g tissue*

Furthermore it was tested whether ^{18}F-labeling of polymers cannot only be used for body distribution studies *ex vivo* but also for imaging and quantification of the compound's uptake into tumors. For this purpose, tumor-bearing rats (AT1) were used, the tumor cell line was implanted subcutaneously on the hind food dorsum. The polymer was taken up into the tumor tissue, however, only to a very low amount. Despite the considerably higher concentration found for the copolymer systems in the blood pool 2 h p.i., no significant differences in tumor uptake was observed for all polymers tested. In fact, the concentration in tumor tissue was only marginally higher than in the reference tissue (testis) in the field of view. Lammers et al. [39] reported for the same tumor model a much higher tumor uptake for large polymers (molecular weight 65 kDa) over a period of 168 h. Since in the present study only an observation period of 2 hours was used (due to the short half-life of ^{18}F) the results are not directly comparable. Besides, the fact that during 168 h AT1 tumors are markedly growing which leads to a visual overestimation of polymer uptake in the images, the elimination (renal or liver / bile) of the polymer used by Lammers et al. seems to be much lower resulting in a longer persistance of the polymer in the circulation. However, the uptake in the lung described by Lammers et al. [39] was not seen with any of the polymers in the present study (Fig. 1) and cannot be explained at present.

3.6 *In vivo* stability of polymer-radionuclide binding

Using radiolabeling to trace polymeric architectures *in vivo,* metabolic stability of the radiolabel should be high. Loss of the radiolabel from the polymer due to radiolysis or enzymatic dehalogenation might lead to false estimation of accumulation patterns or to undesirable accumulation in sensitive tissues, as in

the case of iodine which accumulates in the thyroid [39, 55], limiting diagnostic imaging e.g. with high gamma energy emitting ^{131}I. To study whether low molecular weight radioactive byproducts are present in the blood, blood samples were taken 140 min p.i. and blood plasma was analyzed using SEC. As shown in Figure 3 for random copolymer **^{18}F-P4*** the SEC chromatogram comprised only one radioactive fraction of high molecular weight, indicating that the radioactivity remains associated with the polymers over a time period of more than 2 h.

3.7 µPET imaging

In addition to the biodistribution, differences in the pharmacokinetics of the various polymeric structures were visualized using µPET as non-invasive method with high spatial resolution. Therefore dynamic PET images were obtained over 120 min after i.v. injection of the labeled polymers. Representative whole body µPET images of both radiolabeled homopolymer systems of low and high molecular weight are shown in Fig. 4.

µPET images of low molecular weight homopolymer **^{18}F-P1*** (12 kDa) reveals that after 2 h almost the entire radioactivity localizes in kidneys and bladder (Fig. 4A) whereas accumulation in other organs was barely visible. In correspondence with the biodistribution data obtained (Fig. 1A), µPET imaging of homopolymer **^{18}F-P1*** precisely identifies a renal clearance as expected for a hydrophilic polymeric system of 12 kDa being below the renal threshold for HPMA copolymers (M_w < 40 kDa) [45].

In contrast, whole-body µPET images of the high molecular weight homopolymer **^{18}F-P2*** (77 kDa) demonstrate enrichment predominant in liver and spleen (Fig. 4B), thereby again reflecting the findings of the biodistribution experiments. Despite the high molecular weight of 77 kDa (above the renal excretion threshold), small amounts of radioactivity can still be found in the kidneys but excretion via the bladder was extremely slow. The µPET images obtained for **^{18}F-P1*** and **^{18}F-P2*** are demonstrated in Fig.4.

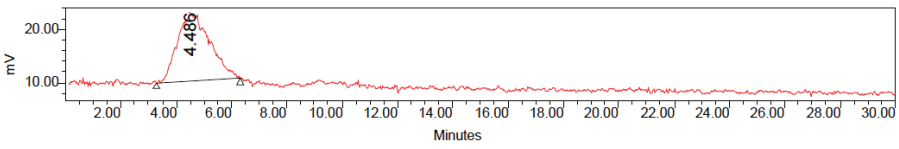

Figure 3: *Sephadex G-25 chromatography of a blood plasma sample taken 140 min p.i. of the random copolymer* ***^{18}F-P4**** *showing only one radioactive fraction of high molecular weight.*

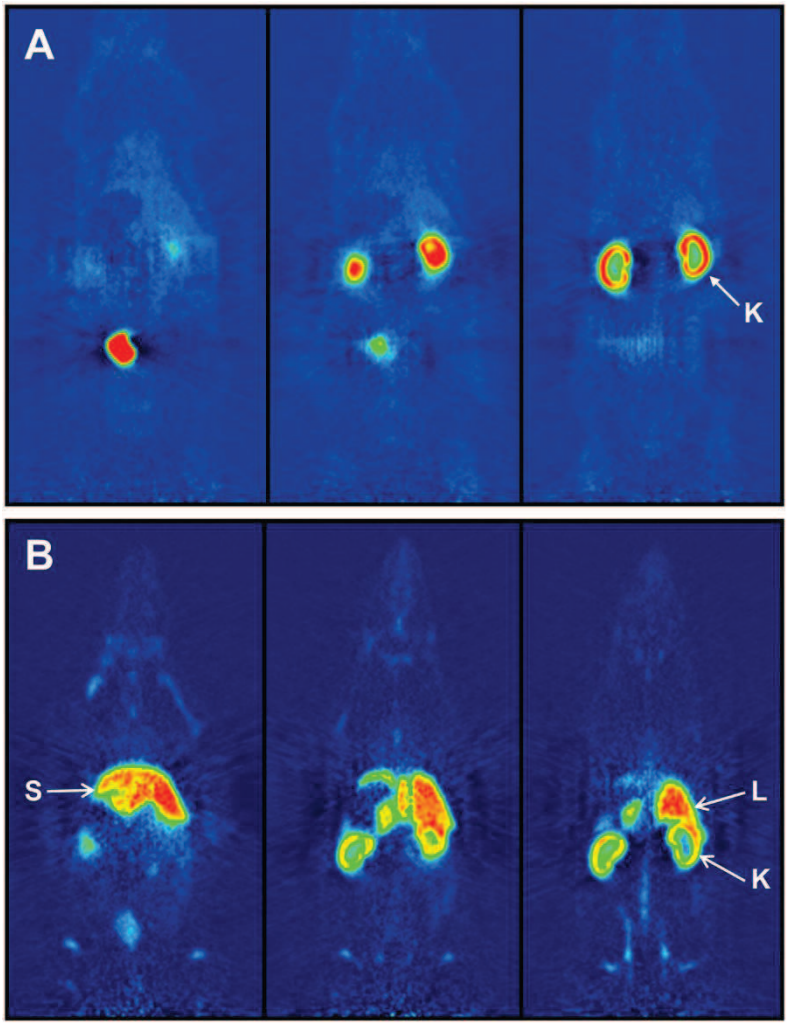

Figure 4: *µPET imaging of ^{18}F-labeled homopolymers. Representative coronar µPET summed images in different depths 120-135 min after i.v. injection. (A) M_w= 12 kDa homopolymer* ***^{18}F-P1**** *showing kidney elimination (K). (B) M_w= 77 kDa homopolymer* ***^{18}F-P2**** *indicating accumulation in liver (L), spleen (S) and kidneys (K).*

In contrast, imaging the distribution pattern of the large HPMA-*ran*-LMA copolymer **^{18}F-P4*** *in vivo*, it clearly shows a reduced liver uptake (which is in good correspondence to the biodistribution experiments) (Fig. 5) as compared to the large homopolymer (Fig. 4B).

Elimination of **^{18}F-P4*** via the kidneys is comparable to the high molecular weight homopolymer **^{18}F-P2*.** In contrast to the homopolymer, the retention of the copolymer in the circulation (blood compartment) 2 h post injection is much higher (Fig. 5, heart, aorta), already indicated by the biodistribution measurement.

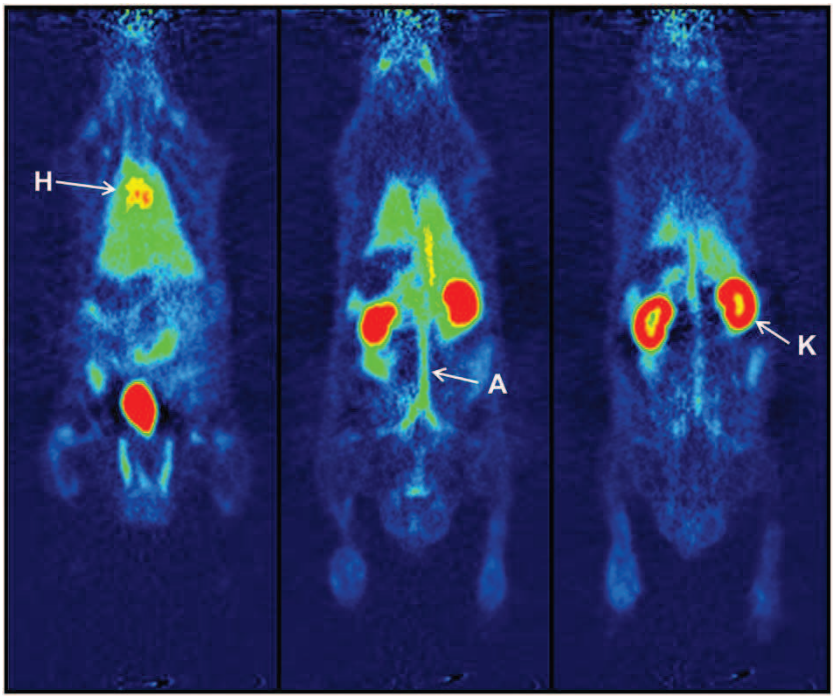

Figure 5: *Representative coronar µPET images of HPMA-ran-LMA copolymer* ^{18}***F-P4**** *(55 kDa) 2 h after i.v. injection. The images show accumulation in kidneys (K) and bladder as well as remaining activity in the blood (heart (H); aorta (A)).*

4. Conclusion

In this study we could demonstrate that the introduction of a radioactive probe allows systematic insights into the correlation between chemical structure and biodistribution of HPMA based polymers of different M_w. In our case we compared homopolymers *vs.* random copolymers exhibiting lauryl methacrylate as hydrophobic segment. As stability of the polymers could be ensured, the results emphasize the special benefit of introducing a radioactive label, in particular when applying positron emission tomography, PET. It enables a precise tracing of the different polymer architectures in the organism and thereby gaining detailed knowledge about structure-property relationships of the polymers influencing their early-phase organ accumulation. The differing structures (**P1*** and **P2*** homopolymers *vs.* **P3*** and **P4*** random copolymers) had a major impact on the biodistribution pattern in the living organism. Our results differ from the results of Lammers [39] by the fact that the relative ratio of the accumulation in different tissue depends strongly on aggregate formation or not. Especially the retention of the high M_w homopolymer and random copolymer is quite different. Despite a large superstructure formation of the HPMA-

ran-LMA copolymers, renal clearance could still be proven and liver accumulation was comparably low. Furthermore the random copolymer **P4*** exhibited increased enrichment in the blood stream (nearly 60 % after 2 h p.i.), underlining its feasibility as model system for the design of amphiphilic transport vehicles for therapeutics *in vivo*. These results emphasize the significance of both (1) a good characterization of the polymers and their aggregates and (2) the use of *in vivo* pharmacokinetics – as it is available by PET - to evaluate the potential of biocompatible polymers as potential drug carriers.

5. Acknowledgement

The authors would like to thank Nicole Bausbacher, Bengü Yilmaz and Hans-Georg Buchholz for their support during animal studies and following interpretation. Furthermore we gratefully acknowledge Dr. Clemens K. Weiss and Elke Muth for their assistance during cmc determination measurements. We also want to thank the Max-Planck Graduate Center (MPGC, M. Allmeroth) as well as the Graduate School Materials Science in Mainz (Excellence Initiative, DFG/GSC 266, D. Moderegger) for financial support. In addition the authors are very thankful for financial support of the DFG (Rösch: RO 985/30-1; Thews: TH 482/4-1, Zentel: ZE 230/21-1) and SAMT Initiative Mainz. We also thank Prof. Helmut Ringsdorf, Prof. Dr. Ruth Duncan and Dr. Matthias Barz for stimulating discussions.

Supporting Information Available: Experimental section-including polymer synthesis, FCS and ring tensiometry setup, radioactive labeling, animal model and μPET setup. This material is available free of charge via the Internet at http://pubs.acs.org.

References

1. Duncan, R., The dawning era of polymer therapeutics. *Nat Rev Drug Discov* **2003,** 2, (5), 347-360.
2. Matsumura, Y.; Maeda, H., A New Concept for Macromolecular Therapeutics in Cancer Chemotherapy: Mechanism of Tumoritropic Accumulation of Proteins and the Antitumor Agent Smancs. *Cancer Research* **1986,** 46, (12 Part 1), 6387-6392.
3. Maeda, H.; Bharate, G. Y.; Daruwalla, J., Polymeric drugs for efficient tumor-targeted drug delivery based on EPR-effect. *European Journal of Pharmaceutics and Biopharmaceutics* **2009,** 71, (3), 409-419.
4. Ringsdorf, H., Structure and properties of pharmacologically active polymers. *Journal of Polymer Science: Polymer Symposia* **1975,** 51, (1), 135-153.

5. Obereigner, B.; Burešová, M.; Vrána, A.; Kopeček, J., Preparation of polymerizable derivatives of N-(4-aminobenzenesulfonyl)-n′-butylurea. *Journal of Polymer Science: Polymer Symposia* **1979,** 66, (1), 41-52.
6. Solovsky, M. V.; Ulbrich, K.; Kopecek, J., Synthesis of N-(2-hydroxypropyl) methacrylamide copolymers with antimicrobial activity. *Biomaterials* **1983,** 4, (1), 44-48.
7. Duncan, R.; Seymour, L. W.; O'Hare, K. B.; Flanagan, P. A.; Wedge, S.; Hume, I. C.; Ulbrich, K.; Strohalm, J.; Subr, V.; Spreafico, F.; Grandi, M.; Ripamonti, M.; Farao, M.; Suarato, A., Preclinical evaluation of polymer-bound doxorubicin. *Journal of Controlled Release* **1992,** 19, (1-3), 331-346.
8. Kopecek, J.; Kopecková, P.; Minko, T.; Lu, Z.-R., HPMA copolymer-anticancer drug conjugates: design, activity, and mechanism of action. *European Journal of Pharmaceutics and Biopharmaceutics* **2000,** 50, (1), 61-81.
9. Duncan, R., Development of HPMA copolymer-anticancer conjugates: Clinical experience and lessons learnt. *Advanced Drug Delivery Reviews* **2009,** 61, (13), 1131-1148.
10. Kataoka, K.; Harada, A.; Nagasaki, Y., Block copolymer micelles for drug delivery: design, characterization and biological significance. *Advanced Drug Delivery Reviews* **2001,** 47, (1), 113-131.
11. Gaucher, G.; Dufresne, M.-H.; Sant, V. P.; Kang, N.; Maysinger, D.; Leroux, J.-C., Block copolymer micelles: preparation, characterization and application in drug delivery. *Journal of Controlled Release* **2005,** 109, (1-3), 169-188.
12. Barz, M.; Luxenhofer, R.; Zentel, R.; Kabanov, A. V., The uptake of N-(2-hydroxypropyl)-methacrylamide based homo, random and block copolymers by human multi-drug resistant breast adenocarcinoma cells. *Biomaterials* **2009,** 30, (29), 5682-5690.
13. Talelli, M.; Rijcken, C. J. F.; van Nostrum, C. F.; Storm, G.; Hennink, W. E., Micelles based on HPMA copolymers. *Advanced Drug Delivery Reviews* **2010,** 62, (2), 231-239.
14. Duncan, R.; Gac-Breton, S.; Keane, R.; Musila, R.; Sat, Y. N.; Satchi, R.; Searle, F., Polymer-drug conjugates, PDEPT and PELT: basic principles for design and transfer from the laboratory to clinic. *Journal of Controlled Release* **2001,** 74, (1-3), 135-146.
15. Vicent, M. J.; Greco, F.; Nicholson, R. I.; Paul, A.; Griffiths, P. C.; Duncan, R., Polymer Therapeutics Designed for a Combination Therapy of Hormone-Dependent Cancer. *Angewandte Chemie International Edition* **2005,** 44, (26), 4061-4066.
16. Greco, F.; Vicent, M. J., Combination therapy: Opportunities and challenges for polymer-drug conjugates as anticancer nanomedicines. *Advanced Drug Delivery Reviews* **2009,** 61, (13), 1203-1213.
17. Duncan, R.; Vicent, M. J., Do HPMA copolymer conjugates have a future as clinically useful nanomedicines? A critical overview of current status and future opportunities. *Advanced Drug*

Delivery Reviews **2010,** 62, (2), 272-282.

18. Lammers, T.; Subr, V.; Ulbrich, K.; Hennink, W. E.; Storm, G.; Kiessling, F., Polymeric nanomedicines for image-guided drug delivery and tumor-targeted combination therapy. *Nano Today* **2010,** 5, (3), 197-212.
19. Lammers, T.; Kiessling, F.; Hennink, W. E.; Storm, G., Nanotheranostics and Image-Guided Drug Delivery: Current Concepts and Future Directions. *Molecular Pharmaceutics* **2010,** 7, (6), 1899-1912.
20. Herth, M. M.; Barz, M.; Moderegger, D.; Allmeroth, M.; Jahn, M.; Thews, O.; Zentel, R.; Rösch, F., Radioactive Labeling of Defined HPMA-Based Polymeric Structures Using [18F]FETos for In Vivo Imaging by Positron Emission Tomography. *Biomacromolecules* **2009,** 10, (7), 1697-1703.
21. Herth, M. M.; Barz, M.; Jahn, M.; Zentel, R.; Rösch, F., 72/74As-labeling of HPMA based polymers for long-term in vivo PET imaging. *Bioorganic & Medicinal Chemistry Letters* **2010,** 20, (18), 5454-5458.
22. Pimm, M. V.; Perkins, A. C.; Strohalm, J.; Ulbrich, K.; Duncan, R., Gamma Scintigraphy of the Biodistribution of 123I-Labelled N-(2-Hydroxypropyl) methacrylamide Copolymer-Doxorubicin Conjugates in Mice with Transplanted Melanoma and Mammary Carcinoma. *Journal of Drug Targeting* **1996,** 3, (5), 375-383.
23. Mitra, A.; Nan, A.; Ghandehari, H.; McNeil, E.; Mulholland, J.; Line, B., Technetium-99m-Labeled N-(2-Hydroxypropyl) Methacrylamide Copolymers: Synthesis, Characterization, and in Vivo Biodistribution. *Pharmaceutical Research* **2004,** 21, (7), 1153-1159.
24. Šprincl, L.; Exner, J.; Štěrba, O.; Kopeček, J., New types of synthetic infusion solutions. III. Elimination and retention of poly-[N-(2 hydroxypropyl) methacrylamide] in a test organism. *Journal of Biomedical Materials Research* **1976,** 10, (6), 953-963.
25. Minko, T.; Kopecková, P.; Pozharov, V.; Kopecek, J., HPMA copolymer bound adriamycin overcomes MDR1 gene encoded resistance in a human ovarian carcinoma cell line. *Journal of Controlled Release* **1998,** 54, (2), 223-233.
26. Kopecek, J.; Kopecková, P., HPMA copolymers: Origins, early developments, present, and future. *Advanced Drug Delivery Reviews* **2010,** 62, (2), 122-149.
27. Barz, M.; Luxenhofer, R.; Zentel, R.; Vicent, M. J., Overcoming the PEG-addiction: well-defined alternatives to PEG, from structure-property relationships to better defined therapeutics. *Polymer Chemistry* **2011**.
28. Kopecek, J., Soluble biomedical polymers. *Polim. Med.* **1977,** 7, 191-221.
29. Kopecek, J.; Bazilová, H., Poly[N-(2 hydroxypropyl) methacrylamide]--I. Radical polymerization and copolymerization. *European Polymer Journal* **1973,** 9, (1), 7-14.
30. Rathi, R. C.; Kopečková, P.; Říhová, B.; Kopeček, J., N-(2-hydroxypropyl)

methacrylamide copolymers containing pendant saccharide moieties: Synthesis and bioadhesive properties. *Journal of Polymer Science Part A: Polymer Chemistry* **1991,** 29, (13), 1895-1902.

31. Ulbrich, K.; Subr, V.; Strohalm, J.; Plocová, D.; Jelínková, M.; Ríhová, B., Polymeric drugs based on conjugates of synthetic and natural macromolecules: I. Synthesis and physico-chemical characterisation. *Journal of Controlled Release* **2000,** 64, (1-3), 63-79.
32. Seymour, L. W.; Duncan, R.; Strohalm, J.; Kopeček, J., Effect of molecular weight (Mw) of N-(2-hydroxypropyl) methacrylamide copolymers on body distribution and rate of excretion after subcutaneous, intra-peritoneal, and intravenous administration to rats. *Journal of Biomedical Materials Research* **1987,** 21, (11), 1341-1358.
33. Chiefari, J.; Chong, Y.K.; Ercole, F.; Krstina, J.; Jeffery, J.; Le, T.; Mayadunne, R.; Meijs, G.; Moad, C.; Moad, G.; Rizzardo, E.; Thang, S.H., Living Free-Radical Polymerization by Reversible Addition-Fragmentation Chain Transfer: The RAFT Process. *Macromolecules* **1998,** 31, 5559-5562.
34. G. Moad, E. R., S. H. Thang, Living Radical Polymerization by the RAFT process. *Aust. J. Chem.* **2005,** 58, 379-410.
35. Matyjaszewski, K.; Xia, J., Atom Transfer Radical Polymerization. *Chemical Reviews* **2001,** 101, (9), 2921-2990.
36. Scales, C. W.; Vasilieva, Y. A.; Convertine, A. J.; Lowe, A. B.; McCormick, C. L., Direct, Controlled Synthesis of the Nonimmunogenic, Hydrophilic Polymer, Poly(N-(2-hydroxypropyl)methacrylamide) via RAFT in Aqueous Media *Biomacromolecules* **2005,** 6, (4), 1846-1850.
37. Gauthier, M. A.; Gibson, M. I.; Klok, H.-A., Synthesis of Functional Polymers by Post-Polymerization Modification. *Angewandte Chemie International Edition* **2009,** 48, (1), 48-58.
38. Maeda, H.; Wu, J.; Sawa, T.; Matsumura, Y.; Hori, K., Tumor vascular permeability and the EPR effect in macromolecular therapeutics: a review. *Journal of Controlled Release* **2000,** 65, (1-2), 271-284.
39. Lammers, T.; Kühnlein, R.; Kissel, M.; Subr, V.; Etrych, T.; Pola, R.; Pechar, M.; Ulbrich, K.; Storm, G.; Huber, P.; Peschke, P., Effect of physicochemical modification on the biodistribution and tumor accumulation of HPMA copolymers. *Journal of Controlled Release* **2005,** 110, (1), 103-118.
40. Julyan, P. J.; Seymour, L. W.; Ferry, D. R.; Daryani, S.; Boivin, C. M.; Doran, J.; David, M.; Anderson, D.; Christodoulou, C.; Young, A. M.; Hesslewood, S.; Kerr, D. J., Preliminary clinical study of the distribution of HPMA copolymers bearing doxorubicin and galactosamine. *Journal of Controlled Release* **1999,** 57, (3), 281-290.
41. L. W. Seymour, D. R. F., D. J. Kerr, D. Rea, M. Whitlock, R. Poyner, C. Boivin, S. Hesslewood, C. Twelves, R. Blackie, A. Schatzlein, D. Jodrell, D. Bissett, H. Calvert, M. Lind, A. Robbins, S.

Burtles, R. Duncan, J. Cassidy, Phase II studies of polymer-doxorubicin (PK1, FCE28068) in the treatment of breast, lung and colorectal cancer. *Int. J. Oncol.* **2009,** 34, 1629-1636.

42. M. Hemmelmann, C. K., U. Schmitt,*; M. Allmeroth, D. M., M. Barz,; K. Koynov, C. H., F. Rösch, R. Zentel*, HPMA based amphiphilic copolymers mediate central nervous effects of domperidone. *Macromolecular Rapid Communications* **2011,** 32(9-10):712-7
43. Workman P, T. P., Balkwill F, Balmain A, Chaplin DJ, Double JA et al. , United Kingdom Co-ordinating Committee on Cancer Research (UKCCCR), Guidelines for the Welfare of Animals in Experimental Neoplasia (2nd edit.). *Br J Cancer* **1998**, (77), 1-10.
44. Boyer, C.; Bulmus, V.; Davis, T. P.; Ladmiral, V.; Liu, J.; Perrier, S. b., Bioapplications of RAFT Polymerization. *Chemical Reviews* **2009,** 109, (11), 5402-5436.
45. Seymour, L. W.; Miyamoto, Y.; Maeda, H.; Brereton, M.; Strohalm, J.; Ulbrich, K.; Duncan, R., Influence of molecular weight on passive tumour accumulation of a soluble macromolecular drug carrier. *European Journal of Cancer* **1995,** 31, (5), 766-770.
46. Eberhardt, M.; Mruk, R.; Zentel, R.; Théato, P., Synthesis of pentafluorophenyl(meth)acrylate polymers: New precursor polymers for the synthesis of multifunctional materials. *European Polymer Journal* **2005,** 41, (7), 1569-1575.
47. Theato, P., Synthesis of well-defined polymeric activated esters. *Journal of Polymer Science Part A: Polymer Chemistry* **2008,** 46, (20), 6677-6687.
48. Brandrup, J.; Immergut, E. H.; Grulke, E. A.; Abe, A.; Bloch, D. R., Polymer Handbook (4th Edition). In John Wiley & Sons.
49. Perrier, S.; Takolpuckdee, P.; Mars, C. A., Reversible Addition-Fragmentation Chain Transfer Polymerization:End Group Modification for Functionalized Polymers and Chain Transfer Agent Recovery. *Macro-molecules* **2005,** 38, (6), 2033-2036.
50. Lee, H. B.; Blaufox, M. D., Blood Volume in the Rat. *J Nucl Med* **1985,** 26, (1), 72-76.
51. Yu, K.; Eisenberg, A., Bilayer Morphologies of Self-Assembled Crew-Cut Aggregates of Amphiphilic PS-b-PEO Diblock Copolymers in Solution. *Macromolecules* **1998,** 31, (11), 3509-3518.
52. Trappmann, B.; Ludwig, K.; Radowski, M. R.; Shukla, A.; Mohr, A.; Rehage, H.; Böttcher, C.; Haag, R., A New Family of Nonionic Dendritic Amphiphiles Displaying Unexpected Packing Parameters in Micellar Assemblies. *Journal of the American Chemical Society* **2010,** 132, (32), 11119-11124.
53. Owens Iii, D. E.; Peppas, N. A., Opsonization, biodistribution, and pharmacokinetics of polymeric nanoparticles. *International Journal of Pharmaceutics* **2006,** 307, (1), 93-102.
54. Ulbrich, K.; Subr, V., Structural and chemical aspects of HPMA copolymers as drug carriers. *Advanced Drug*

Delivery Reviews **2010,** 62, (2), 150-166.

55. Wilbur, D. S., Radiohalogenation of proteins: An overview of radionuclides, labeling methods and reagents for conjugate labeling. *Bioconjugate Chemistry* **1992,** 3, (6), 433-470.

Supplementary information to Manuscript 5.1

Modifying the body distribution of HPMA based copolymers as potential drug carriers by molecular weight and aggregate formation

Mareli Allmeroth[1, §], [redacted]

Contents

1. Experimental section

I. Synthesis of 4-cyano-4-((thiobenzoyl)sulfanyl)pentanoic acid (CTP)

4-cyano-4-((thiobenzoyl)sulfanyl)pentanoic acid was used as chain transfer agent (CTA) and synthesized according to the literature [1].

II. Synthesis of pentafluorophenyl methacrylate (PFPMA)

Pentafluorophenyl methacrylate was prepared according to reference [2].

III. Synthesis of reactive ester homopolymers

RAFT polymerization of pentafluorophenyl methacrylate with 4-cyano-4-((thiobenzoyl) sulfanyl)pentanoic acid was carried out in a schlenk tube [3, 4]. For this purpose, 4 g of PFPMA were dissolved in 5 mL of absolute dioxane, furthermore CTP and AIBN were added. The molar ratio of CTP/AIBN was chosen 8:1. After three freeze-vacuum-thaw cycles, the mixture was immersed in an oil bath at 65 °C and stirred over night. Afterwards, the polymeric solution was precipitated three times in hexane, centrifuged and dried under vacuum at 40 °C over night. A slightly pink powder was obtained. Yield: 52 %. ^{1}H-NMR (300 MHz, $CDCl_3$) δ/ ppm: 1.20-1.75 (br), 2.00-2.75 (br s). ^{19}F-NMR (400 MHz, $CDCl_3$) δ/ ppm: -162.03 (br), -156.92 (br), -152 to -150 (br).

IV. Synthesis of random copolymers

RAFT polymerization of PFPMA with lauryl methacrylate (LMA) by help of CTP was performed in a schlenk tube as well. As an example, 4 g of PFPMA dissolved in 5 mL dioxane, lauryl methacrylate, AIBN and CTP were mixed. The molar ratio of CTP/AIBN was chosen to be 8:1. After three freeze-vacuum-thaw cycles, the mixture was immersed in an oil bath at 65 °C and stirred over night. Afterwards, poly(PFPMA)-*ran*-poly(LMA) was precipitated three times in hexane, centrifuged and dried under vacuum at 40 °C over night. A slightly pink powder was obtained. Yield: 54 %. ^{1}H-NMR (300 MHz, $CDCl_3$) δ/ ppm: 0.84 (br t), 1.20-1.75 (br), 2.00-2.75 (br s). ^{19}F-NMR (400 MHz, $CDCl_3$) δ/ ppm: -162.01 (br), -156.95 (br), -152 to -150 (br).

V. Removal of dithioester endgroups

The dithiobenzoate endgroup was removed using the protocol reported by Perrier et al. 2005 [5]. Therefore a 25-fold molar excess of AIBN was added to the polymer dissolved in

dioxane. After four hours of heating the solution in an oil bath at 70 °C, the polymer was precipitated twice in hexane and collected by centrifugation. The polymer was dried under vacuum over night, a colorless powder was obtained. Yield: 75 %. Removal of the dithioester endgroup could be proven by UV-Vis spectroscopy.

VI. Polymer analogous reaction of homopolymers

Depending on the labeling technique necessary, either for a fluorescent or radioactive marker, two different routes were applied. For subsequent radioactive labeling, the protocol was carried out as follows. As example, 100 mg of the polymeric precursor (M_n = 18000 g/mol) were diluted in 2 mL of absolute dioxane. 5 mg of tyramine, diluted in a DMSO/dioxane mixture, and 10 mg of triethylamine were added. After stirring for four hours at 35 °C, 30 mg of 2-hydroxypropylamine as well as 40 mg of triethylamine were added and the solution was stirred over night. For final removal of reactive ester side groups, further 30 mg of 2-hydroxypropylamine were added the next morning. The solution was precipitated two times in diethyl ether, centrifuged and finally dissolved in a DMSO/water solution for dialysis. After lyophilization a white powder could be obtained. Yield: 79 %. ^{1}H-NMR (400 MHz, d. DMSO) δ/ ppm: 0.60-1.40 (br), 1.45-2.20 (br), 2.75-3.10 (br), 3.50-3.80 (br), 4.60-4.80 (br), 6.60-6.70 (br) and 6.85-7.00 (br). For additional fluorescent labeling, the fluorescent marker Oregon Green 488 cadaverine was used. 100 mg of polymeric precursor were diluted in 2 mL of absolute dioxane and 2.75 mg of Oregon Green 488 cadaverine added. Afterwards tyramine and 2-hydroxypropylamine were added, as described by the procedure above.

VII. Polymer analogous reaction of random copolymers

For radioactive labeling of random copolymers the protocol was applied as follows. 100 mg of poly(PFPMA)-*ran*-poly(LMA) copolymer was dissolved in 2 mL of absolute dioxane. As example, for the polymeric system **P3*-R** (M_n= 17000 g/mol) 5 mg of tyramine and 10 mg of triethylamine were diluted in a DMSO/dioxane mixture and added to the vessel. After stirring for four hours at 35 °C, 30 mg of 2-hydroxypropylamine as well as 40 mg of triethylamine were added and the solution stirred over night. For final removal of reactive ester side groups further 30 mg of 2-hydroxypropylamine were added the next morning. The solution was precipitated two times in diethyl ether, centrifuged and finally dissolved in a DMSO/water solution for dialysis. After lyophilization a white

powder could be obtained. Yield: 51 %. ^{1}H-NMR (400 MHz, d. DMSO) δ/ ppm: 0.70-0.90 (br), 0.90-1.40 (br), 1.40-1.90 (br), 2.75-3.10 (br), 3.50-3.80 (br), 4.50-4.75 (br), 6.60-6.75 (br) and 6.85-7.00 (br). For additional fluorescent labeling, 100 mg of polymeric precursor were diluted in 2 mL of absolute dioxane and 2.9 mg of Oregon Green 488 cadaverine were added. Afterwards tyramine and 2-hydroxypropylamine were added, as described by the procedure above.

VIII. Analytical data obtained in isotonic NaCl solution

Isotonic NaCl solution 0.9 % was obtained by B. Braun Melsungen AG without any purification. Stock solutions were prepared using 1 % of absolute DMSO in isotonic sodium chloride solution.

IX. Critical micelle concentration (cmc) determination by Ring Tensiometry

Cmc determination was accomplished by using the ring tensiometer DCAT 21 of Dataphysics Instruments, Filderstadt. For this purpose, a stock solution of 2 mg polymer/ 20 mL of sodium chloride solution was prepared and stirred for 3 days. By calculation of the SCAT software, version 2.8.1.77, the polymer solution was added dropwise to a known volume of NaCl in a vessel via a Hamilton microsyringe. The temperature in the vessel was kept at 37 °C (± 0.1 °C), maintained by a thermostat. The ring was cleaned by heating in a gas flame. Analysis of the obtained data was carried out by using the software mentioned above and additional plotting with OriginPro Version 8.

X. Size determination by Fluorescence Correlation Spectroscopy (FCS)

The hydrodynamic radii of the polymeric systems were determined by Fluorescence Correlation Spectroscopy using a commercial FCS setup (Zeiss, Germany) consisting of the module ConfoCor 2 and an inverted microscope model Axiovert 200 with a Zeiss C-Apochromat 40 ×/1.2 W water immersion objective. The fluorophores were excited with an Argon laser (λ = 488 nm) and the emission was collected after filtering with a LP505 long pass filter. For detection, an avalanche photodiode, enabling single-photon counting, was used. As sample cell, eight-well, polystyrene-chambered cover glass (Laboratory-Tek, Nalge Nunc International) was applied. For sample preparation, stock solutions of 1 mg fluorescently labeled polymer/mL NaCl were applied, diluted to a final concentration

of 0.1 mg/mL. The solution was kept at room temperature over night. For reference reason, free Oregon Green 488 cadaverine dye in NaCl-solution was also studied. The calibration of the FCS observation volume was done using a dye with known diffusion coefficient, i.e. Rhodamine6 G. For each solution, 5 measurement cycles with a total duration of 150 seconds were applied. Time dependant fluctuations of the fluorescence intensity δI(t) were detected and evaluated by autocorrelation analysis, yielding the diffusion coefficient and hydrodynamic radius of the fluorescent species [6].

XI. Synthesis of [^{18}F]FETos

To an aqueous [^{18}F]fluoride solution (2-8 GBq) 18 mg Kryptofix®2.2.2., potassium carbonate (1 N, 15 µL) and 1 mL acetonitrile were added. The mixture was dried in a stream of nitrogen at 80 °C, the drying procedure was repeated three times. To the dried residue 13 mg of ethyleneglycol-1,2-ditosylate in 1 mL acetonitrile was added and heated under stirring in a sealed vial at 88 °C for 3 min. Purification of the crude product was accomplished using HPLC (Lichrosphere RP18-EC5, 250×10 mm, acetonitrile/water 50:50, flow rate: 5 mL/min, t_R: 8 min). After diluting the HPLC fraction of 2-[^{18}F]fluoroethyl-1-tosylate with water, the product was loaded on a Sep-Pak C18 cartridge, dried with a nitrogen stream and eluted with 0.8 mL of DMSO [7].

XII. Radiolabeling of polymers using [^{18}F]FETos and purification for *ex vivo* and *in vivo* experiments

For radiolabeling, 3 mg of the polymeric precursor were dissolved in 200 µL of dried DMSO. The solution was transferred to a sealed vial and 1 µL of a 5 N sodium hydroxide solution was added. The labeling reaction was started by adding the previously eluted DMSO solution of 2-[^{18}F]fluoroethyl-1-tosylate and the mixture was stirred for 15 min at 120 °C.

For *ex vivo* and *in vivo* experiments, the radiolabeled polymeric systems were freed from low molecular weight byproducts by Sephadex G-25 size exclusion chromatography (HiTrap™ Desalting Column, Sephadex G-25 Superfine, 0.9 % NaCl, flow rate: 0.5 mL/min) leading to a pure, ^{18}F-labeled polymer solution ready for subsequent experiments [8].

XIII. Tumor and animal model

AT1 R3327 prostate carcinoma cells were grown in RPMI medium supplemented with 10 % fetal calf serum (FCS) at 37 °C under a humidified 5 % CO_2 atmosphere and sub cultivated once per week. For *in vivo* experiments male Copenhagen rats (Charles River Wiga, Sulzfeld, Germany; body weight 180 to 300 g), housed in the animal care facility of the University of Mainz, were used. Animals were allowed access to food and acidified water *ad libitum* before the investigation. Solid carcinomas were heterotopically induced by injection of cells (0.4 mL, approximately 10^4 cells/µL) subcutaneously into the dorsum of the hind foot. Tumors grew as flat, spherical segments and replaced the subcutis and corium completely. Volumes were determined by measuring the three orthogonal diameters (d) of the tumors and using an ellipsoid approximation with the formula: $V = d_1 \times d_2 \times d_3 \times \pi/6$. Tumors were used when they reached a volume of between 1.0 to 2.0 mL approx. 8 to 14 days after tumor cell inoculation.

XIV. Small animal PET studies

For *in vivo* imaging, the radiolabeled polymers were injected into tumor bearing rats. Therefore the animals were anaesthetized with pentobarbital (40 mg/kg, i.p., Narcoren, Merial, Hallbergmoos, Germany). PET imaging was performed on a µPET Focus 120 small animal PET (Siemens/Concorde, Knoxville, USA). During PET measurements the animals were placed in supine position and breathed room air spontaneously. After a 15 min transmission scan with an external ^{57}Co source, dynamic PET studies were acquired in 2D mode. The radiolabeled polymer was administered as a bolus injection via the tail vein with a mean activity of 23.3 ± 1.6 MBq. Afterwards, dynamic PET images were obtained for a total measuring interval of 120 min. Finally, a whole body scan (120-135 min post injection) was performed. For quantitative analysis, the PET listmode data were histogrammed into 20 frames with varying time frames (3-10 min) and reconstructed using OSEM algorithm. µPET image quantification was applied using PMOD software (PMOD Technologies Ltd.).

2. References

1. G. Moad, E. R., S. H. Thang, Living Radical Polymerization by the RAFT process. *Aust. J. Chem.* **2005,** 58, 379-410.
2. Eberhardt, M.; Mruk, R.; Zentel, R.; Théato, P., Synthesis of pentafluorophenyl(meth)acrylate polymers: New precursor polymers for the synthesis of multifunctional materials. *European Polymer Journal* **2005,** 41, (7), 1569-1575.
3. Theato, P., Synthesis of well-defined polymeric activated esters. *Journal of Polymer Science Part A: Polymer Chemistry* **2008,** 46, (20), 6677-6687.
4. Barz, M.; Luxenhofer, R.; Zentel, R.; Kabanov, A. V., The uptake of N-(2-hydroxypropyl)-methacrylamide based homo, random and block copolymers by human multi-drug resistant breast adenocarcinoma cells. *Biomaterials* **2009,** 30, (29), 5682-5690.
5. Perrier, S. b.; Takolpuckdee, P.; Mars, C. A., Reversible Addition-Fragmentation Chain Transfer Polymerization:End Group Modification for Functionalized Polymers and Chain Transfer Agent Recovery. *Macromolecules* **2005,** 38, (6), 2033-2036.
6. Rigler, R. E., E.S., Fluorescence Correlation Spectroscopy. *Springer Verlag* **New York 2001**.
7. Bauman, A.; Piel, M.; Schirrmacher, R.; Rösch, F., Efficient alkali iodide promoted 18F-fluoroethylations with 2-[18F]fluoroethyl tosylate and 1-bromo-2-[18F]fluoroethane. *Tetrahedron Letters* **2003,** 44, (51), 9165-9167.
8. Herth, M. M.; Barz, M.; Moderegger, D.; Allmeroth, M.; Jahn, M.; Thews, O.; Zentel, R.; Rösch, F., Radioactive Labeling of Defined HPMA-Based Polymeric Structures Using [18F]FETos for In Vivo Imaging by Positron Emission Tomography. *Biomacromolecules* **2009,** 10, (7), 1697-1703.

This material is available free of charge via the Internet at http://pubs.acs.org.

5.2 Structure and size of HPMA-based polymers decide on tumor accumulation but the tumor model makes a difference: A quantitative *in vivo* PET study

Mareli Allmeroth*[1],

[redacted]

[redacted]

[1] *Institute of Organic Chemistry, Johannes Gutenberg University, Mainz, Germany*

[redacted]

Angewandte Chemie, in preparation

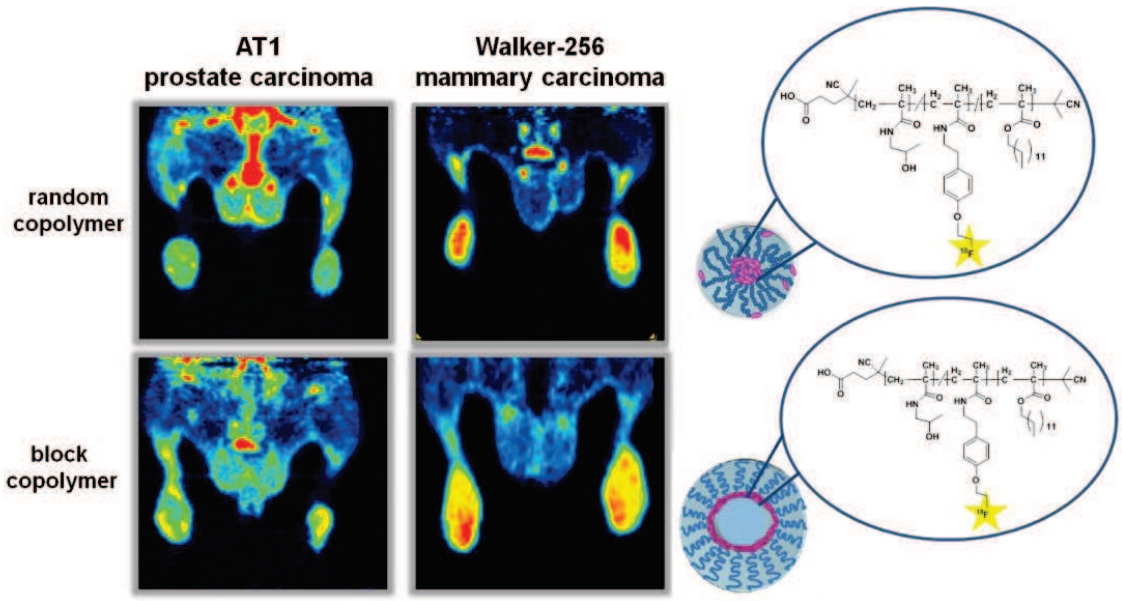

Abstract

Polymeric drug carriers aim to selectively target tumors in combination with protecting normal tissue. In this regard polymer structure and molecular weight are key factors considering organ distribution as well as tumor accumulation of the polymeric drug delivery system. In the present study six different HPMA-based polymer structures (homopolymers, random as well as block copolymers with lauryl methacrylate as hydrophobic group) varying in molecular weight, size and resulting architecture were analyzed in two different tumor models (AT1 prostate carcinoma and Walker 256 mammary carcinoma) *in vivo*. Polymers were labeled with ^{18}F and organ / tumor uptake was followed by *ex vivo* biodistribution as well as *in vivo* μPET imaging. Vascular permeability was measured by dextran extravasation and cell uptake, determined *in vitro* using fluorescence-labeled polymers. Most strikingly, the high molecular weight HPMA-*ran*-LMA copolymer demonstrated highest tumor uptake and blood pool concentration. Obviously the molecular structure (e.g. amphiphilicity) is holding a higher impact on desired *in vivo* properties than polymer size. The results also revealed pronounced differences between the tumor models although vascular permeability was comparable. Accumulation in Walker-256 carcinomas was much higher, presumably due to a better cellular uptake of the polymers in these tumor cells (determined by kinetic cell culture experiments). These investigations clearly indicate that the properties of the individual tumor determine the suitability of polymeric drug carriers. The findings also illustrate the general necessity of a pre-clinical screening to analyze polymer uptake for each individual patient (e.g. by non-invasive imaging) in order to individualize polymer-based chemotherapy.

Keywords: HPMA, fluorine-18 labeling, PET, AT1 Dunning prostate carcinoma R3327, Walker 256 mammary carcinoma, structure- property relationship

1. Introduction

"Polymer therapeutics" [1] are a promising approach for anticancer treatment. The great benefit of polymer based drug delivery systems consists in a decrease of toxic side effects of the chemotherapeutic agent in healthy tissue, an accumulation in the tumor due to the EPR effect [2] and a longer blood circulation time compared to the pure anticancer drug. In this regard poly-*N*-(2-hydroxypropyl)methacrylamide (HPMA) – being non-toxic, non-immunogenic and biocompatible - is holding favorable polymer characteristics for preclinical as well as clinical testing [3-7].

The body distribution of macromolecular therapeutics may not only be affected by specific characteristics of the polymer system such as molecular weight, architecture, lipophilicity or the capability of forming superstructures (resulting in larger diameters). But besides, also biological and physiological properties of the specific tumor may be of high importance. For instance tumor vascularity and perfusion, vascular permeability or metabolic parameters (such as oxygenation, pH or bioenergetic status) may alter the distribution and accumulation of nanotherapeutics [8]. If individual tumors show pronounced differences in their accumulation of specific polymeric structures, the question of a precise pre-therapeutically tailoring of polymer-drug conjugates for each individual patient is arising. Concerning this purpose, non-invasive imaging techniques can be a helpful diagnostic tool providing detailed information of the body distribution as well as tumor accumulation for the individual patient thus enabling to attune polymeric carrier systems for efficient therapy. In this regard, Positron Emission Tomography (PET) constitutes a convenient dynamic imaging technique, allowing a non-invasive visualization of the pharmacokinetics *in vivo,* in real time and with high spatial resolution. Depending on the half-life of the radionuclide applied, the diagnostic time frame can be adjusted from early phase accumulation - using shorter lived isotopes - to long-term imaging over weeks. Until now, studies concerning the *in vivo* behavior of diverse HPMA based formulations have been almost exclusively carried out using γ-imaging radionuclides e.g. Tc-99m or I-125/131 [9],[10] which have a relatively low spatial resolution. By successful radiolabeling of various HPMA based polymers with the positron emitters As-72/74 [11] and F-18 [12], we were able to establish PET imaging to assess the *in vivo* capability

of potential drug delivery systems. By this labeling approach we were able to demonstrate that the ratio of hydrophilicity / hydrophobicity as well as aggregate formation possessed a major impact on body distribution in the living animal [13]. Generally the influence of molecular structure on the tumor accumulation is a question of high importance. Cabral and coworkers [14] already demonstrated the dependency of the polymer size on tumor uptake in poorly permeable tumor models. But in addition, other molecular characteristics (lipophilicity, superstructures) have to be taken into account as well as tumor properties like vascular permeability or cellular uptake in different tumor lines. The impact of these parameters on polymer accumulation of diverse polymer architectures still remains unclear. Taking these demands into consideration, the aim of the present study was to analyze a broad spectrum of HPMA-based polymer architectures concerning their biological distribution *in vivo* in dependency of the tumor specific model. The polymer structures included homopolymers, random copolymers as well as block copolymers consisting of hydrophilic HPMA and hydrophobic lauryl methacrylate (LMA) segments. Both random as well as block copolymers form hydrophilic / hydrophobic superstructures and are interesting as drug delivery vehicles [15-17]. These polymers were tested in two different tumor lines (AT1 subline of the R3327 Dunning prostate and Walker 256 mammary carcinoma) in order to analyze the impact of tumor specific properties. For this purpose we used radio-labeling with the positron emitting isotope fluorine-18 in order to investigate tumor accumulation as well as whole body distribution by application of μPET imaging and *ex-vivo* biodistribution. The study particularly demonstrates the capability of PET imaging for potential polymeric drug carriers and their use for individual patient therapy.

2. Results and Discussion

2.1 Synthetic route of HPMA-based nanoparticles and their radioactive labeling

In these studies we have synthesized a library of HPMA-based polymeric nanoparticles aiming for deepening knowledge on their structure-property relationships *in vivo*. Starting from the reactive ester precursor penta-fluorophenyl methacrylate, we combined reactive ester chemistry with the controlled radical polymerization technique RAFT [18],[19] for polymer preparation. By incorporation of the

hydrophobic lauryl methacrylate monomer and subsequent polymer-analogous reaction with 2-hydroxy-propylamine [20, 21], nanoparticles with diverse polymer architectures – homo-polymers, random as well as block copolymers – are easily realized (Figure 1).

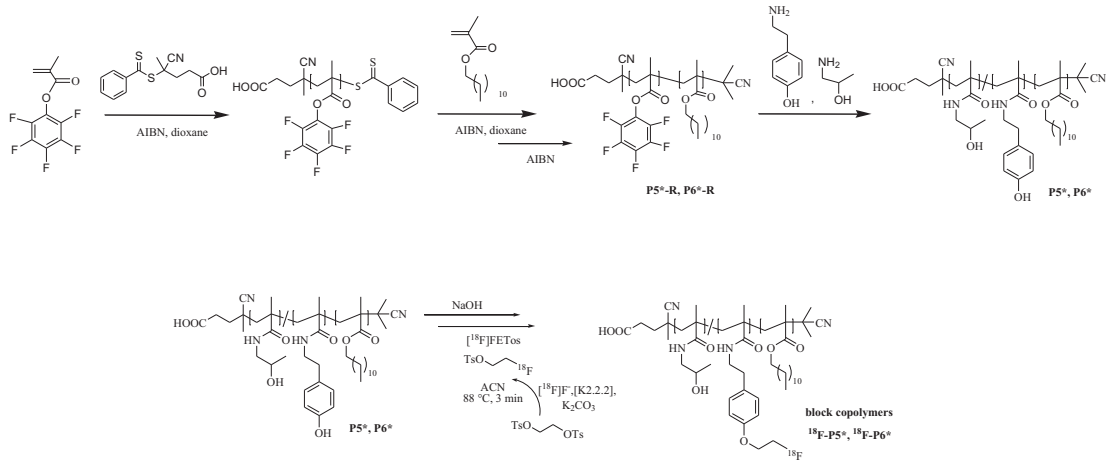

Scheme 1: *Reaction scheme of polymeric precursor systems (exemplary block copolymers **P5*** and **P6***), their polymeranalogous conversion and radioactive labeling procedure.*

Due to the RAFT concept, these HPMA-based polymer systems can be varied in molecular weight as well as hydrophobic content [12, 13, 15]. The hydrophobically modified polymers form aggregates in water solutions (e.g. buffer). Thus the particle size can be varied between some nm (size of an individual hydrophilic polymer coil depending on the molecular weight) and up to 100 nm for the aggregates. The resulting nanoparticles could be visualized by means of Transmission Electron Microscopy (TEM) [22]. Their molecular structure and the size of the nanoparticles (aggregates) are collected in table 1. The hydrodynamic radii of the nanosystems were determined by Fluorescence Correlation Spectroscopy (FCS). This method found a minimum of around 1 nm for the low molecular weight homopolymer **P1*** and showed a slow increase to 3 nm for particle **P2*** with higher molecular weight. The random copolymers **P3*** and **P4*** exhibited a hydrodynamic radius of ~ 33 nm and 40 nm, thereby displaying the middle-sized nanoparticles in the herein presenting study. The biggest sizes were achieved for the block copolymer structures **P5*** and **P6*** with an R_h of around 59 and 113 nm. Taking these values into account, the correlation of size, molecular weight and architecture (e.g. amphiphilicity) of

the HPMA-based nanoparticles is crucial for understanding their biological uptake in the living organism. Related to former studies [13] which demonstrated a major impact of aggregate formation on the polymer biodistribution pattern for random copolymer particles, the herein presented nanosystems – also including HPMA-LMA block copolymers – were tested *in vivo* with respect to organ distribution and tumor accumulation.

Table 1: *Analytical data of reactive ester homopolymers (**P1*-R** and **P2*-R**), random copolymers (**P3*-R** and **P4*-R**) and block copolymers (**P5*-R** and **P6*-R**) as well as the final polymers **P1*-P6***

Nomen-clature	Polymeric structure	Monomer ratio	M_n in g/mol	M_w in g/mol	PDI[2]	R_h[5] in nm
P1*-R	Homopolymer	100%[1]	18000[2]	23000[2]	1.29	n.d.
P2*-R	Homopolymer	100%[1]	87000[2]	130000[2]	1.49	n.d.
P3*-R	Random copolymer	80:20%[1]	17000[2]	21000[2]	1.26	n.d.
P4*-R	Random copolymer	80:20%[1]	57000[2]	80000[2]	1.41	n.d.
P5*-R	Block copolymer	60:40%[1]	14000[2]	18000[2]	1.26	n.d.
P6*-R	Block copolymer	60:40%[1]	25000[2]	31000[2]	1.25	n.d.
P1*	Homopolymer	100%[3]	9000[4]	12000[4]	1.29	1.1
P2*	Homopolymer	100%[3]	52000[4]	77000[4]	1.49	3.0
P3*	Random copolymer	82:18[3]	11000[4]	14000[4]	1.26	33.4
P4*	Random copolymer	75:25[3]	39000[4]	55000[4]	1.41	39.9
P5*	Block copolymer	79:21[3]	9000[4]	12000[4]	1.24	58.7
P6*	Block copolymer	75:25[3]	17000[4]	21000[4]	1.24	112.8

*[1] =Calculated monomer ratio; [2] =Determination by GPC in THF as solvent; [3] =Monomer ratio determined by ^{1}H-NMR spectroscopy after polymeranalogous reaction with 2-hydroxypropylamine; [4] =Calculated from the molecular weights of the reactive ester polymers **P1*-R** to **P6*-R** as determined by GPC in THF as solvent; [5] =Hydrodynamic radii determined by Fluorescence Correlation spectroscopy (FCS)*

For this purpose polymeric systems were labeled with the positron emitting radionuclide [^{18}F]fluorine which exhibits favorable nuclear characteristics ($t_{1/2}$=110 min, high β^+-branching, low beta energy) for high resolution non-invasive PET imaging. Radiolabeling was accomplished in two steps using the prosthetic labeling synthon [^{18}F]FETos, attached to the hydrophilic part of the polymer backbone by covalent linkage to tyramine groups (incorporation efficiency ~ 4%) (Scheme 1) [12]. Within each polymer architecture, radiolabeling efficiencies were shown to be higher for polymers of lower molecular weight (**P1***, **P3***, **P5***) and highest RCYs were achieved for the homopolymer **P1*** (RCY = 37 ± 6). This might be due to the better accessibility of the tyramine groups. Following ^{18}F-labeling, bio-distribution of the labeled compounds was analyzed by μPET imaging as well as *ex vivo* organ concentration measurements in rats. To investigate the impact of tumor specific tissue and cell properties on the uptake of the varying polymer structures, accumulation was followed in two different tumor lines (subline AT1 of the Dunning prostate carcinoma R3327 and the Walker 256 mammary carcinoma) of the rat.

2.2 Organ distribution

Using μPET imaging and *ex vivo* biodistribution analysis allows quantification of the polymer uptake in different organs. Fig. 1A shows the whole body distribution pattern of the different polymers 2 h after i.v. injection. The images clearly indicate pronounced differences with low molecular weight nanoparticles (**P1***, **P3***, **P5***) predominantly found in the kidney whereas high molecular weight polymer particles (**P2***, **P4***, **P6***) were found to a greater extend in liver and spleen. The images also show that the two HPMA-*ran*-LMA copolymers (**P3***, **P4***) stayed much longer in the blood compartment than the other polymer architectures. In these animals the aorta and the femoral artery are clearly visible as well as the well perfused lung (Suppl. Fig. 1). By administration of the large homopolymer (**P2***) the liver is (at least partially) clearly visualized whereas the small homopolymer (**P1***) is only seen in the kidney.

Using PET imaging also the time course of uptake into the tissues can be traced. By defining ROIs over different organs the time-activity curve (TAC) displays temporal redistribution.

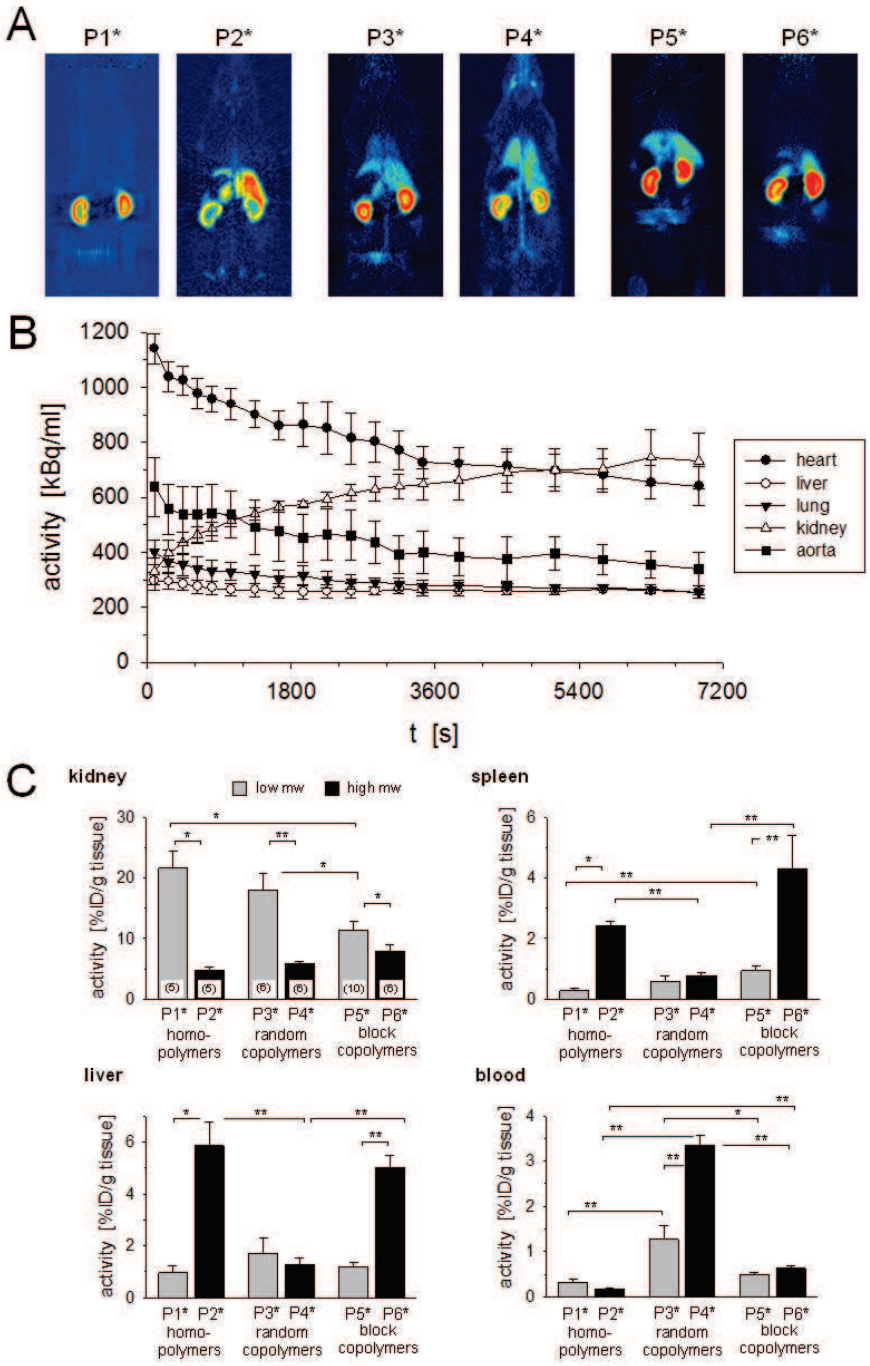

Figure 1: *Organ distribution of the polymers (**P1*** and **P2*** homopolymers, **P3***and **P4*** random copolymers as well as **P5*** and **P6*** block copolymers with low or high molecular weight respectively). **(A)** Whole body PET images of the distribution of the polymers 2h after polymer injection. **(B)** Time activity curves (TAC) for different organs after injection of the random copolymer with high molecular weight (**P4***). n=2. **(C)** Quantification of the polymer uptake in different tissues. Uptake is expressed by the fraction of the injected dose (ID) of the polymer per gram tissue 2 h after i.v. injection. n=5-10, (*) p<0.05, (**)p<0.01.*

As Fig. 1B demonstrates, the high molecular weight HPMA-*ran*-LMA copolymer (**P4***) is continuously excreted by the kidney (as indicated by a continuous increase in activity in this organ) whereas in all other organs the tissue concentration is steadily decreasing.

In order to quantify the organ uptake, biodistribution was measured *ex vivo* 2 h and 4 h after particle injection. The measurements showed pronounced disparities between various organs depending on polymer architecture as well as molecular weight. For the low molecular weight polymers the highest concentrations were found in the kidney (Fig. 1C, Tab. 2, $p<0.001$ ANOVA). Since the molecular weight of these polymeric systems is close to the renal filtration threshold, they can be easily filtrated into primary urine which will lead to the high whole tissue concentration observed. The polymer architecture (homo- *vs*. random copolymers) plays only an insignificant role for renal uptake (or urinary excretion). However, the renal concentration of the low molecular weight block copolymer (**P5***) was significantly lower than for both other polymer structures which probably might be the result of their superstructure formation resulting in a much larger molecular diameter (Tab. 1). After 4 h the renal concentration further increased (not statistically significant) for all polymers (Fig. 2) which corresponds well to the TAC curves shown in Fig. 1B.

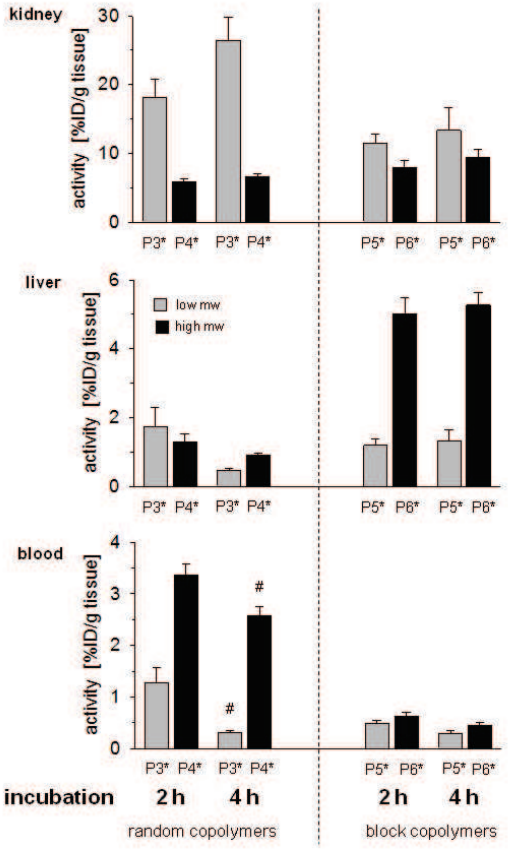

Figure 2: *Comparison of the organ distribution of random and block copolymers 2 h and 4 h after injection, respectively. n=3-10, (#) $p<0.05$ 2 h vs. 4 h.*

The high molecular weight homo-polymer **P2*** as well as the block copolymer **P6*** were taken up most prominently into liver and spleen. The liver concentrations of these polymers

were 5-times higher than for all other polymers (Fig. 1C, Tab. 2) indicating that polymer structure is of high importance regarding liver uptake ($p=0.029$ ANOVA). The other polymers showed concentrations on comparable levels. After 4 h the liver concentrations of the random copolymers were markedly, however not statistically significant, lower (Fig. 2) whereas for the block copolymers the concentration remained constant. The organ distribution stays in good accordance to data described by Kissel et al. [9] who investigated an HPMA homopolymer with a molecular weight of 27 kDa - thereby being in between the two here presented homopolymers **P1*** and **P2***. On the other hand the results are partially in contrast to the findings depicted by Lammers et al. [23] where the authors described a much higher accumulation of the HPMA homopolymers in the spleen as compared to the liver. In the present study liver concentration was 2-3-times higher than in the spleen. The mentioned disparities might be a result of different time points of measurement.

As a result of low renal excretion and low hepatic elimination of the copolymers **P3*** and **P4***, the blood levels of both random copolymers 2 h after injection were significantly higher than those of the homo- and block copolymers. Regarding the high molecular weight polymers **P2***, **P4*** and **P6***, the blood concentration of the HPMA-*ran*-LMA copolymer was almost 5-20-times higher (Fig. 1C, $p<0.0001$ ANOVA) and stayed elevated for the whole observation frame of 4 h (Fig. 2). The most probable reason of the prolonged stay of the copolymer in vasculature seems to be the higher lipophilicity of the LMA-containing copolymers [13] and consequential a diminished renal excretion. The blood levels of the homopolymers were markedly lower than described by a previous study [23]. This distinction still remains unclear.

The organ distribution in other tissues was not pronouncedly different among the studied polymer systems or the organ levels directly reflect the disparities in blood compartment (Tab. 2).

Table 2: *Polymer uptake in different organs expressed by the fraction of the injected dose (ID) of the polymer per gram tissue 2 h after i.v. injection. n=5-10.*

	polymer concentration [%ID/g tissue]					
organ	**P1***	**P2***	**P3***	**P4***	**P5***	**P6***
lung	0.23±0.04	0.27±0.04	0.49±0.09	1.33±0.13	0.28±0.05	0.39±0.06
liver	0.96±0.28	5.87±0.9	1.73±0.57	1.3±0.24	1.2±0.18	5.01±0.47
spleen	0.28±0.08	2.41±0.17	0.58±0.18	0.77±0.09	0.94±0.14	4.3±1.1
kidney	24.52±0.94	4.83±0.49	18.06±2.68	5.86±0.4	11.44±1.33	7.95±0.96
muscle	0.09±0.01	0.04±0.01	0.11±0.02	0.16±0.05	0.08±0.03	0.07±0.01
heart	0.12±0.01	0.09±0.01	0.37±0.07	0.72±0.11	0.16±0.02	0.22±0.03
blood	0.33±0.06	0.18±0.03	1.27±0.3	3.36±0.22	0.49±0.05	0.63±0.07
small intestine	0.16±0.02	0.36±0.06	0.29±0.1	0.46±0.11	0.21±0.05	0.23±0.02
testis	0.1±0.01	0.06±0.01	0.15±0.01	0.18±0.02	0.09±0.01	0.1±0.01

2.3 Tumor accumulation

The major aim of the presented study was to analyze the uptake of six nanosized polymer architectures in two different tumor models (AT1 prostate carcinoma, Walker 256 mammary carcinoma of the rat) applying PET as a fast and versatile imaging tool. Both tumor cell lines were implanted subcutaneously into the hind foot dorsum and grew with a comparable rate, 7 to 14 days to reach a mean volume of 1.32±0.10 ml. Even though both tumor models show similar growth rate and comparable histology, the uptake of the polymers was fundamentally different.

All polymers accumulate poorly in AT1 tumors with nearly no influence of molecular structure and aggregate size (Fig. 3). Neither polymeric structure ($p=0.952$ ANOVA) nor molecular weight ($p=0.304$) had a relevant impact on intratumoral concentrations – although the blood levels were varying noticeably between the different polymer architectures (especially for **P3*** and **P4***, Fig. 1C). The accumulation of the homopolymers was comparable to that described by others [23] who investigated

the tumor uptake in the same tumor model, however, at a later time point after polymer injection. Nevertheless they described a better uptake of the large homopolymer as compared to low molecular weight HPMA based homopolymers which could not be confirmed in the present study. In principle, AT1 prostate carcinomas do not accumulate any of the polymers very well.

When analyzing the spatial distribution of the intratumoral uptake in AT1 tumors, PET imaging revealed that the highest concentrations were found in the outer rim of AT1 tumors, a phenomenon seen more or less with all polymers (Fig. 3A).

For more detailed evaluation of the spatial heterogeneity, autoradiograms have been generated and correlated with the histological structure. These microscopic images illustrated that the high concentration in the rim corresponds to the subcutis around the tumor and not to the tumor tissue itself (Fig. 6A). Since the *ex vivo* biodistribution studies were performed in tumor tissue without skin, the values shown in Fig. 3B are not biased by the subcutaneous blood compartment.

In Walker 256 tumors the uptake was highly different, depending on the polymer architecture as well as the molecular weight. Whereas the homo- and the block copolymers were accumulated poorly in the Walker tumors (comparable to AT1 tumors), the uptake of the HPMA-*ran*-LMA copolymers was significantly higher (Fig. 3B). The intratumoral concentration of the large random copolymer (**P4***) was 4.6-times higher than for the large homopolymer (**P2***) and almost 3-times higher than the HPMA-*ran*-LMA copolymer levels in AT1 tumors (Fig. 3B). Since the random copolymer particles stay much longer in the circulation (blood pool, Fig. 1C) one possible explanation would be the difference of vascularity of AT1 and Walker 256 carcinoma. However, investigation of microvessel density by immunochemistry revealed that there were no profound disparities between both tumor models [24-26]. A marginal indication for the impact of the fraction of blood vessels within the tumor on the polymer uptake might be the fact that in AT1 tumors vascular density increases in larger tumors [27] which slightly correlates with the polymer accumulation (data not shown).

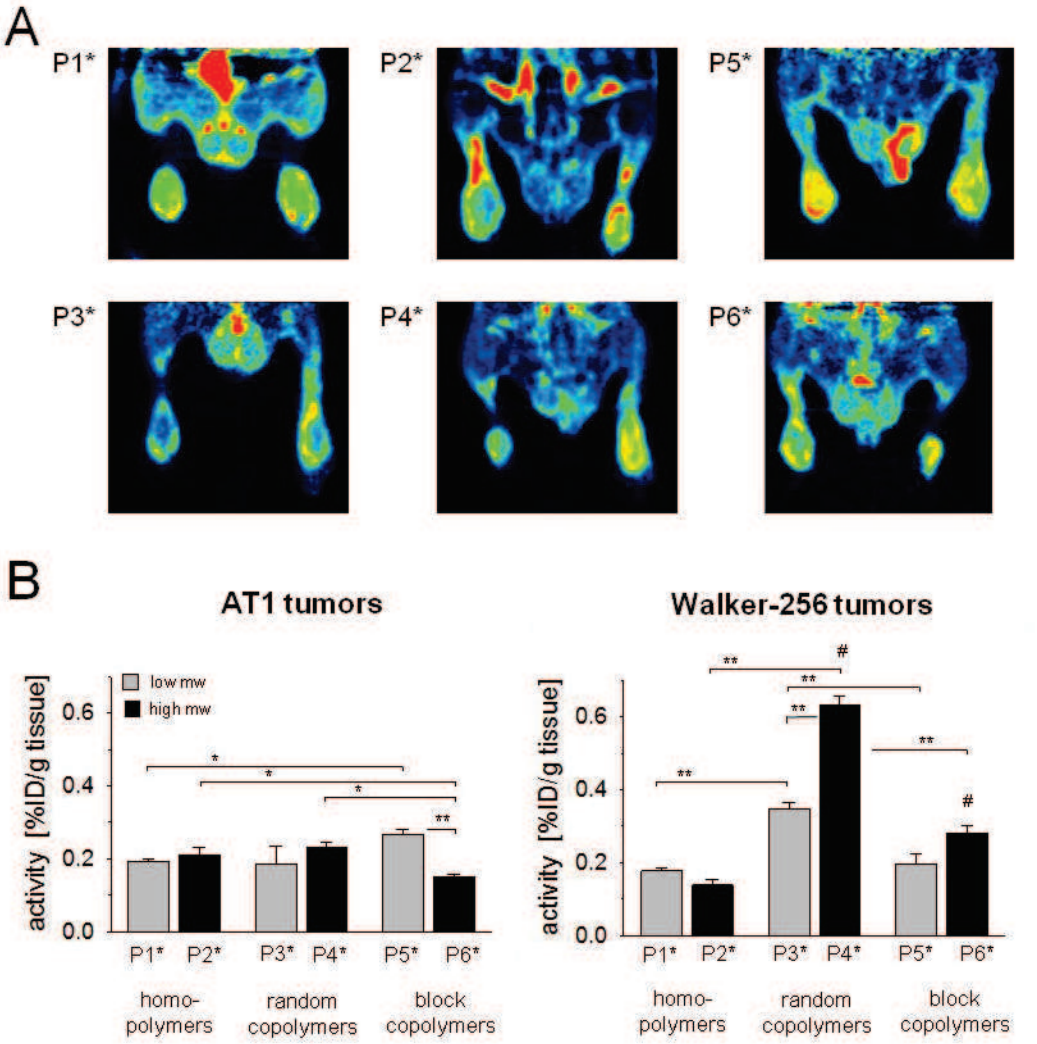

Figure 3: *Tumor uptake of the polymers (**P1*** and **P2*** homopolymers; **P3*** and **P4*** random copolymers; **P5*** and **P6*** block copolymers with low or high molecular weight, respectively).* ***(A)*** *Example PET images of polymer accumulation in AT1 prostate carcinomas.* ***(B)*** *Intratumoral polymer concentration in AT1 prostate carcinomas and Walker 256 mammary carcinomas determined by biodistribution measurements 2h after polymer application. n=5-6; (*) p<0.05, (**) p<0.01; (#) p<0.01 Walker-256 vs. AT1 tumors.*

The low molecular weight random copolymer (**P3***) also showed a markedly (however not statistically significant p=0.055) higher concentration in Walker carcinomas as compared to AT1 tumors. The absolute level of **P3***, however, was lower than for **P4*** (Fig. 3B) which might be the result of a lower blood concentration of **P3*** (Fig. 1C). Besides others, one possible explanation might be the lower hydrophobicity of the small random copolymer **P3*** (incorporation efficiency of 18 % LMA) compared to its high

molecular weight counterpart **P4*** (25 % of LMA-fraction). Obviously the uptake of the random copolymer nanoparticles depends mainly on the tumor entity which was confirmed by ANOVA ($p<0.0001$). The uptake of the block copolymers was also much lower than for the random copolymers (approx. at the same level as for the homopolymers). These data clearly reveal that the intratumoral uptake of polymers is not only a question of molecular size [14] (which is highest for the block polymer particles, Tab. 1) but also strongly dependent on the chemical properties of the polymer architectures (e.g. hydrophobicity / hydrophilicity). However, for a distinct polymeric structure the differences between the tumor lines are tremendous (at least for the random copolymers) indicating that specific tumor cell properties also mainly affect intratumoral accumulation of polymers.

Analysis of the time course of polymer uptake in both tumor lines by PET imaging (Fig. 4A) showed that a stable intratumoral concentration was reached 15-20 min after injection (Fig. 4B). The concentrations of the random and block copolymer (**P4***, **P6***) remained constant even over a longer time span up to 4 h (Fig. 5) although the blood concentration was decreasing over time (Fig. 2).

Furthermore, similar results were found in experiments using ^{131}I-labeled random copolymer **P4*** over a time span of 72 hours. Even tumor enrichment over time – whilst blood pool concentration of the polymer decreased - could be observed (data not shown). One important aspect resulting from the findings on the HPMA-*ran*-LMA copolymers addresses the cause of the differences between the tumor lines responsible for the diverging uptake. Two tumor specific factors should be taken into account: (1) differences in vascular permeability and (2) differences in cellular uptake of the polymer.

Since former studies of Cabral and coworkers could already demonstrate that vascular permeability affects the tumor uptake of nanosized structures [14], this parameter was also measured in the tumor models used in the present study determining the extravasation of dextrans with different molecular weights (10, 70, 200 kDa).

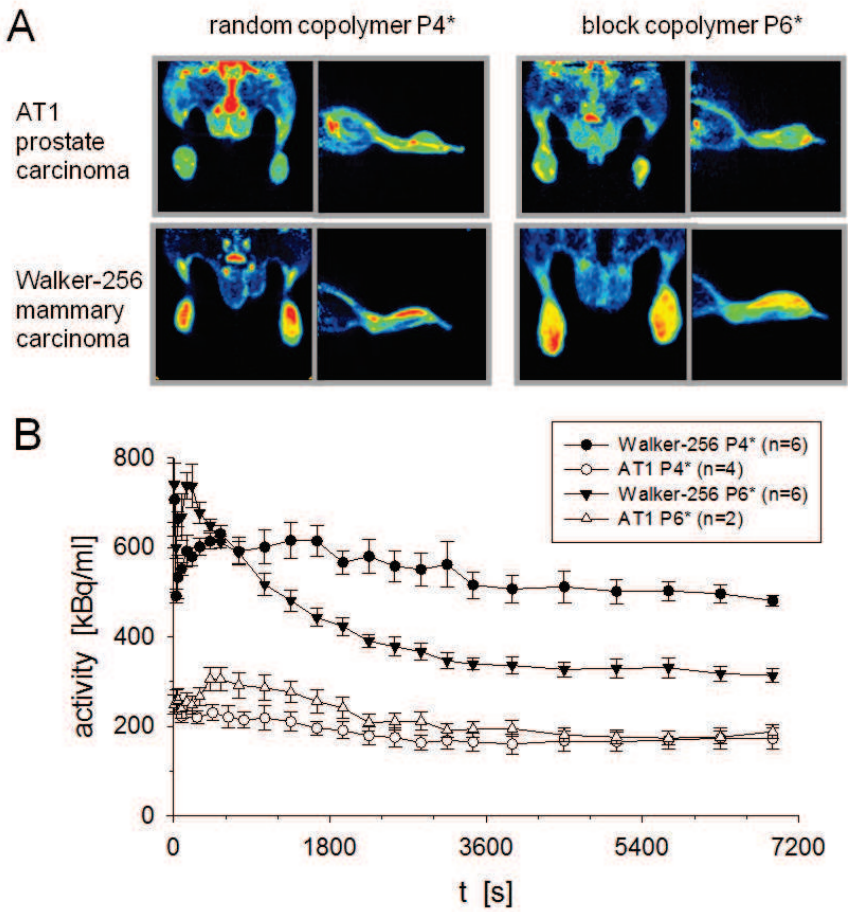

Figure 4: *Comparison of polymer uptake in different tumor lines.* ***(A)*** *Example PET images of the accumulation of the large HPMA-ran-LMA and HPMA-b-LMA copolymers in AT1 and Walker 256 carcinomas.* ***(B)*** *Time course of the relative polymer uptake of the high molecular weight random (**P4***) and block copolymer (**P6***) in Walker 256 and AT1 tumors. Values were normalized to the concentration of the reference tissue (testis).*

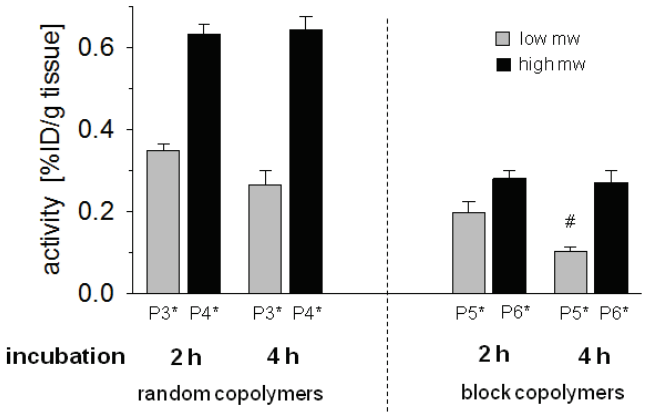

Figure 5: *Intratumoral concentration of random and block copolymers in Walker-256 mammary carcinomas 2 and 4 h after injection, respectively. n=4-6, (#) $p<0.05$ 2 h vs. 4 h.*

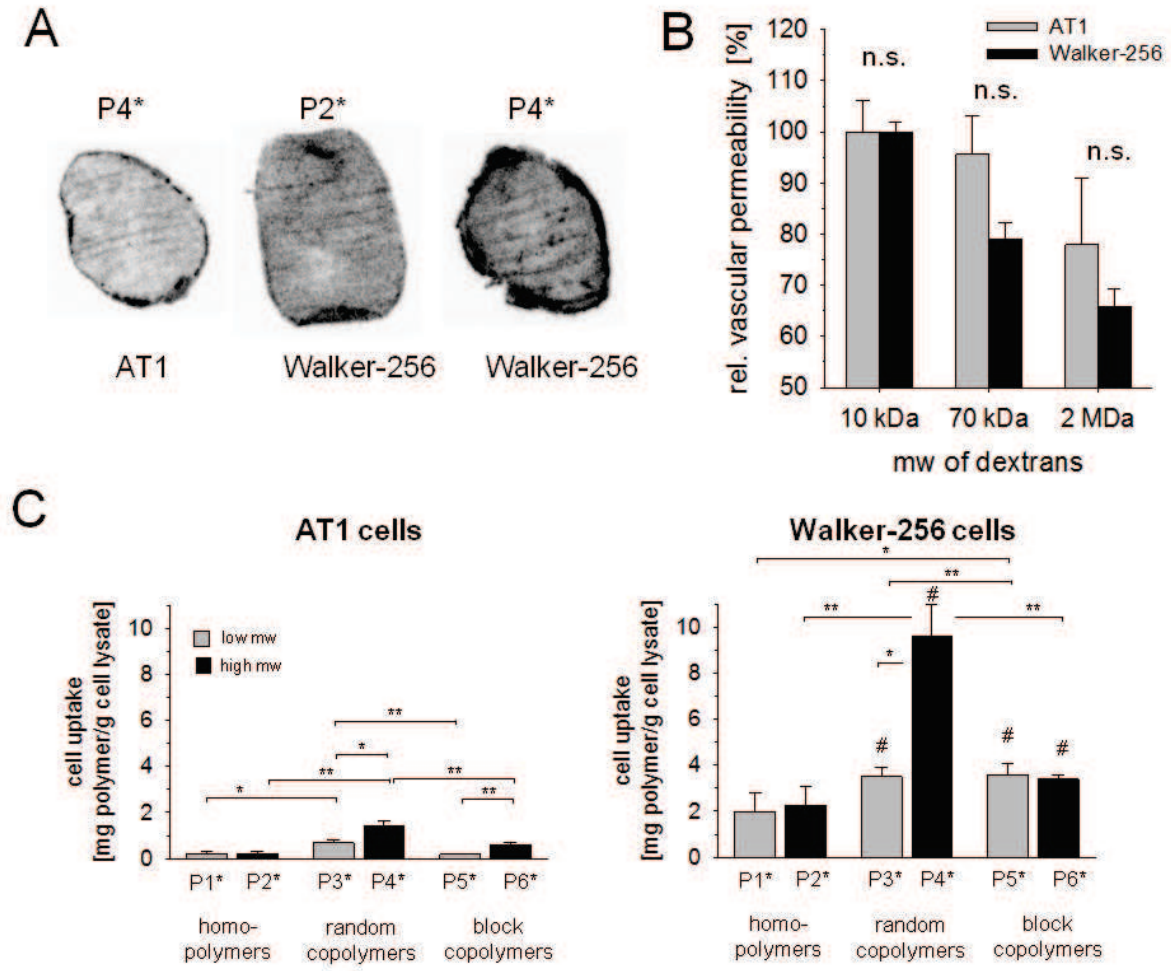

Figure 6. *Differences of intratumoral uptake distribution.* ***(A)*** *Autoradiographic images of the polymer distribution within the tumor.* ***(B)*** *Vascular permeability of AT1 and Walker 256 tumors in vivo measured by extravasation of dextrans of different molecular weights (M_w). n=2-6.* ***(C)*** *Cellular uptake of the polymers after 2 h incubation at 37 °C in AT1 and Walker 256 carcinoma cells in vitro; n=6-12, (*) p<0.05, (**) p<0.01. (#) p<0.01 Walker-256 vs. AT1 cells.*

As shown in Fig. 6B, the vascular permeability for high molecular weight dextrans was slightly (but not statistically significant) different between the two tumor lines.

However, although AT1 tumors showed a much lower uptake of the HPMA-*ran*-LMA copolymers compared to Walker 256 tumors, the vascular permeability of these tumors was found to be even higher (Fig. 6B). Studies by other groups analyzing the vascular permeability of these tumor lines also showed that both tumors were moderately permeable for molecules up to a molecular weight of approximately 50-60 kDa but they seem to be more or less impermeable for molecules over 90 kDa [28, 29]. Nonetheless, the results of these studies are difficult to compare with each other

due to different techniques used for measuring vascular permeability whereas the results of the present study (as shown in Fig. 6B) used the same experimental procedure under identical conditions. In the previous studies an equilibrium between blood pool and interstitial space for molecules up to 50-60 kDa was reached at least 60 min post injection [29]. For this reason it seems to be plausible that the low and high molecular weight homo- and block copolymers show comparable uptake in both tumor lines. The results concerning the HPMA-*ran*-LMA copolymers however are somehow surprising. In contrast to the other polymer structures, these nanoparticles are markedly accumulated in Walker 256 tumors but not in AT1 tumors (although the vascular permeability was lower, Fig. 6B). Beyond that, the high molecular weight random copolymer **P4*** (M_n= 39 kDa) was taken up much stronger than its low molecular weight counterpart **P3*** (M_n= 11 kDa). Therefore other mechanisms besides vascular permeability have to be considered.

In a further *in vitro* study the cellular uptake of the polymers into AT1 and Walker 256 cells was measured. The cell uptake depended significantly on the tumor cell line (p=0.0001, ANOVA). As shown in Fig. 6C all polymers were taken up in AT1 cells to only a very small extent. However, the uptake of the HPMA-*ran*-LMA copolymers in Walker 256 cells was approximately 4-6 times higher than in AT1 cells (Fig. 6C). Obviously, these tumor cells exhibit distinct features leading to a much better cellular uptake which might explain the differences in the *ex vivo* biodistribution experiments. Although differences in the endocytic processes of both lines might explain these findings, the reason for this differential behavior presently still remains unclear. The cellular uptake of the homopolymers in Walker 256 cells was markedly lower than for the random copolymers. The uptake pattern (Fig. 6C) was therefore similar to the whole tumor tissue results (Fig. 3B) indicating that the combination of *in vivo* and *in vitro* experiments constitutes a beneficial platform for determining the suitability of polymers as drug carrier systems.

3. Conclusion

The present study clearly demonstrates that polymer architecture as well as molecular weight and size affect the body distribution of HPMA-based polymers. Using radiolabeling of the polymers with positron emitting isotopes (^{18}F) allows biodistribution analyses as well as non-invasive Positron Emission

Tomography (PET) imaging for quantification purposes. Applying these techniques, the results underline the important role of molecular weight concerning renal excretion whereas polymer structure influences the hepatic uptake as well as elimination and consequential intravascular disposition. In contrast to homo- and block copolymers, HPMA-LMA random copolymers - exhibiting a higher percentage of hydrophobic segments - remain in the blood compartment for several hours which can be easily followed by PET. When analyzing the tumor uptake of the varying polymer architectures in two different carcinoma lines of the rat, surprisingly, the polymeric nanoparticles demonstrated strongly differing tumor accumulation properties, depending on the respective tumor line. Whereas in AT1 tumors all polymers were accumulated equally to a low extent, Walker 256 tumors remarkably have taken up the HPMA-*ran*-LMA copolymers approximately 5-times stronger. Since the site of tumor growth, the proliferation rate as well as histological and vascular characteristics were comparable between both tumor lines, other tumor specific properties seem to be responsible for the different polymer accumulation. Cell experiments clearly show that the cellular uptake of the polymers varies markedly between the two cell lines used and could explain (at least partially) the differences seen *in vivo*.

It can be concluded that the variation of structure and size of the herein presented HPMA-based nanoparticles has a dominant influence on a prolonged stay in circulation and on a pronounced uptake of these molecules in the tumor tissue *in vivo*. The results also clearly reveal that the efficacy of a tumor treatment by polymer drug nanocarriers depends strongly on the properties of each individual tumor (depending on the tumor line). The perfect polymer fit has to be chosen for individual tumors. Concerning the clinical setting, the present studies underline the necessity of a precise polymer characterization in combination with its pre-clinical screening to tailor the polymer carrier system for each individual tumor and patient to be treated. In this regard both radiolabeling as well as imaging of the polymeric architectures using PET is emphasizing a favorable and promising analytical tool for the individualization of polymer-based chemotherapy to the patient's needs, applicable to a variety of nanocarrier systems.

4. Materials and methods

Materials

All solvents were of analytical grade, as obtained by Sigma Aldrich and Acros Organics. Dioxane was distilled over a sodium/potassium composition. Lauryl methacrylate was distilled to remove the stabilizer and stored at -18 °C. 2,2'-azoisobutyronitrile (AIBN) was recrystallized from diethyl ether and stored at -18 °C as well.

Methods

Polymer Synthesis

Synthesis of 4-cyano-4-((thiobenzoyl) sulfanyl)pentanoic acid (CTP). 4-cyano-4((thiobenzoyl)sulfanyl)pentanoic acid was used as chain transfer agent (CTA) and synthesized according to the literature[19].

Synthesis of pentafluorophenyl methacrylate (PFPMA). Pentafluoro-phenyl methacrylate was prepared according to reference [21].

Synthesis of reactive ester homo-polymers. RAFT polymerization of pentafluorophenyl methacrylate with 4-cyano-4-((thiobenzoyl) sulfanyl)pentanoic acid was carried out in a schlenk tube [13, 15, 20]. For this purpose, 4 g of PFPMA were dissolved in 5 mL of absolute dioxane, furthermore CTP and AIBN were added. The molar ratio of CTP/AIBN was chosen 8:1. After three freeze-vacuum-thaw cycles, the mixture was immersed in an oil bath at 65 °C and stirred overnight. Afterwards, the polymeric solution was precipitated three times in hexane, centrifuged and dried under vacuum at 40 °C overnight. A slightly pink powder was obtained. Yield: 52 %. 1H-NMR (300 MHz, CDCl3) δ/ ppm: 1.20-1.75 (br), 2.00-2.75 (br s). 19F-NMR (400 MHz, CDCl3) δ/ ppm: -162.03 (br), -156.92 (br), -152 to -150 (br).

Synthesis of random copolymers. RAFT polymerization of PFPMA with lauryl methacrylate (LMA) by help of CTP was performed in a schlenk tube as well. As an example, 4 g of PFPMA dissolved in 5 mL dioxane, lauryl methacrylate, AIBN and CTP were mixed. The molar ratio of CTP/AIBN was chosen to be 8:1. After three freeze-vacuum-thaw cycles, the mixture was immersed in an oil bath at 65 °C and stirred overnight. Afterwards, poly(PFPMA)-ran-poly(LMA) was pre-cipitated three times in hexane, centrifuged and dried under vacuum at 40 °C overnight. A slightly pink powder was obtained. Yield: 54%. 1H-NMR

(300 MHz, CDCl3) δ/ ppm: 0.84 (br t), 1.20-1.75 (br), 2.00-2.75 (br s). 19F-NMR (400 MHz, CDCl3) δ/ ppm: -162.01 (br), -156.95 (br), -152 to -150 (br).

Synthesis of block copolymers. The macro-CTA obtained after homo-polymerization of PFPMA was dissolved in dioxane, afterwards lauryl methacrylate as well as AIBN were added. As an example, 250 mg of macro initiator were dissolved in 5 mL dioxane, lauryl methacrylate and AIBN (8:1 ratio macro-CTA/AIBN) were mixed. After three freeze-vacuum-thaw cycles, the mixture was immersed in an oil bath at 65 °C and stirred for three days. Afterwards, poly(PFPMA)-*b*-poly(LMA) was pre-cipitated three times in ethanol, centrifuged and dried under vacuum at 40 °C overnight. A slightly pink powder was obtained. Yield: 54%. 1H-NMR (300 MHz, CDCl3) δ/ ppm: 0.84 (br t), 1.20-1.75 (br), 2.00-2.75 (br s). 19F-NMR (400 MHz, CDCl3) δ/ ppm: -162.01 (br), -156.95 (br), -152 to -150 (br).

Removal of dithioester endgroups. The dithiobenzoate endgroup was removed using the protocol reported by Perrier et al. [30]. Therefore a 25-fold molar excess of AIBN was added to the polymer dissolved in dioxane. After four hours of heating the solution in an oil bath at 70 °C, the polymer was precipitated twice in hexane and collected by centrifugation. The polymer was dried under vacuum overnight, a colorless powder was obtained. Yield: 75%. Removal of the dithioester endgroup could be proven by UV-Vis spectroscopy.

Polymer analogous reaction of homo-polymers. Depending on the labeling technique necessary, either for a fluorescent or radioactive marker, two different routes were applied. For subsequent radioactive labeling, the protocol was carried out as follows. As example, 100 mg of the polymeric precursor (Mn = 18000 g/mol) were diluted in 2 mL of absolute dioxane. 5 mg of tyramine, diluted in a DMSO/dioxane mixture, and 10 mg of triethylamine were added. After stirring for four hours at 35 °C, 30 mg of 2-hydroxypropylamine as well as 40 mg of triethylamine were added and the solution was stirred overnight. For final removal of reactive ester side groups, further 30 mg of 2-hydroxypropylamine were added the next morning. The solution was precipitated two times in

diethyl ether, centrifuged and finally dissolved in a DMSO/water solution for dialysis. After lyophilization a white powder could be obtained. Yield: 79%. 1H-NMR (400 MHz, d. DMSO) δ/ ppm: 0.60-1.40 (br), 1.45-2.20 (br), 2.75-3.10 (br), 3.50-3.80 (br), 4.60-4.80 (br), 6.60-6.70 (br) and 6.85-7.00 (br). For additional fluorescent labeling, the fluorescent marker Oregon Green 488 cadaverine was used. 100 mg of polymeric precursor were diluted in 2 mL of absolute dioxane and 2.75 mg of Oregon Green 488 cadaverine added. Afterwards tyramine and 2-hydroxypropylamine were added, as described by the procedure above.

Polymer analogous reaction of random copolymer. For radioactive labeling of random copolymers the protocol was applied as follows. 100 mg of poly(PFPMA)-*ran*-poly(LMA) co-polymer was dissolved in 2 mL of absolute dioxane. As example, for the polymeric system **P3*-R** (M_n = 17000 g/mol) 5 mg of tyramine and 10 mg of triethylamine were diluted in a DMSO/dioxane mixture and added to the vessel. After stirring for four hours at 35 °C, 30 mg of 2-hydroxypropylamine as well as 40 mg of triethylamine were added and the solution stirred overnight. For final removal of reactive ester side groups further 30 mg of 2-hydroxypropylamine were added the next morning. The solution was precipitated two times in diethyl ether, centrifuged and finally dissolved in a DMSO/water solution for dialysis. After lyophilization a white powder could be obtained. Yield: 51%. 1H-NMR (400 MHz, d. DMSO) δ/ ppm: 0.70-0.90 (br), 0.90-1.40 (br), 1.40-1.90 (br), 2.75-3.10 (br), 3.50-3.80 (br), 4.50-4.75 (br), 6.60-6.75 (br) and 6.85-7.00 (br). For additional fluorescent labeling, 100 mg of polymeric precursor were diluted in 2 mL of absolute dioxane and 2.9 mg of Oregon Green 488 cadaverine were added. Afterwards tyramine and 2-hydroxypropylamine were added, as described by the procedure above.

Polymeranalogous reaction of block copolymers. For radioactive labeling as well as for fluorescent labeling the above mentioned synthetic route (see polymeranalogous reaction of random copolymers) can be applied.

Characterization

1H-NMR spectra were obtained by a Bruker AC 300 spectrometer at 300 MHz, 19F-NMR analysis was carried out with a Bruker DRX-400 at 400 MHz. All

measurements were accomplished at room temperature and spectroscopic data were analyzed using ACDLabs 9.0 1D NMR Manager. The synthesized polymers were dried at 40 °C under vacuum overnight, followed by Gel Permeation Chromatography (GPC). GPC was performed in tetrahydrofuran (THF) as solvent, using following equipment: pump PU 1580, autosampler AS 1555, UV detector UV 1575 and RI detector RI 1530 from Jasco as well as a miniDAWN Tristar light scattering detector from Wyatt. Columns were used from MZ Analysentechnik, 300x8.0 mm: MZ-Gel SDplus 106 Å 5 µm, MZ-Gel SDplus 104 Å 5 µm and MZ-Gel SDplus 102 Å 5 µm. GPC data were evaluated by using the software PSS WinGPC Unity from Polymer Standard Service Mainz. The flow rate was set to 1 mL/min with a temperature of 25 °C.

For synthesis of 2-[18F]fluoroethyl-1-tosylate ([18F]FETos), a Sykam S 1100 pump and a Knauer UV-detector (K-2501) HPLC system were used. Size Exclusion Chromatography (SEC) of 18F-labeled polymers was performed using HiTrap™ Desalting Column, Sephadex G-25 Superfine and a waters pump (1500 series), a Waters UV-detector (2487 λ absorbance detector) and a Berthold LB 509 radiodetector.

Size determination by Fluorescence Correlation Spectroscopy (FCS). The hydrodynamic radii of the polymeric systems were determined by Fluorescence Correlation Spectroscopy using a commercial FCS setup (Zeiss, Germany) consisting of the module ConfoCor 2 and an inverted microscope model Axiovert 200 with a Zeiss C-Apochromat 40 ×/1.2 W water immersion objective. The fluorophores were excited with an Argon laser (λ= 488 nm) and the emission was collected after filtering with a LP505 long pass filter. For detection, an avalanche photodiode, enabling single-photon counting, was used. As sample cell, eight-well, polystyrene-chambered cover glass (Laboratory-Tek, Nalge Nunc Inter-national) was applied. For sample preparation, stock solutions of 0.1 mg fluorescently labeled polymer/mL NaCl were applied. The solution was kept at room temperature overnight. For reference reason, free Oregon Green 488 cadaverine dye in NaCl-solution was also studied. The calibration of the FCS observation volume was done using a dye with known diffusion coefficient, i.e. Rhodamine6 G. For each solution, 5 measurement cycles with a total duration of 150 seconds were applied. Time dependant fluctuations of the

fluorescence intensity δI(t) were detected and evaluated by autocorrelation analysis, yielding the diffusion coefficient and hydrodynamic radius of the fluorescent species [31].

Radioactive labeling

Synthesis of [^{18}F]FETos. To an aqueous [^{18}F]fluoride solution (2-8 GBq) 18 mg Kryptofix®2.2.2., potassium carbonate (1 N, 15 µL) and 1 mL acetonitrile were added. The mixture was dried in a stream of nitrogen at 80 °C, the drying procedure was repeated three times. To the dried residue 13 mg of ethyleneglycol-1,2-ditosylate in 1 mL acetonitrile was added and heated under stirring in a sealed vial at 88 °C for 3 min. Purification of the crude product was accomplished using HPLC (Lichrosphere RP18-EC5, 250×10 mm, acetonitrile/water 50:50, flow rate: 5 mL/min, t_R: 8 min). After diluting the HPLC fraction of 2-[^{18}F]fluoroethyl-1-tosylate with water, the product was loaded on a Sep-Pak C18 cartridge, dried with a nitrogen stream and eluted with 0.8 mL of DMSO [32].

Radiolabeling of polymers. For radio-labeling, 3 mg of the polymeric precursor were dissolved in 200 µL of dried DMSO. The solution was transferred to a sealed vial and 1 µL of a 5 N sodium hydroxide solution was added. The labeling reaction was started by adding the previously eluted DMSO solution of 2-[^{18}F]fluoroethyl-1-tosylate and the mixture was stirred for 15 min at 120 °C. For *ex vivo* and *in vivo* experiments, the radiolabeled polymeric systems were freed from low molecular weight byproducts by Sephadex G-25 size exclusion chromatography (HiTrap™ Desalting Column, Sephadex G-25 Superfine, 0.9% NaCl, flow rate: 0.5 mL/min) leading to a pure, ^{18}F-labeled polymer solution ready for subsequent experiments [12, 13].

Tumor and animal models

Tumor and animal models. For animal experiments two rat tumor cell lines were used: (1) Walker 256 mammary carcinoma, (2) subline AT1 of the Dunning prostate carcinoma R3327. Both cell lines were grown in culture in RPMI medium supplemented with 10 mM L-glutamine and 10% fetal calf serum (FCS) at 37°C under a humidified 5% CO_2 atmosphere and sub-cultivated twice per week. For tumor implantation male Sprague-Dawley rats (for Walker 256 tumors) or male Copenhagen rats (for R3327 AT1 tumors) (Charles River Wiga, Sulzfeld, Germany; body weight

150 to 300 g) housed in the animal care facility of the University of Mainz were used in this study. All experiments had previously been approved by the regional animal ethics committee and were conducted in accordance with the German Law for Animal Protection and the UKCCCR Guidelines [33]. Animals were allowed access to food and acidified water *ad libitum* before the investigation. Solid carcinomas of both cell lines were heterotopically induced by injection of cell suspension of the respective tumor line (0.4 ml approx. 10^4 cells/µl) subcutane-ously into the dorsum of the hind foot. Tumors grew as flat, spherical segments and replaced the subcutis and corium completely. Volumes were determined by measuring the three orthogonal diameters (d) of the tumors and using an ellipsoid approximation with the formula: $V = d_1 \times d_2 \times d_3 \times \pi/6$. Tumors were used when they reached a volume of between 0.5 to 3.0 ml approx. 7 to 14 days after tumor cell inoculation.

Cellular studies and permeability assay

Cellular uptake of polymers. Cellular uptake of homo- and random copolymers into AT1- and Walker 256 cells was measured *in vitro*. Therefore, low and high molecular weight reactive precursor polymers were labeled with the fluorochrome Oregon Green 488 cadaverine. Uptake experiments were performed using collagen-coated 24-well plates. Collagen A (Biochrom, Berlin, Germany) was diluted with water and pH-adjusted (3.5). Plates were incubated for 30 min and dried. Cells were grown until wells reached ~ 70% confluence when they were incubated with 500 µl HEPES-buffered Ringer solution (pH = 7.4) containing 0.02 mg polymer/ml for 2 h at 37 °C. After washing, the cells were lysed with 250 µl Triton X-MOPS lysis buffer (15 min, room temperature) and mechanically removed from the plate surface. After centrifugation, 100 µl supernatant was pipetted in 96-well black bottom microplates and analyzed in a microplate-reader (Infinite 200, Tecan, Männedorf, Switzerland) excitation 485 nm, emission 532 nm). Protein content of each sample was determined using Bradford reagent. The polymer uptake was expressed by the content of polymer/per gram cell protein.

Permeability assay. Vascular permeability of the tumor lines was measured by the extravasation of macromolecular dextrans. Therefore FITC- or Texas-Red-labeled dextrans with molecular weights of 10 kDa, 70

kDa or 200 kDa (Invitrogen, Darmstadt, Germany), respectively, were dissolved in saline at a concentration of 12.5 mg/ml. 400 µl of these solutions was injected into the tail vein of tumor bearing animals. After 15 min (10 kDa dextran), 1 h (70 kDa dextran) or 3 h (200 kDa dextran) animals were sacrificed, the tumors were removed, rapidly frozen in liquid nitrogen and cryosections (10 µm) prepared. Using fluorescence microscopy (Keyence, Neu-Isenburg, Germany) at low resolution, images of dextran extravasation were taken from 2 to 3 different regions of each cryosection. Approx. 3 to 4 sections from each tumor were analyzed resulting in 9 to 11 images per tumor. Dextran diffusion (described by the area fraction of the cryosection positive for the fluorochrome) was determined by image analysis software (ImageJ, National Institutes of Health, Bethesda MD, USA). The molecular diameter of the dextrans was determined by Fluorescence Correlation Spectroscopy using Rhodamine6G as calibration dye. Stock solutions of 0.1 mg dextran/mL NaCl were prepared. The diameters of the three dextrans were 1.77±0.1 nm (10 kDa, FITC-labeled), 14.42±1.0 nm (70 kDa, Texas Red-labeled) and 34.99±2.2 nm (200 kDa, FITC-labeled), respectively.

In vivo µPET imaging and ex vivo biodistribution studies

µPET imaging. For µPET imaging, rats were anaesthetized either with pentobarbital (40 mg/kg, intraperitoneal, Narcoren, Merial, Hallbergmoos, Germany) or with isofluran (2 %). Polymers were injected via tail vein puncture.

The µPET imaging was performed on a microPET Focus 120 small animal PET (Siemens/Concorde, Knoxville, USA). During PET measurements the animals were placed in supine position and breathed room air spontaneously. Dynamic PET studies were acquired in listmode. The radiolabeled polymers were administered as a bolus injection of 0.4 - 0.7 mL simultaneously with the start of the PET scan. The mean injected activity of labeled polymers was 23.6±1.3 MBq. The PET listmode data were histogrammed into 25 frames and reconstructed using OSEM2D algorithm. Volumes-of-interests (VOIs) were defined for tumor and reference tissue (testis). The testis was used as a reference since it was in the field of view when imaging the tumors on the feet and because the tissue concentration was relatively constant between all animals

on a low level. Time activity curves (TAC) were obtained with varying time frames (1.5-10 min) for a total measuring interval of 120 min. Ratios of tumor to reference tissue were calculated from integral images between 15' and 120' after polymer injection.

For PET imaging of the time course of body distribution in different internal organs the field of view was located over the trunk from the neck region to the pelvis. TACs were analyzed for VOIs of heart, liver, lung, kidney and aorta.

Biodistribution studies. In order to assess the distribution of the radiolabeled polymers in different organs of the animals, the polymer (concentration of 1 mg in 1 mL sodium chloride solution) was injected i.v. in anaesthetized tumor-bearing rats via the tail vein with a mean activity of 11.9 ± 0.7 MBq. After 120 or 240 min, the animals were sacrificed and different organ (kidney, liver, lung, spleen, heart, skeletal muscle, small intestine, testis, blood) and tumor samples were taken. The tissue samples were weighed and minced. Finally, the ^{18}F-activity in the organs was measured in a γ-counter.

In vitro assays

Autoradiography and histological staining. For autoradiography, animals were treated in the same way as in the biodistribution experiments. Directly after sacrifice (120 or 240 min after polymer injection) tumors were excised and rapidly frozen in liquid nitrogen cooled isopentane. The tissue was then embedded (Tissue-Tek, O.C.T. Compound, Sakura Finetek Europe, Leiden, The Netherlands) and coronar slices (thickness 20 µm) were cut with a cryostat (Slee, Mainz, Germany). The specimens were transferred on coated object holders and dried at room temperature until they were placed on Fuji imaging plates (BAS-SR 2040. 20x40 cm, Fujifilm Europe, Düsseldorf, Germany). After 5 hours of exposure, the phosphor screen was laser scanned in a 50 µm-pixel size mode using an image reader FLA-7000 (Fujifilm). Afterwards autoradiography sections were HE stained (hematoxylin 2 min, rinsed with tap water, eosin 30 s, rinsed) and dehydrated (ethanol) before coverslipped using aquatex mounting medium (Merck, Darmstadt, Germany). HE sections were digitized using digital microscopy (Keyence BZ-8000, Osaka, Japan).

Statistical analysis. Results are expressed as means±SEM. Differences between groups were assessed by the two-tailed Wilcoxon test for paired samples and by multi-factorial ANOVA. The significance level was set at α=5% for all comparisons.

Acknowledgement

The authors would like to thank Nicole Bausbacher and Bengü Yilmaz for their support during animal studies and following interpretation. We also want to thank the Max-Planck Graduate Center (MPGC, M. Allmeroth) as well as the Graduate School Materials Science in Mainz (Excellence Initiative, DFG/GSC 266, D. Moderegger) for financial support. In addition the authors are very thankful for financial support of the DFG (Rösch: RO 985/30-1; Thews: TH 482/4-1, Zentel: ZE 230/21-1) and SAMT Initiative Mainz. Furthermore thanks to Dr. Matthias Barz for fruitful discussion.

Additional information

The authors declare no competing financial interests.

References

[1] R. Duncan, *Nat Rev Drug Discov* **2003**, *2*, 347.

[2] Y. Matsumura, H. Maeda, *Cancer Research* **1986**, *46*, 6387.

[3] R. Duncan, *Advanced Drug Delivery Reviews* **2009**, *61*, 1131.

[4] T. Lammers, *Advanced Drug Delivery Reviews* **2010**, *62*, 203.

[5] T. Minko, P. Kopecková, V. Pozharov, J. Kopecek, *Journal of Controlled Release* **1998**, *54*, 223.

[6] D. P. Nowotnik, E. Cvitkovic, *Advanced Drug Delivery Reviews* **2009**, *61*, 1214.

[7] K. Ulbrich, V. Subr, *Advanced Drug Delivery Reviews* **2010**, *62*, 150.

[8] L. S. Heuser, F. N. Miller, *Cancer* **1986**, *57*, 461.

[9] M. Kissel, P. Peschke, V. Subr, K. Ulbrich, A. Strunz, R. Kühnlein, J. Debus, E. Friedrich, *European Journal of Nuclear Medicine and Molecular Imaging* **2002**, *29*, 1055.

[10] Z.-R. Lu, *Advanced Drug Delivery Reviews* **2010**, *62*, 246.

[11] M. M. Herth, M. Barz, M. Jahn, R. Zentel, F. Rösch, *Bioorganic & Medicinal Chemistry Letters* **2010**, *20*, 5454.

[12] M. M. Herth, M. Barz, D. Moderegger, M. Allmeroth, M. Jahn, O. Thews, R. Zentel, F. Rösch, *Biomacromolecules* **2009**, *10*, 1697.

[13] M. Allmeroth, D. Moderegger, B. Biesalski, K. Koynov, F. Rösch, O. Thews, R. Zentel, *Biomacromolecules* **2011** *12*, 2841.

[14] Y. M. H. Cabral, K. Mizuno, Q. Chen, M. Murakami, M. Kimura, Y. Terada,

M.R. Kano, K. Miyazono, M. Uesaka, N. Nishiyama & K. Kataoka, *Nature Nanotechnology* **2011**, *6*, 815.

[15] M. Barz, R. Luxenhofer, R. Zentel, A. V. Kabanov, *Biomaterials* **2009**, *30*, 5682.

[16] K. Kataoka, A. Harada, Y. Nagasaki, *Advanced Drug Delivery Reviews* **2001**, *47*, 113.

[17] M. Talelli, C. J. F. Rijcken, C. F. van Nostrum, G. Storm, W. E. Hennink, *Advanced Drug Delivery Reviews* **2010**, *62*, 231.

[18] J. Chiefari, Y. K. Chong, F. Ercole, J. Krstina, J. Jeffery, T. P. T. Le, R. T. A. Mayadunne, G. F. Meijs, C. L. Moad, G. Moad, E. Rizzardo, S. H. Thang, *Macromolecules* **1998**, *31*, 5559.

[19] E. R. G. Moad, S. H. Thang, *Aust. J. Chem.* **2005**, *58*, 379.

[20] P. Theato, *Journal of Polymer Science Part A: Polymer Chemistry* **2008**, *46*, 6677.

[21] M. Eberhardt, R. Mruk, R. Zentel, P. Théato, *European Polymer Journal* **2005**, *41*, 1569.

[22] M. Barz, M. Tarantola, K. Fischer, M. Schmidt, R. Luxenhofer, A. Janshoff, P. Theato, R. Zentel, *Biomacromolecules* **2008**, *9*, 3114.

[23] T. Lammers, R. Kühnlein, M. Kissel, V. Subr, T. Etrych, R. Pola, M. Pechar, K. Ulbrich, G. Storm, P. Huber, P. Peschke, *Journal of Controlled Release* **2005**, *110*, 103.

[24] S. Häggström, A. Bergh, J.-E. Damber, *The Prostate* **2000**, *45*, 42.

[25] P. Mukherjee, A. V. Sotnikov, H. J. Mangian, J.-R. Zhou, W. J. Visek, S. K. Clinton, *Journal of the National Cancer Institute* **1999**, *91*, 512.

[26] F. G. Wu HP, Liang HM, Zheng CS, Li X., *World J Gastroenterol* **2004**, *6*, 813.

[27] S. Halin, P. Hammarsten, P. Wikström, A. Bergh, *The Prostate* **2007**, *67*, 370.

[28] A. Gossmann, Y. Okuhata, D. M. Shames, T. H. Helbich, T. P. L. Roberts, M. F. Wendland, S. Huber, R. C. Brasch, *Radiology* **1999**, *213*, 265.

[29] M.-Y. Su, A. Mühler, X. Lao, O. Nalcioglu, *Magnetic Resonance in Medicine* **1998**, *39*, 259.

[30] S. b. Perrier, P. Takolpuckdee, C. A. Mars, *Macromolecules* **2005**, *38*, 2033.

[31] R. E. Rigler, E.S., *Springer Verlag* **New York 2001**.

[32] A. Bauman, M. Piel, R. Schirrmacher, F. Rösch, *Tetrahedron Letters* **2003**, *44*, 9165.

[33] P. Workman, E. O. Aboagye, F. Balkwill, A. Balmain, G. Bruder, D. J. Chaplin, J. A. Double, J. Everitt, D. A. H. Farningham, M. J. Glennie, L. R. Kelland, V. Robinson, I. J. Stratford, G. M. Tozer, S. Watson, S. R. Wedge, S. A. Eccles, *Br J Cancer* **2010**, *102*, 1555.

Additional results

The impact of the hydrophobic lauryl methacrylate group on the pharmacokinetics of HPMA based random copolymers *in vivo*

Polymer based nanocarrier systems gained high importance in the field of drug delivery over the last decades. Their application *in vivo* revealed major advantages compared to the free therapeutic agent, including a decrease in toxic side effects in healthy tissue, prolonged blood circulation times as well as accumulation in tumor tissue due to the EPR-effect. Besides these benefits, polymer therapeutics have to meet special requirements regarding the elimination from the body. In this regard, the herein investigated synthetic polymer poly(HPMA) – since it is biocompatible but not biodegradable – has to be renally cleared in an adequate time frame. In respect to the aforementioned key factors for a successful delivery of pharmacologically active drugs to the target site, our studies highlighted an HPMA based random copolymer system holding the majority of desired criteria. In this case, random copolymerization with lauryl methacrylate (LMA) as hydrophobic group was carried out, leading to an incorporation ratio of 25 %. Molecular weight was chosen to be above the renal threshold of HPMA copolymers [1] and aggregate formation could be proven by means of Fluorescence Correlation Spectroscopy (FCS). This HPMA-*ran*-LMA copolymer (here named **P4***) exhibited favorable *in vivo* characteristics, including low hepatic as well as spleenic uptake, enhanced retention in the blood pool (nearly 60 % remained in the blood stream after 2 hours p.i.), comparatively highest tumor accumulation and despite its molecular weight still renal clearance (see chapter 5.1 and 5.2). Based on these results, the question was arising whether the observed pharmacokinetic profile is attributed to the incorporation ratio of the hydrophobic lauryl methacrylate moiety. Due to this assumption, we decided on the synthesis of two more HPMA-*ran*-LMA copolymers with lower amounts of hydrophobic groups, 16 % (**P2***) and 20 % (**P3***) respectively. Furthermore, the obtained data was directly compared to a high molecular weight HPMA homopolymer (**P1***) – not exhibiting hydrophobic lauryl methacrylate chains - since the influence of hydrophilicity / hydrophobicity seems to be a major factor for subsequent organ accumulation of the polymeric compounds. Their evaluation *in vivo* was accomplished by introducing the short-lived radionuclide fluorine-18 and subsequent monitoring via Positron Emission Tomography (PET) as well as *ex vivo* biodistribution studies in Walker 256 mammary

carcinoma bearing rats. The obtained findings were directly compared to the already received results of the random copolymer **P4*** (LMA content = 25 %). Analytical data of the different HPMA based polymer structures are depicted in table 1.

Table 1**: Analytical data of reactive ester homopolymer and random copolymers (**P1*-R – P4*-R**) as well as their conversion to final polymer structures (**P1* - P4).*

Notation	Polymer structure	Monomer ratio	M_n [g/mol]	M_w [g/mol]	PDI[b)]	R_h in nm[e)]
P1*-R	Homopolymer	100 %[a)]	87000 [b)]	130000 [b)]	1.49	-
P2*-R	Random copolymer	85:15[a)]	61000[b)]	106000[b)]	1.73	-
P3*-R	Random copolymer	82:18[a)]	61000[b)]	98000[b)]	1.59	-
P4*-R	Random copolymer	80:20[a)]	57000[b)]	80000[b)]	1.41	-
P1*	Homopolymer	100 %[c)]	52000 [d)]	77000 [d)]	1.49	3.0
P2*	Random copolymer	84:16[c)]	40000[d)]	70000[d)]	1.73	30.9
P3*	Random copolymer	80:20[c)]	41000[d)]	65000[d)]	1.59	36.3
P4*	Random copolymer	75:25[c)]	39000[d)]	55000[d)]	1.41	39.9

*[a)] = Calculated monomer ratio; [b)] = Determination by GPC in THF as solvent; [c)] = Monomer ratio determined by ^{1}H-NMR spectroscopy after polymeranalogous reaction with 2-hydroxypropylamine; [d)] = Calculated from the molecular weight of the reactive ester polymers **P1*-R –P3*-R** as determined by GPC in THF as solvent; [e)] = Hydrodynamic radii of the aggregates determined by Fluorescence Correlation Spectroscopy (FCS)*

As clearly seen from the data, M_w of all investigated polymer structures was > 45 kDa and thus above the renal threshold of HPMA copolymers [2]. Hydrodynamic radii were determined to be in the range of 3 nm for the high molecular weight homopolymer **P1***and 31 to 40 nm for the random copolymer structures. Thus, in isotonic solution the homopolymer is dissolving as individual random coil whereas the HPMA-*ran*-LMA copolymers demonstrated superstructure formation. Regarding the last-mentioned, they show a slight decrease in size with lower lauryl methacrylate content. Denser superstructures in aqueous environment are formed, attributed to higher hydrophilicity of **P2*** and **P3***. These findings stay in good correspondence with former studies of Ulbrich et al. who determined a decrease in R_h for HPMA based copolymers with decreasing dodecyl content [3].

Radioactive labeling of the compounds was accomplished by [^{18}F]fluoroethylation using similar conditions compared to former studies on HPMA based polymer architectures

(see 5.1 and 5.2). Radiochemical yields are summarized in table 2. An obvious trend can be derived from the received data. Highest RCYs were obtained for the polymer without any hydrophobic modification, namely homopolymer **P1***. With increasing amount of lauryl methacrylate, radiolabeling efficiencies are falling down, implying that the phenolic groups are less accessible in highly hydrophobic polymer structures.

Table 2**: Polymer characteristics as well as Radiochemical Yields (RCYs) for HPMA homopolymer (**P1) as well as HPMA-ran-LMA copolymers with different LMA incorporation ratios (**P2*-P4***).*

Notation	Polymer structure	LMA ratio[c)]	M_n in [g/mol]	M_w in [g/mol]	RCY in % [f)]
P1*	Homopolymer	0 %	52000 [d)]	77000 [d)]	24±2
P2*	Random copolymer	16 %	40000[d)]	70000[d)]	16 ± 3
P3*	Random copolymer	20 %	41000[d)]	65000[d)]	12 ± 3
P4*	Random copolymer	25 %	39000[d)]	55000[d)]	9 ± 2

[f)] = *Corrected Radiochemical Yields (RCYs) determined via SEC (represented as mean±SEM)*

Organ distribution studies

To study the influence of the hydrophobic moiety of HPMA-*ran*-LMA copolymers on organ distribution as well as tumor accumulation *in vivo*, biodistribution studies in Walker 256 mammary carcinoma bearing rats were carried out. Quantification of the recovered dose of radiofluorinated HPMA based polymer structures was accomplished in selected organs (liver, spleen, kidney, blood, heart, lung, muscle small intestine, testis and tumor) 2 and 4 hours after intravenous administration.

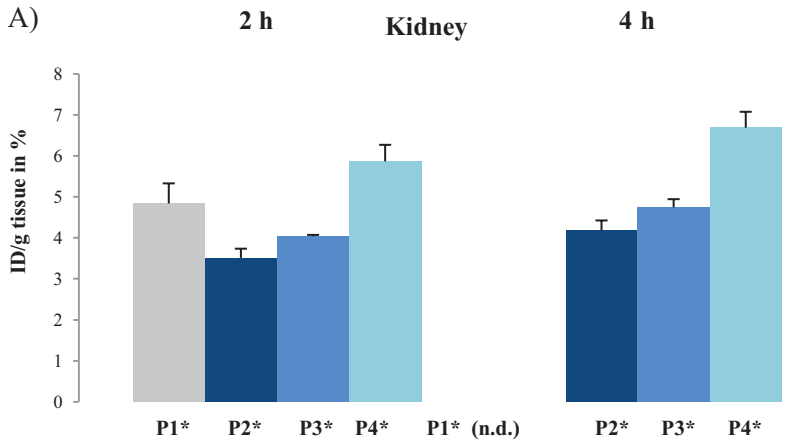

Figure 1A**: Biodistribution data of polymers **P1*- P4 in the kidney 2 and 4 hours p.i.. **P1*** at 4 h was not determined (n.d.).*

Figure 1A illustrates the renal excretion pattern of all four polymers over a time span of 4 hours. In comparison, **P2*** showed lowest kidney uptake (3.51±0.22 % ID/g tissue) whereas **P4*** was the one exhibiting highest glomerular filtration after 2 hours (5.86±0.40 % ID/g tissue). Kidney accumulation of all investigated random copolymer structures was increasing over time thus demonstrating a slow but appearing renal elimination from the body. Seymour et al. already revealed the tremendous effect of M_w of HPMA based copolymers on the resulting biodistribution characteristics [2]. They could demonstrate that polymers with molecular weights of less than 45 kDa were rapidly excreted from the blood stream resulting in fast urinary elimination. In addition, molecules with molecular weights above the renal threshold were determined to be still able to pass through the glomerular pore as long as they exhibit a flexible structure (also shown for HPMA) [4, 5]. These findings stay in good correspondence to our results, since the herein investigated polymers **P1*- P4*** possessed higher molecular weights (M_w = 55 kDa – 77 kDa) than the renal threshold for HPMA copolymers but were still renally cleared.

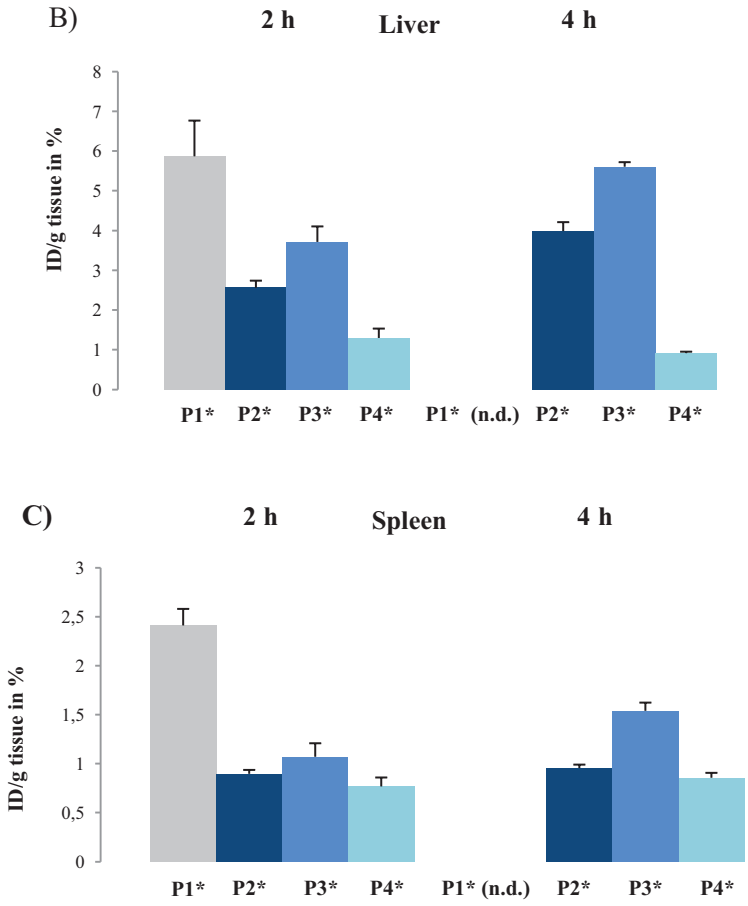

Figure 1B and 1C**: Biodistribution data of polymers **P1*- P4 in liver (1B) and spleen (1C) 2 and 4 h p.i.. **P1*** at 4 h was not determined (n.d.).*

Biodistribution data of the three random copolymer systems in liver and spleen demonstrated an opposite trend compared to kidney accumulation. The organs of the mononuclear phagocyte system showed lowest concentrations for polymer **P4*** with highest hydrophobic content (2 h liver: 0.30±0.24 and spleen: 0.77±0.09 % ID/g tissue) as well as predominant hepatic uptake of random copolymer **P3***, still increasing over time (2 h = 3.72±0.39 and 4 h = 5.61±0.11 % ID/g tissue). In this regard, no direct correlation between the percentage of incorporated hydrophobic lauryl methacrylate and resulting MPS recognition can be drawn. The difference in polymer size (nm-range of 31 – 40) can only play a minor role since nanoparticles with sizes up to 20 µm can be recognized and transported by the cells of the mononuclear phagocyte system (Kupffer cells) [7]. This is a size limit far beyond the here presented polymer systems. The only parameter which was explicitly varied in this study was the ratio of hydrophobic moiety - thus assuming that an adequate balance of hydrophilicity / hydrophobicity of the random copolymer structures (as seen for a polymer **P4*** with a LMA content of 25 %) is preventing opsonization and hepatobiliary excretion. This idea is in accordance with former studies on organic cations of Meijer et al. [8] who suggested that not lipophilicity *per se* but the amphiphilic balance plays a major role in hepatic uptake [9]. The aforementioned assumption seems to be a major factor regarding liver and spleen accumulation of polymeric systems, further supported by the observation of a nearly 3-fold increase in both hepatic as well as spleenic uptake of the hydrophilic HPMA homopolymer **P1*** compared to the amphiphilic copolymer structures. Besides, the issue of flexibility and deformability has to be addressed, having an important influence on blood circulation times as well as macrophage uptake [10]. Due to the high incorporation ratio of lauryl methacrylate in **P4***, the random copolymer may be in a strong disequilibrium and hence more dynamic / flexible in its conformation *in vivo*.

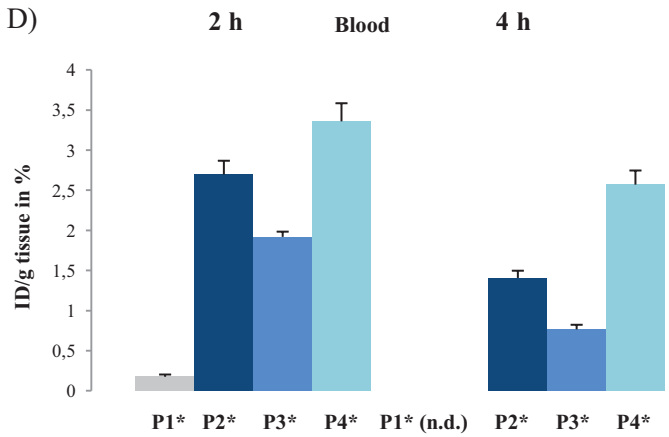

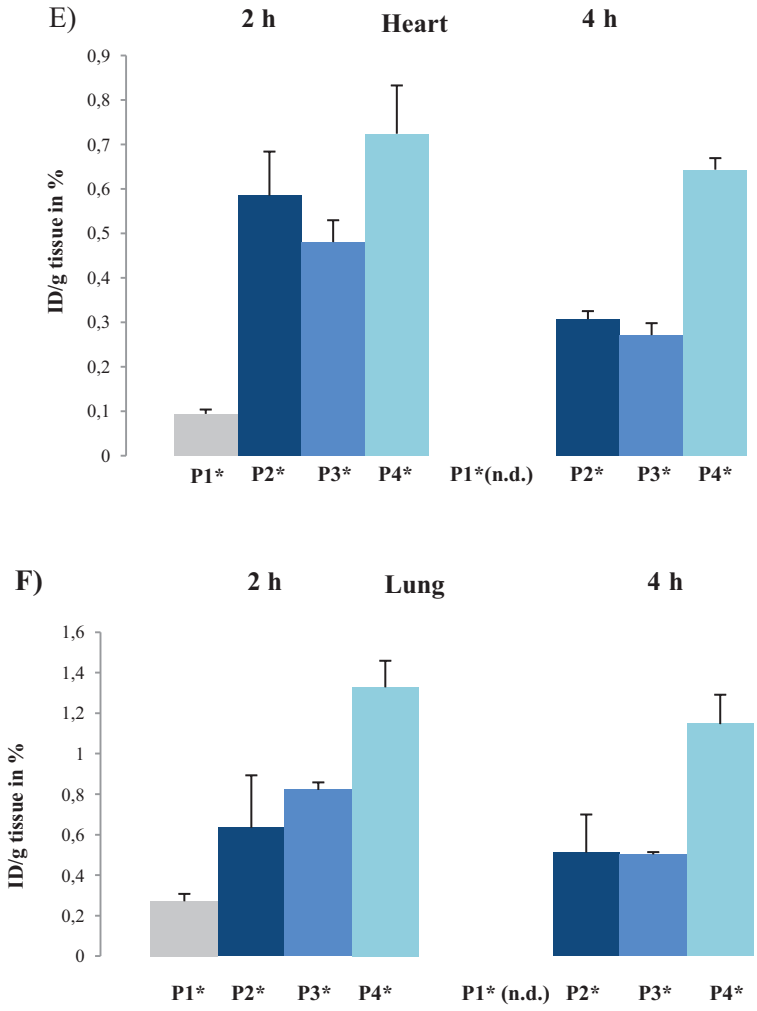

Figure 1D-1F**: Biodistribution data of polymers **P1 - **P4*** in blood (1D), heart (1E) and lung (1F) 2 and 4 hours p.i.. **P1*** at 4 h was not determined (n.d.).*

As seen in Fig. 1D, distinct disparities in blood pool concentration could be observed for the varying random copolymer structures. Polymer **P4* -** with highest LMA content - showed supreme plasma-half life, nearly staying constant over time (2 h = 3.36±0.23 and 4 h = 2.57±0.18 % ID/g tissue). Its recovered dose after 4 hours corresponds to more than 40 % of polymer remaining in the blood stream [11]. In contrast, HPMA homopolymer **P1*** demonstrated lowest blood pool concentrations - with predominant clearance from the blood stream within 2 hours (2 h = 0.18±0.03 % ID/g tissue). These findings may be attributed to its efficient hepatic as well as spleenic uptake over time hence eliminating the homopolymer from the blood pool. A closely related pattern can be seen for polymer **P3*** (20 % LMA) which exhibits medium levels in the blood, drastically decreasing with enhanced liver accumulation in the examined time span. In conclusion, the already

observed characteristics of the investigated polymer systems in the organs of the MPS directly reflect their behavior in the blood pool. Highly blood supplied organs such as heart and lung are displaying the general trend of polymer concentration in the blood stream, possessing the highest values for polymer **P4*** (25 % LMA) over time (4 h heart = 0.64±0.03 and 4 h lung = 1.15±0.14 % ID/g tissue). With decreasing blood presence, levels in heart and lung are also reduced, as clearly seen for homopolymer **P1*** after 2 hours (heart = 0.09±0.01 and lung = 0.27±0.04 % ID/g tissue) and for random copolymer **P2*** after 4 hours (heart = 0.27±0.03 and lung = 0.50±0.01 % ID/g tissue). Besides, the concentration of the herein investigated HPMA based polymer structures in muscle and small intestine was comparatively low and stayed constant over time. An overview of the obtained biodistribution data in organs of interest (2 and 4 hours p.i.) is given in table 3.

Table 3**: Ex vivo biodistribution data of the investigated random copolymer structures **P1 - **P4*** in major organs of interest 2 and 4 hours after intravenous administration in Walker 256 mammary carcinoma bearing rats. Data is represented as % ID/g tissue (means±SEM).*

2 h p.i.	**Polymer concentration in % ID/g tissue**			
Organ	**Polymer P1*** (0 % LMA)	**Polymer P2*** (16 % LMA)	**Polymer P3*** (20 % LMA)	**Polymer P4*** (25 % LMA)
lung	0.27±0.04	0.63±0.26	0.82±0.04	1.33±0.13
liver	5.87±0.90	2.56±0.18	3.71±0.40	1.30±0.24
spleen	2.41±0.17	0.90±0.04	1.07±0.14	0.77±0.09
kidney	4.83±0.49	3.51±0.22	4.04±0.03	5.86±0.40
muscle	0.04±0.01	0.10±0.01	0.08±0.01	0.16±0.05
heart	0.09±0.01	0.59±0.10	0.48±0.05	0.72±0.11
blood	0.18±0.03	2.70±0.17	1.92±0.07	3.36±0.23
small intestine	0.36±0.06	0.42±0.06	0.32±0.01	0.46±0.11
testis	0.06±0.01	0.10±0.02	0.11±0.01	0.18±0.02
W 256 tumor	0.14±0.02	0.56±0.14	0.56±0.10	0.63±0.13

4 h p.i.	**Polymer concentration in % ID/g tissue**			
Organ		**Polymer P1*** (16 % LMA)	**Polymer P2*** (20 % LMA)	**Polymer P3*** (25 % LMA)
lung	n.d.	0.51±0.19	0.50±0.01	1.15±0.14
liver	n.d.	3.99±0.22	5.61±0.11	0.92±0.04
spleen	n.d.	0.95±0.04	1.54±0.08	0.86±0.05
kidney	n.d.	4.17±0.25	4.74±0.20	6.68±0.39

muscle	n.d.	0.04±0.00	0.05±0.01	0.09±0.01
heart	n.d.	0.31±0.02	0.27±0.03	0.64±0.03
blood	n.d.	1.41±0.01	0.77±0.06	2.57±0.18
small intestine	n.d.	0.36±0.04	0.26±0.02	0.33±0.01
testis	n.d.	0.12±0.01	0.12±0.01	0.16±0.01
W 256 tumor	n.d.	0.49±0.03	0.52±0.12	0.64±0.02

Tumor accumulation

Besides the closer investigation of the effect of amphiphilicity on the biodistribution profile of HPMA-*ran*-LMA copolymers *in vivo*, main focus was furthermore laid on polymer dependent tumor accumulation in the Walker 256 mammary carcinoma model. Due to the favorable characteristics of polymer **P4*** regarding both organ and tumor uptake, we aimed to gain further knowledge about the hydrophilic / hydrophobic balance influencing tumor accumulation. Based on this concept, two random copolymer systems with lower lauryl methacrylate ratios (**P2*** = 16 % and **P3*** = 20 %) as well as a high molecular weight homopolymer (**P1***) were comparatively examined to **P4*** over a time span of 4 hours (see Fig. 2A).

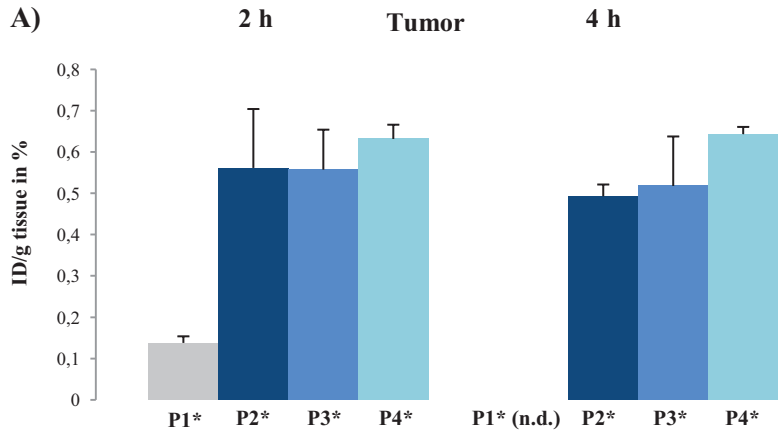

Figure 2A**: Biodistribution data of polymers **P1*- P4 in Walker 256 mammary carcinoma tissue 2 and 4 h p.i. **P1*** at 4 h was not determined (n.d.).*

Unfortunately due to a high discrepancy in tumor volume in the herein presented study, relatively high SEM values for the different random copolymers in tumor tissue were obtained. Nevertheless, a general trend can be determined over time. Polymer **P4*** with highest LMA content (25 %) is also demonstrating major tumor uptake within 4 hours (0.64±0.02 % ID/g tissue). In comparison, HPMA-*ran*-LMA copolymer **P2*** - with only

16 % of hydrophobic lauryl methacrylate groups - exhibits lowest tumor concentrations among the amphiphilic copolymers in the same time frame (0.49±0.03 % ID/g tissue). In this regard, it can be assumed that the increased incorporation of the hydrophobic moiety has a major impact on the resulting tumor uptake *in vivo*, also maintained by the observation of a 5-fold lower tumor accumulation of the hydrophilic homopolymer **P1*** (0.14±0.02 % ID/g tissue). The augmented interaction between the hydrophobic parts of the tumor membrane and the randomly distributed lauryl methacrylate chains – also present along the hydrophilic corona of the polymeric micelles - may be a possible explanation. These findings stay in good accordance with former *in vitro* studies in our group (see chapter 5.2) in Walker 256 mammary carcinoma cells. Three different HPMA based polymer architectures were examined (homopolymers, random as well as block copolymers) and among these the high molecular weight random copolymer **P4*** was the one showing supreme cellular uptake. In addition, studies of Barz et al. [12] with the MCF7/ADR cell line revealed an identical *in vitro* behavior. HPMA based polymers with higher molecular weight were predominantly taken up, possessing a maximum for a 40 kDa HPMA-*ran*-LMA copolymer. The observed polymer dependent characteristics were also attributed to the higher cell-membrane affinity of random copolymer structures. Furthermore, studies of Ulbrich et al. clearly demonstrated that the type and content of the hydrophobic substituent in Dox modified HPMA random copolymers had a considerable influence on tumor accumulation / regression in mice bearing EL-4 T-cell lymphoma [3]. Their investigations revealed that higher hydrophobicity was a key factor for prolonged blood circulation as well as enhanced tumor concentrations, particularly found for a randomly distributed cholesterol moiety.

Finally, selected tumor to organ ratios of the here examined HPMA based polymer structures are summarized in table 4 thus allowing a better determination of tumor targeting abilities of the three different structures. Tumor-to-organ ratio < 1 illustrates increased accumulation in healthy tissue; a ratio > 1 indicates a more effective tumor concentration of the compounds.

Table 4**: Tumor to organ ratios of polymers **P1 - **P4*** 4 hours post injection*

2 h p.i.	P1* (0 % LMA)	P2* (16 % LMA)	P3* (20 % LMA)	P4* (25 % LMA)
tumor	1	1	1	1
lung	0.52	0.96	1.04	0.56
liver	0.02	0.12	0.09	0.70
spleen	0.06	0.52	0.34	0.74
kidney	0.03	0.12	0.11	0.10
muscle	3.50	12.25	10.40	7.11
heart	1.55	1.58	1.93	1.00
small intestine	0.39	1.36	2.00	1.94
testis	2.33	4.08	4.33	4.00

As clearly seen for all polymer systems, tumor-to-organ ratio was always higher for muscle, heart, small intestine (except of **P1***) and testis. In contrast, organs such as lung, liver, spleen and kidney showed tumor-to-organ ratios < 1 hence indicating increased polymer accumulation in healthy tissues. Nevertheless, among the examined nanocarrier systems, the random copolymer **P4*** illustrated enhanced ratios regarding liver and spleen (0.70 and 0.74 respectively) thereby underlining the importance of an appropriate hydrophilic / lipophilic balance for preventing the recognition by the cells of the mononuclear phagocyte system.

MicroPET imaging in Walker 256 carcinoma bearing rats

In addition to the already obtained quantitative results of organ / tumor distribution, both static as well as dynamic microPET imaging was accomplished for *in vivo* monitoring of the different polymer systems. Whole body images (Fig. 3A), acquired 2 hours post injection – were in good correlation to the observed pharmacokinetic profile by means of *ex vivo* biodistribution studies (see Fig. 1A-1F). **P2*** and **P4*** showed distinct blood circulation properties (visualized by the aorta (A)) thus being consistent with the quantitative results in the blood stream (see Fig. 1D). In contrast, random copolymer **P2*** possessed lower levels in the blood pool which was concordantly detected by means of Positron Emission Tomography, too. Furthermore, the HPMA based homopolymer **P1*** was not present in the blood stream any more – staying in accordance with the obtained *ex vivo* results.

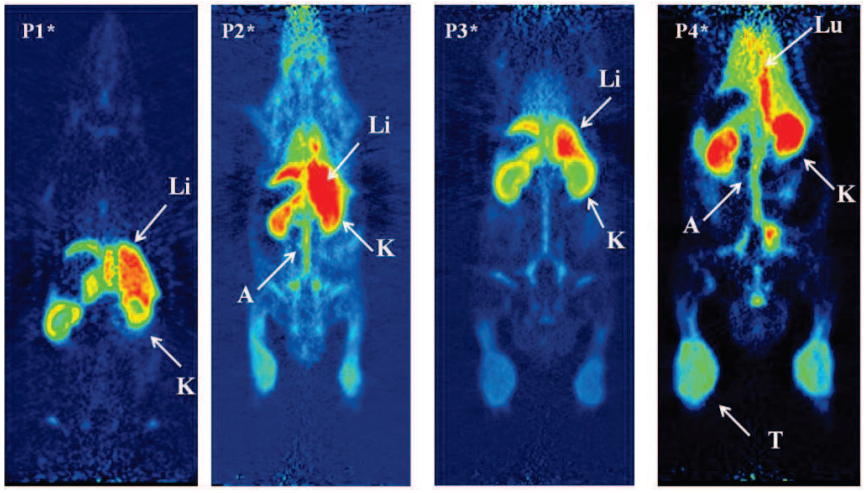

Figure 3A**: Whole body microPET image sections obtained 120-125 min after i.v. administration of ^{18}F-labeled polymers **P1*-P4. Organs of interest: kidney (K); aorta (A); liver (Li); lung (Lu) and tumor (T)*

All investigated polymer systems exhibited renal clearance as monitored via the kidneys (K). In addition, enhanced liver (Li) uptake for polymers **P1***, **P2*** and **P3*** could be seen. The HPMA-*ran*-LMA copolymer **P4*** furthermore revealed increased concentrations in lung (Lu) and tumor tissue (T). Besides, tumor accumulation was visualized using dynamic µPET imaging over a time course of 2 hours p.i. (Fig. 3B). Coronal slices of summed microPET images through the tumors – implanted at the hind foot dorsum – clearly displayed tumor uptake for the three random polymers.

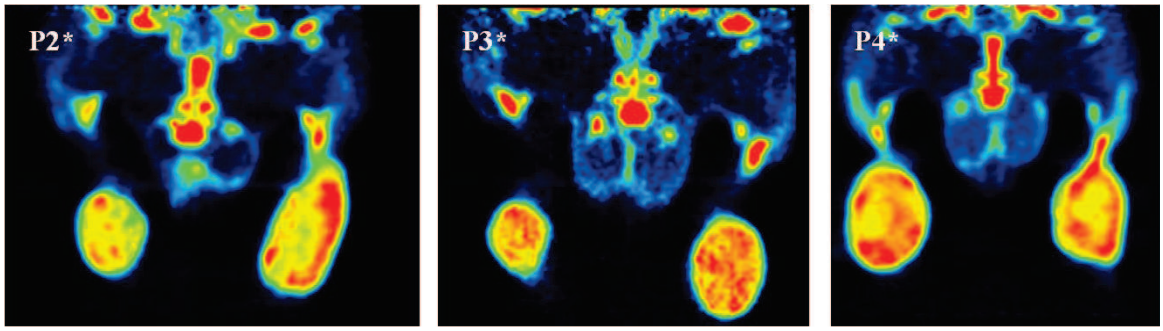

Figure 3B**: Examples of coronal µPET image sections of Walker 256 mammary carcinoma 60-120 min p.i.. **P1 was not monitored.*

In conclusion, the present study demonstrates the promising potential of HPMA-*ran*-LMA copolymers in the field of polymer drug delivery – with special focus on the effect of hydrophobic modification on their pharmacokinetic profile *in vivo*. Compared to the hydrophilic homopolymer **P1***, random copolymers with increasing lauryl methacrylate

content showed improved tumor accumulation and especially polymer **P4*** (25 % LMA) exhibited low hepatic as well as spleenic uptake. It can be assumed that the hydrophilic / lipophilic balance has a major influence on the recognition of the investigated nanoparticles by the MPS and thus the incorporation ratio of 25 % hydrophobic groups seems to be a reasonable approach for HPMA based polymer therapeutics. The protection toward opsonization is also leading to prolonged blood circulation times of random copolymer **P4*** - fundamental for the widely known EPR-effect.

References

1. Seymour, L. W.; Miyamoto, Y.; Maeda, H.; Brereton, M.; Strohalm, J.; Ulbrich, K.; Duncan, R., Influence of molecular weight on passive tumour accumulation of a soluble macromolecular drug carrier. *European Journal of Cancer* **1995,** 31, (5), 766-770.
2. Seymour, L. W.; Duncan, R.; Strohalm, J.; Kopeček, J., Effect of molecular weight (Mw) of N-(2-hydroxypropyl)methacrylamide copolymers on body distribution and rate of excretion after subcutaneous, intraperitoneal, and intravenous administration to rats. *Journal of Biomedical Materials Research* **1987,** 21, (11), 1341-1358.
3. Chytil, P.; Etrych, T.; Konak, C.; Sirova, M.; Mrkvan, T.; Boucek, J.; Rihova, B.; Ulbrich, K., New HPMA copolymer-based drug carriers with covalently bound hydrophobic substituents for solid tumour targeting. *Journal of Controlled Release* **2008,** 127, (2), 121-130.
4. Renkin, E. M.; Gilmore, J. P., Renal Physiology. *Handbook of Physiology (VIII)* **1973,** J. Orloff and R.W. Berliner (Eds.).
5. Rennke, H. G.; Venkatachalam, M. A., Glomerular permeability of macromolecules. Effect of molecular configuration on the fractional clearance of uncharged dextran and neutral horseradish peroxidase in the rat. *The Journal of Clinical Investigation* **1979,** 63, (4), 713-717.
6. Alexis, F.; Pridgen, E.; Molnar, L. K.; Farokhzad, O. C., Factors Affecting the Clearance and Biodistribution of Polymeric Nanoparticles. *Molecular Pharmaceutics* **2008,** 5, (4), 505-515.
7. Bertrand, N.; Leroux, J.-C., The journey of a drug-carrier in the body: An anatomo-physiological perspective. *Journal of Controlled Release* 161, (2), 152-163.
8. Meijer, D. K. F.; Mol, W. E. M.; Müller, M.; Kurz, G., Carrier-mediated transport in the hepatic distribution and elimination of drugs, with special reference to the category of organic cations. *Journal of Pharmacokinetics and Pharmacodynamics* **1990,** 18, (1), 35-70.
9. Neef, K.; Jonkman, J. H. G.; Meijer, D. K. F., Hepatic disposition and biliary excretion of the organic cations thiazinamium and thiazinamium sulfoxide in rats. *Journal of Pharmaceutical Sciences* **1978,** 67, (8), 1147-1150.
10. Banquy, X.; Suarez, F.; Argaw, A.; Rabanel, J.-M.; Grutter, P.; Bouchard, J.-F.; Hildgen, P.; Giasson, S., Effect of mechanical properties of hydrogel nanoparticles on macrophage cell uptake. *Soft Matter* **2009,** 5, (20), 3984-3991.
11. Lee, H. B.; Blaufox, M. D., Blood Volume in the Rat. *J Nucl Med* **1985,** 26, (1), 72-76.

12. Barz, M.; Luxenhofer, R.; Zentel, R.; Kabanov, A. V., The uptake of N-(2-hydroxypropyl)-methacrylamide based homo, random and block copolymers by human multi-drug resistant breast adenocarcinoma cells. *Biomaterials* **2009,** 30, (29), 5682-5690.

5.3 PEGylation of HPMA-based block copolymers enhances tumor accumulation *in vivo*: A quantitative study using radiolabeling and Positron Emission Tomography

***Mareli Allmeroth*[1,§],** [redacted]

[redacted]

[redacted]

[§] *Institute of Organic Chemistry, Johannes Gutenberg University, Duesbergweg 10-14, 55099 Mainz, Germany;* [redacted]

[redacted]

Journal of Controlled Release, in preparation

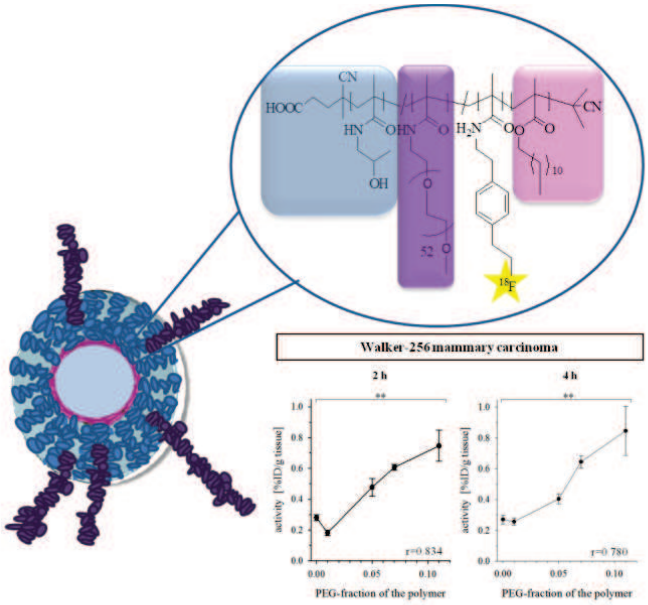

PEGylation of HPMA-*b*-LMA copolymers improves their *in vivo* pharmacokinetics in a linear trend-monitored by PET-

Abstract

Block copolymer micelles are widely established drug delivery systems, particularly in the field of anticancer treatment. Due to their amphiphilic core-shell structure, hydrophobic (chemo) therapeutics can be easily encapsulated. Polymer size as well as surface properties highly determine the *in vivo* potential / performance with PEGylation being the most commonly applied approach to tune pharmacokinetics for efficient drug delivery. In the present study five different HPMA based block copolymers - with lauryl methacrylate as hydrophobic block - were investigated in the Walker 256 mammary carcinoma *in vivo*. They varied in incorporation ratio of a PEG_{2000} side chain fragment in the hydrophilic block, ranging from block copolymers with 0 % PEG to 11 % degree of PEGylation. Polymers were labeled with the positron emitter ^{18}F and organ / tumor uptake was quantified by *ex vivo* biodistribution as well as microPET imaging. Tumor cell uptake *in vitro* was studied using fluorescence labeled polymers. Most remarkably, the *in vivo* results revealed a linear trend in tumor accumulation – with lowest tumor uptake of the pure block copolymer to highest enrichment with 11 % PEG side chains. Within the studied polymers, the block copolymer of 7 % PEGylation exhibited the most favorable organ distribution pattern, showing highest blood-circulation level as well as lowest hepatic and spleenic uptake. However, no direct correlation between PEGylation dependent increase in tumor accumulation *in vivo* and the polymer uptake of Walker 256 tumor cells *in vitro* was observed where highest cellular uptake was determined for block copolymers with lowest PEG content (0 and 1 %). These findings emphasize the need for reliable (non-invasive) *in vivo* techniques revealing overall polymer distribution and helping to identify drug carrier systems for efficient therapy such as radiolabeling in combination with PET imaging.

1. Introduction

Over the last four decades "Polymer therapeutics", a term describing polymeric drugs, polymer-drug conjugates, polymer-protein conjugates, polymeric micelles as well as polyplexes, have been intensively studied regarding their potential in anticancer treatment [1]. The key benefits of polymer based drug delivery systems compared to the low molecular weight free drug rely on the reduction of usually occurring toxic side effects in healthy tissue, their enhanced accumulation in the tumor due to the EPR effect [2, 3] and an increase in plasma half-life toward the pure chemotherapeutic agent.

Demonstrated by the moderate number of clinically tested polymers, some essential requirements need to be fulfilled by the polymer drug carrier system. Besides being non-toxic, non-immunogenic, biodegradable or respectively biocompatible with an adequate molecular weight to allow body elimination, the carrier system should be narrowly distributed to ensure homogeneity of the final conjugates. In this regard, poly(HPMA) is holding favorable characteristics, already validated by diverse preclinical and clinical studies [4-10].

Nevertheless, major obstacles still have to be overcome. These include the protection of the polymer drug delivery systems versus degrading enzymes or fast uptake by the reticuloendothelial system (RES) resulting in a rapid elimination of the carrier system from the blood stream. Considering these demands, PEG has become firmly established as promising candidate to prolong the pharmacokinetic properties of drugs, with special focus on protein modification as generally described by the term PEGylation [11-16]. The so called "stealth properties" of polyethylene glycol – responsible for low immunogenicity and antigenicity of the coated material - are mainly based on the high hydrophilicity as well as flexibility of the PEG-chains forming a protective layer, thereby e.g. minimizing the identification by opsonin proteins responsible for phagocytic uptake [12, 17, 18]. Regarding their shielding efficacy, optimal molecular weights for polyethylene glycol have been reported to be between 1500 – 5000 g/mol [17, 19]. The above mentioned favorable characteristics of PEG render this polymer valuable for a variety of biomedical applications and particularly in combination with the multifunctional poly(HPMA), polymer drug carrier

systems with beneficial synergetic effects can be created.

Previous studies on ^{18}F-radiolabeled HPMA homopolymers and random copolymers revealed that the ratio of hydrophilicity / hydrophobicity as well as aggregate formation possessed a major impact on the body distribution in the living animal [20]. Taking this knowledge into consideration, we subsequently concentrated on the correlation between specific polymer characteristics (e.g. molecular weight, architecture and lipophilicity) and their influence on tumor uptake in two different tumor models. Amphiphilic HPMA-LMA random and block copolymers – both forming super-structures in aqueous media - revealed promising results of tumor accumulation *in vivo* and thus may be attractive candidates for drug delivery [21-23]. Due to the aforementioned results, the question was arising whether the pharmacokinetics of the HPMA based block copolymers can be improved by incorporation of PEG side chains into the hydrophilic block. To our knowledge, no attempts of combining the favorable characteristics of HPMA and PEG into one polymer chain of a block copolymer have been reported so far.

In contrast to the dynamic nature of random copolymers, amphiphilic block copolymers are characterized by higher stability in hydrophilic media (contributed to their tendency to self-assemble in water driven by a gain of entropy) which is especially advantageous for the entrapment of hydrophobic drugs into the core. Due to their small sizes as well as the formation of a hydrophilic shell providing steric hindrance, prolonged circulation times can be achieved for micellar carriers [24]. With regard to the need of forming well-defined polymers, controlled radical polymerization techniques like ATRP or RAFT [25-28] introduced the facile access to narrowly distributed polymer structures and especially in combination with reactive ester chemistry [21, 29, 30], RAFT offers an elegant route to a variety of polymer architectures and functional groups. Not only imaging moieties (e.g. fluorescent or radioactive markers) and therapeutics can be attached, also the polymer nature of the hydrophilic shell can be easily modified.

The previous results [20] also demonstrated the need for appropriate preclinical screening methodologies to select a suitable therapy for the individual patient [8, 31]. Concerning this purpose, radiolabeling and Positron

Emission Tomography (PET) are helpful diagnostic tools providing detailed information on body distribution as well as tumor accumulation in the living organism. Depending on the radionuclide's half-life, the diagnostic time frame can be adjusted from early phase accumulation to long-term imaging over weeks or months. Until now, studies concerning the *in vivo* behavior of diverse HPMA and PEG based nanoparticles have been almost exclusively carried out using either γ-imaging radionuclides like ^{99m}Tc, ^{111}In or $^{125/131}$I [32-36] providing relatively low spatial resolution or by means of the metallic positron emitter ^{64}Cu which requires chelating agents [37-40]. In contrast to these approaches, we demonstrated the successful radio-labeling of various HPMA based polymers with the positron emitters $^{72/74}$As [41] and ^{18}F [42], thereby establishing PET imaging to assess the *in vivo* capability of potential drug delivery systems.

In this work we have focused on a precise modification of HPMA-*b*-LMA copolymers by incorporating different percentages of a linear, amine-functionalized PEG_{2000Da} fragment into the hydrophilic block. This approach was aimed to optimize both blood retention time as well as tumor uptake of HPMA based block copolymers, taking advantage of the so called "stealth properties" of PEG chains > 1500 Dalton towards opsonization processes. In order to correlate the influence of PEG content on the resulting pharmacokinetics *in vivo*, the block copolymers were radiolabeled with the positron emitting nuclide ^{18}F holding ideal nuclear characteristics concerning PET imaging ($t_{1/2}$: 109.7 min, β^+: 635 keV, 96.7%). This enabled to investigate tumor accumulation as well as body distribution in the experimental Walker 256 mammary carcinoma model by means of μPET imaging and *ex vivo* biodistribution studies. In addition, the cellular uptake into tumor cells of PEGylated block copolymers was analyzed.

2. Material and methods

2.1 Materials

All solvents were of analytical grade, as obtained by Sigma Aldrich and Acros Organics. Dioxane was distilled over a sodium / potassium composition, di-chloromethane over calcium hydride. Lauryl methacrylate was distilled to remove the stabilizer and stored at -18 °C. 2,2'-azoisobutyronitrile (AIBN) was

recrystallized from diethyl ether and stored at -18 °C as well.

2.2 Experimental setups

Experimental setups can be found in the supplementary information.

2.3 Synthesis of the polymers

The polymers $\mathbf{P_{0\%}}$ to $\mathbf{P_{11\%}}$ were prepared in analogy to reference [20, 21, 42]. The details are added as supplementary information.

2.4 Characterization of the polymers

The hydrodynamic radii of the polymeric systems were determined by Fluorescence Correlation Spectroscopy (FCS) using a commercial FCS setup. Thereby aggregate formation of the block copolymers can be proven. The details can be found in the supplementary information.

2.5 Radiolabeling and purification for *ex vivo* and *in vivo* experiments

Radiolabeling and subsequent purification of the polymers for *ex vivo* and *in vivo* experiments was accomplished using an ^{18}F-fluoro-ethylation method modified from Herth et al. [42]. In brief, 3 mg polymer was dried azeotropically three times each with 1 mL of acetonitrile prior to [^{18}F]fluorination. 100 µL of dry DMSO as well as 1 µL of 5M Cs_2CO_3 solution was added and the labeling reaction was started by adding a dry solution of [^{18}F]FETos in DMSO. Radiolabeling was performed at 120 °C for 18 min. Further details are given in the supporting information.

2.6 Animal experiments

2.6.1 Tumor and animal model

For animal experiments the rat tumor cell line Walker 256 mammary carcinoma was used. Experimental details can be found in the supplementary. All experiments had previously been approved by the regional animal ethics committee and were conducted in accordance with the German Law for Animal Protection and the UKCCCR Guidelines [43].

2.6.2 *In vivo* µPET imaging

For µPET imaging, rats were anaesthetized with pentobarbital (40 mg/kg, intraperitoneal, Narcoren, Merial, Hallbergmoos, Germany). ^{18}F-labeled polymers were injected via tail vein puncture. Experimental setup of the microPET is described in the supporting information.

2.6.3 Biodistribution and cellular uptake studies

Further information on biodistribution as well as cellular studies can be found in the supplementary information.

2.6.4 Statistical analysis

Results are expressed as means ± SEM. Differences between groups were assessed by the two-tailed Wilcoxon or Kruskal-Wallis test for unpaired samples. The significance level was set at α=5% for all comparisons. Correlation analysis was performed by calculating the Pearson correlation coefficient.

3. Results and discussion

3.1 Synthesis and radioactive labeling of HPMA-*b*-LMA copolymers with varying PEG_{2000Da} content

The aim of the present study focused on the impact of PEG_{2000Da} fragments in HPMA-LMA block copolymers on tumor uptake as well as body distribution of the polymer systems *in vivo*. By combining the controlled radical polymerization technique RAFT (Reversible Addition-Fragmentation Chain Transfer) [27, 28] with reactive ester chemistry [44] we could already demonstrate the facile synthesis of well-defined and narrowly distributed HPMA based polymer systems - differing in molecular weight as well as incorporation of hydrophobic segments - in former studies [20, 21].

In addition, radioactive labeling using the positron emitter Fluorine-18 [42] illustrated successful monitoring of the polymer carrier system in the living organism and further examinations emphasized that particularly polymer architecture as well as molecular weight had a tremendous effect on organ distribution, blood circulation properties and tumor uptake *in vivo* [20]. Taking these results into account, here the focus was laid on the optimization of the *in vivo* characteristics of HPMA-LMA block copolymers, representing the most defined and stable polymer structures. By incorporation of different ratios of PEG_{2000} side chains into the hydrophilic part of the block copolymer structure (0, 1, 5, 7 and 11 % respectively) we investigated how hydrodynamic radii, amphiphilicity and aggregate formation as well as spacer linkage is affecting the polymer fate in the living organism. A key aspect of these polymer-dependent features was the correlation to blood pool concentration as well as tumor accumulation. Overall, five different block copolymer structures were synthesized (**$P_{0\%}$** to **$P_{11\%}$**), starting from the same reactive block copolymer precursor system (**P*-R**).

The polymer characteristics are summarized in table 1.

As depicted in table 1, well-defined and narrowly distributed block copolymer systems could be synthesized (PDI = 1.25). The hydrophobic lauryl methacrylate segment was incorporated to an extent of 25 %, as determined by gel permeation chromatography and ^{1}H-NMR spectroscopy. Molecular weights (M_n) of the final polymer structures were between 17000 and 39000 g/mol, increasing with higher PEG content. PEG_{2000} segments were linked to the hydrophilic block with efficiencies of 1, 5, 7 and 11 % as calculated by ^{1}H-NMR spectroscopy. The pure HPMA-LMA block copolymer **$P_{0\%}$** exhibited a hydrodynamic radius of 112.8 nm, thereby representing the highest aggregate structure investigated in this study. Based on the higher hydrophilicity of polyethylene glycol compared to HPMA, we examined a decrease of R_h values with increasing PEG incorporation, possessing a minimum for **$P_{5\%}$** and **$P_{7\%}$** (~ 38 nm). This result stays in good correlation with earlier studies on PEG-coated nanoparticles by Gref at al. [45] assuming that the higher incorporation ratio of PEG imparts lower interfacial tension between the aqueous surrounding and the hydrophobic core. Nevertheless polymer **$P_{11\%}$** - exhibiting a linkage efficiency of 11 % PEG segments – demonstrated an increase of hydrodynamic radius to 53 nm, probably due to steric hindrance in the polymer chain [46]. A reaction scheme of the polymer synthesis is illustrated in figure 1.

Table 1: *Analytical data of reactive ester precursor polymer (**P*-R**) and final polymer structures (**$P_{0\%}$** to **$P_{11\%}$**)*

Nomenclature	Polymer structure	Monomer ratio	PEG_{2000} incorp.[5]	M_n in g/mol	M_w in g/mol	PDI[2]	R_h[6] in nm
P*-R	Block copolymer	60:40%[1]	-	25.000[2]	31000[2]	1.25	n.d.
$P_{0\%}$	Block copolymer	75:25%[3]	0%	17000[4]	21000[4]	1.25	112.8 +/- 5.7
$P_{1\%}$	Block copolymer	75:25%[3]	1%	20000[4]	24000[4]	1.25	55.4 +/- 2.9
$P_{5\%}$	Block copolymer	75:25%[3]	5%	26000[4]	33000[4]	1.25	38.0 +/- 2.1
$P_{7\%}$	Block copolymer	75:25%[3]	7%	30000[4]	38000[4]	1.25	38.1 +/- 2.1
$P_{11\%}$	Block copolymer	75:25%[3]	11%	39000[4]	47000[4]	1.25	53.0 +/- 2.8

*[1] = Calculated monomer ratio; [2] = Determination by GPC in THF as solvent ; [3] = Monomer ratio determined by ^{1}H-NMR spectroscopy after polymeranalogous reaction with 2-hydroxypropylamine; [4] = Calculated from the molecular weight of the reactive ester polymer **P*-R** as determined by GPC in THF as*

solvent; [5] = PEG_{2000} incorporation (incorp.) ratio determined by ^{1}H-NMR spectroscopy after polymeranalogous reaction; [6] = Hydrodynamic radii of the aggregates determined by Fluorescence Correlation Spectroscopy (FCS)

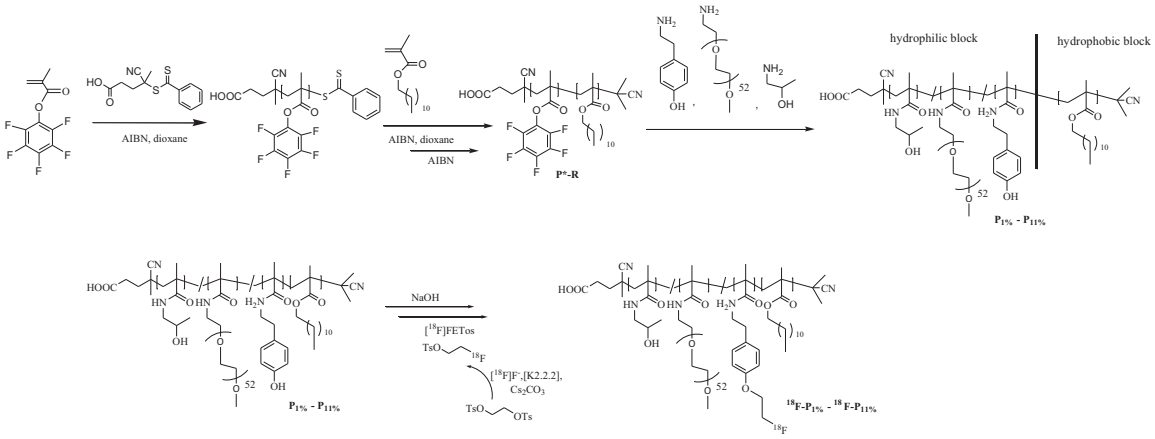

Figure 1: *Polymer synthesis as well as radioactive labeling procedure (exemplified for PEG_{2000} modified polymers)*

Table 2*: Corrected radiochemical yields for HPMA based block copolymers* ***$P_{0\%}$*** *to* ***$P_{11\%}$***

Nomenclature	Polymeric structure	PEG_{2000} incorp.[5]	Monomer ratio[3]	M_w in g/mol[4]	RCY in %
^{18}F-$P_{0\%}$	Block copolymer	0%	75:25%	21000[4]	7±0
^{18}F -$P_{1\%}$	Block copolymer	1%	75:25%	24000[4]	11±1
^{18}F -$P_{5\%}$	Block copolymer	5%	75:25%	33000[4]	15±8
^{18}F-$P_{7\%}$	Block copolymer	7%	75:25%	38000[4]	5±1
^{18}F -$P_{11\%}$	Block copolymer	11%	75:25%	47000[4]	18±2

Starting from the reactive ester monomer pentafluorophenyl methacrylate (PFPMA) the macro-CTA was synthesized and further converted to reactive ester block copolymer **P*-R**. By polymeranalogous reaction of the hydrophilic block, tyramine groups (incorporation of ~ 3 %) for radiolabel attachment as well as the amine-functionalized PEG_{2000} fragment and 2-hydroxypropylamine were covalently linked. To perform non-invasive small animal PET imaging as well as for quantification by *ex vivo* biodistribution measurements, the positron emitter fluorine-18 was introduced via [^{18}F]fluoroethylation, a method already established for various HPMA based copolymers [20, 42]. In order to promote the incorporation of the fluoroethyl radiolabel, the previously applied radiolabeling conditions [42] were

adjusted by using Cs_2CO_3 as base as well as azeotropic drying of the polymer precursors prior to radiolabeling.

Nevertheless, radiolabeling efficiencies - as listed in Table 2 - were still comparably low, with highest RCYs achieved for block copolymer **$P_{11\%}$** (RCY = 18±2 %).

3.2 Organ distribution

Regarding the influence of surface chemistry on pharmacokinetics, both PEG length and surface density on block copolymer derived nanoparticles was shown to hold a tremendous impact on clearance from the bloodstream [38, 40, 47].

Quantification of the recovered dose of radiofluorinated block copolymers was accomplished in selected organs (liver, spleen, kidney, heart, blood, lung, muscle, small intestine and testis) 2 h and 4 h after i.v. administration.

Biodistribution data of polymers with different degree of PEGylation in the organs is illustrated in Figure 2 and Table 3 (4 h values are depicted in table S1 see supporting information).

As clearly visible, a major dependency of the PEG_{2000} content in the hydrophilic block regarding organ accumulation can be detected. The pure block copolymer **$P_{0\%}$** exhibited the highest uptake in the kidney; further increasing over time and hence demonstrating renal clearance (see Fig. 2A). With higher PEG_{2000} percentage a decrease in kidney accumulation could be observed (r=-0.881), possessing a minimum for **$P_{7\%}$**. Apparently the hydrodynamic radii (Tab. 1) of the PEGylated compounds reveal a correlation to their observed kidney uptake. Block copolymers with larger sizes (**$P_{0\%}$**, **$P_{1\%}$** and **$P_{11\%}$** with R_h = 112, 55 and 53 nm respectively) also showed highest kidney accumulation. A decrease in polymer size resulted in a diminished renal excretion, underlining the high impact of molecular architecture besides size on the clearance of polymer carriers [48]. Furthermore, higher hydrophilicity and PEG surface coverage may gradually lower glomerular filtration, probably attributed to a better shielding efficacy of the highly modified block copolymers toward plasma proteins. In general it has to be noted that all herein presented block copolymers illustrated renal clearance, a major requirement for non-biodegradable nanocarriers to circumvent chronic accumulation in the body.

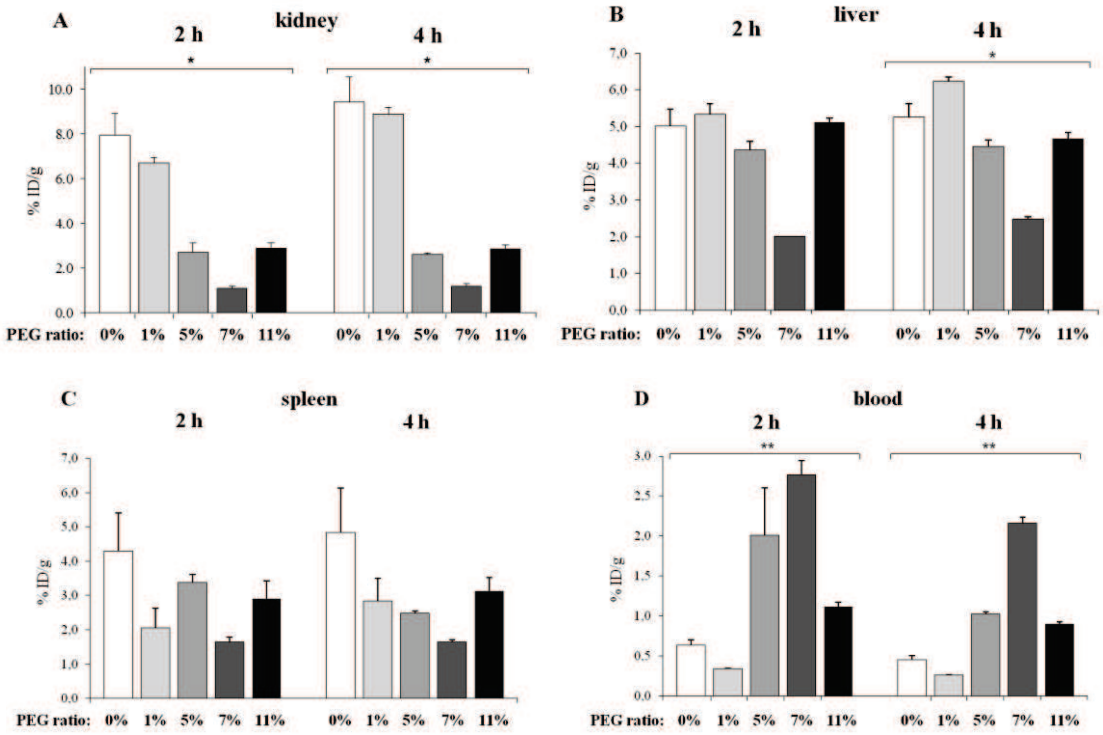

Figure 2: *Biodistribution of polymer structures* $\mathbf{P_{0\%}}$ *to* $\mathbf{P_{11\%}}$*, in selected organs (kidney, liver, spleen and blood) 2 and 4 hours p.i. n=2-6, (*) p<0.05, (**) p<0.01.*

Table 3: *Polymer uptake in different organs expressed by the fraction of the injected dose (ID) of the polymer per gram tissue 2 h after i.v. injection. n=2-6.*

	polymer concentration [%ID/g tissue]				
organ	**0% PEG**	**1% PEG**	**5% PEG**	**7% PEG**	**11% PEG**
lung	0.39±0.06	0.23±0.01	0.74±0.18	1.15±0.01	0.89±0.26
liver	5.01±0.47	5.34±0.29	4.37±0.23	2.01±0.01	5.11±0.13
spleen	4.30±1.10	2.06±0.57	3.39±0.51	1.64±0.15	2.90±0.52
kidney	7.95±0.96	6.72±0.22	2.71±0.41	1.09±0.11	2.91±0.20
muscle	0.07±0.01	0.04±0.01	0.10±0.03	0.05±0.01	0.07±0.01
heart	0.22±0.03	0.11±0.01	0.39±0.08	0.61±0.01	0.31±0.03
blood	0.63±0.07	0.34±0.01	2.01±0.59	2.76±0.18	1.12±0.05
small intestine	0.23±0.02	0.14±0.01	0.22±0.02	0.25±0.05	0.31±0.06
testis	0.10±0.01	0.07±0.01	0.19±0.03	0.19±0.01	0.17±0.01

Interestingly, polymer **$P_{7\%}$** which exhibited lowest kidney elimination also showed lowest liver (Fig. 2B; 2.47±0.06 % ID/g tissue) and spleen uptake (Fig. 2C; 1.64±0.07 % ID/g tissue) over a time span of 4 hours, thereby combining favorable characteristics for the application as polymeric nanocarrier *in vivo*. However, it has to be noticed that the hepatic or spleenic uptake only slightly depends (not statistically significant) on the PEGylation of the polymer. Probably as a result of the differences seen in renal excretion and liver uptake, PEGylation plays an important role for the blood level of the polymers (Fig. 2D, Tab. 3). An augmentation in PEG content resulted in an almost linear increase of polymer concentration in the blood (r=0.878). Only the polymer containing 11 % of PEG_{2000} segments showed lower levels. This correlation could either be the result of reduced renal excretion of PEGylated polymers or maybe caused by differences in polymer binding to plasma proteins which should be analyzed in further studies. These findings stay in good correlation to investigations of Torchilin et al., showing that a higher percentage of PEG-content led to an improved plasma-half life of "stealth" liposomes in mice [49]. Nevertheless, there seems to be a limit of PEGylation efficacy as demonstrated for decreasing blood concentration of block copolymer **$P_{11\%}$** (0.90±0.02 % ID/g tissue after 4h). In general, blood levels of all polymers decreased over the prolonged observation time of 4 h (Fig. 2D) indicating the ongoing excretion of the polymers, presumably by the kidney (Fig. 2A). Highly blood supplied organs such as heart and lung directly reflect the blood concentration pattern – exhibiting a minimum level of block copolymer **$P_{1\%}$** and highest values for **$P_{7\%}$** (see Tab. 3 and Fig. / Tab. S1 supporting info). In addition to these findings, polymer accumulation in muscle, small intestine and testis was comparatively low, not demonstrating great differences between the five examined block copolymers varying in PEG_{2000} incorporation efficiencies (cf. Tab. S1 supporting info).

3.3 Tumor accumulation

For analysis of the polymer uptake *in vivo* Walker 256 mammary carcinomas were used with a volume of 1.46±0.16 mL. Quantitative biodistribution studies of the tumor tissue were accomplished 2 and 4 h post-injection of the polymer compounds. The dependency of PEGylation on the % ID/g tumor is depicted in Figure 3.

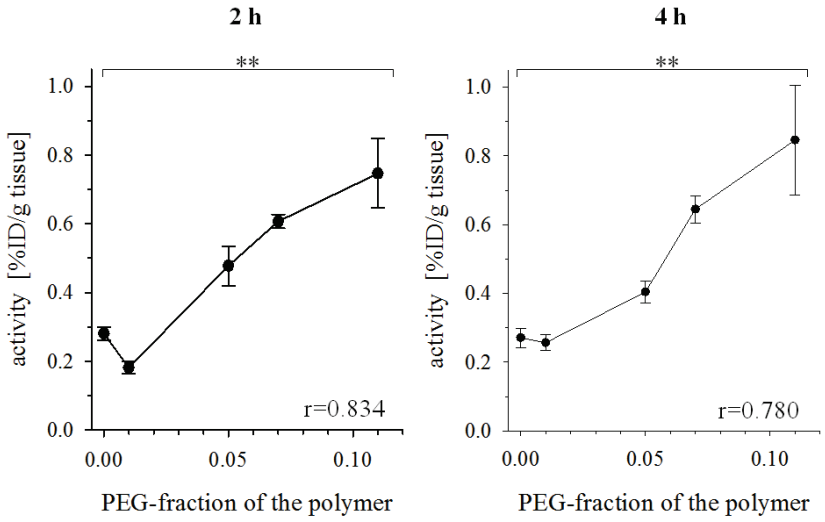

Figure 3: *Tumor accumulation of polymers as a function of the incorporated amount of PEG_{2000}. n=4-6, (**) p<0.01.*

Based on these results, a direct correlation between PEG_{2000} incorporation ratio and tumor uptake can be drawn (r=0.834 and r=0.780, respectively). Even though organ distribution studies (see Figure 2) revealed most favorable characteristics for block copolymer **$P_{7\%}$**, including highest blood retention and low renal clearance, the tumor data demonstrate a gradual increase in tumor uptake with ascending PEG content. In this regard, the block copolymer with highest PEG level (**$P_{11\%}$**) also achieved highest tumor uptake - despite lower blood levels compared to **$P_{7\%}$**. As expected, tumor accumulation is not solely affected by the retention of the polymers in the circulation. Analyzing the tumor accumulation of the polymers after 4 hours revealed a similar pattern versus the time point of 120 min. An almost linear correlation between the amount of PEGylation and tumor uptake could be seen. Notably - despite a decrease in blood levels of all polymers after 4 h (Fig. 2) - tumor uptake was even increasing in the tumor tissue. This observation indicated that tumor accumulation is not only the result of a passive redistribution between the blood compartment and the tumor tissue.

3.4 MicroPET imaging studies in Walker 256 carcinoma bearing rats

Besides quantification of organ accumulation - clearly demonstrating a correlation of PEGylation on organ distribution and tumor uptake *ex vivo* - both static and dynamic µPET studies

were accomplished. Whole-body µPET images (Fig. 4), acquired 2 h post injection, stay in good accordance to the distribution data obtained in major organs (Fig. 2). PET images reveal kidney and bladder accumulation for all block copolymers hence confirming renal clearance. Furthermore, PET studies clearly displayed the disparities regarding blood circulation lifetimes according to different degrees of PEG incorporation.

Whereas neither heart nor aorta are displayed in case of $\mathbf{P_{0\%}}$ and $\mathbf{P_{1\%}}$, PET images of block copolymers exhibiting higher PEG content ($\mathbf{P_{5\%}}$, $\mathbf{P_{7\%}}$, $\mathbf{P_{11\%}}$) explicitly show remaining activity in the blood compartment. This observation is illustrating the enhanced circulation of PEGylated block copolymers in the blood pool which is essential for effective drug delivery (in correspondence with the *ex vivo* biodistribution data, Fig. 2).

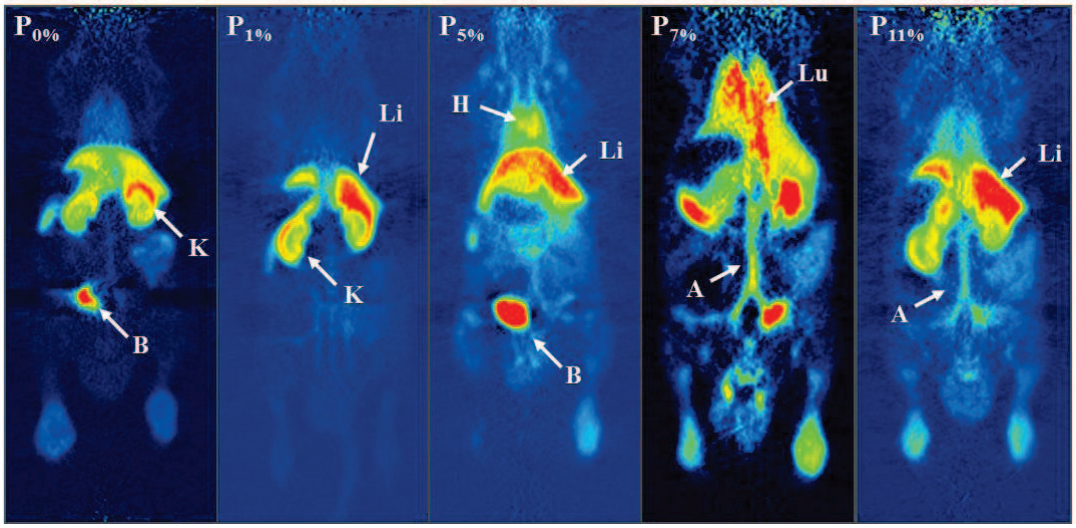

Figure 4: *Whole body µPET image sections obtained 120-135 min after administration of ^{18}F-polymers showing renal clearance (kidney (K), bladder (B)), distribution in liver (Li) and lung (Lu) as well as enhanced blood retention (heart (H), aorta (A)) of PEGylated polymers.*

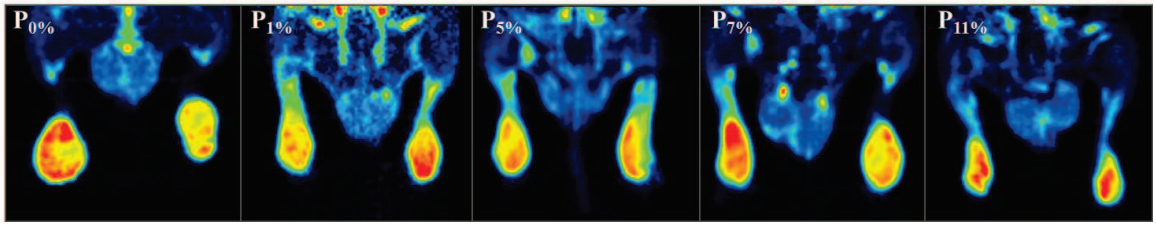

Figure 5: *Examples of coronal µPET image sections of Walker 256 tumors 60-120 min after i.v. administration of polymers with varying PEG content illustrating tumor accumulation.*

Based on the findings regarding enhanced tumor accumulation with increasing PEGylation, the uptake of PEG modified block copolymers in the Walker 256 carcinoma was furthermore studied using dynamic µPET imaging over the course of 2 h after i.v. injection. Coronal slices of summed µPET images through the tumors - implanted at the hind food dorsum - (Fig. 5) clearly display polymer uptake for all ^{18}F-labeled polymers.

Finally the question arises how the observed disparities in tumor accumulation can be explained. Despite the differences in long term blood concentration of the polymers (seen in the biodistribution experiments, Fig. 2) which may increase the diffusive intratumoral extravasation of the highly PEGylated polymers, the uptake of polymers into the tumor cells might be responsible. Due to this assumption, we additionally investigated the cellular uptake of the presented polymers into Walker 256 cells *in vitro*. Fig. 6 clearly indicates pronounced differences between the block polymers. However, in contrast to the *in vivo* data, the cellular uptake was highest for non- and low PEGylated polymers (**$P_{0\%}$** and **$P_{1\%}$**) whereas the highly PEGylated compounds showed a distinct lower intracellular accumulation. Another reason for the observed disparities in tumor uptake *in vivo* could be the vascular permeability, since the hydrodynamic radii were markedly different. Polymer structures around an R_h of 50 nm demonstrate most effective tumor enrichment thus staying in good accordance with studies suggesting this radius as suitable limit for nanoparticles regarding cancer therapy [50-52]. Presumably a combination of the increased blood levels together with the reduction of hydrodynamic radius seems to be responsible for the tumor accumulation of the highly PEGylated polymers.

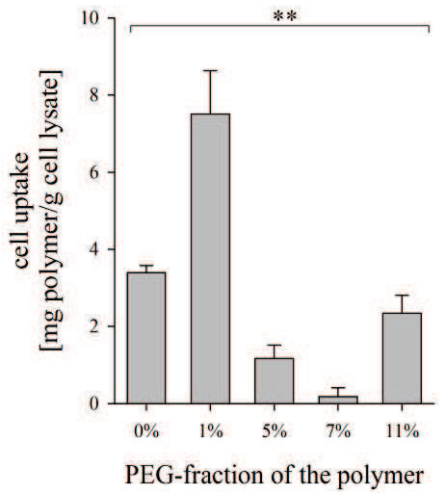

Figure 7: *Cellular uptake of the polymers after 2 h incubation at 37 °C in Walker 256 carcinoma cells in vitro; n=6, (*) p<0.05.*

4. Conclusion

The present study clearly demonstrates that a controlled modification of HPMA-LMA block copolymers by means of PEGylation has a tremendous impact on their pharmacokinetic profile *in vivo*. Radiolabeling of polymers with positron emitting isotopes such as fluorine-18 in combination with non-invasive Positron Emission Tomography (PET) imaging enables to monitor their biodistribution pattern, particularly regarding tumor accumulation, in a quantitative way. By means of these techniques, we could observe that the degree of PEGylation of block copolymers was responsible for severe disparities in their biodistribution characteristics. Block copolymers with low amounts of PEG_{2000} side chains - exhibiting highest hydrodynamic radii - showed major kidney and RES uptake. Blood retention as well as tumor accumulation was comparatively low. In contrast, higher PEG content caused prolonged blood circulation times of the HPMA based block copolymers, even resulting in a linear trend of tumor accumulation with increased PEGylation efficacy. Interestingly, $\mathbf{P_{7\%}}$ exhibited most favorable *in vivo* characteristics – including lowest hepatic and spleenic uptake as well as highest blood pool concentration 4 h p.i. – but nevertheless $\mathbf{P_{11\%}}$ was the block copolymer with highest tumor accumulation in the Walker 256 mammary carcinoma over time. So far, there seems to be a general dependency of polymer size combined with the degree of PEGylation on resulting tumor uptake. This correlation has to be further examined but in general it opens the discussion of selectively induce smaller block copolymer sizes by systematic PEG incorporation to fine-tune them for efficient anticancer therapy. In contrast to the obtained *in vivo* results, an opposite trend could be observed for the *in vitro* studies on this tumor cell line. Notably, in this case highest cellular uptake was determined for non- or low PEGylated compounds. These results clearly indicate that *in vitro* studies cannot be directly transferred to the *in vivo* situation. In particular they underline the importance of (non-invasive) *in vivo* techniques for assessing the intratumoral polymer uptake in order to tailor polymer based (chemo) therapy to the patient needs. Furthermore the herein presented approach emphasizes the versatility of selective PEGylation of amphiphilic block copolymers helping to improve their pharmacokinetic profiles and thus designing potential polymeric drug carrier systems for anticancer treatment.

5. Acknowledgement

The authors would like to thank Barbara Biesalski, Nicole Bausbacher and Bengü Yilmaz for their support during animal studies and following interpretation. We also want to thank the Max-Planck Graduate Center (MPGC, M. Allmeroth) as well as the Graduate School Materials Science in Mainz (Excellence Initiative, DFG/GSC 266, D. Moderegger) for financial support. In addition the authors are very thankful for financial support of the DFG (Rösch: RO 985/30-1; Thews: TH 482/4-1, Zentel: ZE 230/21-1) and SAMT Initiative Mainz.

References

[1] R. Duncan, The dawning era of polymer therapeutics. Nat Rev Drug Discov 2(5) (2003) 347-360.

[2] Y. Matsumura, H. Maeda, A New Concept for Macromolecular Therapeutics in Cancer Chemotherapy: Mechanism of Tumoritropic Accumulation of Proteins and the Antitumor Agent Smancs. Cancer Research 46(12 Part 1) (1986) 6387-6392.

[3] H. Maeda, J. Wu, T. Sawa, Y. Matsumura, K. Hori, Tumor vascular permeability and the EPR effect in macromolecular therapeutics: a review. Journal of Controlled Release 65(1-2) (2000) 271-284.

[4] K. Ulbrich, V. Subr, Structural and chemical aspects of HPMA copolymers as drug carriers. Advanced Drug Delivery Reviews 62(2) (2010) 150-166.

[5] R. Duncan, L.W. Seymour, K.B. O'Hare, P.A. Flanagan, S. Wedge, I.C. Hume, K. Ulbrich, J. Strohalm, V. Subr, F. Spreafico, M. Grandi, M. Ripamonti, M. Farao, A. Suarato, Preclinical evaluation of polymer-bound doxorubicin. Journal of Controlled Release 19(1-3) (1992) 331-346.

[6] M.V. Pimm, A.C. Perkins, J. Strohalm, K. Ulbrich, R. Duncan, Gamma Scintigraphy of the Biodistribution of 123I-Labelled N-(2-Hydroxypropyl) methacrylamide Copolymer-Doxo-rubicin Conjugates in Mice with Transplanted Melanoma and Mammary Carcinoma. Journal of Drug Targeting 3(5) (1996) 375-383.

[7] R. Duncan, Development of HPMA copolymer-anticancer conjugates: Clinical experience and lessons learnt. Advanced Drug Delivery Reviews 61(13) (2009) 1131-1148.

[8] T. Lammers, V. Subr, K. Ulbrich, W.E. Hennink, G. Storm, F. Kiessling, Polymeric nanomedicines for image-guided drug delivery and tumor-targeted combination therapy. Nano Today 5(3) (2010) 197-212.

[9] T. Minko, P. Kopecková, V. Pozharov, J. Kopecek, HPMA copolymer bound adriamycin overcomes MDR1 gene encoded resistance in a human ovarian carcinoma cell line. Journal of Controlled Release 54(2) (1998) 223-233.

[10] D.P. Nowotnik, E. Cvitkovic, ProLindac(TM) (AP5346): A review of

the development of an HPMA DACH platinum Polymer Therapeutic. Advanced Drug Delivery Reviews 61(13) (2009) 1214-1219.

[11] A. Abuchowski, T. van Es, N.C. Palczuk, F.F. Davis, Alteration of immunological properties of bovine serum albumin by covalent attachment of polyethylene glycol. Journal of Biological Chemistry 252(11) (1977) 3578-3581.

[12] R. Gref, A. Domb, P. Quellec, T. Blunk, R.H. Müller, J.M. Verbavatz, R. Langer, The controlled intravenous delivery of drugs using PEG-coated sterically stabilized nanospheres. Advanced Drug Delivery Reviews 16(2-3) (1995) 215-233.

[13] J.M. Harris, R.B. Chess, Effect of pegylation on pharmaceuticals. Nat Rev Drug Discov 2(3) (2003) 214-221.

[14] G. Pasut, F.M. Veronese, Polymer-drug conjugation, recent achievements and general strategies. Progress in Polymer Science 32(8-9) (2007) 933-961.

[15] G. Pasut, F.M. Veronese, PEG conjugates in clinical development or use as anticancer agents: An overview. Advanced Drug Delivery Reviews 61(13) (2009) 1177-1188.

[16] M.J. Joralemon, S. McRae, T. Emrick, PEGylated polymers for medicine: from conjugation to self-assembled systems. Chemical Communications 46(9) 1377-1393.

[17] M.D. Howard, M. Jay, T.D. Dziubla, X. Lu, PEGylation of Nanocarrier Drug Delivery Systems: State of the Art. Journal of Biomedical Nanotechnology 4(2) (2008) 133-148.

[18] A.S. Karakoti, S. Das, S. Thevuthasan, S. Seal, PEGylated Inorganic Nanoparticles. Angewandte Chemie International Edition 50(9) (2011) 1980-1994.

[19] D.E. Owens Iii, N.A. Peppas, Opsonization, biodistribution, and pharmacokinetics of polymeric nanoparticles. International Journal of Pharmaceutics 307(1) (2006) 93-102.

[20] M. Allmeroth, D. Moderegger, B. Biesalski, K. Koynov, F. Rösch, O. Thews, R. Zentel, Modifying the Body Distribution of HPMA-Based Copolymers by Molecular Weight and Aggregate Formation. Biomacromolecules 12(7) (2011) 2841-2849.

[21] M. Barz, R. Luxenhofer, R. Zentel, A.V. Kabanov, The uptake of N-(2-hydroxypropyl)-methacrylamide based homo, random and block copolymers by human multi-drug resistant breast adenocarcinoma cells. Biomaterials 30(29) (2009) 5682-5690.

[22] K. Kataoka, A. Harada, Y. Nagasaki, Block copolymer micelles for drug delivery: design, characterization and biological significance. Advanced Drug Delivery Reviews 47(1) (2001) 113-131.

[23] M. Talelli, C.J.F. Rijcken, C.F. van Nostrum, G. Storm, W.E. Hennink, Micelles based on HPMA copolymers. Advanced Drug Delivery Reviews 62(2) (2010) 231-239.

[24] G. Gaucher, M.-H. Dufresne, V.P. Sant, N. Kang, D. Maysinger, J.-C. Leroux, Block copolymer micelles: preparation, characterization and application in drug

delivery. Journal of Controlled Release 109(1-3) (2005) 169-188.

[25] K. Matyjaszewski, J. Xia, Atom Transfer Radical Polymerization. Chemical Reviews 101(9) (2001) 2921-2990.

[26] C.W. Scales, Y.A. Vasilieva, A.J. Convertine, A.B. Lowe, C.L. McCormick, Direct, Controlled Synthesis of the Nonimmunogenic, Hydrophilic Polymer, Poly(N-(2-hydroxypropyl)methacrylamide) via RAFT in Aqueous Media Biomacromolecules 6(4) (2005) 1846-1850.

[27] J. Chiefari, Y.K. Chong, F. Ercole, J. Krstina, J. Jeffery, T. Le, R. Mayadunne, G. Meijs, C. Moad, G. Moad, E. Rizzardo, S.H. Thang, Living Free-Radical Polymerization by Reversible Addition-Fragmentation Chain Transfer: The RAFT Process. Macromolecules 31 (1998) 5559-5562.

[28] E.R. G. Moad, S. H. Thang, Living Radical Polymerization by the RAFT process. Aust. J. Chem. 58 (2005) 379-410.

[29] M. Eberhardt, R. Mruk, R. Zentel, P. Théato, Synthesis of pentafluoro-phenyl(meth)acrylate polymers: New precursor polymers for the synthesis of multifunctional materials. European Polymer Journal 41(7) (2005) 1569-1575.

[30] M.A. Gauthier, M.I. Gibson, H.-A. Klok, Synthesis of Functional Polymers by Post-Polymerization Modification. Angewandte Chemie International Edition 48(1) (2009) 48-58.

[31] T. Lammers, Improving the efficacy of combined modality anticancer therapy using HPMA copolymer-based nanomedicine formulations. Advanced Drug Delivery Reviews 62(2) (2010) 203-230.

[32] B. Hoang, H. Lee, R.M. Reilly, C. Allen, Noninvasive Monitoring of the Fate of 111In-Labeled Block Copolymer Micelles by High Resolution and High Sensitivity MicroSPECT/CT Imaging. Molecular Pharmaceutics 6(2) (2009) 581-592.

[33] Z.-R. Lu, Molecular imaging of HPMA copolymers: Visualizing drug delivery in cell, mouse and man. Advanced Drug Delivery Reviews 62(2) (2010) 246-257.

[34] Y. Zhang, Y. Sun, X. Xu, X. Zhang, H. Zhu, L. Huang, Y. Qi, Y.-M. Shen, Synthesis, Biodistribution, and Microsingle Photon Emission Computed Tomography (SPECT) Imaging Study of Technetium-99m Labeled PEGylated Dendrimer Poly(amidoamine) (PAMAM)-Folic Acid Conjugates. Journal of Medicinal Chemistry 53(8) (2010) 3262-3272.

[35] M. Kissel, P. Peschke, V. Subr, K. Ulbrich, A. Strunz, R. Kühnlein, J. Debus, E. Friedrich, Detection and cellular localisation of the synthetic soluble macromolecular drug carrier pHPMA. European Journal of Nuclear Medicine and Molecular Imaging 29(8) (2002) 1055-1062.

[36] Z. Yang, S. Zheng, W.J. Harrison, J. Harder, X. Wen, J.G. Gelovani, A. Qiao, C. Li, Long-Circulating Near-Infrared Fluorescence Core-Cross-Linked

Polymeric Micelles: Synthesis, Characterization, and Dual Nuclear / Optical Imaging. Biomacro-molecules 8(11) (2007) 3422-3428.

[37] H. Xie, Z.J. Wang, A. Bao, B. Goins, W.T. Phillips, In vivo PET imaging and biodistribution of radiolabeled gold nanoshells in rats with tumor xenografts. International Journal of Pharmaceutics 395(1-2) (2010) 324-330.

[38] G. Sun, A. Hagooly, J. Xu, A.M. Nyström, Z. Li, R. Rossin, D.A. Moore, K.L. Wooley, M.J. Welch, Facile, Efficient Approach to Accomplish Tunable Chemistries and Variable Biodistributions for Shell Cross-Linked Nanoparticles. Biomacromolecules 9(7) (2008) 1997-2006.

[39] X. Sun, R. Rossin, J.L. Turner, M.L. Becker, M.J. Joralemon, M.J. Welch, K.L. Wooley, An Assessment of the Effects of Shell Cross-Linked Nanoparticle Size, Core Composition, and Surface PEGylation on in Vivo Biodistribution. Biomacromolecules 6(5) (2005) 2541-2554.

[40] K.-i. Fukukawa, R. Rossin, A. Hagooly, E.D. Pressly, J.N. Hunt, B.W. Messmore, K.L. Wooley, M.J. Welch, C.J. Hawker, Synthesis and Characterization of Core-Shell Star Copolymers for In Vivo PET Imaging Applications. Biomacromolecules 9(4) (2008) 1329-1339.

[41] M.M. Herth, M. Barz, M. Jahn, R. Zentel, F. Rösch, 72/74As-labeling of HPMA based polymers for long-term in vivo PET imaging. Bioorganic & Medicinal Chemistry Letters 20(18) (2010) 5454-5458.

[42] M.M. Herth, M. Barz, D. Moderegger, M. Allmeroth, M. Jahn, O. Thews, R. Zentel, F. Rösch, Radioactive Labeling of Defined HPMA-Based Polymeric Structures Using [18F]FETos for In Vivo Imaging by Positron Emission Tomography. Biomacromolecules 10(7) (2009) 1697-1703.

[43] P. Workman, E.O. Aboagye, F. Balkwill, A. Balmain, G. Bruder, D.J. Chaplin, J.A. Double, J. Everitt, D.A.H. Farningham, M.J. Glennie, L.R. Kelland, V. Robinson, I.J. Stratford, G.M. Tozer, S. Watson, S.R. Wedge, S.A. Eccles, Guidelines for the welfare and use of animals in cancer research. Br J Cancer 102(11) (2010) 1555-1577.

[44] P. Theato, Synthesis of well-defined polymeric activated esters. Journal of Polymer Science Part A: Polymer Chemistry 46(20) (2008) 6677-6687.

[45] R. Gref, M. Lück, P. Quellec, M. Marchand, E. Dellacherie, S. Harnisch, T. Blunk, R.H. Müller, "Stealth" corona-core nanoparticles surface modified by polyethylene glycol (PEG): influences of the corona (PEG chain length and surface density) and of the core composition on phagocytic uptake and plasma protein adsorption. Colloids and Surfaces B: Biointerfaces 18(3-4) (2000) 301-313.

[46] H. Lee, R.G. Larson, Effects of PEGylation on the Size and Internal Structure of Dendrimers: Self-Penetration of Long PEG Chains into the Dendrimer Core. Macromolecules 44(7) 2291-2298.

[47] F. Alexis, E. Pridgen, L.K. Molnar, O.C. Farokhzad, Factors Affecting the

Clearance and Biodistribution of Polymeric Nanoparticles. Molecular Pharmaceutics 5(4) (2008) 505-515.

[48] M.E. Fox, F.C. Szoka, J.M.J. Fréchet, Soluble Polymer Carriers for the Treatment of Cancer: The Importance of Molecular Architecture. Accounts of Chemical Research 42(8) (2009) 1141-1151.

[49] V.P. Torchilin, V.G. Omelyanenko, M.I. Papisov, A.A. Bogdanov Jr, V.S. Trubetskoy, J.N. Herron, C.A. Gentry, Poly(ethylene glycol) on the liposome surface: on the mechanism of polymer-coated liposome longevity. Biochimica et Biophysica Acta (BBA) - Biomembranes 1195(1) (1994) 11-20.

[50] M.R. Dreher, W. Liu, C.R. Michelich, M.W. Dewhirst, F. Yuan, A. Chilkoti, Tumor Vascular Permeability, Accumulation, and Penetration of Macromolecular Drug Carriers. Journal of the National Cancer Institute 98(5) (2006) 335-344.

[51] J.A. Barreto, W. O'Malley, M. Kubeil, B. Graham, H. Stephan, L. Spiccia, Nanomaterials: Applications in Cancer Imaging and Therapy. Advanced Materials 23(12) H18-H40.

[52] Y.M. H. Cabral, K. Mizuno, Q. Chen, M. Murakami, M. Kimura, Y. Terada, M.R. Kano, K. Miyazono, M. Uesaka, N. Nishiyama & K. Kataoka, Accumulation of sub-100 nm polymeric micelles in poorly permeable tumours depends on size. Nature Nanotechnology 6 (2011) 815-823.

Supplementary information to Manuscript 5.3

PEGylation of HPMA-based block copolymers enhances tumor accumulation *in vivo*: A quantitative study using radiolabeling and Positron Emission Tomography

Mareli Allmeroth[1,§], [redacted]

Contents

1. Experimental section

I. Experimental setup

^{1}H-NMR spectra were obtained by a Bruker AC 300 spectrometer at 300 MHz, ^{19}F-NMR analysis was carried out with a Bruker DRX-400 at 400 MHz. All measurements were accomplished at room temperature and spectroscopic data were analyzed using ACDLabs 9.0 1D NMR Manager. The synthesized polymers were dried at 40 °C under vacuum over night, followed by Gel Permeation Chromatography (GPC). GPC was performed in tetrahydrofuran (THF) as solvent, using following equipment: pump PU 1580, autosampler AS 1555, UV detector UV 1575 and RI detector RI 1530 from Jasco as well as a miniDAWN Tristar light scattering detector from Wyatt. Columns were used from MZ Analysentechnik, 300x8.0 mm: MZ-Gel SDplus 10^6 Å 5 µm, MZ-Gel SDplus 10^4 Å 5 µm and MZ-Gel SDplus 10^2 Å 5 µm. GPC data were evaluated by using the software PSS WinGPC Unity from Polymer Standard Service Mainz. The flow rate was set to 1 mL/min with a temperature of 25 °C.

Synthesis of 2-[^{18}F]fluoroethyl-1-tosylate ([^{18}F]FETos), was performed using a homemade automated synthesis module including a Knauer K-501 pump, a Knauer K-2501 UV-detector (Herbert Knauer GmbH, Berlin, Germany) and a radiodetector connected in series. HPLC purification was accomplished using a LiChrospher RP-18 EC 5µ (250 x 10 mm) (50:50 water–acetonitrile at 5 mL/min). ^{18}F-labeled polymers were isolated using a chromatographic system consisting of a waters pump (1500 series), a Waters UV-detector (2487 λ absorbance detector), a Berthold LB 509 radio detector and a HiTrap™ Desalting Column, Sephadex G-25 Superfine.

Recovered radioactive doses were determined using a Perkin Elmer 2470 Wizard^2 γ-counter.

II. Synthesis of 4-cyano-4-((thiobenzoyl)sulfanyl)pentanoic acid (CTP)

4-cyano-4-((thiobenzoyl)sulfanyl)pentanoic acid was used as chain transfer agent (CTA) and synthesized according to the literature [1].

III. Synthesis of pentafluorophenyl methacrylate (PFPMA)

Pentafluorophenyl methacrylate was prepared according to reference [2].

IV. Synthesis of reactive ester homopolymer (macro-CTA)

RAFT polymerization of pentafluorophenyl methacrylate with 4-cyano-4-((thiobenzoyl) sulfanyl)pentanoic acid was carried out in a schlenk tube [3, 4]. For this purpose, 4 g of PFPMA were dissolved in 5 mL of absolute dioxane, furthermore CTP and AIBN were added. The molar ratio of CTP/AIBN was chosen 1:8. After three freeze-vacuum-thaw cycles, the mixture was immersed in an oil bath at 65 °C and stirred over night. Afterwards, the polymeric solution was precipitated three times in hexane, centrifuged and dried under vacuum at 40 °C over night. A slightly pink powder was obtained. Yield: 52 %. ^{1}H-NMR (300 MHz, $CDCl_3$) δ/ ppm: 1.20-1.75 (br), 2.00-2.75 (br s). ^{19}F-NMR (400 MHz, $CDCl_3$) δ/ ppm: -162.03 (br), -156.92 (br), -152 to -150 (br).

V. Synthesis of reactive ester block copolymers

The macro-CTA obtained after homopolymerization of PFPMA was dissolved in dioxane, afterwards lauryl methacrylate as well as AIBN were added. As an example, 250 mg of macro initiator were dissolved in 5 mL dioxane, lauryl methacrylate and AIBN (8:1 ratio macro-CTA/AIBN) were mixed. After three freeze-vacuum-thaw cycles, the mixture was immersed in an oil bath at 65 °C and stirred for three days. Afterwards, poly(PFPMA)-*b*-poly(LMA) was precipitated three times in ethanol, centrifuged and dried under vacuum at 40 °C over night. A slightly pink powder was obtained. Yield: 54 %. ^{1}H-NMR (300 MHz, CDCl3) δ/ ppm: 0.84 (br t), 1.20-1.75 (br), 2.00-2.75 (br s). ^{19}F-NMR (400 MHz, $CDCl_3$) δ/ ppm: -162.01 (br), -156.95 (br), -152 to -150 (br).

VI. Removal of dithioester endgroups

The dithiobenzoate endgroup was removed using the protocol reported by Perrier et al. 2005 [5]. Therefore a 25-fold molar excess of AIBN was added to the polymer dissolved in dioxane. After four hours of heating the solution in an oil bath at 70 °C, the polymer was precipitated twice in hexane and collected by centrifugation. The polymer was dried under vacuum over night, a colorless powder was obtained. Yield: 75 %. Removal of the dithioester endgroup could be proven by UV-Vis spectroscopy.

VII. Synthesis of amine functionalized PEG_{2000} fragment

To synthesize the PEG_{2000}-amine fragment, a modified two step synthesis was accomplished [6]. For the first step as example, 50 g of $mPEG_{2k}$ (n = 0.025 mol) were dissolved in 250 mL of toluene. The PEG solution in toluene was azeotropically dried by distilling off 125 mL of solvent. Afterwards the solution was cooled to room temperature and 100 mL of anhydrous dichloromethane were added. Subsequent, the solution was cooled to 0-5 °C and 3.66 mL (n = 0.0362 mol) of triethylamine as well as 3.72 mL of methanesulfonyl chloride (n = 0.032 mol) were dropwise added via a rubber septa. The mixture was stirred for 2 hours at ca. 4 °C and then stirred at room temperature over night under argon gas. The next morning the mixture was concentrated on a rotary evaporator and filtered through a coarse glass frit (glass frit should be heated up to prevent solidifying). Precipitation of the product was carried out with approx. 500 mL of a mixture (30:70 v/v) of cold isopropyl alcohol and diethyl ether. The product was collected and dried under vacuum over night to give 34.61 g (yield: 67 %) of a white powder. ^{1}H-NMR (300 MHz, $CDCl_3$) δ/ ppm: 3.05 (s), 3.34 (t), 3.61 (br t), 4.35 (t). For the second step, a 1L, round-bottom flask equipped with a magnetic stirrer as well as a nitrogen inlet bubbler was charged with 3 g of mPEG 2 kDa mesylate (n = 0.0015 mol) and 900 mL of ammonium hydroxide aqueous solution (30 % v/v). To this solution 90 mg of ammonium chloride was added. The solution was warmed carefully to dissolve all of the PEG mesylate. The solution was stirred at room temperature for 5 days while venting excess gases through a bubbler to prevent pressure buildup. After completion of the reaction, 80 g of sodium chloride were added and the mixture was 4 times extracted with 200 mL of dichloromethane. The combined organic extracts were dried over sodium sulfate for 1 h, filtered and evaporated (not completely). Precipitation was carried out by addition of 900 mL of cold diethyl ether, filtered and dried under vacuum over night. Yield: 2.14 g (67%) of a white powder. ^{1}H-NMR (300 MHz, $CDCl_3$) δ/ ppm: 2.92 (t), 3.35 (t), 3.61 (br t), 3.85 (t).

VIII. Polymeranalogous reaction of block copolymers

For radioactive labeling of block copolymers the protocol was applied as follows. 100 mg of poly(PFPMA)-*b*-poly(LMA) copolymer was dissolved in 2 mL of absolute dioxane. Exemplary for $\mathbf{P_{7\%}}$ (M_n = 25000 g/mol), 5.4 mg of tyramine and 4 mg of triethylamine were diluted in a DMSO/dioxane mixture and added to the vessel. After stirring for 10

hours at 45 °C, 160 mg of amine-functionalized PEG_{2k} in 500 µL DMSO as well as 8 mg of triethylamine were added and the solution stirred for 1 ½ days. Thereafter, 21 mg of 2-hydroxypropylamine and 28 mg of Et_3N were added and the solution further stirred for 48 hours. For final removal of reactive ester side groups 20 mg of 2-hydroxypropylamine were additionally added the next morning. The solution was precipitated two times in diethyl ether, centrifuged and finally dissolved in a DMSO/water solution for dialysis. After lyophilization a white, crystalline powder could be obtained. Yield: 51 %. ^{1}H-NMR (400 MHz, d. DMSO) δ/ ppm: 0.70-0.90 (br), 0.90-1.40 (br), 1.40-1.90 (br), 2.75-3.10 (br), 3.20-3.25 (s), 3.45-3.55 (br), 3.65-3.85 (br), 4.50-4.75 (br), 6.60-6.75 (br) and 6.85-7.00 (br). For additional fluorescent labeling, 100 mg of polymeric precursor were diluted in 2 mL of absolute dioxane and 2.9 mg of Oregon Green 488 cadaverine were added. Afterwards tyramine, $PEG\text{-}amine_{2kDa}$ and 2-hydroxypropylamine were added, as described by the procedure above.

IX. Size determination by Fluorescence Correlation Spectroscopy (FCS)

The hydrodynamic radii of the polymeric systems were determined by Fluorescence Correlation Spectroscopy using a commercial FCS setup (Zeiss, Germany) consisting of the module ConfoCor 2 and an inverted microscope model Axiovert 200 with a Zeiss C-Apochromat 40 ×/1.2 W water immersion objective. The fluorophores were excited with an Argon laser (λ = 488 nm) and the emission was collected after filtering with a LP505 long pass filter. For detection, an avalanche photodiode, enabling single-photon counting, was used. As sample cell, eight-well, polystyrene-chambered cover glass (Laboratory-Tek, Nalge Nunc International) was applied. For sample preparation, stock solutions of 0.1 mg fluorescently labeled polymer/mL NaCl were applied. The solution was kept at room temperature over night. For reference reason, free Oregon Green 488 cadaverine dye in NaCl-solution was also studied. The calibration of the FCS observation volume was done using a dye with known diffusion coefficient, i.e. Alexa Fluor 488. For each solution, 5 measurement cycles with a total duration of 150 seconds were applied. Time dependant fluctuations of the fluorescence intensity δI(t) were detected and evaluated by autocorrelation analysis, yielding the diffusion coefficient and hydrodynamic radius of the fluorescent species [7].

X. Radiolabeling of polymers and purification for *ex vivo* and *in vivo* experiments

Radiolabeling of the polymers was accomplished by means of [^{18}F]fluoroethylation using a two-step synthesis procedure modified from [8]. In a first step, the labeling synthon [^{18}F]fluoroethyl tosylate ([^{18}F]FETos) was synthesized using a homemade automated synthesis module. The modular synthesis started with collecting the aqueous [^{18}F]F$^-$ solution (800-6000 MBq) on a SepPak-QMA cartridge (Waters, USA). [^{18}F]F$^-$ was eluted from the cartridge with 15 µL 1M K_2CO_3 solution, 18 mg Kryptofix 2.2.2 (Merck) in 1 mL acetonitrile and residual water was removed by azeotropic drying. To the dried K^+/[^{18}F]F$^-$/Kryptofix 2.2.2/carbonate complex, 14 mg of 1,2-ethylene ditosylate in 1 mL of MeCN were added and the mixture was heated at 87 °C for 3 min. Purification of the crude product was accomplished using semipreparative HPLC (Lichrospher RP18-EC5, 250 × 10 mm, MeCN/H_2O 1:1 (v/v), flow rate: 5 mL/min, R_t: 8 min). The HPLC fraction of [^{18}F]FETos was diluted with 50 mL of H_2O and collected on a SPE cartridge (Strata X, Phenomenex, USA). After drying in a stream of He, the purified labeling synthon was eluted from the cartridge with 0.9 mL of DMSO yielding [^{18}F]FETos in about 60 % decay-corrected RCY after a total synthesis time of 50 min. In order to promote the second step the radioactive labeling procedure, 3 mg of the polymeric labeling precursor were dried azeotropically using acetonitrile (3x1 mL) and solved subsequently in 200 µL of dried DMSO. 1 µL of a 5M Cs_2CO_3 solution was added and the clear solution was heated for 1 min at 120 °C. The radiolabeling reaction was started by adding 0.8 mL of [^{18}F]FETos in DMSO to the clear polymer solution and the mixture was heated for 18 min at 120 °C. After cooling to RT, purification of the ^{18}F-labeled polymer was accomplished using Size Exclusion Chromatography (HiTrap™ Desalting Column, Sephadex G-25 Superfine, 0.9 % NaCl solution, flow rate: 0.5 mL/min) leading to a pure, ^{18}F-labeled polymer solution ready for subsequent *ex vivo* and *in vivo* experiments.

XI. Tumor and animal model

Cells lines were grown in culture in RPMI medium supplemented with 10 mM L-glutamine and 10 % fetal calf serum (FCS) at 37 °C under a humidified 5 % CO_2 atmosphere and sub-cultivated twice per week. For tumor implantation male Sprague-Dawley rats (Charles River Wiga, Sulzfeld, Germany; body weight 195 to 315 g) housed in the animal care facility of the University of Mainz were used in this study. Animals were allowed access to food and acidified water ad libitum before the investigations.

Solid carcinomas were heterotopically induced by injection of cell suspension (0.4 mL approx. 10^4 cells/µL) subcutaneously into the dorsum of the hind foot. Tumors grew as flat, spherical segments and replaced the subcutis and corium completely. Volumes were determined by measuring the three orthogonal diameters (d) of the tumors and using an ellipsoid approximation with the formula: $V = d_1 \times d_2 \times d_3 \times \pi/6$. Tumors were used when they reached a volume of between 0.5 to 3.0 mL approx. 7 to 14 days after tumor cell inoculation.

XII. *In vivo* µPET imaging

The µPET imaging was performed on a microPET Focus 120 small animal PET (Siemens/Concorde, Knoxville, USA). Animals were placed supine and breathed room air spontaneously. Dynamic PET studies were acquired in listmode. The radiolabeled polymers were administered as a bolus injection of 0.4 - 0.7 mL simultaneously with the start of the PET scan. The mean injected activity of labeled polymers was 21.7±2.2 MBq. The PET listmode data were histogrammed into 25 frames and reconstructed using OSEM2D algorithm. Volumes-of-interests (VOIs) were defined for tumor and reference tissue (testis). The testis was used as a reference since it was in the field of view when imaging the tumors on the feet and because the tissue concentration was relatively constant between all animals on a low level. Time activity curves (TAC) were obtained with varying time frames (1.5 - 10 min) for a total measuring interval of 120 min. Ratios of tumor to reference tissue were calculated from integral images between 15' and 120' after polymer injection.

XIII. Biodistribution and cellular uptake studies

In order to assess the distribution of the radiolabeled polymers in different organs of the animals, the polymer (concentration of 1 mg in 1 mL sodium chloride solution) was injected i.v. in anaesthetized tumor-bearing rats via the tail vein with a mean activity of 11.1±0.4 MBq. After 120 or 240 min, the animals were sacrificed and different organ (kidney, liver, lung, spleen, heart, skeletal muscle, small intestine, testis, blood) and tumor samples were taken. The tissue samples were weighed and minced. Finally, the ^{18}F-activity in the organs was measured in a γ-counter.

Cellular uptake of pure and PEGylated block copolymers into Walker 256 cells was measured *in vitro*. Therefore, the polymeric precursors were labeled with the fluorochrome Oregon Green 488 cadaverine (see VIII: polymeranalogous reaction of

block copolymers). Uptake experiments were performed using collagen-coated 24-well plates. Collagen A (Biochrom, Berlin, Germany) was diluted with water and pH-adjusted (3.5). Plates were incubated for 30 min and dried. Cells were grown until wells reached ~ 70% confluence when they were incubated with 500 µl HEPES-buffered Ringer solution (pH = 7.4) containing 0.02 mg polymer/mL for 2 h at 37 °C. After washing, the cells were lysed with 250 µl Triton X-MOPS lysis buffer (15 min, room temperature) and mechanically removed from the plate surface. After centrifugation, 100 µl supernatant was pipetted in 96-well black bottom microplates and analyzed in a microplate-reader (Infinite 200, Tecan, Männedorf, Switzerland; excitation 485 nm, emission 532 nm). Protein content of each sample was determined using Bradford reagent. The polymer uptake was expressed by the content of polymer/per gram cell protein.

2. Tables

Table S1*: Organ distribution 4 hours post injection. Polymer uptake in different organs expressed by the fraction of the injected dose (ID) of the polymer per gram tissue. n=2-3.*

4h p.i.	**polymer concentration [%ID/g tissue]**				
Organ	**$P_{0\%}$**	**$P_{1\%}$**	**$P_{5\%}$**	**$P_{7\%}$**	**$P_{11\%}$**
lung	0.35±0.04	0.21±0.03	0.61±0.08	0.74±0.24	0.62±0.04
liver	5.27±0.35	6.24±0.11	4.45±0.17	2.47±0.06	4.68±0.17
spleen	4.84±1.30	2.84±0.66	2.48±0.06	1.64±0.07	3.14±0.38
kidney	9.45±1.12	8.89±0.29	2.61±0.06	1.20±0.12	2.86±0.18
muscle	0.05±0.01	0.05±0.01	0.07±0.01	0.05±0.01	0.07±0.01
heart	0.15±0.01	0.09±0.01	0.33±0.01	0.52±0.05	0.29±0.01
blood	0.45±0.05	0.26±0.01	1.03±0.02	2.16±0.07	0.90±0.02
small intestine	0.32±0.05	0.15±0.02	0.26±0.01	0.32±0.02	0.29±0.03
testis	0.09±0.01	0.07±0.01	0.17±0.01	0.26±0.02	0.20±0.01

Figures

Figure S1: *Biodistribution of polymer structures* $P_{0\%}$ *to* $P_{11\%}$*, in heart and lung 2 and 4 hours p.i. Uptake is expressed by the fraction of the injected dose (ID) of the polymer per gram tissue. n=2-6, (*) p<0.05, (**) p<0.01.*

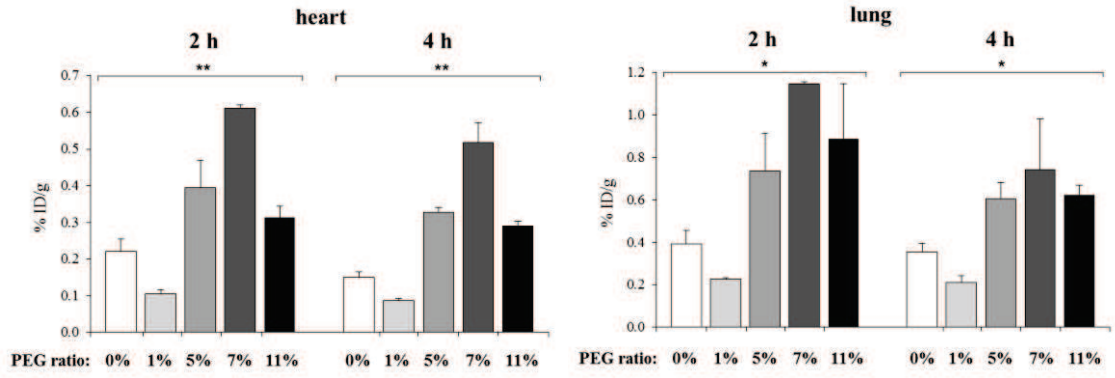

3. References

[1] E.R. G. Moad, S. H. Thang, Living Radical Polymerization by the RAFT process. Aust. J. Chem. 58 (2005) 379-410.

[2] M. Eberhardt, R. Mruk, R. Zentel, P. Théato, Synthesis of pentafluorophenyl(meth)acrylate polymers: New precursor polymers for the synthesis of multifunctional materials. European Polymer Journal 41(7) (2005) 1569-1575.

[3] P. Theato, Synthesis of well-defined polymeric activated esters. Journal of Polymer Science Part A: Polymer Chemistry 46(20) (2008) 6677-6687.

[4] M. Barz, R. Luxenhofer, R. Zentel, A.V. Kabanov, The uptake of N-(2-hydroxypropyl)-methacrylamide based homo, random and block copolymers by human multi-drug resistant breast adenocarcinoma cells. Biomaterials 30(29) (2009) 5682-5690.

[5] S.b. Perrier, P. Takolpuckdee, C.A. Mars, Reversible Addition-Fragmentation Chain Transfer Polymerization:End Group Modification for Functionalized Polymers and Chain Transfer Agent Recovery. Macromolecules 38(6) (2005) 2033-2036.

[6] Hoffmann-La ROCHE AG, K. Conde-Knape, W. Danho, G. Ehrlich, N. Fotouhi, D.C. Fry, W. Khan, A. Konkar, C.M. Rondinone, J. Swistok, R.A. Taub, J.W. Tilley, NEUROPEPTIDE-2 RECEPTOR-AGONISTS Patent WO/2007/065808 (2007).

[7] R.E. Rigler, E.S., Fluorescence Correlation Spectroscopy. Springer Verlag (New York 2001).

[8] M.M. Herth, M. Barz, D. Moderegger, M. Allmeroth, M. Jahn, O. Thews, R. Zentel, F. Rösch, Radioactive Labeling of Defined HPMA-Based Polymeric Structures Using [18F]FETos for In Vivo Imaging by Positron Emission Tomography. Biomacromolecules 10(7) (2009) 1697-1703.

Additional results

The impact of PEGylation on HPMA-*b*-LMA copolymers and their cellular uptake in the human breast adenocarcinoma cell line MCF-7

Block copolymer micelles are widely established in the field of polymer therapeutics, especially regarding anticancer treatment. Due to the core-shell morphology of amphiphilic block copolymers, the hydrophobic inner core enables the storage of pharmacologically active drugs which are either encapsulated by chemical, physical or electrostatic interactions. A major requirement for an effective application of amphiphilic block copolymers in cancer therapy is the appropriate polymer size. It has been suggested that nanoparticles have to be smaller than 100 nm in diameter to achieve favorable *in vivo* characteristics [1, 2]. Furthermore they have to exhibit sizes bigger than the renal excretion cut-off size (~ 5.5 nm [3]) to avoid rapid clearance from the blood stream. Polymeric micelles with diameters above 200 nm possess the fundamental drawback of enhanced recognition by the mononuclear phagocyte system and thus increased hepatic as well as spleenic uptake can be observed [4, 5]. Due to these findings, a major demand regarding HPMA-LMA block copolymers established in our laboratory was the reduction in polymer size. Former studies of Barz et al. revealed a hydrodynamic radius of approx. 100 nm for HPMA-*b*-LMA copolymers with molecular weights of ~ 30 kDa and further *in vivo* investigations of comparable block copolymer structures demonstrated their enhanced hepatobiliary excretion (see section 5.2). Based on these observations we aimed to improve the pharmacokinetic profile of HPMA based block copolymers by incorporating PEG_{2000} fragments into the hydrophilic block. On one hand the introduction of a more hydrophilic group induces a decrease in block copolymer size in aqueous environment and on the other hand particularly poly(ethylene glycol) is widely known for its shielding efficacy toward the MPS [6-8]. Due to this concept, we synthesized five different HPMA-*b*-LMA copolymers - varying in degree of PEGylation and exhibiting R_h of < 100 nm – to examine their biodistribution pattern in Walker 256 mammary carcinoma bearing rats (see section 5.3). We could observe a linear trend of tumor accumulation, possessing highest levels for block copolymers with increasing PEG content. Based on these promising results, we wanted to gain deepening knowledge on polymer-tumor cell interactions, endocytic pathways as well as polymer specific characteristics depending on the respective tumor cell line. Thus comparative cellular

studies in the human breast adenocarcinoma cell line MCF-7 were carried out. Analytical data of the differing block copolymer structures are depicted in table 1.

Table 1: *Analytical data of reactive ester precursor polymer (**P*-R**) and final polymer structures (**$P_{0\%}$** to **$P_{15\%}$**)*

Nomenclature	Polymer structure	Monomer ratio	PEG_{2000} incorp.[5]	M_n [g/mol]	M_w [g/mol]	PDI[2]	R_h[6] [nm]
P*-R	Block copolymer	60:40%[1]	-	25.000[2]	31000[2]	1.25	n.d.
$P_{0\%}$	Block copolymer	75:25%[3]	0%	17000[4]	21000[4]	1.25	112.8 +/- 5.7
$P_{1\%}$	Block copolymer	75:25%[3]	1%	20000[4]	24000[4]	1.25	55.4 +/- 2.9
$P_{5\%}$	Block copolymer	75:25%[3]	5%	26000[4]	33000[4]	1.25	38.0 +/- 2.1
$P_{7\%}$	Block copolymer	75:25%[3]	7%	30000[4]	38000[4]	1.25	38.1 +/- 2.1
$P_{15\%}$	Block copolymer	75:25%[3]	15%	46000[4]	55000[4]	1.25	63.1+/- 5.1

*[1] = Calculated monomer ratio; [2] = Determination by GPC in THF as solvent; [3] = Monomer ratio determined by ^{1}H-NMR spectroscopy after polymeranalogous reaction with 2-hydroxypropylamine; [4] = Calculated from the molecular weight of the reactive ester polymer **P*-R** as determined by GPC in THF as solvent; [5] = PEG_{2000} incorporation (incorp.) ratio determined by ^{1}H-NMR spectroscopy after polymeranalogous reaction; [6] = Hydrodynamic radii of the aggregates determined by Fluorescence Correlation Spectroscopy (FCS)*

As illustrated in table 1, well-defined and narrowly distributed (PDI = 1.25) block copolymers were synthesized. The hydrophobic lauryl methacrylate moiety was incorporated with a ratio of 25 % - determined via gel permeation chromatography as well as ^{1}H-NMR spectroscopy. Molecular weights (M_n) were in the range of 17000 g/mol for the pure block copolymer **$P_{0\%}$** to a maximum of 46000 g/mol for polymer **$P_{15\%}$**. Hydrodynamic radii were investigated by means of Fluorescence Correlation Spectroscopy (FCS) with highest R_h of ~ 113 nm for non PEGylated block copolymer **$P_{0\%}$**. By incorporation of the more hydrophilic polyethylene glycol compared to HPMA a decrease in hydrodynamic radius could be observed. With increasing PEG content, R_h values became smaller, possessing a minimum for **$P_{5\%}$** and **$P_{7\%}$** with ~ 38 nm. These findings stay in good accordance to Gref et al. [7] who assumed that with increasing PEG ratio a lower interfacial tension between aqueous environment and hydrophobic core can

be achieved. In contrast, the block copolymer with highest degree of PEGylation ($\mathbf{P_{15\%}}$) is demonstrating again an increase to 63 nm hence presuming an alteration in polymer structure: e.g. the formation of polymer brushes.

Cellular studies were accomplished by introducing a fluorescent dye – Oregon Green 488 Cadaverine – into the hydrophilic block via polymeranalogous reaction (calculated to be 1 mol %).

Cell viability assay

Cytotoxicity of the block copolymers $\mathbf{P_{0\%}}$ to $\mathbf{P_{15\%}}$ was evaluated using the MTS [3-(4,5-dimethylthiazol-2-yl)-5-(3-carboxymethoxyphenyl)-2-(4-sulfophenyl)-2H-tetrazolium] cell viability assay. MTS is a tetrazolium analog of MTT [3-(4,5-dimethylthiazol-2-yl)-2, 5-diphenyltetrazolium bromide] and with addition of the electron donor phenazine methosulfate (PMS) it is reduced to a water soluble, purple formazan product by means of mitochondrial dehydrogenases of living cells [9]. The formation of this product can be – due to its absorbance maximum of 490 - 500 nm – colorimetrically determined and hence the amount of colored product is proportional to the number of living cells.

In this regard, MCF-7 cells were seeded into sterile 96-well microtitre plates at 8000 cells/well. Cells were allowed to settle for 24 hours and then different concentrations (1, 0.8, 0.4, 0.2, 0.1, 0.05 and 0.025 mg/mL respectively) of unlabeled block copolymers were added. Final polymer concentrations contained 1 % of dimethylsulfoxide (v/v). Due to this preparation step, cells were furthermore treated with the same percentage of DMSO as control to evaluate solvent toxicity. They were incubated for 72 hours and afterwards MTS and PMS (20:1 v/v %) were added. Cells were further incubated for 2 hours and the plates finally read spectrophotometrically at 490 nm using a Victor2 Wallac plate reader. Absorbance values are represented as the percentage of cell viability compared to control cells (control equalized 100 %). Cell viabilities of the investigated HPMA-*b*-LMA copolymers are described in Figure 1A-E.

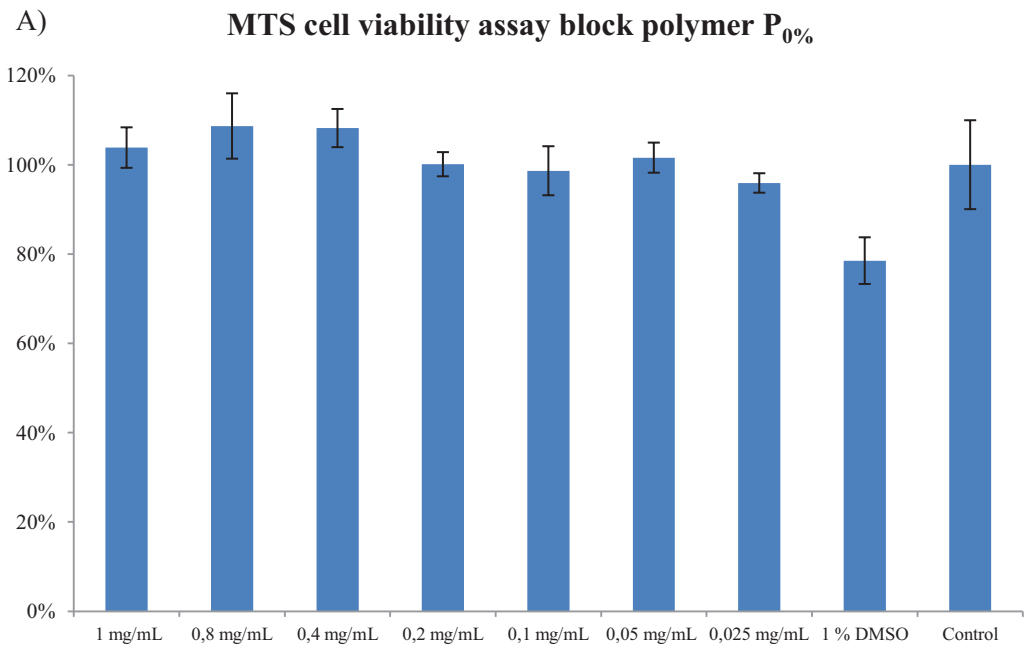

***Figure 1A**: Cell viability assay (MTS) of pure block copolymer **$P_{0\%}$** at different concentrations*

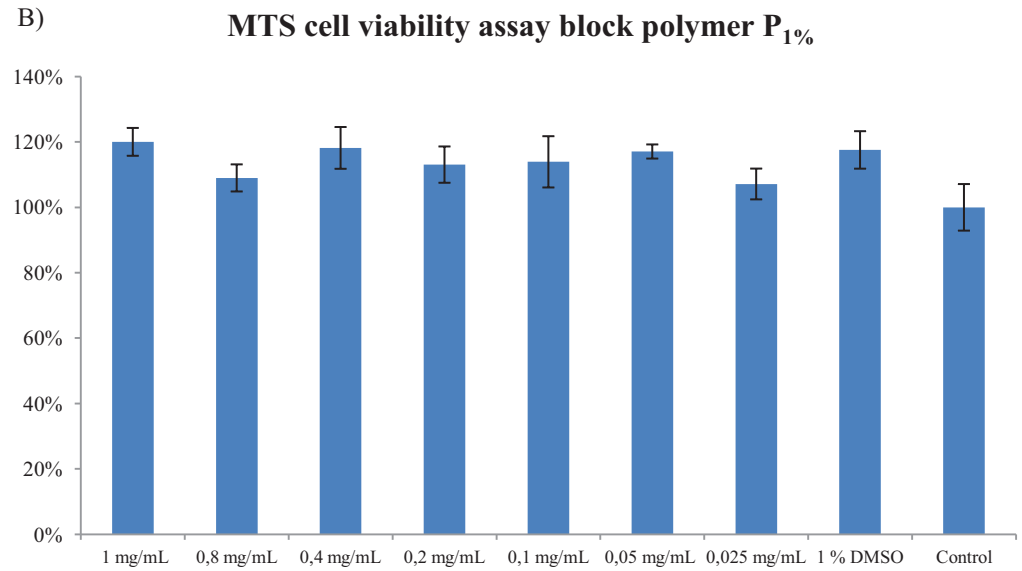

***Figure 1B**: Cell viability assay (MTS) of block copolymer **$P_{1\%}$** at different concentrations*

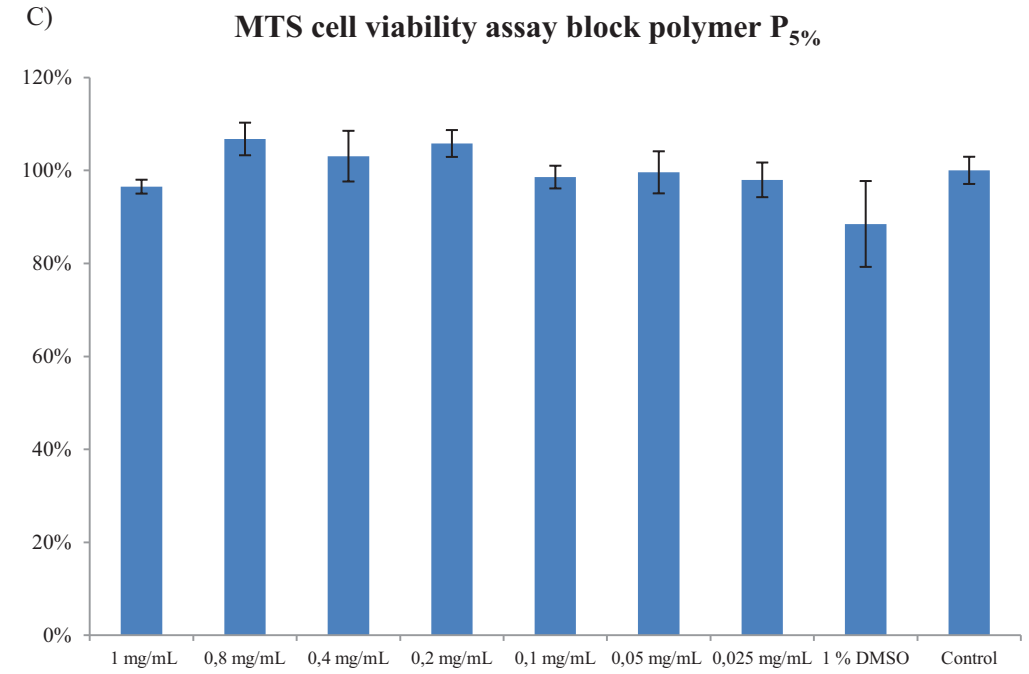

***Figure 1C**: Cell viability assay (MTS) of block copolymer **$P_{5\%}$** at different concentrations*

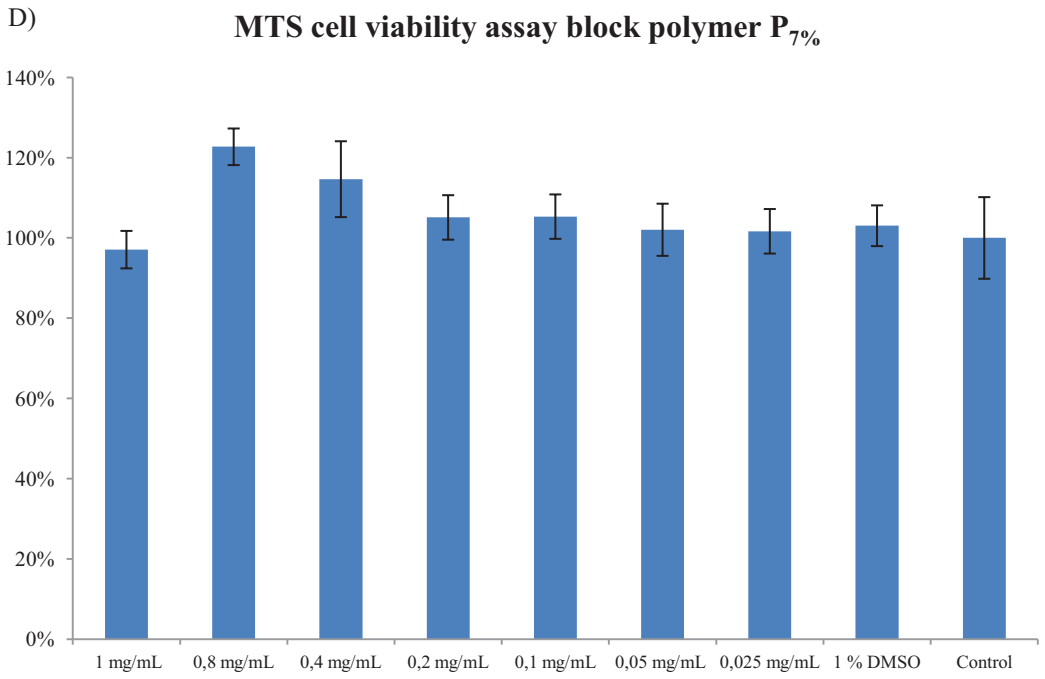

***Figure 1D**: Cell viability assay (MTS) of block copolymer **$P_{7\%}$** at different concentrations*

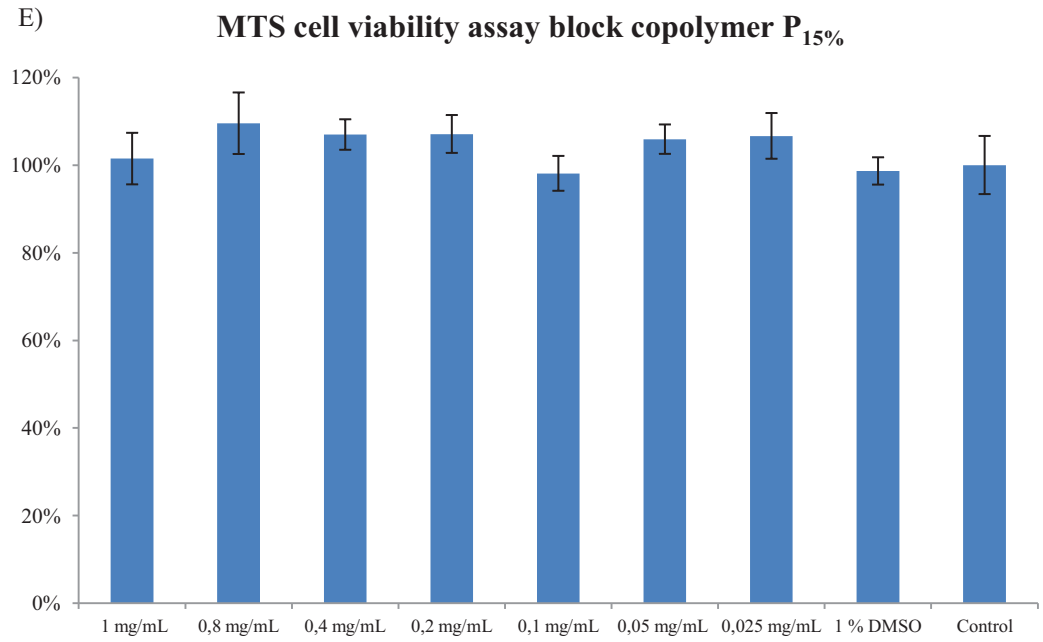

***Figure 1E**: Cell viability assay (MTS) of block copolymer **$P_{15\%}$** at different concentrations*

As clearly seen in the MTS assays, none of the investigated block copolymers is demonstrating cytotoxicity in the MCF-7 cell line after 72 hours of incubation at concentrations of up to 1 mg/mL. Thus the degree of PEGylation is not influencing cell viability. Furthermore, 1 % of DMSO only has a marginal effect on cell viability, ensuring the applied polymer preparation.

Cellular uptake studies by means of fluorescence-activated cell sorting (FACS)

Fluorescence-activated cell sorting (FACS) constitutes a special type of flow cytometry. This technology is based on simultaneously measuring and analyzing multiple physical characteristics of single particles – commonly cells – during their flow in a fluid stream through a beam of light. By means of this methodology, relative size, granularity or internal complexity as well as relative fluorescence intensity of a particle / cell can be determined. A flow cytometer is consisting out of three main systems, namely fluidics, optics and electronics. The fluidics system is responsible for the particle transport to the laser beam. Each particle in the fluid stream scatters light when passing through the laser beam and furthermore fluorescent moieties which are present in the particle or covalently coupled to it may be excited with subsequent emission of light. A combination of beam splitters and filters directs the scattered and fluorescent light to adequate detectors inside the flow cytometer. The detectors then produce electronic signals proportional to the

obtained optical signals which can be processed by the computer. Based on this principle, three types of data can be generated. These include Forward scatter (FSc) – for determining the approximate cell size -, Side or orthogonal scatter (SSc) – giving information about cell complexity or granularity – as well as fluorescence intensity to investigate cell structure and function.

Regarding our studies, we applied fluorescence-activated cell sorting to investigate time-dependent cellular uptake of the presented block copolymer systems in MCF-7 cells. A final polymer concentration of 0.25 mg/mL was used for cell incubation and the following time points were chosen for studying polymer dependent uptake kinetics: 0, 0.25, 0.5, 1, 2, 5 and 24 hours. All experiments were accomplished at 37 °C (determination of total uptake) and 4 °C (determination of cell binding) to evaluate whether the cellular uptake of the herein investigated block copolymer structures is energy-dependent. Real cellular uptake (expressed as uptake at 37 °C minus uptake at 4 °C) of the differing polymers in MCF-7 cells is illustrated as % positive gated cells *vs.* time in Figure 2A.

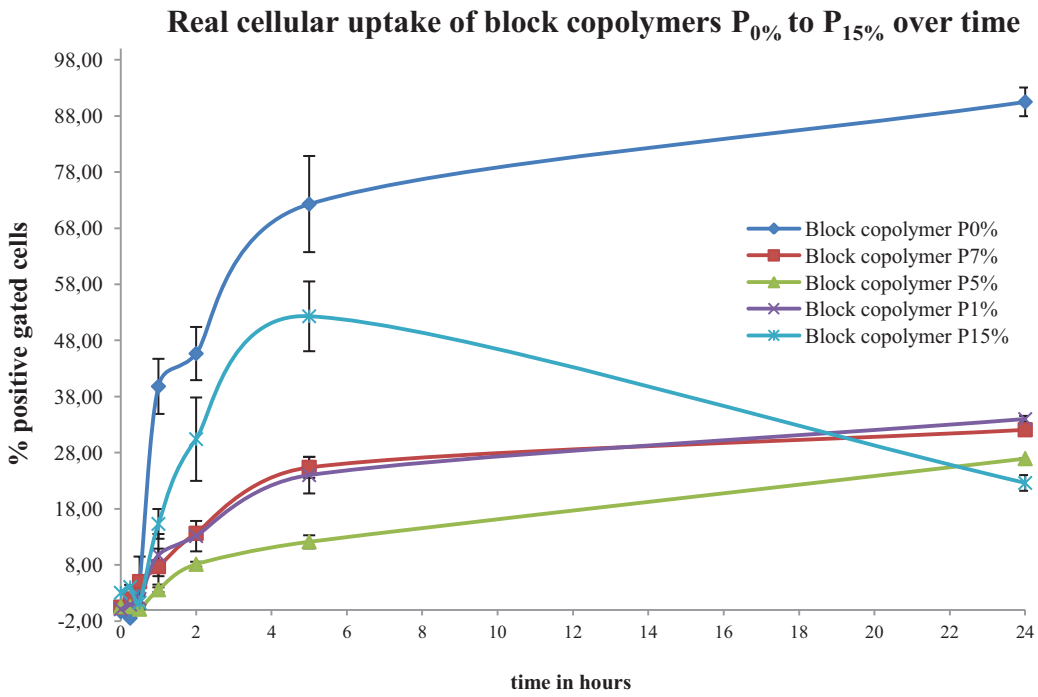

***Figure 2A**: Real cellular uptake of block copolymers **$P_{0\%}$** to **$P_{15\%}$** over time (in % positive gated cells vs. time in hours)*

The cellular uptake profiles in Fig. 2A clearly indicate an energy-dependent cell-internalization mechanism, confirmed by high disparities between FACS values obtained at 37 °C and 4 °C (data not shown). Furthermore, a major trend among the herein investigated block copolymer structures can be derived. The pure block copolymer without any PEGylation demonstrates major internalization into MCF-7 cells as indicated by more than 90 % of positive gated cells at 24 hours of incubation and a general increase over time. These findings stay in accordance with former studies on the cellular uptake of HPMA-*b*-LMA copolymers in the MCF-7/ADR cell line in our group [10]. The herein obtained results on block copolymer uptake may be attributed to two different factors. On one hand, nanoparticle size seems to have a crucial effect on the internalization of nanoparticles by biological cells [11]. During the endocytic process the surface energy of the nanoparticulate system is sacrificed to provide bending energy for the formation of a shell on the nanoparticle surface by the lipid bilayer membrane. Studies of Feng et al. [12] assumed that nanoparticles of less than 100 nm in diameter do not possess enough surface energy to provide the necessary bending energy to form the curvature of the desired size. This could be confirmed by computer simulation of the internalization process of nanoparticles by Ferrari et al. [13]. In our case, the pure block copolymer $\mathbf{P_{0\%}}$ exhibits a hydrodynamic radius of 112 nm thus being in the required range for efficient intracellular uptake. On the other hand, the surface structure is playing an important role in terms of cell-internalization mechanisms. In this regard, the issue of the so called "PEG-dilemma" in gene therapy has to be addressed [14]. Studies revealed that PEGylation can be beneficial concerning the biodistribution and tumor accumulation of nanoparticles but at the same time possesses major disadvantages in terms of intracellular trafficking of cellular uptake as well as endosomal escape [15]. The frequently occurring decrease in transfection efficiency of PEGylated nanoparticles is explained by the steric hindrance introduced by PEG hence inhibiting the interactions between the surface positive charge of lipoplexes and anionic molecules on the cell surface. This observation in gene delivery may also be conferred to our studies since we investigated highest tumor accumulation of polymers with increasing PEG content *in vivo* (see section 5.3) but an inverse pattern regarding cellular uptake *in vitro*. It seems to be that the pure block copolymer is facilitating polymer-cell interactions, probably attributed to the absence of polyethylene glycol as shielding moiety.

Besides, block copolymer $\mathbf{P_{15\%}}$ exhibits second highest values for time-dependent cellular uptake studies in MCF-7 cells (Fig. 2A) and being the only one with a severe decrease in cell-internalization from 5 to 24 hours. Due to the observed drop in cellular uptake, we further investigated the collected cell media of block copolymer $\mathbf{P_{15\%}}$ after different time points of incubation to gain deepening knowledge about endocytic / exocytic processes of this specific block copolymer system at 37 °C over time (see Fig. 2B).

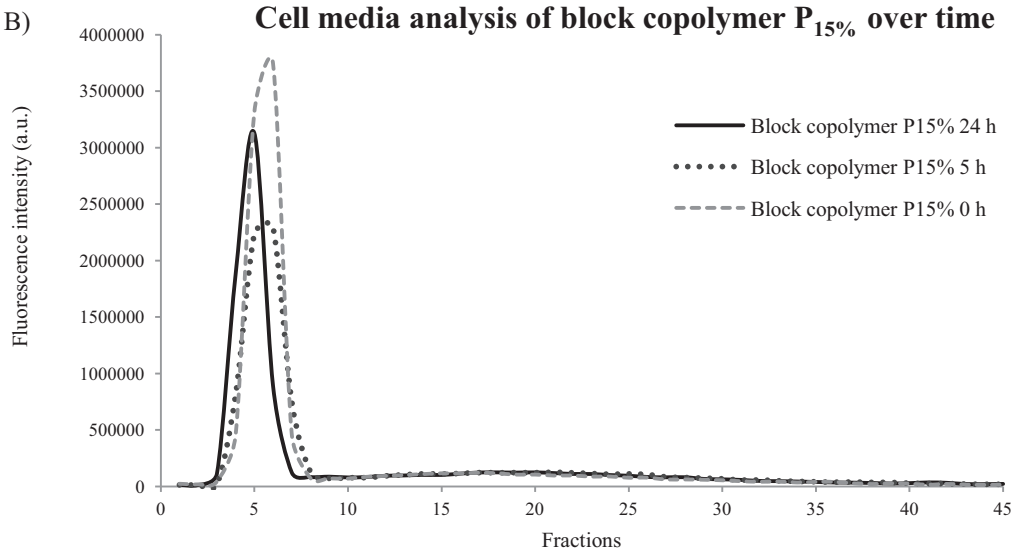

***Figure 2B**: Cell media analysis of block copolymer $\boldsymbol{P_{15\%}}$ after 0, 5 and 24 hours of incubation in MCF-7 cells at 37 °C*

As indicated in Fig. 2B, block copolymer $\mathbf{P_{15\%}}$ showed highest levels in cell media at 0 h, confirming that endocytic uptake has not occurred so far. More importantly, lowest fluorescent intensity in the cell media could be detected after 5 hours of incubation hence directly reflecting the obtained FACS data of $\mathbf{P_{15\%}}$ in Fig. 2A. Due to the highest cellular uptake of block copolymer $\mathbf{P_{15\%}}$ at this time point, its levels in the cell media are comparatively low. In contrast, supernatant analysis after 24 hours of incubation demonstrates comparatively higher values of $\mathbf{P_{15\%}}$ in the cell media thus proofing its exocytic elimination from MCF-7 cells over a time span of one day. These findings support the already observed trend of cellular uptake of block copolymer $\mathbf{P_{15\%}}$ by means of fluorescence-activated cell sorting as seen in Fig. 2A and underline the influence of the degree of PEGylation on intracellular trafficking and resulting exocytic processes.

Furthermore it has to be noted that the two aforementioned factors influencing cellular uptake – nanoparticle size and surface modification by PEG – are of different importance

for the block copolymer with highest degree of PEGylation. PEGylation seems to play a minor role regarding the endocytic uptake of **$P_{15\%}$** in the investigated breast adenocarcinoma cell line since second highest cellular uptake among the studied polymer structures could be determined within 5 hours. Its hydrodynamic radius of ~ 63 nm has to be the major determinant regarding the cell-internalization process – providing the required bending energy for endocytic uptake.

Besides, the block copolymers **$P_{1\%}$** and **$P_{7\%}$** demonstrate a similar uptake pattern in MCF-7 cells over time, possessing comparatively low levels of cell-internalization – with approx. 30 % of positive gated cells after 24 hours of incubation. Also in this case, PEGylation efficiency is not defining polymer-cell interactions since otherwise block copolymer **$P_{1\%}$** should display only marginal lower cellular uptake than its pure polymer analog **$P_{0\%}$**. In contrast, both polymer structures are internalized to the same extent, probably attributed to their small polymer sizes of around (for **$P_{1\%}$**) and below (for **$P_{7\%}$**) 100 nm in diameter. Even though block copolymer **$P_{5\%}$** exhibits a similar R_h than **$P_{7\%}$** (~ 38 nm) it displays lower cellular uptake in MCF-7 cells (particularly at 5 hours of incubation), an observation which cannot be explained to date.

Intracellular localization by means of live cell confocal fluorescence microscopy

To further examine the intracellular pathways of the herein presented block copolymer structures, live cell confocal fluorescence microscopy was applied. Confocal laser scanning microscopy (CLSM or LSCM) is a technique enabling high resolution optical images with depth selectivity [16]. The characteristic feature of confocal microscopy lies in its capability to acquire in-focus images from selected depths, so-called optical sectioning. Images are obtained point-by-point and reconstruction is accomplished with a computer. Thus three-dimensional images of topologically complex objects can be generated. In contrast to a conventional microscope, confocal microscopy only images one depth level at a time (z-level). By means of CLSM a controlled and highly limited depth of focus can be realized hence facilitating the precise localization of fluorescently labeled nanoparticles inside the cell. The principle of confocal microscopy is illustrated in Fig. 3A.

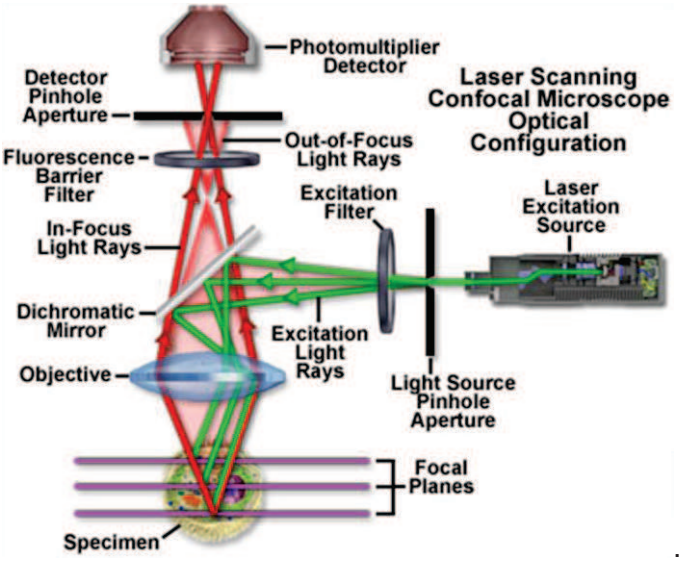

***Figure 3A**: Principle of confocal microscopy. Image source Olympus*

Coherent light which is emitted by the laser system – the excitation source – is passing through a light source pinhole aperture that is situated in a conjugate plane (confocal) with a scanning point on the specimen and a second pinhole aperture located in front of a photomultiplier detector [17]. As the laser is reflected by a dichromatic mirror and scanned across the specimen in a defined focal plane, secondary fluorescence which is emitted from points on the investigated object in the same focal plane is focused as a confocal point at the detector pinhole aperture. A significant percentage of fluorescence emission is appearing at points above and below the objective focal plane and thus is not confocal with the pinhole. These are termed out-of-focus light rays and they create extended Airy disks in the aperture plane. Since only a small amount of the out-of-focus fluorescence emission is delivered through the pinhole aperture, most of this light is not detected by the photomultiplier and hence is not contributing to the resulting image. The photomultiplier tube is then transforming the light signal into an electrical signal which is subsequently recorded by a computer. Due to the suppression of out-of-focus light, sharper images compared to conventional fluorescence microscopy techniques as well as z-stack images at various depths within the specimen can be obtained [16].

In the previous study we have focused on a closer examination of the fluorescently labeled block copolymers in terms of their intracellular localization. Live cell confocal fluorescence microscopy images of block copolymers $\mathbf{P_{0\%}}$ - $\mathbf{P_{15\%}}$ were produced. Co-localization experiments were carried out by means of the lysosomal marker dextrane Texas Red and dextrane Cascade Blue, Hoechst 33342 for nucleus staining as well as the

endoplasmic reticulum marker BODIPY TR glibenclamide. MCF-7 cells were seeded on a cover glass and allowed to settle for 24 hours. Polymer concentration was chosen to be 0.25 mg/mL, accordant to FACS measurements. Cells were incubated for 4, 5, 16 and 24 hours – depending on the investigated polymer system.

Since earlier studies on HPMA based copolymers revealed their endocytic internalization into cells [18] and lysosomes being a principle component of this pathway (also responsible for the degradation of macromolecules), we started with the investigation on a potential lysosomal uptake of HPMA-*b*-LMA copolymers in MCF-7 cells. Cells were incubated with polymer solution for four hours and lysosomal marker (dextrane Texas Red) was added (see Figure 3B).

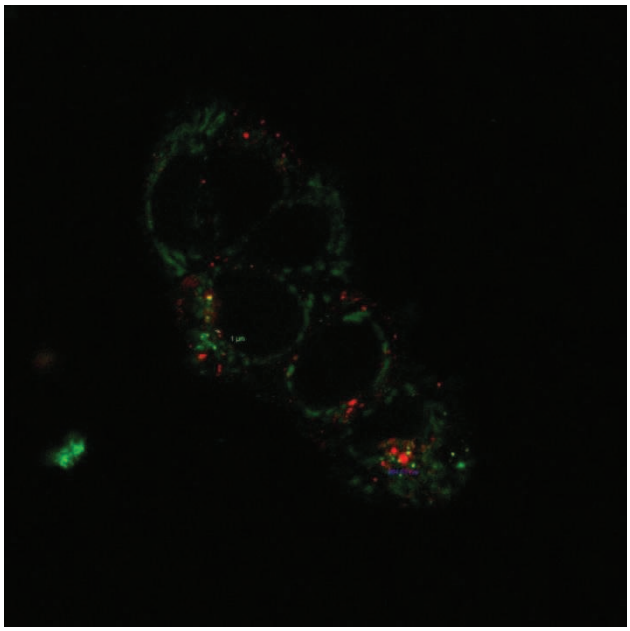

***Figure 3B**: Confocal image of block copolymer **$P_{0\%}$** after 4 hours of incubation. (Green): Oregon Green 488 labeled block copolymer; (red): lysosomal tracker dextrane Texas Red*

Figure 3B clearly demonstrates intracellular uptake of block copolymer **$P_{0\%}$** after 4 hours of incubation, with predominant accumulation around the cell nucleus (not stained). Co-localization of the polymer with lysosomal marker was very low (nearly no overlay of green and red fluorescence) thus not showing lysosomal uptake of the pure block copolymer after endocytosis. Due to the preferential enrichment of **$P_{0\%}$** around the nucleus of MCF-7 cells, we decided on the addition of an ER (Endoplasmic Reticulum) tracker to better determine the intracellular localization of the block copolymer. The resulting confocal images are displayed in Fig. 3C-F.

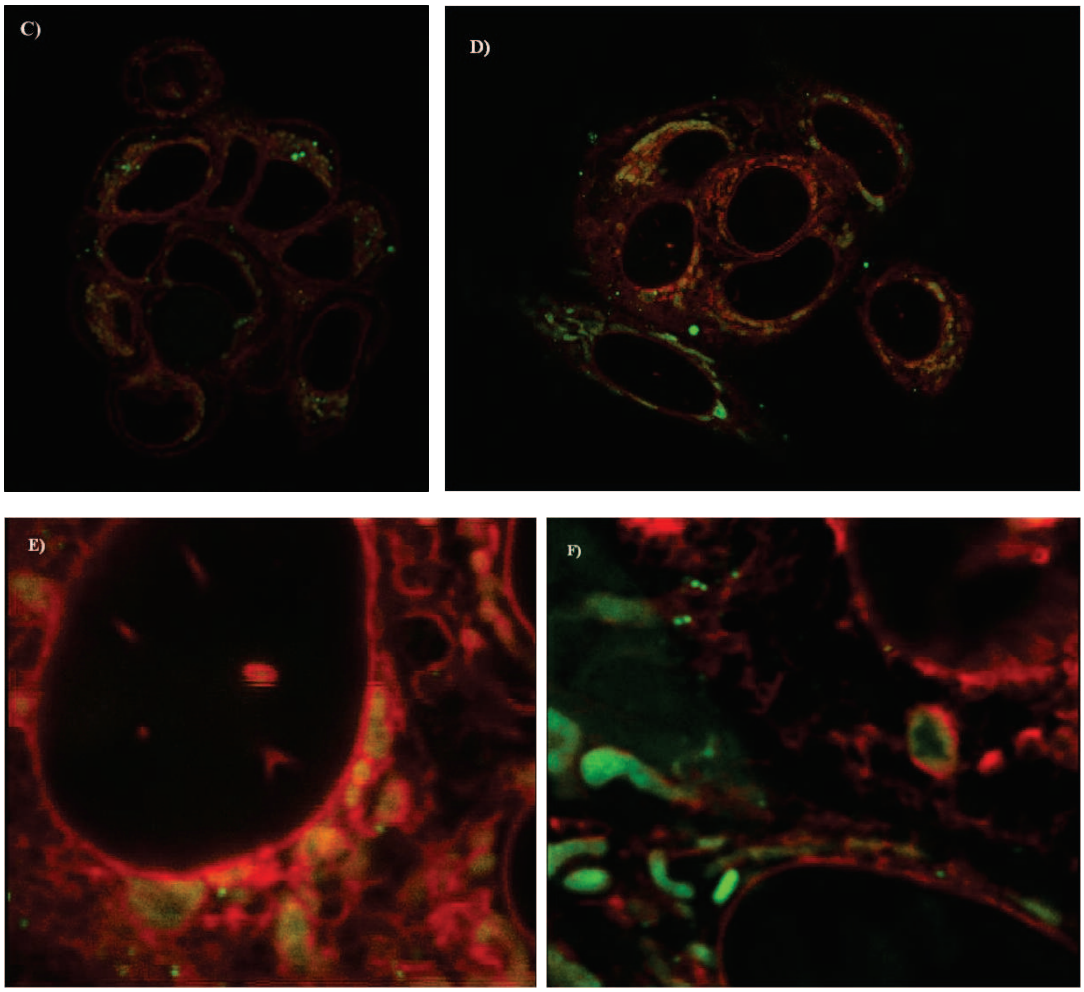

***Figure 3C/D**: Confocal images of block copolymer **$P_{0\%}$** after 4 hours of incubation. **Figure 3E/F**: 3D confocal images of block copolymer **$P_{0\%}$** after 4 h of incubation (zoomed in from Fig. 3D). (Green): Oregon Green 488 labeled block copolymer; (red): ER tracker BODIPY TR glibenclamide*

By means of the endoplasmic reticulum marker, predominant localization of the pure block copolymer in the ER could be determined. In particular the 3D images (seen in Fig. 3E/F) revealed the overlay of green (polymer-related) and red (ER tracker-related) fluorescence thus confirming the presence of **$P_{0\%}$** in the endoplasmic reticulum. Unfortunately, these results could not be verified again (as seen in Fig. 3G) with additional nucleus staining, raising the question whether the obtained localization of **$P_{0\%}$** in the ER after 4 hours was a process occurring within seconds / minutes and thus the subsequent experiments were not able to be accomplished in the appropriate time-window or the observed results were only a single appearing phenomenon following from deviant preparation procedures (e.g. in terms of cell seeding, cell density, contamination or polymer concentration). Due to the limited time frame during the foreign research visit,

the monitored disparities have to be further examined in continuative studies since a repeat of the experiment of n = 2 is not sufficient for a reasonable explanation, respectively neglecting the observed findings. Furthermore – related to the aforementioned issue - the concept of cellular fractionation should be addressed, enabling a quantitative determination of fluorescently labeled polymer in fractionated organelles of the cell. This technology constitutes an important complementary tool providing further insights into cellular pathways of polymeric nanoparticles and thus may be extremely beneficial regarding the clarification of the herein observed accumulation pattern.

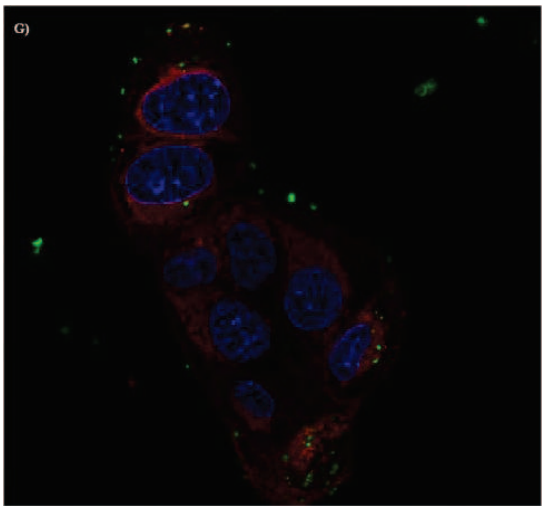

***Figure 3G**: Confocal images of block copolymer **$P_{0\%}$** after 4 hours of incubation. (Green): Oregon Green 488 labeled block copolymer; (red): ER tracker BODIPY TR glibenclamide; (blue): nucleus marker Hoechst 33342*

Besides - based on the promising results regarding the increased cellular uptake of block copolymer **$P_{0\%}$** over 24 hours determined via FACS - we wanted to examine its intracellular localization at this time point by means of confocal fluorescence microscopy, too. As illustrated in Fig. 3H/I, low-membrane associated fluorescence could be detected (in accordance with the previous results) hence internalization of polymer **$P_{0\%}$** into MCF-7 cells was proven.

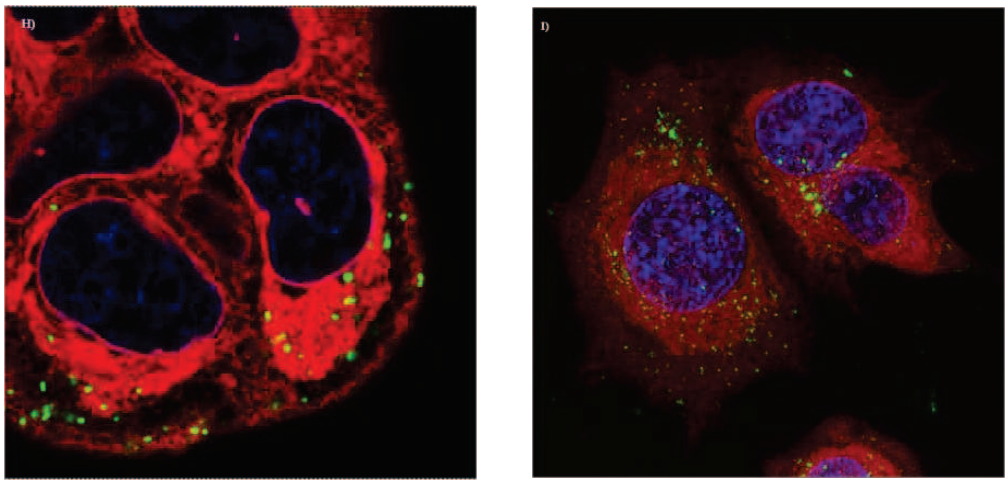

***Figure 3H/I**: 3D confocal images of block copolymer $\mathbf{P_{0\%}}$ after 24 hours of incubation. (Green): Oregon Green 488 labeled block copolymer; (red): ER tracker BODIPY TR glibenclamide; (blue): nucleus marker Hoechst 33342*

Furthermore, increased polymer accumulation around the nucleus (particularly depicted in Fig. 3I) can be seen within 24 hours, demonstrating an overlay of OG 488 labeled block copolymer and the endoplasmic reticulum marker. These findings are partially in compliance with the distinct localization of $\mathbf{P_{0\%}}$ in the ER after 4 hours (see Fig. 3C-F) but in general it has to be noted that one major drawback of the applied ER marker lies in its diffuse visualization of the endoplasmic reticulum also imaging its surrounding (e.g. cytosol and cell membrane). Thus the interpretation of the obtained results is rather difficult and either a more defined fluorescent ER tracker or cellular fractionation should be employed to enable an accurate intracellular trafficking of the polymer compound.

Among the investigated polymer structures, $\mathbf{P_{1\%}}$ was the block copolymer with highest co-localization with lysosomal marker dextrane Texas Red after 5 hours but still not showing 100 % compliance as seen in Fig. 3J.

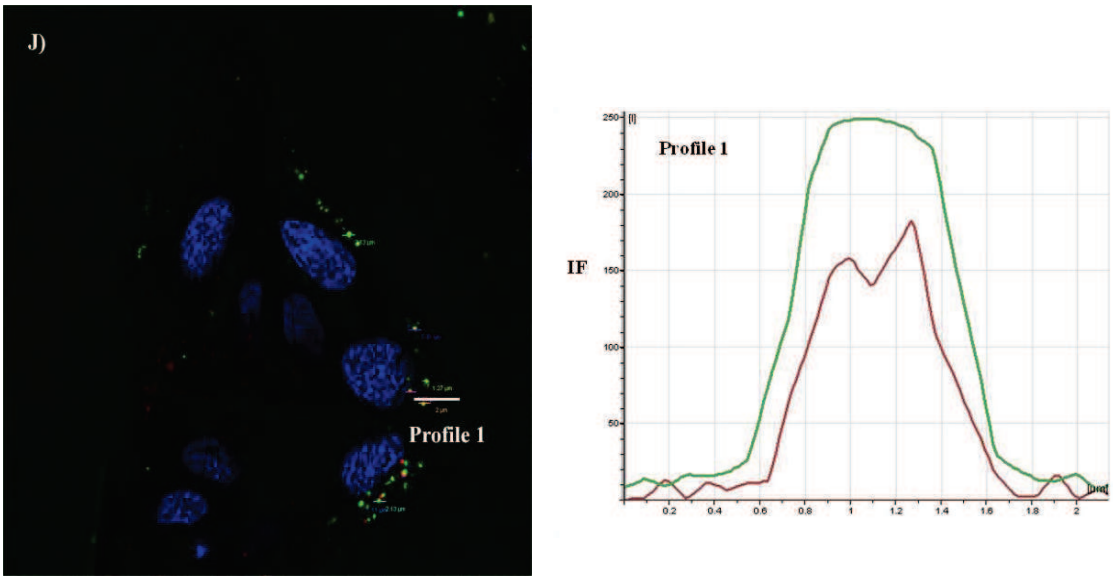

***Figure 3J**: Live-cell confocal image of block copolymer $P_{1\%}$ after 5 hours of incubation (left) as well as proof of co-localization with lysosomal marker by means of overlaying fluorescence (right). (Green): Oregon Green 488 labeled block copolymer; (red): lysosomal marker dextrane Texas Red; (blue): nucleus marker Hoechst 33342. IF = Intensity Fluorescence*

Regarding block copolymers $\mathbf{P_{5\%}}$ and $\mathbf{P_{7\%}}$, live-cell confocal imaging demonstrated comparatively low cellular uptake into MCF-7 cells (in accordance with fluorescence-activated cell sorting) within 5 hours and additionally displayed only minor co-localization with the lysosomal marker dextrane Texas Red (data not shown). In contrast, block copolymer $\mathbf{P_{15\%}}$ with highest degree of PEGylation was illustrating enhanced cellular internalization in the same time frame, directly reflecting the obtained FACS-values (see Fig. 2A). Partial co-localization with the lysosomal tracker could be detected but still being considerably below the findings for block copolymer $\mathbf{P_{1\%}}$ (Fig. 3K). Further ER staining by means of BODIPY TR glibenclamide revealed a similar internalization pattern for $\mathbf{P_{15\%}}$ compared to the pure block copolymer $\mathbf{P_{0\%}}$ after 24 hours of incubation (Fig. 3H/I *vs.* 3L), showing fluorescently labeled polymer in the area around the nucleus but also to some extent close to the cellular membrane.

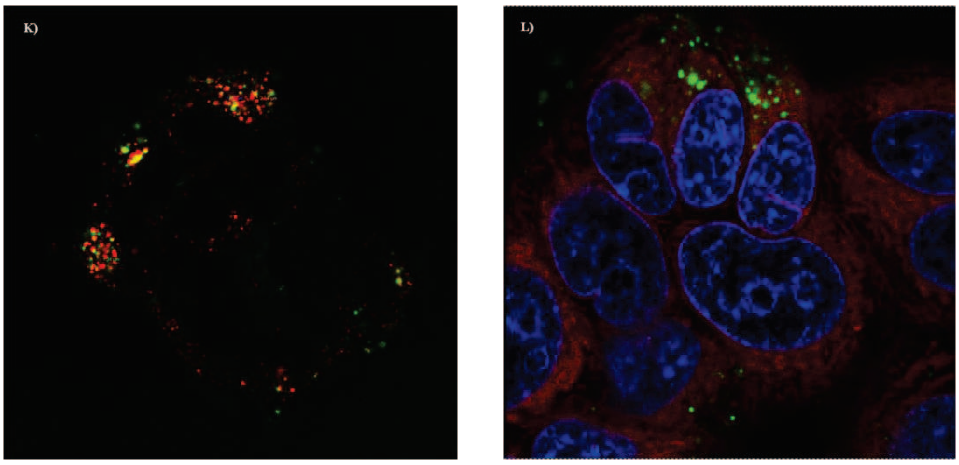

***Figure 3K (left)**: Live-cell confocal image of block copolymer **$P_{15\%}$** after 5 hours incubation. (Green): Oregon Green 488 labeled block copolymer; (red): lysosomal marker dextrane Texas Red; **Figure 3L (right)**: Live-cell confocal image of block copolymer **$P_{15\%}$** after 24 hours incubation. (Green): Oregon Green 488 labeled block copolymer; (red): ER marker BODIPY TR glibenclamide; (blue): nucleus marker Hoechst 33342*

As already mentioned earlier, the application of the endosomal marker in MCF-7 cells includes several issues such as a diffuse overall staining of the entire cell and thus complicating the interpretation of the obtained confocal images (see Fig. 3L). Since it cannot be exactly determined whether the herein presented polymer structures are really localizing within the endoplasmic reticulum, we aimed to further investigate the presence of organelles inside the stained region. Based on this idea, we used three different fluorescent dyes: Oregon Green, Texas Red and Cascade Blue. Oregon Green 488 was used for intracellular polymer tracking, BODIPY TR glibenclamide for ER staining as well as dextrane Cascade Blue as lysosomal marker. After 24 h incubation of polymer **$P_{15\%}$**, false color pictures of selected cells were taken (representative image see Fig. 3M) and it was clearly shown that the lysosomes were also preferentially localized within the interstitium of the endoplasmic reticulum and hence in the fluorescently labeled region of the ER tracker. This finding is emphasizing the complexity of cellular staining and furthermore opens the discussion for the presence of other cell organelles within the interstitial space of the ER in MCF-7 cells.

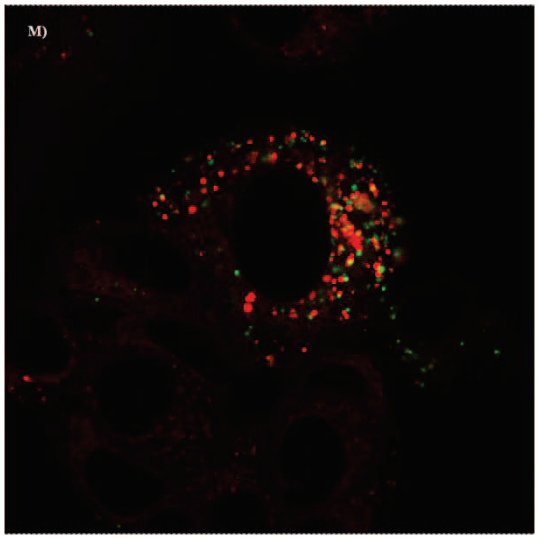

***Figure 3M**: Live-cell confocal false color image of block copolymer **$P_{15\%}$** 24 hours after incubation. (Green): Oregon Green 488 labeled block copolymer; (red): ER marker BODIPY TR glibenclamide and lysosomal marker dextrane Cascade Blue*

Since both organelle markers (for lysosomal as well as ER tracking) did not achieve distinct results on the endocytic uptake of the herein investigated block copolymers, different intracellular pathways have to be considered. In this regard, the polymer pattern inside the cell is playing a major role because the absence of bigger polymer agglomerates (mostly single spots are visible within the cells) rather excludes polymer uptake by larger organelles such as mitochondria or the golgi complex. More reasonable, small organelles distributed within the interstitial space of the ER as well as in the cytosol seem to be responsible for the intracellular uptake of the polymeric nanoparticles after endocytosis. In this regard, further examinations are particularly focusing on peroxisomes [19] which belong to the microbody family and constitute a class of ubiquitous and essential cell organelles [20]. They are considered as "multipurpose" organelles which possess different metabolic functions depending on the respective organism, cell type as well as developmental stage. Peroxisomes are not only responsible for cleaning up the cell's garbage but more importantly, significant roles in lipid metabolism – e.g. α- and β-oxidation of certain fatty acids as well as biosynthesis of ether lipids, bile acids, cholesterol and dolichol – are attributed to these subcellular organelles [21]. Noteworthy, there is strong evidence that peroxisomes and mitochondria are metabolically linked organelles and thus working together on different processes. Since peroxisomes hold a major role in the breakdown of very long chain fatty acids via β-oxidation, there may be a direct correlation between the observed intracellular pathways of the herein investigated

block copolymer structures – exhibiting the fatty acid lauryl methacrylate as hydrophobic block – and the metabolic function of these organelles. This assumption is under closer investigation in ongoing studies.

Inhibition of endocytic pathways monitored via fluorescence-activated cell sorting

Regarding a closer examination on the endocytic internalization process of the herein presented block copolymer structures (particularly concentrating on $\mathbf{P_{0\%}}$ and $\mathbf{P_{15\%}}$), we focused on the application of three different endocytic inhibitors: methyl-β-cyclodextrin, sucrose and cytochalasin D and their influence on polymer uptake into MCF-7 cells. In general macromolecules have to be transported into the cell in membrane bound vesicles - provided by the invagination and pinching-off of pieces of the plasma membrane - during a process called endocytosis [22]. Endocytosis can be divided into two main categories: phagocytosis (uptake of large particles) and pinocytosis (uptake of fluids and solutes). The latter can be further differentiated into four basic mechanisms, namely macropinocytosis, clathrin-mediated endocytosis (CME), caveolae-mediated endocytosis as well as clathrin- and caveolae-independent endocytosis. A general overview of the diversity of endocytic pathways is depicted in Fig. 4.

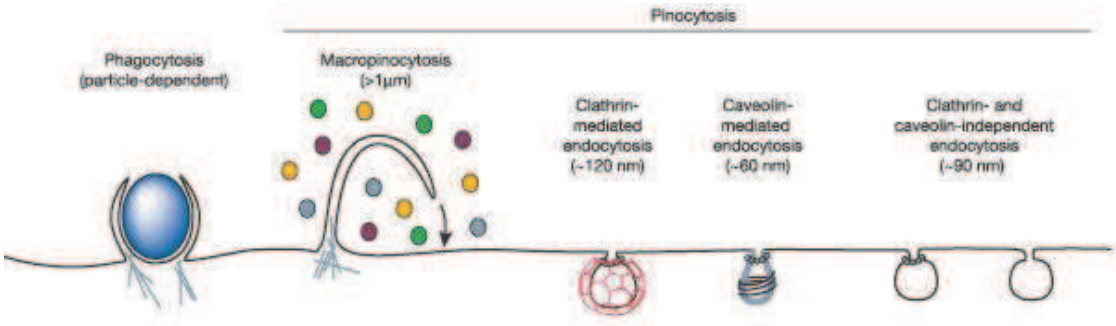

***Figure 4**: The diversity of endocytic pathways – depending on size of the endocytic vesicle, nature of the cargo as well as mechanism of vesicle formation [22].*

In the present study, the three applied endocytic inhibitors are known for the inhibition of different pinocytic pathways. Beginning with methyl-β-cyclodextrin, it is a cyclic oligomer of glucopyranoside inhibiting cholesterol-dependent endocytic processes by reversibly extracting the steroid out of the plasma membrane [23]. It is commonly used to investigate whether endocytosis is depending on the integrity of lipid rafts. Thus methyl-

β-cyclodextrin is a cholesterol-depletion reagent inhibiting the lipid raft (belonging to the clathrin- and caveolae-independent endocytosis) as well as the caveolae and clathrin-mediated pathway [24, 25]. In contrast, hypertonic sucrose only inhibits clathrin-dependent endocytosis by removing membrane-associated clathrin lattices and hence resulting in disappearance of clathrin-coated vesicles, plasma membrane-coated pits as well as clathrin-coated buds on the trans-golgi network [26]. Besides, cytochalasin D is leading to depolymerization of filamentous actin and thus destroying the actin cytoskeleton [24]. It is known for the inhibition of macropinocytosis [27].

In our case, MCF-7 cells were pretreated with the aforementioned endocytic inhibitors 30 min before polymer incubation, washed and then simultaneous addition of inhibitor and polymer was accomplished. Incubation with both components was carried out for 2 and 5 hours and then cells were prepared for fluorescence-activated cell sorting. To further investigate the general impact of the inhibitors concerning cell viability / cytotoxicity in the human breast adenocarcinoma cell line, controls without polymer were additionally prepared (not showing any cell toxicity via FACS within the observed time-window). The influence of methyl-β-cyclodextrin, sucrose as well as cytochalasin D on the pure block copolymer $\mathbf{P_{0\%}}$ is illustrated in Fig. 5A.

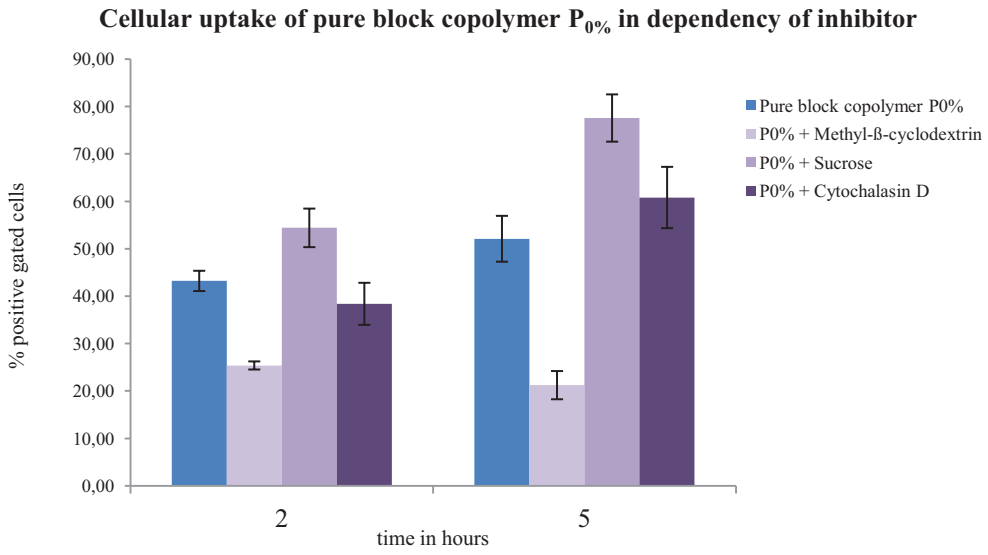

***Figure 5A**: Influence of inhibitors (methyl-β-cyclodextrin, sucrose as well as cytochalasin D) on the cellular uptake of block copolymer $\boldsymbol{P_{0\%}}$ in MCF-7 cells over time*

Based on the results seen in Fig. 5A, some important characteristics can be derived. Comparing the cellular uptake of the pure block copolymer $\mathbf{P_{0\%}}$ with its internalization efficiency by simultaneous addition of methyl-β-cyclodextrin, a significant trend can be observed. In the presence of the mentioned inhibitor, cellular uptake of $\mathbf{P_{0\%}}$ is distinctly decreasing over time, nearly ½ of positive gated cells can only be detected by means of FACS after 2 hours of incubation. This discrepancy between block copolymer alone and $\mathbf{P_{0\%}}$ with methyl-β-cyclodextrin is further increasing over time (5 hours after incubation: 52 % *vs.* 21 % positive gated cells) and demonstrates a major dependency of the endocytic uptake of HPMA-*b*-LMA copolymers via a cholesterol-dependent pathway. The absence of cholesterol is explicitly reducing the internalization of $\mathbf{P_{0\%}}$ and emphasizes the importance of this steroid for endocytosis of the presented block copolymer. Clathrin and caveolin-dependent uptake require cholesterol [22, 25, 28] but since wild type MCF-7 cells do not express a detectable amount of caveolin [29], the observed cellular uptake may be via clathrin-dependent or the lipid raft pathway. These findings stay in correspondence with former studies on HPMA based Dox-AGM copolymers of Greco et al. [30], also showing a pronounced decrease of cellular uptake of the aforementioned copolymers in MCF-7 cells due to methyl-β-cyclodextrin.

Beside, closer investigations on the addition of hypertonic sucrose revealed another important result. As clearly seen in Fig. 5A, the addition of sucrose – inhibiting clathrin-dependent endocytosis – resulted in an enhanced cellular uptake of $\mathbf{P_{0\%}}$ compared to the pure block copolymer, even increasing over time. Based on these findings, the clathrin-dependent endocytic pathway does not seem to be the preferential route of block copolymer uptake into MCF-7 cells. Nevertheless it has to be noted that hypertonic sucrose – despite its application as clathrin-dependent inhibitor – possesses some major drawbacks. It is well-known that extracellular hypertonicity induces cell shrinkage which is leading to compensatory activation of a number of plasma membrane ion transporters, pumps and channels [31]. Thus the hypertonic stress might also induce a reorganization of the cellular membrane leading to an uncontrolled uptake of the polymeric compounds. This issue has to be closely investigated in further studies. However simultaneously applied control studies with sucrose did not reveal any influence on cell viability by means of FACS. Besides, the depolymerization of filamentous actin by means of cytochalasin D is not holding a particular effect on the internalization of the HPMA-*b*-LMA copolymer in the human breast adenocarcinoma cell line, illustrated by accordant

cellular uptake levels compared to the free block copolymer (slight disparities are in the range of the standard deviation).

In conclusion some major statements can be derived. The inhibitor methyl-β-cyclodextrin demonstrated a major impact of block copolymer uptake on a cholesterol-dependent endocytic pathway (e.g. clathrin-dependent, caveolae-dependent or clathrin- and caveolae-independent pathway). Since wild-type MCF-7 cells are not expressing caveolin to a detectable amount, only clathrin-dependent or clathrin- and caveolae-independent endocytosis is of importance. Due to the observed findings of hypertonic sucrose, the clathrin-dependent pathway can also be excluded (as long as cell integrity is further ensured in ongoing studies). Furthermore, cytochalasin D is not affecting the cellular uptake of the pure block copolymer in MCF-7 cells and consequentially a clathrin- and caveolae independent endocytic pathway should be involved. This is subdivided into 4 different classes: Arf6-dependent, flotilin-dependent, Cdc42-dependent and RhoA-dependent [32]. Further examinations should directly focus on the aforementioned routes.

At the end it has to be noted that a general issue regarding chemical inhibitors relies in their rare selectivity and disturbance of multiple endocytic pathways [33]. Hence, it is from fundamental importance to use such inhibitors in combination with endocytosis markers as positive controls and additional methods (such as cell transfection with GFP or FRET imaging) to validate the inhibitory mechanism in the particular cell type. But this is beyond the scope of the herein presented experiment.

Even though the here obtained *in vitro* results in the human breast adenocarcinoma cell line MCF-7 cannot be directly compared to the predominantly applied *in vivo* tumor model (Walker 256 mammary carcinoma) some major correlations can be drawn. The presented study is explicitly showing that a combination of *in vitro* and *in vivo* evaluations is crucial to understand the overall characteristics of polymeric nanocarriers. Particularly focusing on the herein presented HPMA block copolymers, the *in vivo* results were quite promising, demonstrating enhanced blood circulation time with increasing PEG ratio as well as highest tumor accumulation of the block copolymer with highest degree of PEGylation (see chapter 5.3). But not only is the distribution to the target site of major importance regarding efficient anticancer therapy, it has to be further guaranteed that intracellular uptake of the polymeric drug delivery vehicle is actually taking place. In this regard – as seen by the predominant cellular uptake of pure block copolymer in

MCF-7 cells via FACS - PEGylation can possess some major disadvantages (e.g. shielding of nanoparticle toward polymer-cell interactions). Thus *in vitro* studies are essentially required to complement already obtained *in vivo* information in order to reflect the design of potential polymer based (chemo) therapeutics from different standpoints.

References

[1] J.A. Barreto, W. O'Malley, M. Kubeil, B. Graham, H. Stephan, L. Spiccia, Nanomaterials: Applications in Cancer Imaging and Therapy. Advanced Materials 23(12) H18-H40.

[2] M.E. Davis, Z. Chen, D.M. Shin, Nanoparticle therapeutics: an emerging treatment modality for cancer. Nat Rev Drug Discov 7(9) (2008) 771-782.

[3] F. Alexis, E. Pridgen, L.K. Molnar, O.C. Farokhzad, Factors Affecting the Clearance and Biodistribution of Polymeric Nanoparticles. Molecular Pharmaceutics 5(4) (2008) 505-515.

[4] E. Gullotti, Y. Yeo, Extracellularly Activated Nanocarriers: A New Paradigm of Tumor Targeted Drug Delivery. Molecular Pharmaceutics 6(4) (2009) 1041-1051.

[5] C. Fang, B. Shi, Y.-Y. Pei, M.-H. Hong, J. Wu, H.-Z. Chen, In vivo tumor targeting of tumor necrosis factor-a-loaded stealth nanoparticles: Effect of MePEG molecular weight and particle size. European Journal of Pharmaceutical Sciences 27(1) (2006) 27-36.

[6] R. Gref, A. Domb, P. Quellec, T. Blunk, R.H. Müller, J.M. Verbavatz, R. Langer, The controlled intravenous delivery of drugs using PEG-coated sterically stabilized nanospheres. Advanced Drug Delivery Reviews 16(2-3) (1995) 215-233.

[7] R. Gref, M. Lück, P. Quellec, M. Marchand, E. Dellacherie, S. Harnisch, T. Blunk, R.H. Müller, "Stealth" corona-core nanoparticles surface modified by polyethylene glycol (PEG): influences of the corona (PEG chain length and surface density) and of the core composition on phagocytic uptake and plasma protein adsorption. Colloids and Surfaces B: Biointerfaces 18(3-4) (2000) 301-313.

[8] F.M. Veronese, G. Pasut, PEGylation, successful approach to drug delivery. Drug Discovery Today 10(21) (2005) 1451-1458.

[9] A. Cory, T. Owen, J. Barltrop, J. Cory, Use of an aqueous soluble tetrazolium/formazan assay for cell growth assays in culture. Cancer Commun. 3(7) (1991) 207-212.

[10] M. Barz, R. Luxenhofer, R. Zentel, A.V. Kabanov, The uptake of N-(2-hydroxypropyl)-methacrylamide based homo, random and block copolymers by human multi-drug resistant breast adenocarcinoma cells. Biomaterials 30(29) (2009) 5682-5690.

[11] Y. Liu, J. Pan, S.-S. Feng, Nanoparticles of lipid monolayer shell and biodegradable polymer core for controlled release of paclitaxel: Effects of surfactants on particles size, characteristics and in vitro performance. International Journal of Pharmaceutics 395(1-2) (2010) 243-250.

[12] K. Yin Win, S.-S. Feng, Effects of particle size and surface coating on cellular uptake of polymeric nanoparticles for oral delivery of anticancer drugs. Biomaterials 26(15) (2005) 2713-2722.

[13] P. Decuzzi, M. Ferrari, The role of specific and non-specific interactions in receptor-mediated endocytosis of nanoparticles. Biomaterials 28(18) (2007) 2915-2922.

[14] M.J. Joralemon, S. McRae, T. Emrick, PEGylated polymers for medicine: from conjugation to self-assembled systems. Chemical Communications 46(9) (2010) 1377-1393.

[15] H. Hatakeyama, H. Akita, H. Harashima, A multifunctional envelope type nano device (MEND) for gene delivery to tumours based on the EPR effect: A strategy for overcoming the PEG dilemma. Advanced Drug Delivery Reviews 63(3) 152-160.

[16] J. Pawley, Handbook of Biological Confocal Microscopy. Springer 3rd edition (2006).

[17] T. Fellers, M. Davidson, Introduction to Confocal Microscopy. Olympus Fluoview Resource Center (2007).

[18] R. Duncan, P. Rejmanova, J. Kopecek, J.B. Lloyd, Pinocytic uptake and intracellular degradation of N-(2-hydroxypropyl)methacrylamide copolymers a potential drug delivery system. Biochimica et Biophysica Acta (BBA) - General Subjects 678(1) (1981) 143-150.

[19] C.D. Duve, The Peroxisome: A New Cytoplasmic Organelle. Proceedings of the Royal Society of London. Series B. Biological Sciences 173(1030) (1969) 71-83.

[20] R.J.A. Wanders, H.R. Waterham, Biochemistry of Mammalian Peroxisomes Revisited. Annual Review of Biochemistry 75(1) (2006) 295-332.

[21] M. Schrader, Y. Yoon, Mitochondria and peroxisomes: Are the ‘Big Brother’ and the ‘Little Sister’ closer than assumed? BioEssays 29(11) (2007) 1105-1114.

[22] S.D. Conner, S.L. Schmid, Regulated portals of entry into the cell. Nature 422(6927) (2003) 37-44.

[23] D. Vercauteren, R.E. Vandenbroucke, A.T. Jones, J. Rejman, J. Demeester, S.C. De Smedt, N.N. Sanders, K. Braeckmans, The Use of Inhibitors to Study Endocytic Pathways of Gene Carriers: Optimization and Pitfalls. Mol Ther 18(3) 561-569.

[24] L.W. Zhang, N.A. Monteiro-Riviere, Mechanisms of Quantum Dot Nanoparticle Cellular Uptake. Toxicological Sciences 110(1) (2009) 138-155.

[25] S.K. Rodal, G. Skretting, O. Garred, F. Vilhardt, B. van Deurs, K. Sandvig, Extraction of Cholesterol with Methyl-ß-Cyclodextrin Perturbs Formation of Clathrin-coated Endocytic Vesicles. Molecular Biology of the Cell 10(4) (1999) 961-974.

[26] S.H. Hansen, K. Sandvig, B. van Deurs, Clathrin and HA2 adaptors: effects of potassium depletion, hypertonic medium, and cytosol acidification. The Journal of Cell Biology 121(1) (1993) 61-72.

[27] S. Gold, P. Monaghan, P. Mertens, T. Jackson, A Clathrin Independent Macropinocytosis-Like Entry Mechanism Used by Bluetongue Virus-1 during Infection of BHK Cells. PLoS ONE 5(6) e11360.

[28] D. Hailstones, L.S. Sleer, R.G. Parton, K.K. Stanley, Regulation of caveolin and caveolae by cholesterol in MDCK cells. Journal of Lipid Research 39(2) (1998) 369-379.

[29] G. Fiucci, D. Ravid, R. Reich, M. Liscovitch, Caveolin-1 inhibits anchorage-independent growth, anoikis and invasiveness in MCF-7 human breast cancer cells. Oncogene 21(15) (2002) 2365-2375.

[30] F. Greco, M.J. Vicent, S. Gee, A.T. Jones, J. Gee, R.I. Nicholson, R. Duncan, Investigating the mechanism of enhanced cytotoxicity of HPMA copolymer-Dox-AGM in breast cancer cells. Journal of Controlled Release 117(1) (2007) 28-39.

[31] A. Ivanov, Exocytosis and Endocytosis. Methods in Molecular Biology (2008).

[32] G. Sahay, D.Y. Alakhova, A.V. Kabanov, Endocytosis of nanomedicines. Journal of Controlled Release 145(3) 182-195.

[33] A.I. Ivanov, Vol. 440, 2008, pp. 15-33.

5.4 Comparative study on short and long-term distribution of HPMA-*ran*-LMA copolymers *in vivo* by means of ^{18}F and ^{131}I-labeling revealing tumor retention over time

[redacted], ***Mareli Allmeroth***, [redacted] *Rudolf Zentel* [redacted] *Frank Rösch** [redacted]

[redacted]

[redacted], *Dipl. Chem. M. Allmeroth*

Institute of Organic Chemistry, Johannes Gutenberg University Mainz, Duesbergweg 10-14, 55099 Mainz, Germany [redacted]

[redacted]

Macromolecular Rapid Communications, in preparation

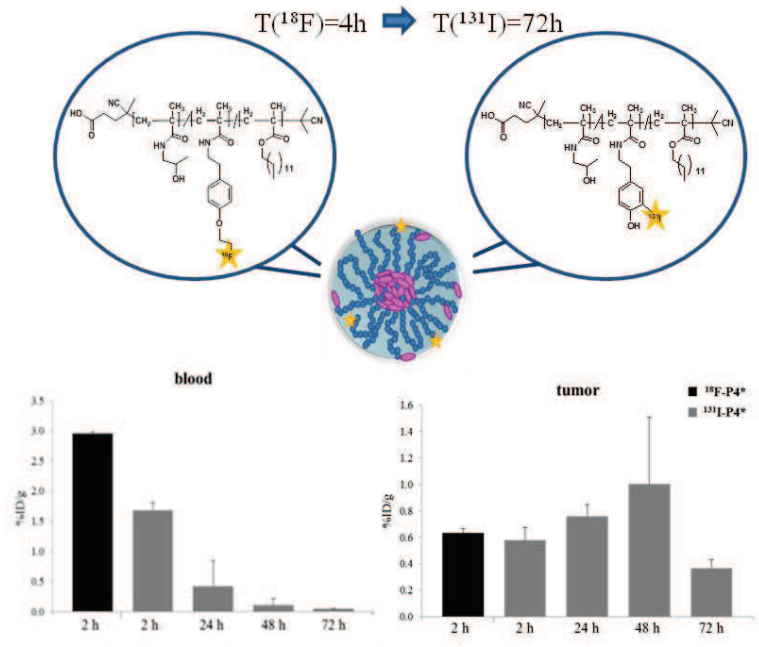

Abstract

With the discovery of the enhanced permeability and retention effect of macromolecules in tumor tissue an increasing need for suitable pre-clinical monitoring of potential nanocarrier systems has emerged. In this regard, both short as well as long term *in vivo* tracking is crucial for understanding structure-property relationships of polymer carrier systems and their resulting pharmacokinetic profile. Based on former studies revealing favorable *in vivo* characteristics for ^{18}F-labeled HPMA based random copolymers – including prolonged plasma half-life as well as enhanced tumor accumulation over a time span of 4 hours - the presented work focuses on their long term investigation in the living organism. In this respect, four different HPMA based polymers (homopolymers as well as random copolymers with lauryl methacrylate as hydrophobic segment) were synthesized and subsequent radioactive labeling was accomplished via the long-lived radioisotope iodine-131. *In vivo* results, concentrating on the pharmacokinetics of a high molecular weight HPMA-*ran*-LMA copolymer, were obtained by means of biodistribution studies in the Walker 256 mammary carcinoma model over a time-span of three days. Special emphasis was laid on the time-dependant correlation between blood circulation properties and corresponding tumor accumulation, particularly regarding the EPR-effect. Studies revealed that despite a polymer clearance from the blood within 72 hours, there was still an increase in tumor uptake observed over time. This characteristic strongly underlines the “proof-of-principle”, namely the EPR-effect, and hence demonstrates the potential of the investigated polymer in terms of efficient anticancer therapy. Furthermore, the findings illustrate the need to combine information of different labeling approaches and *in vivo* evaluation techniques to generate an overall pharmacokinetic picture of potential nanocarriers in the pre-clinical setting.

Keywords: EPR · HPMA · Imaging · Iodine-131 · RAFT

Introduction

Polymeric nanocarrier systems are of emerging interest regarding their potential for anticancer therapy. In contrast to the low molecular weight free drug – suffering from short plasma-half lives, high clearance rates and undesirable side effects in healthy tissue – macromolecular based drug delivery vehicles can significantly improve the pharmacokinetic profile of (chemo) therapeutic agents. Prolonged blood-circulation times, enhanced tumor accumulation due to the EPR-effect [1] as well as a decrease of toxic side effects are only some advantages to be named. The EPR-effect has been proposed to lead to a further increase in intratumoral drug concentration over a longer period of time even with a decrease in plasma level.

Regarding clinical implementation, a polymeric drug carrier has to be non-toxic, non-immunogenic, biodegradable or at least biocompatible with appropriate molecular weight to ensure body excretion. Furthermore, narrow molecular weight distributions are needed to guarantee homogeneity of the final conjugates. [2, 3] Among various clinically investigated polymer structures, so far six HPMA anticancer conjugates entered clinical trials - demonstrating the versatility of this multifunctional synthetic polymer in tumor treatment. [4-7]

In terms of their therapeutic application area, it is essential that the developed polymer systems are as well-defined as possible. [8] The introduction of controlled radical polymerization techniques like ATRP (Atom Transfer Radical Polymerization) [9] or RAFT (Reversible Addition-Fragmentation Chain Transfer) [10, 11] thus facilitated the access to narrowly-distributed and well-defined polymer structures. Notably, the combination of RAFT with reactive ester chemistry [12-14] is demonstrating an elegant route to diverse polymer architectures. [15-17]

Besides the aforementioned high demands on the macromolecular carrier system, especially adequate pre-clinical screening tools are crucial in order to provide an appropriate therapy for the individual patient. [18, 19] In this regard, non-invasive molecular imaging techniques such as Positron Emission Tomography (PET) or Single Photon Emission Computed Tomography (SPECT) constitute helpful diagnostic tools enabling detailed information on the body disposition as well as tumor accumulation of the polymer-drug conjugate in the living organism. In

dependency of the incorporated radionuclide, and its particular half-life, the diagnostic time frame can be adjusted from early phase accumulation – by means of shorter lived isotopes – to long term imaging over weeks or months.

Former studies in our group already illustrated the successful radiolabeling of various HPMA based polymers by means of the positron emitters As-72/74 [20] and F-18 [21] thereby establishing µPET imaging for time-efficient screening of potential drug delivery systems. Further investigations on ^{18}F-labeled HPMA based polymer systems revealed the major impact of molecular weight and aggregate formation on the body distribution in the living animal. [22] The examined polymer structures included homopolymers as well as random copolymers composed of a hydrophilic HPMA and a hydrophobic lauryl methacrylate (LMA) segment. In direct comparison, the high molecular weight random copolymer (M_w = 55 kDa, LMA ratio 25%) exhibited most favorable *in vivo* characteristics – combining prolonged blood circulation times with highest tumor uptake as well as low liver accumulation and renal excretion properties. However, this specific pharmacokinetic profile was investigated by means of fluorine-18 ($t_{1/2}$ = 110 min) as radioactive marker, enabling a diagnostic time frame of only up to 4 hours. But particularly the observation of enhanced plasma-half life of the random copolymer (after 4 h p.i. ~ 40 % of the polymer still remained in the blood pool) was asking for a selective monitoring of this polymer architecture in the long term. In this regard, the enhanced permeability and retention of macromolecules in tumor tissue has to be addressed, not just being a temporary phenomenon of passive targeting to the tumor site but notably allowing a sustained release and accumulation of drugs over weeks and longer. [23, 24] To proof the "EPR-effect" for the herein presented HPMA-*ran*-LMA copolymer system, we decided on its radioactive labeling by incorporating the longer-lived γ-emitter iodine-131 ($t_{1/2}$ = 8.1 days). Radioisotopes of iodine are highly suitable for studying the long term pharmacokinetics of HPMA based polymer architectures, attributed to their longer half-lives, facile access to radiolabeling procedures as well as direct availability. [4, 7, 19, 25] In addition, the convenience of incorporating iodine-131 at tyramine groups likewise used for ^{18}F-labeling via [^{18}F]fluoroethylation enables the direct comparison of short term

pharmacokinetics of the applied polymer system (^{131}I- *vs.* O-[^{18}F]fluoroethyl-tyramine labeling). Furthermore, long term distribution of the identical polymer batch by means of I-131 can be accomplished, too.

The aim of the present study focused on radiolabeling of HPMA based polymers via iodine-131 and the consequent long term monitoring of an HPMA-*ran*-LMA copolymer *in vivo*, particularly regarding its blood residence time as well as tumor accumulation / retention properties ("EPR-effect") over a time-window of three days. Due to an additional time point in the short-range (2 h), a direct correlation to former studies with ^{18}F-labeled HPMA based random copolymer can be drawn. [22]

Experimental Section

Materials

All solvents were of analytical grade, as obtained by Sigma Aldrich and Acros Organics. Dioxane was distilled over a sodium/potassium composition. Lauryl methacrylate was distilled to remove the stabilizer and stored at -18 °C. 2,2'-azobisisobutyronitrile (AIBN) was recrystallized from diethyl ether and stored at -18 °C as well. Iodine-131 was obtained from GE Healthcare (Braunschweig, Germany).

Polymer synthesis

Synthesis of 4-cyano-4-((thiobenzoyl) sulfanyl)pentanoic acid (CTP)

4-cyano-4-((thiobenzoyl)sulfanyl)pentanoic acid was used as chain transfer agent (CTA) and synthesized according to the literature.[11]

Synthesis of pentafluorophenyl methacrylate (PFPMA)

Pentafluorophenyl methacrylate was prepared according to reference. [26]

Synthesis of homopolymers and random copolymers

The synthesis of reactive ester homopolymers as well as copolymers can be found in the supporting information.

Removal of dithioester endgroups

The dithiobenzoate endgroup was removed using the protocol reported by Perrier et al. 2005. [27] The procedure is further explained in the supplementary information.

Polymer analogous reaction of homopolymers and random copolymer

The polymeranalogous reaction of homopolymers and random copolymers are explained in more detail in the supplementary information.

Radiolabeling

Radiolabeling procedures applied to study ^{131}I-radiolabeling of different HPMA based polymers are provided as supplementary information.

Radioiodination for *in vivo* experiments was performed using the following optimized labeling conditions applying the CAT procedure yielding 49±3 % of ^{131}I-labeled HPMA-*ran*-LMA copolymer **P4***: 1 mg **P4*** in 100 µL of DMSO, 200 µg CAT, 200 µL PBS and 96±16 MBq of [^{131}I]iodide solution.

Polymer characterization (including experimental setups and FCS measurements) as well as animal experiments are provided as supporting information.

Results and Discussion

To investigate the long-term *in vivo* distribution of HPMA based polymer structures - with special focus on tumor accumulation characteristics and the EPR (Enhanced Permeability and Retention) effect – two HPMA based polymer architectures (homopolymers and random copolymers with lauryl methacrylate as hydrophobic group) were synthesized by combining reactive ester chemistry with the RAFT polymerization technique [10, 26, 28]. This approach enables the synthesis of well-defined and narrowly distributed polymer systems and polymeranalogous reaction with primary amines facilitates the incorporation of imaging moieties such as fluorescent dyes or radiolabels. Former studies in our group already demonstrated the tremendous impact of polymer structure (molecular weight, amphiphilicity and superstructure formation) on cellular uptake [15] and in particular on the *in vivo* fate. [22] Since closer investigations revealed favorable *in vivo* characteristics – including prolonged blood-circulation time, low hepatic uptake as well as renal clearance – for a high molecular weight HPMA-*ran*-LMA copolymer over a time span of 4 hours by means of the positron emitter fluorine-18 ($t_{1/2}$ = 110 min) [22], we decided to selectively examine its long term fate using the γ-emitter iodine-131 ($t_{1/2}$ = 8 d). For a detailed comparison of the radiolabeling process, HPMA homopolymers (**P1*** and **P2***) as well as random copolymers (**P3*** and **P4***) - varying in molecular weight - were investigated. Polymer synthesis and radioactive labeling procedure are depicted in figure 1; polymer characterization in table 1.

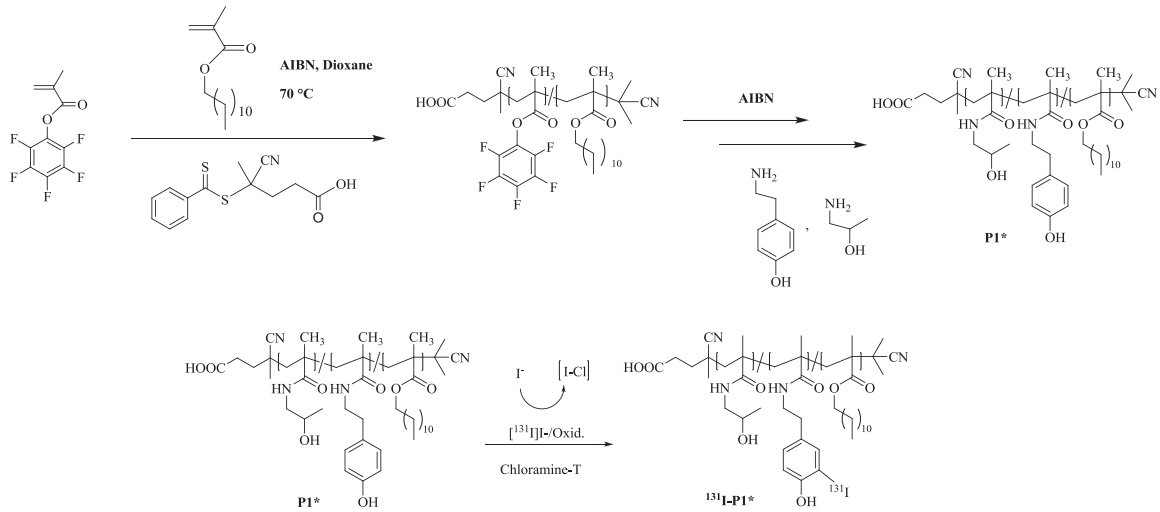

***Figure 1**: Polymer synthesis via reactive ester approach with subsequent polymeranalogous reaction as well as radioactive labeling procedure by means of iodine-131*

Table 1**: Analytical data of reactive ester precursor polymers (**P1*-R - P4*-R**) as well as final polymeric structures (**P1* - P4)*

Notation	Polymeric structure	Monomer ratio	M_n [g/mol]	M_w [g/mol]	PDI [b]	R_h [e] [nm]
P1*-R	Homopolymer	100 %[a]	18000[b]	23000[b]	1.29	n.d.
P2*-R	Homopolymer	100 %[a]	87000[b]	130000[b]	1.49	n.d.
P3*-R	Random copolymer	80:20[a]	17000[b]	21000[b]	1.26	n.d.
P4*-R	Random copolymer	80:20[a]	57000[b]	80000[b]	1.41	n.d.
P1*	Homopolymer	100 %[c]	9000[d]	12000[d]	1.29	1.1
P2*	Homopolymer	100 %[c]	52000[d]	77000[d]	1.49	3.0
P3*	Random copolymer	82:18[c]	11000[d]	14000[d]	1.26	33.4
P4*	Random copolymer	75:25[c]	39000[d]	55000[d]	1.41	39.9

*[a] Calculated monomer ratio; [b] Determination by GPC in THF as solvent; [c] Monomer ratio determined by ^{1}H-NMR spectroscopy after polymeranalogous reaction with 2-hydroxypropylamine; [d] Calculated from the molecular weights of the reactive ester polymers **P1*-R – P4*-R** as determined by GPC in THF as solvent; [e] Hydrodynamic radii determined by Fluorescence Correlation spectroscopy (FCS)*

Former ^{18}F-labeling of HPMA based polymer systems has been accomplished via [^{18}F]fluoroethylation of tyramine groups [21, 22] (~ 2 - 4 % incorporation as determined by ^{1}H-NMR) which provide highly activated phenolic rings. Hence, I-131 incorporation can be accomplished by means of electrophilic aromatic substitution; enabling ^{131}I-labeling of the same HPMA based polymers without prior derivatization of the polymer structure. This approach allows for a direct correlation of structure-property relationships between the ^{18}F- and the ^{131}I-labeled HPMA-*ran*-LMA copolymer *in vivo*.

In order to promote incorporation of ^{131}I *via* direct electrophilic aromatic substitution, reaction conditions were studied to optimize the labeling technique for different HPMA based architectures. Since direct electrophilic radioiodination requires the generation of an electrophilic radioiodine species by oxidation from [^{131}I]NaI, two different in-situ oxidants were tested, being commonly applied for radioiodination of proteins: Chloramine-T (N-chloro-4-methylbenzenesulfonamide sodium salt, CAT) and Iodogen™ (1,3,4,6-Tetra-chloro-3a,6a-diphenylglycoluril). [29, 30] Radioactive labeling of polymers was performed in phosphate buffered saline (pH = 7.2) and succeeded within 4 minutes reaction time. Investigations on type and amount of oxidant revealed highest radiochemical yields (RCYs) for CAT regarding I-131 labeling of HPMA homopolymers (**P1*** M_w = 12 and **P2*** M_w = 77 kDa respectively); with higher RCY for the high molecular weight homopolymer (see figure S1 supplementary info). Stability of the radiolabel was ensured by means of SEC purification in combination with thin layer chromatography, indicating less than 1 % radioiodine detachment from the polymer after 2 days of storage in NaCl at 4 °C. Radioiodination of HPMA-LMA random copolymers (**P3*** M_w = 11 kDa; **P4*** M_w = 55 kDa) additionally concentrated on the appropriate choice of reaction solvents since the hydrophobic lauryl methacrylate side chains avoid complete dissolution of the polymers in PBS (solvent dependency see figure S2 and S3 supplementary info).

Concerning the labeling efficiencies, the low molecular weight random copolymer **P3*** showed highest RCYs (41 %, decay corrected) for Iodogen whereas its high molecular weight counterpart **P4*** exhibited best labeling yields (corrected RCY = 44 %) using Chloramine-T.

Due to former short term studies by means of [^{18}F]fluoroethylation, exposing the high molecular weight HPMA-*ran*-LMA copolymer as most suitable candidate for polymer drug delivery [22], we here aimed to investigate its potential as polymeric nanocarrier in more detail and with respect to long term pharmacokinetics. Hence [^{131}I]radio-iodination of HPMA-LMA random copolymer **P4*** for subsequent *in vivo* evaluation was accomplished using CAT as oxidizing agent as well as DMSO in order to promote ^{131}I incorporation in sufficient high yields - using 1 mg of polymer precursor in a total synthesis time (including SEC purification) of less than 20 min. Biodistribution studies of ^{131}I-labeled polymer were carried out in Walker 256 tumor bearing rats.

In order to follow the long term biodistribution and tumor accumulation (EPR-effect), time points were chosen to be 2, 24, 48 and 72 h post injection. Radioiodination efficiencies were determined to be 49±3% (decay corrected) after preparative SEC purification. Figure 2 displays the biodistribution of **^{131}I-P4*** in organs of interest (liver, spleen, kidney, lung, heart and blood), investigated over up to 72 h in comparison to short term pharmacokinetics observed for **^{18}F-P4***.

Concerning relevant organs of body clearance - i.e. liver, spleen and kidney – striking differences between short term distribution obtained with **^{18}F-P4*** and long term disposition measured with the ^{131}I-labeled analog were observed. Hepatic and spleenic uptake of ^{131}I-labeled **P4*** was much higher (over a time span of 72 h) when comparing to the data of the ^{18}F-labeled polymer. Even at the same time point (2 h p.i.), the liver concentration of the ^{131}I-labeled compound was 5-times higher compared to ^{18}F-labeling whereas the spleen showed 10-times higher values for **^{131}I-P4*** (Figure 2A/B, table S1). This observation may be attributed to an enhanced lipophilicity of the random copolymer system induced by the more hydrophobic iodine radiolabel. Besides, an inverse pattern was observed regarding kidney concentrations of the herein examined high molecular weight random copolymer.

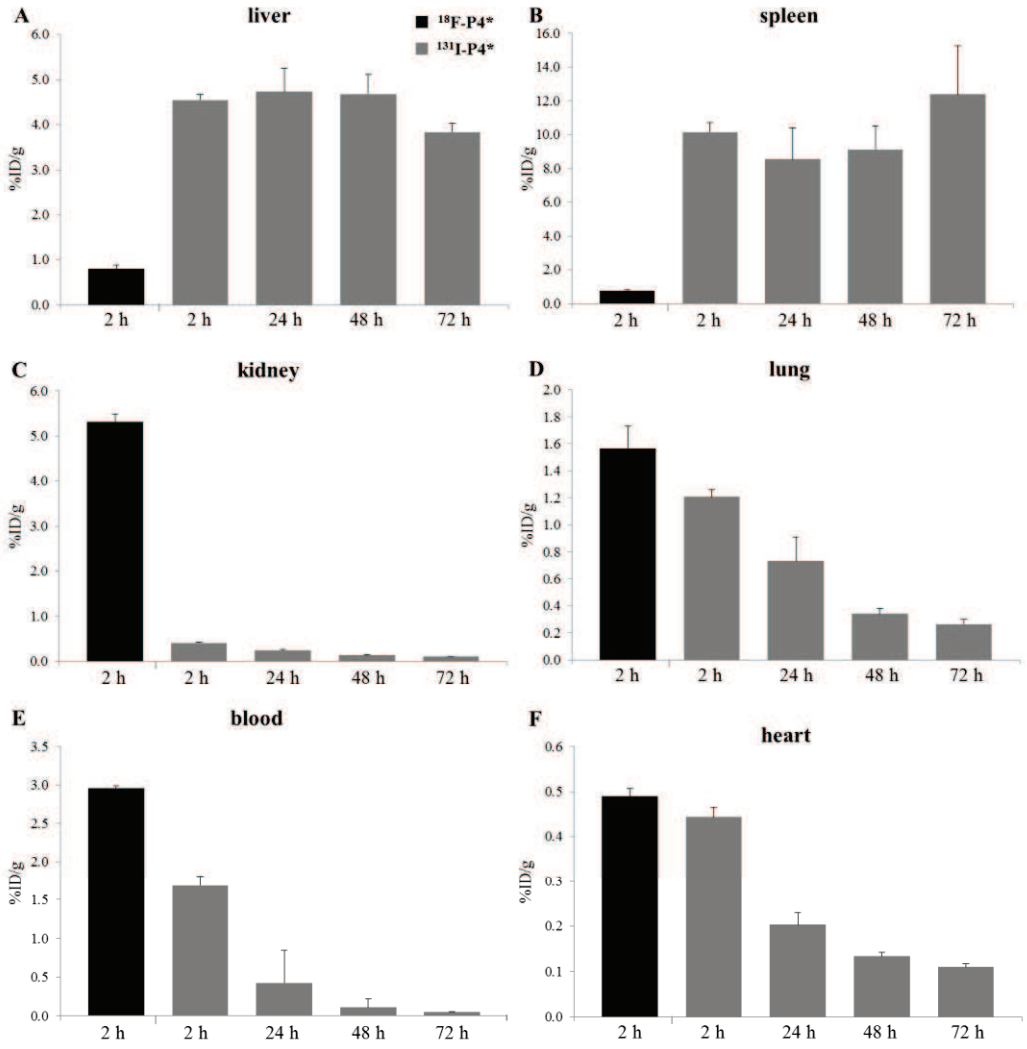

Figure 2**: Biodistribution studies of the large HPMA-ran-LMA copolymer **P4 in different organs (liver, spleen, kidney, lung, heart and blood) 2 h p.i. using **^{18}F-P4*** and for up to 72 h by means of **^{131}I-P4*.** Data is expressed as % ID/g tissue (mean±SEM). n=2-3 Almost linear decrease in **^{131}I-P4*** level in the kidney (r=-0.934), lung (r=-0.896) and heart (r=-0.881).*

Kidney uptake (Figure 2C) of **^{131}I-P4*** was strongly reduced, displaying about 14-times lower concentrations compared to **^{18}F-P4***. According to the observed pharmacokinetic shifts in organ uptake between the differently labeled random copolymer **P4*** it has to be mentioned that the minute amounts of a reporter probe should allow to study pharmacokinetics without effectively altering surface properties or architecture of the carrier system. However *in vivo,* the radiolabel - or its anchoring moiety - might be subjected to degradation (e.g. in the liver) resulting in higher concentrations of lipophilic radio-metabolites in the liver or enhanced clearance of hydrophilic metabolites via

the kidney. Former studies on a [^{18}F]fluoroethylated HPMA homopolymer revealed low initial metabolism rates in the blood, with no further increase for up to 1 h after i.v. administration. Here, no radiometabolites were detected in the urine implying plasma binding of the initially formed ^{18}F-metabolites. Furthermore, no radioactive accumulation in the skeleton due to released [^{18}F]fluoride was observed up to 2 h after polymer administration. [22] Besides, in the present study nearly 1.8-times lower concentrations of **^{131}I-P4*** were found in the blood compared to **^{18}F-P4*** (1.69±0.12 % ID/g *vs.* 2.60±0.03 % ID/g, respectively) 2 h p.i. which might be ascribed to the observed plasma binding of ^{18}F-radiometabolites leading to an overestimation of initial blood pool concentrations upon ^{18}F-polymer administration. Although the observed disparities in organ distribution are likely attributed to differences in the metabolism of the radiolabels, a potential influence of the radionuclide itself on polymer characteristics and subsequent clearance has to be addressed. Pozzi et al. studied the influence of the radioisotope (^{18}F *vs.* ^{131}I-prosthetic group) on the *in vivo* pharmacokinetics of a model peptide. Notably, the ^{131}I-labeled peptide showed mainly hepatic as well as spleenic uptake (likely due to the higher lipophilicity of iodine) whereas the respective ^{18}F-labeled peptide was cleared via the renal system. [31] Based on these findings not only the degree of isotope release and its reutilization by plasma binding or organ uptake might account for the discrepancy in organ distribution but also the radionuclide *per se* might impart higher liver and spleenic uptake (as seen for **^{131}I-P4***).

In order to effectively deliver drugs to the target tissue (tumor), a suitable drug carrier system has to meet unique requirements - particularly prolonged retention in the blood pool as well as an EPR mediated accumulation in the tumor tissue is most desired. Regarding these special demands, we wanted to study the potential of the high molecular weight HPMA-LMA random copolymer **P4*** in the Walker 256 carcinoma model. Investigation of the polymer concentration in the blood compartment over up to three days (Fig. 2E, blood; Fig. 2F, heart) revealed a continuous clearance of **P4***. Major blood clearance was observed within the first 24 h after administration of **^{131}I-P4*** with 25 % (0.42±0.04 % ID/g) of **^{131}I-P4*** remaining in the blood compartment

after 1 day. These findings demonstrate even higher blood levels compared to a study of Lammers et al. [32] determining the blood residence time of an iodine-131 labeled HPMA copolymer of 31 kDa. In addition, concentrations at 72 h (0.05±0.01 % ID/g) indicated a total blood clearance of **P4*** in less than three days. The blood concentration was decreasing almost linearly (r= -0.867). Highly blood supplied organs such as lung (Figure 2D) and heart (Figure 2F) reflect the already investigated course of iodine-131 labeled polymer in the blood. Besides the aforementioned characteristics of the polymer in the blood pool, the observed trend in tumor accumulation is much more remarkable. Even though we investigated a significant blood clearance of the random copolymer over time, the concentrations found for **^{131}I-P4*** gradually increased over a time window of 2 days (Figure 3). Considering that more than 90 % of the polymer is being cleared from the blood within this time frame (Figure 2E), the increased retention of **P4*** in the tumor is directly correlating to the characteristics of EPR-mediated passive tumor accumulation of polymeric nanocarrier systems. [1, 24, 33]

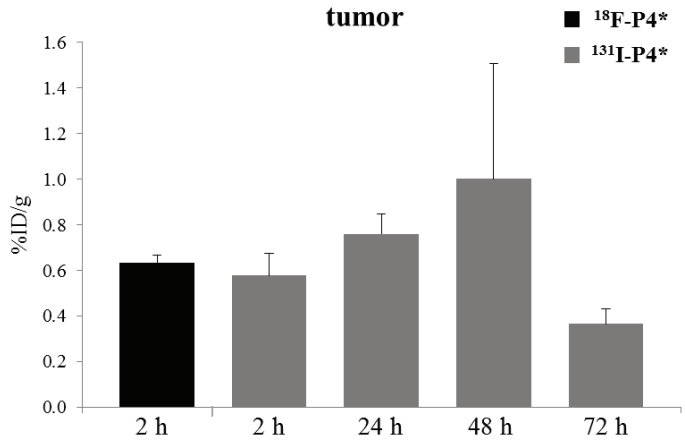

Figure 3**: Tumor uptake of high molecular weight HPMA-ran-LMA copolymer **P4 in the Walker 256 mammary carcinoma model. Distribution was studied 2 h p.i. using **^{18}F-P4*** and for up to 72 h by means of **^{131}I-P4***. Data is expressed as % ID/g tissue (mean±SEM).*

Former studies in our group already revealed a significant cellular uptake of the high molecular weight random copolymer **P4*** in the Walker 256 mammary carcinoma cell line (data not shown). Based on these findings we assume that the *in vivo* observed tumor characteristics are related to a combination of increased extravasation of polymer to the tumor tissue (EPR-effect) as well as polymer-cell specific interactions at the tumor site. However, highest tumor uptake of **^{131}I-P4*** was observed 48 h after administration (1.00±0.51 % ID/g) thus demonstrating the suitability of this HPMA based copolymer system for anticancer treatment within a time frame of 2 days. The decreasing value found at 72 h after injection (Figure 3) could be the result of differences in tumor growth which might affect the tumor accumulation of the polymer.

Noteworthy both, **^{18}F-P4*** and **^{131}I-P4***, showed similar initial tumor concentrations of about 0.6 % ID/g - despite the observed differences in initial organ and blood pool concentrations. With these findings, both labeling strategies are assumed to be suitable to determine the tumor targeting ability of polymer based drug carrier systems. Although the shorter half-life of ^{18}F (110 min) limits the diagnostic time frame to several hours, [^{18}F]fluoroethylation allows to assess the suitability of drug carriers for efficient tumor treatment profiting from additional PET imaging as valuable short term preclinical tool. However, despite fast and efficient screening of potential polymeric drug delivery vehicles is enabled - with respect to assessing intratumoral distribution - careful interpretation regarding initial organ distribution has to be accomplished. Here application of diverse labeling approaches, not demanding for a prior variation of the polymer structure, are crucial in order to reveal overall pharmacokinetic as well as long term distribution, facilitating the choice of promising drug delivery compounds in the future.

Conclusion

In the present study we could demonstrate the successful introduction of a long-lived radioisotope into HPMA-*ran*-LMA copolymer structures, enabling their precise tracing in terms of body distribution and especially tumor accumulation over a time span of several days. Radioactive labeling by means of iodine-131 enabled *ex vivo* bio-distribution studies of the high molecular weight HPMA based random copolymer,

underlining the significance of tracking the pharmacokinetic profile of polymers in the long run. Based on an observation frame of 3 days, enhanced retention of the random copolymer **P4*** in tumor tissue could be proven (at least over 48 hours) – despite its concurrent clearance from the blood pool. These characteristics can be directly correlated to the well-known EPR-effect. Furthermore, due to a comparative short term study of ^{18}F-labeled copolymer **P4***, the additional labeling approach indicated an accordant tumor uptake pattern for **^{131}I-P4*** at the same time point (2 h p.i.). This observation is of major importance since initial organ distribution of the differently labeled high molecular weight HPMA based random copolymer revealed strong disparities in organ accumulation. In this regard, metabolic studies on the *in vivo* stability of the polymer-bound radiolabels are ongoing. In conclusion, the herein obtained results underline the significance of applying multiple and versatile labeling approaches to determine the potential of polymeric carrier systems for efficient anticancer therapy.

Acknowledgement

The authors would like to thank Barbara Biesalski, Martin Nowak and Achim Reibel for their support during animal studies. Special thanks go to Danielle Vugts for providing introduction into radioiodination procedures. We also want to thank the Max-Planck Graduate Center (MPGC, M. Allmeroth) as well as the Graduate School Materials Science in Mainz (Excellence Initiative, DFG/GSC 266, D. Moderegger) for financial support. In addition the authors are very thankful for financial support of the DFG (Rösch: RO 985/30-1; Thews: TH 482/4-1, Zentel: ZE 230/21-1) and SAMT Initiative Mainz.

References

[1] Y. Matsumura, H. Maeda, Cancer Research **1986**, 46, 6387.

[2] R. Duncan, Nat Rev Drug Discov **2003**, 2, 347.

[3] R. Duncan, Nat Rev Cancer **2006**, 6, 688.

[4] D. R. F. L. W. Seymour, D. J. Kerr, D. Rea, M. Whitlock, R. Poyner, C. Boivin, S. Hesslewood, C. Twelves, R. Blackie, A. Schatzlein, D. Jodrell, D. Bissett, H. Calvert, M. Lind, A. Robbins, S. Burtles, R. Duncan, J. Cassidy, Int. J. Oncol. **2009**, 34, 1629.

[5] R. Duncan, Advanced Drug Delivery Reviews **2009**, 61, 1131.

[6] R. Duncan, M. J. Vicent, Advanced Drug Delivery Reviews **2010**, 62, 272.

[7] L. W. Seymour, D. R. Ferry, D. Anderson, S. Hesslewood, P. J. Julyan, R. Poyner, J. Doran, A. M. Young, S. Burtles, D. J. Kerr, Journal of Clinical Oncology **2002**, 20, 1668.

[8] M. Barz, R. Luxenhofer, R. Zentel, M. J. Vicent, Polymer Chemistry **2011**, 2, 1900.

[9] K. Matyjaszewski, J. Xia, Chemical Reviews **2001**, 101, 2921.

[10] J. Chiefari, Y. K. Chong, F. Ercole, J. Krstina, J. Jeffery, T. P. T. Le, R. T. A. Mayadunne, G. F. Meijs, C. L. Moad, G. Moad, E. Rizzardo, S. H. Thang, Macromolecules **1998**, 31, 5559.

[11] E. R. G. Moad, S. H. Thang, Aust. J. Chem. **2005**, 58, 379.

[12] M. Eberhardt, P. Théato, Macromolecular Rapid Communications **2005**, 26, 1488.

[13] P. Theato, Journal of Polymer Science Part A: Polymer Chemistry **2008**, 46, 6677.

[14] M. A. Gauthier, M. I. Gibson, H.-A. Klok, Angewandte Chemie International Edition **2009**, 48, 48.

[15] M. Barz, R. Luxenhofer, R. Zentel, A. V. Kabanov, Biomaterials **2009**, 30, 5682.

[16] M. I. Gibson, E. Fröhlich, H.-A. Klok, Journal of Polymer Science Part A: Polymer Chemistry **2009**, 47, 4332.

[17] C. Boyer, V. Bulmus, T. P. Davis, V. Ladmiral, J. Liu, S. b. Perrier, Chemical Reviews **2009**, 109, 5402.

[18] T. Lammers, V. Subr, K. Ulbrich, W. E. Hennink, G. Storm, F. Kiessling, Nano Today **2010**, 5, 197.

[19] T. Lammers, Advanced Drug Delivery Reviews **2010**, 62, 203.

[20] M. M. Herth, M. Barz, M. Jahn, R. Zentel, F. Rösch, Bioorganic & Medicinal Chemistry Letters **2010**, 20, 5454.

[21] M. M. Herth, M. Barz, D. Moderegger, M. Allmeroth, M. Jahn, O. Thews, R. Zentel, F. Rösch, Biomacromolecules **2009**, 10, 1697.

[22] M. Allmeroth, D. Moderegger, B. Biesalski, K. Koynov, F. Rösch, O. Thews, R. Zentel, Biomacromolecules **2011** 12, 2841.

[23] H. Maeda, G. Y. Bharate, J. Daruwalla, European Journal of Pharmaceutics and Biopharmaceutics **2009**, 71, 409.

[24] J. Fang, H. Nakamura, H. Maeda, Advanced Drug Delivery Reviews **2011**, 63, 136.

[25] Z.-R. Lu, Advanced Drug Delivery Reviews **2010**, 62, 246.

[26] M. Eberhardt, R. Mruk, R. Zentel, P. Théato, European Polymer Journal **2005**, 41, 1569.

[27] S. b. Perrier, P. Takolpuckdee, C. A. Mars, Macromolecules **2005**, 38, 2033.

[28] G. R. Moad, E.; Thang, S.H., Aust. J. Chem. **2005**, 58, 379.

[29] P. R. P. Salacinski, C. McLean, J. E. C. Sykes, V. V. Clement-Jones, P. J. Lowry, Analytical Biochemistry **1981**, 117, 136.

[30] F. C. Greenwood, W. M. Hunter, Biochem. J. **1963**, 89, 114.

[31] O. R. Pozzi, E. O. Sajaroff, M. n. M. Edreira, Applied Radiation and Isotopes **2006**, 64, 668.

[32] T. Lammers, R. Kühnlein, M. Kissel, V. Subr, T. Etrych, R. Pola, M. Pechar, K. Ulbrich, G. Storm, P. Huber, P. Peschke, Journal of Controlled Release **2005**, 110, 103.

[33] H. Maeda, Journal of Controlled Release **2012**.

Supplementary information to Manuscript 5.4

Comparative study on short and long-term distribution of HPMA-*ran*-LMA copolymers *in vivo* by means of ^{18}F and ^{131}I-labeling revealing tumor retention over time

[redacted], **Mareli Allmeroth**, [redacted]

Contents

1. Experimental section

I. Characterization of polymers

1H-NMR spectra were obtained by a Bruker AC 300 spectrometer at 300 MHz, 19F-NMR analysis was carried out with a Bruker DRX-400 at 400 MHz. All measurements were accomplished at room temperature and spectroscopic data were analyzed using ACDLabs 9.0 1D NMR Manager. The synthesized polymers were dried at 40 °C under vacuum overnight, followed by Gel Permeation Chromatography (GPC). GPC was performed in tetrahydrofuran (THF) as solvent, using following equipment: pump PU 1580, autosampler AS 1555, UV detector UV 1575 and RI detector RI 1530 from Jasco as well as a miniDAWN Tristar light scattering detector from Wyatt. Columns were used from MZ Analysentechnik, 300x8.0 mm: MZ-Gel SDplus 106 Å 5 µm, MZ-Gel SDplus 104 Å 5 µm and MZ-Gel SDplus 102 Å 5 µm. GPC data were evaluated by using the software PSS WinGPC Unity from Polymer Standard Service Mainz. The flow rate was set to 1 mL/min with a temperature of 25 °C.

Analytical Size Exclusion Chromatography (SEC) of ^{131}I-labeled polymers was performed using HiTrap™ Desalting Column, Sephadex G-25 Superfine and HPLC system consisting of a waters pump (1500 series), a Waters UV-detector (2487 λ absorbance detector) and a Berthold LB 509 radiodetector. Radiochemical purity was determined using Tec Control chromatography strips (Biodex Medical Systems, Inc., USA). Preparative SEC for removal of free iodine was accomplished using disposable PD-10 Desalting Columns (GE Healthcare) which were preconditioned and eluted with 0.9% (w/v) sodium chloride solution.

II. Synthesis of reactive ester homopolymers

RAFT polymerization of pentafluorophenyl methacrylate with 4-cyano-4-((thiobenzoyl) sulfanyl)pentanoic acid was carried out in a schlenk tube. [1-3] For this purpose, 4 g of PFPMA were dissolved in 5 mL of absolute dioxane, furthermore CTP and AIBN were added. The molar ratio of CTP/AIBN was chosen 8:1. After three freeze-vacuum-thaw cycles, the mixture was immersed in an oil bath at 65 °C and stirred overnight. Afterwards, the polymeric solution was precipitated three times in hexane, centrifuged and dried under vacuum at 40 °C overnight. A slightly pink powder was obtained. Yield: 52 %. 1H-NMR (300 MHz, CDCl3) δ/ ppm: 1.20-1.75 (br), 2.00-2.75 (br s). 19F-NMR (400 MHz, CDCl3) δ/ ppm: -162.03 (br), -156.92 (br), -152 to -150 (br).

III. Synthesis of reactive ester random copolymers

RAFT polymerization of PFPMA with lauryl methacrylate (LMA) by help of CTP was performed in a schlenk tube as well. As an example, 4 g of PFPMA dissolved in 5 mL dioxane, lauryl methacrylate, AIBN and CTP were mixed. The molar ratio of CTP/AIBN was chosen to be 8:1. After three freeze-vacuum-thaw cycles, the mixture was immersed in an oil bath at 65 °C and stirred over night. Afterwards, poly(PFPMA)-*ran*-poly(LMA) was precipitated three times in hexane, centrifuged and dried under vacuum at 40 °C over night. A slightly pink powder was obtained. Yield: 54 %. ^{1}H-NMR (300 MHz, $CDCl_3$) δ/ ppm: 0.84 (br t), 1.20-1.75 (br), 2.00-2.75 (br s). ^{19}F-NMR (400 MHz, $CDCl_3$) δ/ ppm: -162.01 (br), -156.95 (br), -152 to -150 (br).

IV. Polymeranalogous reaction of homopolymers

Depending on the labeling technique necessary, either for a fluorescent or radioactive marker, two different routes were applied. For subsequent radioactive labeling, the protocol was carried out as follows. As example, 100 mg of the polymeric precursor (Mn = 18000 g/mol) were diluted in 2 mL of absolute dioxane. 5 mg of tyramine, diluted in a DMSO/dioxane mixture, and 10 mg of triethylamine were added. After stirring for four hours at 35 °C, 30 mg of 2-hydroxypropylamine as well as 40 mg of triethylamine were added and the solution was stirred overnight. For final removal of reactive ester side groups, further 30 mg of 2-hydroxypropylamine were added the next morning. The solution was precipitated two times in diethyl ether, centrifuged and finally dissolved in a DMSO/water solution for dialysis. After lyophilization a white powder could be obtained. Yield: 79%. 1H-NMR (400 MHz, d. DMSO) δ/ ppm: 0.60-1.40 (br), 1.45-2.20 (br), 2.75-3.10 (br), 3.50-3.80 (br), 4.60-4.80 (br), 6.60-6.70 (br) and 6.85-7.00 (br). For additional fluorescent labeling, the fluorescent marker Oregon Green 488 cadaverine was used. 100 mg of polymeric precursor were diluted in 2 mL of absolute dioxane and 2.75 mg of Oregon Green 488 cadaverine added. Afterwards tyramine and 2-hydroxypropylamine were added, as described by the procedure above.

V. Polymeranalogous reaction of random copolymers

For radioactive labeling of random copolymers the protocol was applied as follows. 100 mg of poly(PFPMA)-*ran*-poly(LMA) copolymer was dissolved in 2 mL of absolute dioxane. As example, for the polymeric system **P3*-R** (M_n= 17000 g/mol) 5 mg of

tyramine and 10 mg of triethylamine were diluted in a DMSO/dioxane mixture and added to the vessel. After stirring for four hours at 35 °C, 30 mg of 2-hydroxypropylamine as well as 40 mg of triethylamine were added and the solution stirred over night. For final removal of reactive ester side groups further 30 mg of 2-hydroxypropylamine were added the next morning. The solution was precipitated two times in diethyl ether, centrifuged and finally dissolved in a DMSO/water solution for dialysis. After lyophilization a white powder could be obtained. Yield: 51 %. ^{1}H-NMR (400 MHz, d. DMSO) δ/ ppm: 0.70-0.90 (br), 0.90-1.40 (br), 1.40-1.90 (br), 2.75-3.10 (br), 3.50-3.80 (br), 4.50-4.75 (br), 6.60-6.75 (br) and 6.85-7.00 (br). For additional fluorescent labeling, 100 mg of polymeric precursor were diluted in 2 mL of absolute dioxane and 2.9 mg of Oregon Green 488 cadaverine were added. Afterwards tyramine and 2-hydroxypropylamine were added, as described by the procedure above.

VI. Analytical data obtained in isotonic NaCl solution

Isotonic NaCl solution 0.9 % was obtained by B. Braun Melsungen AG without any purification. Stock solutions were prepared using 1 % of absolute DMSO in isotonic sodium chloride solution.

VII. Size determination by Fluorescence Correlation Spectroscopy (FCS)

The hydrodynamic radii of the polymeric systems were determined by Fluorescence Correlation Spectroscopy using a commercial FCS setup (Zeiss, Germany) consisting of the module ConfoCor 2 and an inverted microscope model Axiovert 200 with a Zeiss C-Apochromat 40 ×/1.2 W water immersion objective. The fluorophores were excited with an Argon laser (λ= 488 nm) and the emission was collected after filtering with a LP505 long pass filter. For detection, an avalanche photodiode, enabling single-photon counting, was used. As sample cell, eight-well, polystyrene-chambered cover glass (Laboratory-Tek, Nalge Nunc International) was applied. For sample preparation, stock solutions of 1 mg fluorescently labeled polymer/mL NaCl were applied, diluted to a final concentration of 0.1 mg/mL. The solution was kept at room temperature over night. For reference reason, free Oregon Green 488 cadaverine dye in NaCl-solution was also studied. The calibration of the FCS observation volume was done using a dye with known diffusion coefficient, i.e. Rhodamine6 G. For each solution, 5 measurement cycles with a total duration of 150 seconds were applied. Time dependant fluctuations of the fluorescence

intensity δI(t) were detected and evaluated by autocorrelation analysis, yielding the diffusion coefficient and hydrodynamic radius of the fluorescent species. [4]

VIII. Radiolabeling of polymers

In order to optimize ^{131}I-radiolabeling of HPMA based polymers, two different in-situ oxidants were investigated. For radiolabeling using Iodogen™ (1,3,4,6-Tetrachloro-3a,6a-diphenylglycoluril) as oxidizing agent, the reaction vials were coated prior to the radiolabeling with the respective amount of Iodogen™. Consecutively, 50 µL of 0.5 M phosphate buffer (pH = 7.4), 450 µL PBS, 100 µL of the respective polymer as well as 3-10 MBq of ^{131}I (0.05N NaOH solution) was placed into the coated vial. At t = 4 min, 100 µL of an aqueous ascorbic acid solution (25 mg/mL, pH = 5.0) was added and after 1 min of shaking, the labeling mixture was transferred onto a PD-10 column for subsequent purification using fractionated elution with 0.9 % sodium chloride solution.

Radiolabeling procedure using Chloramine-T (N-chloro-4-methylbenzenesulfonamide sodium salt, CAT) was started by placing 3-10 MBq of ^{131}I (0.05 N NaOH solution) in a reaction vial, followed by 50 µL of 0.5M phosphate buffer (pH = 7.4) and 400 µL of PBS. After addition of 200- 500 µg of the respective polymer in 100 µL of solvent, the radiolabeling reaction was started by adding CAT solution (1 mg/mL in 0.9 % sodium chloride solution) resulting in a final volume of 550 µL for the radiolabeling mixture. After 4 min, the reaction was quenched and purified according to the Iodogen procedure.

IX. Tumor and animal model

Tumor experiments were performed with the Walker 256 mammary carcinoma of the rat. The named cell line was grown in culture in RPMI medium supplemented with 10 mM L-glutamine and 10% fetal calf serum (FCS) at 37 °C under a humidified 5 % CO_2 atmosphere and sub-cultivated twice per week. For tumor implantation male Sprague-Dawley rats (Charles River Wiga, Sulzfeld, Germany; body weight 150 to 300 g) housed in the animal care facility of the University of Mainz were used in this study. All experiments had previously been approved by the regional animal ethics committee and were conducted in accordance with the German Law for Animal Protection and the UKCCCR Guidelines. [5] Animals were allowed access to food and acidified water *ad libitum* before the investigation. Solid carcinomas were heterotopically induced by

injection of cell suspension of the respective tumor line (0.4 ml approx. 10^4 cells/µl) subcutaneously into the dorsum of the hind foot. Tumors grew as flat, spherical segments and replaced the subcutis and corium completely. Volumes were determined by measuring the three orthogonal diameters (d) of the tumors and using an ellipsoid approximation with the formula: $V = d_1 \times d_2 \times d_3 \times \pi/6$. Tumors were used when they reached a volume of between 0.3 to 2.2 mL approx. 5 to 8 days after tumor cell inoculation. Three days before i.v. injection of ^{131}I-labeled copolymer, potassium iodide (0.1 % w/v) was added to animal's drinking water to limit thyroid uptake of any free radioiodide.

X. Biodistribution studies

In order to assess the distribution of the radiolabeled polymers in different organs of the animals, the polymer (concentration of 1 mg in 1 mL sodium chloride solution) was injected i.v. in anaesthetized tumor-bearing rats via the tail vein with a mean activity of 9.3 ± 0.3 MBq (for ^{131}I) and 5.1 ± 0.2 MBq (for ^{18}F). After 2, 24, 48 and 72 hours, the animals were sacrificed and different organ (kidney, liver, lung, spleen, heart, skeletal muscle, small intestine, testis, blood) and tumor samples were taken. The tissue samples were weighed and minced. Finally, the ^{131}I-activity in the organs was measured in a γ-counter.

XI. Statistical analysis

Results are expressed as means±SEM. Differences between groups were assessed by the two-tailed Wilcoxon or Kruskal-Wallis test for unpaired samples. The significance level was set at α=5% for all comparisons. Correlation analysis was performed by calculating the Pearson correlation coefficient.

2. Figures

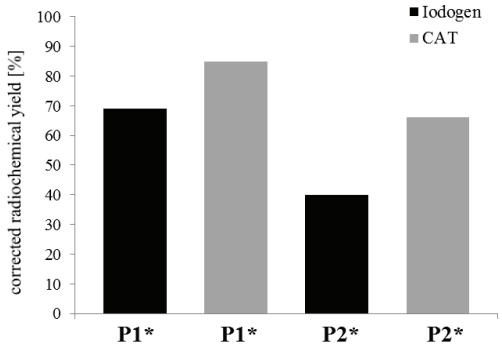

Figure S1**: Corrected radiochemical yields for radioiodination of HPMA based homopolymers **P1 and **P2*** using 25 µg Iodogen™ or 200 µg Chloramine-T as determined using SEC.*

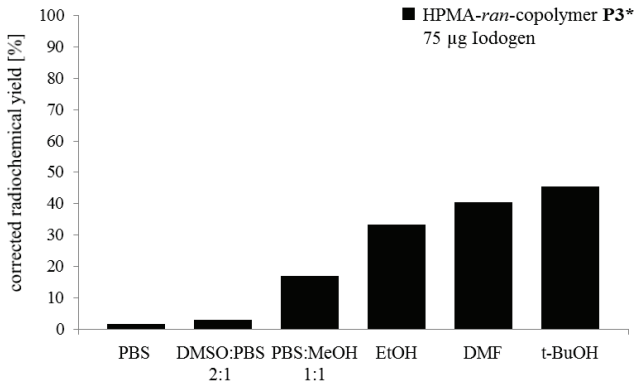

Figure S1**: Influence of solvent on the radioiodination of HPMA-ran-LMA copolymer **P3 using 75 µg of Iodogen™ as determined using SEC.*

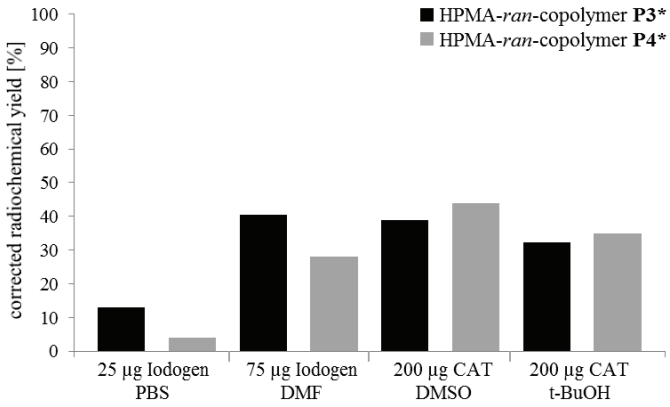

Figure S3**: Corrected radiochemical yields of HPMA-ran-LMA copolymers **P3 and **P4*** using Iodogen™ and CAT for I-131 radiolabeling as determined by means of SEC.*

3. Tables

Table 1**: Biodistribution data of ^{18}F- and ^{131}I-labeled HPMA-ran-LMA copolymer **P4 after i.v. administration in Walker 256 carcinoma bearing rats studied over a time course of up to 3 days. Data is represented as % ID/g tissue (mean±SEM)*

	^{18}F-P4*	**^{131}I-P4***			
organ	**2 h[a]**	**2 h[a]**	**24 h[a]**	**48 h[a]**	**72 h[b]**
lung	1.56±0.17	1.21±0.05	0.73±0.18	0.34±0.04	0.26±0.04
liver	0.80±0.08	4.55±0.11	4.73±0.51	4.68±0.43	3.83±0.20
spleen	0.74±0.09	10.15±0.55	8.55±1.83	9.11±1.41	12.38±2.90
kidney	5.32±0.17	0.41±0.02	0.24±0.02	0.13±0.02	0.10±0.01
muscle	0.09±0.02	0.09±0.02	0.05±0.01	0.03±0.01	0.04±0.01
heart	0.49±0.02	0.44±0.02	0.20±0.03	0.13±0.01	0.11±0.01
blood	2.96±0.03	1.69±0.12	0.42±0.04	0.11±0.01	0.05±0.01
small intestine	0.26±0.01	0.26±0.01	0.44±0.04	0.37±0.03	0.28±0.04
testis	0.14±0.01	0.14±0.01	0.17±0.02	0.14±0.03	0.13±0.02
W-256 tumor	0.63±0.02	0.58±0.8	0.76±0.09	1.00±0.32	0.37±0.04[c]

[a]N = 3, [b]N = 2, [c]N=4.

4. References

[1] M. Allmeroth, D. Moderegger, B. Biesalski, K. Koynov, F. Rösch, O. Thews, R. Zentel, *Biomacromolecules* 2011 *12*, 2841.

[2] M. Barz, R. Luxenhofer, R. Zentel, A. V. Kabanov, *Biomaterials* 2009, *30*, 5682.

[3] P. Theato, *Journal of Polymer Science Part A: Polymer Chemistry* 2008, *46*, 6677.

[4] R. E. Rigler, E.S., *Springer Verlag* New York 2001.

[5] P. Workman, E. O. Aboagye, F. Balkwill, A. Balmain, G. Bruder, D. J. Chaplin, J. A. Double, J. Everitt, D. A. H. Farningham, M. J. Glennie, L. R. Kelland, V. Robinson, I. J. Stratford, G. M. Tozer, S. Watson, S. R. Wedge, S. A. Eccles, *Br J Cancer* 2010, *102*, 1555.

5.5 *In vivo* monitoring of non-linear PEG based copolymers by means of Positron Emission Tomography: The influence of molecular weight on their pharmacokinetic profile

Mareli Allmeroth[§], [redacted]

[§] *Institute of Organic Chemistry, Johannes Gutenberg University, Duesbergweg 10-14, 55099 Mainz, Germany;* [redacted]

Manuscript in preparation

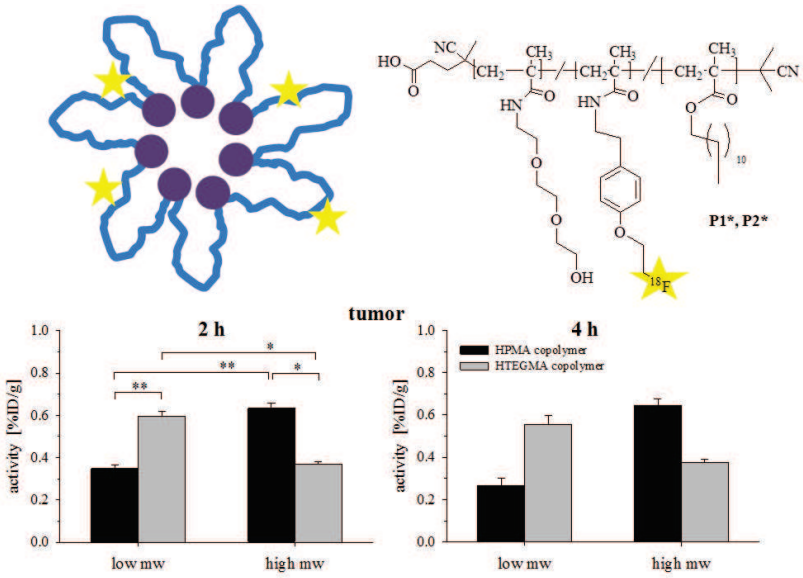

Abstract

Polymeric nanocarrier systems constitute a major research area regarding anticancer therapy. In terms of efficient accumulation at the target site, different parameters such as molecular weight, size, surface charge as well as overall polymer structure demonstrate significant influence. In the present study, four different random copolymer systems varying in molecular weights below and above the renal threshold as well as hydrophilic group (hydroxy-triethylene glycol methacrylamide (HTEGMA) *vs.* *N*-(2-hydroxypropyl) methacrylamide (HPMA)) were investigated in the Walker 256 mammary carcinoma *in vivo*. Lauryl methacrylate was incorporated as hydrophobic group. The polymer structures were radiolabeled with the positron emitter fluorine-18 and organ / tumor uptake was followed using *ex vivo* biodistribution as well as *in vivo* microPET imaging over a time span of 4 hours. Whereas the HTEGMA-*ran*-LMA copolymers (**P1*** and **P2***) exhibited hydrodynamic radii of < 10 nm thus assuming intrachain micellation, the HPMA-*ran*-LMA copolymers **P3*** and **P4*** formed larger aggregates (R_h ~ 40 nm) in isotonic solution – as determined by Fluorescence Correlation Spectroscopy (FCS). A comparative study *in vivo* revealed highest tumor uptake for copolymers **P1*** and **P4***; with the latter also possessing maximum blood retention times. In contrast, **P2*** was subjected to rapid hepatic uptake and **P3*** almost completely cleared via the kidneys within the investigated time-window. Hence low tumor accumulation levels were detected. The findings clearly revealed that molecular weight, size and polymer architecture are major determinants for the pharmacokinetic pattern of polymer drug delivery vehicles and precisely adjusting these parameters is essential for designing efficient polymer based (chemo) therapy in the future. In this regard, non-invasive imaging techniques such as Positron Emission Tomography in combination with short-lived radionuclides constitute a versatile tool for their fast pre-clinical screening.

Keywords: Fluorine-18; HPMA; PEG; PET; RAFT polymerization; Walker 256 mammary carcinoma

1. Introduction

Over the last four decades "Polymer Therapeutics" have become of increasing interest in the field of polymer science. Particularly in the interdisciplinary scope of anticancer treatment, a diversity of polymer nanocarrier systems has been investigated so far [1-7]. The key advantages of polymer based drug delivery vehicles compared to the free therapeutic agent rely on the reduction of toxic side effects in non-target tissue, a prolonged blood-circulation time in the organism followed by their enhanced accumulation / retention in the tumor due to the EPR effect [8, 9] .

Concerning the clinical setting, major requirements have to be fulfilled by the polymeric carrier system. They have to be non-toxic, non-immunogenic as well as biodegradable or at least biocompatible with adequate molecular weight to guarantee body elimination. Furthermore, narrowly-distributed polymeric carriers are needed to secure homogeneity of the final conjugates. In this regard, poly(HPMA) as well as poly(ethylene glycol) belong to the main classes of synthetic polymers applied in drug delivery and being particularly successful in clinical trials [10-12].

Besides selecting the appropriate carrier system for a clinical application, the need for suitable preclinical screening methodologies is gaining more and more importance in the field of individualized patient therapy [13, 14]. Due to these challenges, the introduction of a radioactive probe into the polymeric structure and subsequent monitoring by means of Positron Emission Tomography (PET) constitutes a beneficial diagnostic tool to trace organ distribution as well as tumor accumulation. Depending on the applied radionuclide – and its corresponding half-life – short as well as long term pharmacokinetic studies can be accomplished.

To date, *in vivo* studies on HPMA or PEG based nanoparticles were mainly carried out using either γ-emitting radioisotopes such as Tc-99m, In-111 or I-125/131 [15-19] offering relatively low spatial resolution or by introducing the metallic positron emitter Cu-64 requiring voluminous chelating agents [20-22]. In contrast, we could demonstrate the successful synthesis of F-18 as well as As-72/74 labeled HPMA based polymer structures in former studies [23, 24] thereby establishing PET imaging for fast and versatile screening of potential polymeric nanocarrier systems. Particularly fluorine-18 ($t_{1/2}$ = 110 min) is considered as ideal radioisotope for

positron emission tomography, attributed to its favorable physical and nuclear characteristics combined with only trace amounts incorporated not interfering with the overall polymer structure. Using this [^{18}F]fluoroethylation labeling approach, we were able to reveal that molecular weight as well as aggregate formation of HPMA based polymer architectures possessed a major influence on their biodistribution pattern *in vivo* [25]. Recent studies furthermore identified the significance of the applied tumor model on the resulting accumulation of the carrier system at the tumor site (data not shown).

In addition to adequate imaging techniques, developing a polymer therapeutic is always holding the demand of well-definedness [26]. In this regard, the implementation of controlled radical polymerization methodologies such as ATRP [27] and RAFT [28, 29] enabled the facile access to well-defined and narrowly distributed polymer structures. Especially in the field of biomedical applications, these techniques are becoming more important since they provide diverse possibilities of macromolecular engineering. In this respect, recent achievements in the controlled polymerization of non-linear PEG analogs underline their potential as "smart" biomaterials and thus qualifies their use as alternatives to the widely exploited linear poly(ethylene glycol) moiety [30]. One of their great benefits relies on the accessibility of high-molecular weight PEG based polymers using comparatively mild reaction conditions as well as their feasibility to exhibit stimuli-responsive character-istics. A variety of PEG (macro) monomers has been investigated so far [31-34] and special focus was also laid on their polymerization via the RAFT technique [35-38]. Representing a new approach of PEGylation, studies on their *in vitro* [39] and *in vivo* [21] capability – particularly in comparison to the linear counterpart - are of emerging interest.

From this perspective, the combination of RAFT with the reactive ester approach demonstrates a promising concept of introducing non-linear PEG analogs into polymer structures, accomplished by means of polymer-analogous reaction with primary amines [40]. Besides, the characteristics of RAFT and reactive ester chemistry enable the synthesis of diverse polymer architectures as well as the incorporation of functional moieties such as fluorescent dyes, radioactive probes or pharmacologically active drugs [25, 41-43].

Based on the prospects of implementing non-linear PEG analogs in the field of biomedical applications, the aim of the present study focused on the synthesis and subsequent *in vivo* evaluation of non-linear PEG based random copolymers (HTEGMA-*ran*-LMA). With special emphasis on the impact of both hydrophilic segment as well as molecular weight, *in vivo* pharmaco-kinetics were compared to the findings of the HPMA-ran-LMA copolymer analogs. Polymer structures were labeled via fluorine-18 and *in vivo* μPET imaging as well as *ex vivo* biodistribution studies applied to monitor organ / tumor uptake in Walker 256 mammary carcinoma bearing rats.

2. Materials and Methods

2.1 Materials

All solvents were of analytical grade, as obtained by Sigma Aldrich and Acros Organics. Dioxane was distilled over a sodium/potassium composition, THF over sodium and CH_2Cl_2 as well as acetonitrile over calcium hydride. Lauryl methacrylate was distilled to remove the stabilizer and stored at -18 °C. 2,2'-azoisobutyronitrile (AIBN) was recrystallized from diethyl ether and stored at -18 °C as well.

2.2 Characterization

^{1}H-NMR spectra were obtained by a Bruker AC 300 spectrometer at 300 MHz, ^{19}F-NMR analysis was carried out with a Bruker DRX-400 at 400 MHz. All measurements were accomplished at room temperature and spectroscopic data were analyzed using ACDLabs 9.0 1D NMR Manager. The synthesized polymers were dried at 40 °C under vacuum over night, followed by Gel Permeation Chromatography (GPC). GPC was performed in tetrahydrofuran (THF) as solvent, using following equipment: pump PU 1580, autosampler AS 1555, UV detector UV 1575 and RI detector RI 1530 from Jasco as well as a miniDAWN Tristar light scattering detector from Wyatt. Columns were used from MZ Analysentechnik, 300x8.0 mm: MZ-Gel SDplus 10^6 Å 5 μm, MZ-Gel SDplus 10^4 Å 5 μm and MZ-Gel SDplus 10^2 Å 5 μm. GPC data were evaluated by using the software PSS WinGPC Unity from Polymer Standard Service Mainz. The flow rate was set to 1 mL/min with a temperature of 25 °C.

For synthesis of 2-[^{18}F]fluoroethyl-1-tosylate ([^{18}F]FETos), a Sykam S 1100 pump and a Knauer UV-detector (K-2501) HPLC system were used. Size Exclusion Chromatography (SEC) of ^{18}F-labeled polymers was performed

using HiTrap™ Desalting Column, Sephadex G-25 Superfine and a waters pump (1500 series), a Waters UV-detector (2487 λ absorbance detector) and a Berthold LB 509 radiodetector.

In *ex vivo* studies, fluorine-18 activities were determined using a Perkin Elmer 2470 Wizard^2 γ- counter.

2.2.1 Polymer synthesis

2.3.1 Synthesis of 4-cyano-4-((thiobenzoyl)sulfanyl)pentanoic acid (CTP)

4-cyano-4-((thiobenzoyl)sulfanyl) pentanoic acid was used as chain transfer agent (CTA) and synthesized according to the literature [44].

2.3.2 Synthesis of pentafluorophenyl methacrylate (PFPMA)

Pentafluorophenyl methacrylate was prepared according to reference [41].

2.3.3 Synthesis of random copolymers

RAFT polymerization of PFPMA with lauryl methacrylate (LMA) by help of CTP was performed in a schlenk tube according to the literature [42, 43]. As an example, 4 g of PFPMA dissolved in 5 mL dioxane, lauryl methacrylate, AIBN and CTP were mixed. The molar ratio of CTP/AIBN was chosen to be 8:1. After three freeze-vacuum-thaw cycles, the mixture was immersed in an oil bath at 65 °C and stirred over night. Afterwards, poly(PFPMA)-*ran*-poly(LMA) was precipitated three times in hexane, centrifuged and dried under vacuum at 40 °C over night. A slightly pink powder was obtained. Yield: 54 %. ^{1}H-NMR (300 MHz, $CDCl_3$) δ/ ppm: 0.84 (br t), 1.20-1.75 (br), 2.00-2.75 (br s). ^{19}F-NMR (400 MHz, $CDCl_3$) δ/ ppm: -162.01 (br), -156.95 (br), -152 to -150 (br).

2.3.4 Removal of dithioester endgroups

The dithiobenzoate endgroup was removed using the protocol reported by Perrier et al. 2005 [45]. A 25-fold molar excess of AIBN was added to the polymer dissolved in dioxane. After four hours of heating the solution in an oil bath at 70 °C, the polymer was precipitated twice in hexane and collected by centrifugation. The polymer was dried under vacuum over night, a colorless powder was obtained. Yield: 75 %. Removal of the dithioester endgroup could be proven by UV-Vis spectroscopy.

2.3.5 Synthesis of amine functionalized triethylene glycol

2-[2-(2-aminoethoxy)ethoxy]ethanol was synthesized in a three step procedure according to Lebeau et al. [46]. In a typical reaction, methanesulfonyl chloride (14.60 mL, 188.6 mmol, 1 equiv.) was added dropwise to triethylene glycol (28.32 g, 188.6 mmol, 1 equiv.) and Et_3N (26.4 mL, 1 equiv.) in dry THF (100 mL) at - 5 °C. This mixture was stirred for two hours in the cold, then allowed to warm to room temperature and stirred over night. The next morning the precipitate was filtered and the filtrate evaporated. The residue was column chromatographed (ethyl acetate / hexane 10:3; R_f =0.08) to separate the product from non- and disulfonated byproducts. Yield of 2-{2-{2-[(methylsulfonyl)oxy]ethoxy}ethoxy}ethanol: 38%. ^{1}H-NMR (300 MHz, $CDCl_3$) δ/ ppm: 3.05 (s, 3H), 3.58 (m, 2H), 3.66 (m, 4H), 3.71 (m, 2H), 3.75 (m, 2H) and 4.36 (m, 2H).

In the second step, NaN_3 (2.14 g, 32.9 mmol, 1.5 equiv.) was dissolved in abs. acetonitrile (30 mL). The sulfonated triethylene glycol (5 g, 21.9 mmol, 1 equiv.) – dissolved in 20 mL abs. MeCN – was subsequently added via septa and the solution refluxed for 90 hours. After completion of reaction, 20 mL H_2O were added and the mixture extracted with three times of 70 mL dichloromethane. The organic phases were collected, dried over $MgSO_4$ and the solvent was evaporated. Yield of 2-[2-(2-azido-ethoxy)ethoxy]ethanol: 89%. ^{1}H-NMR (300 MHz, $CDCl_3$) δ/ ppm: 2.84 (t, 2H) and 3.67 (m, 10H).

In the third step, (890 mg, 5.08 mmol, 1 equiv.), PPh_3 (1.47 g, 5.59 mmol, 1.1 equiv.), H_2O (0.14 mL, 7.62 mmol, 1.5 equiv.) and THF (10 mL) were mixed and stirred for 32 hours at room temperature. The solution was afterwards heated to 40 °C and stirred for further 16 hours. The solvent was evaporated and product column chromatographed (methanol / chloroform / triethylamine 2:3:1; R_f = 0.38). Yield of 2-[2-(2-aminoethoxy)ethoxy]ethanol: 79 %. ^{1}H-NMR (300 MHz, $CDCl_3$) δ/ ppm: 2.93 (t, 2H), 3.71-3.45 (m, 10H).

2.3.6 Polymeranalogous reaction of random copolymers

For radioactive labeling of random copolymers the protocol was applied as follows. 100 mg of poly(PFPMA)-*ran*-poly(LMA) copolymer was dissolved in 2 mL of absolute dioxane. Exemplary for **P2*** (M_n= 57000 g/mol), 4 mg of tyramine and 3 mg of triethylamine were diluted in a DMSO/dioxane mixture and added to the vessel. After stirring for

four hours at 35 °C, 40 mg of 2-[2-(2-aminoethoxy)ethoxy]ethanol as well as 30 mg of triethylamine were added and the solution stirred at 45 °C over the weekend. Conversion was subsequently monitored via ^{19}F-NMR and still revealed polymer bound reactive ester groups. Due to this observation, 40 mg of amine functionalized triethylene glycol was additionally added and the solution stirred over night. For final removal of reactive ester side groups further 40 mg of 2-[2-(2-amino-ethoxy)ethoxy]ethanol were added the next morning. The solution was precipitated three times in diethyl ether, centrifuged and finally dissolved in a DMSO / water solution for dialysis. After lyophilization a white powder could be obtained. Yield: 60 %. ^{1}H-NMR (400 MHz, d. DMSO) δ/ ppm: 0.70-0.90 (br), 0.90-1.40 (br), 1.40-1.90 (br), 2.90-3.25 (br), 3.45-3.55 (br), 4.45-4.60 (br), 6.60-6.75 (br) and 6.85-7.00 (br). For additional fluorescent labeling, 100 mg of polymeric precursor were diluted in 2 mL of absolute dioxane and 2.9 mg of Oregon Green 488 cadaverine were added. Afterwards tyramine and [2-(2-aminoethoxy)ethoxy]ethanol were added, as described by the procedure above.

2.4 Analytical data obtained in isotonic NaCl solution

Isotonic NaCl solution 0.9 % was obtained by B. Braun Melsungen AG without any purification. Stock solutions were prepared using 1 % of absolute DMSO in isotonic sodium chloride solution.

2.4.1 Size determination by Fluorescence Correlation Spectroscopy (FCS)

The hydrodynamic radii of the polymeric systems were determined by Fluorescence Correlation Spectroscopy using a commercial FCS setup (Zeiss, Germany) consisting of the module ConfoCor 2 and an inverted microscope model Axiovert 200 with a Zeiss C-Apochromat 40 ×/1.2 W water immersion objective. The fluorophores were excited with an Argon laser (λ = 488 nm) and the emission was collected after filtering with a LP505 long pass filter. For detection, an avalanche photodiode, enabling single-photon counting, was used. As sample cell, eight-well, polystyrene-chambered cover glass (Laboratory-Tek, Nalge Nunc International) was applied. For sample preparation, stock solutions of 1 mg fluorescently labeled polymer/mL NaCl were applied, diluted to a final concentration of 0.1 mg/mL. The

solution was kept at room temperature over night. For reference reason, free Oregon Green 488 cadaverine dye in NaCl-solution was also studied. The calibration of the FCS observation volume was done using a dye with known diffusion coefficient, i.e. Alexa Fluor 488. For each solution, 5 measurement cycles with a total duration of 150 seconds were applied. Time dependant fluctuations of the fluorescence intensity δI(t) were detected and evaluated by autocorrelation analysis, yielding the diffusion coefficient and hydrodynamic radius of the fluorescent species [47].

2.5 Synthesis of [^{18}F]FETos

To an aqueous [^{18}F]fluoride solution (2-8 GBq) 18 mg Kryptofix®2.2.2., potassium carbonate (1N, 15 µL) and 1 mL acetonitrile were added. The mixture was dried in a stream of nitrogen at 80 °C, the drying procedure was repeated three times. To the dried residue 13 mg of ethyleneglycol-1,2-ditosylate in 1 mL acetonitrile was added and heated under stirring in a sealed vial at 88 °C for 3 min. Purification of the crude product was accomplished using HPLC (Lichrosphere RP18-EC5, 250×10 mm, acetonitrile/water 50:50, flow rate: 5 mL/min, t_R: 8 min). After diluting the HPLC fraction of 2-[^{18}F]fluoroethyl-1-tosylate with water, the product was loaded on a Sep-Pak C18 cartridge, dried with a nitrogen stream and eluted with 0.8 mL of DMSO [48].

2.6 Radiolabeling of polymers using [^{18}F]FETos and purification for *ex vivo* and *in vivo* experiments

For radiolabeling, 3 mg of the polymeric precursor were dissolved in 200 µL of dried DMSO. The solution was transferred to a sealed vial and 1 µL of a 5N sodium hydroxide solution was added. The labeling reaction was started by adding the previously eluted DMSO solution of 2-[^{18}F]fluoroethyl-1-tosylate and the mixture was stirred for 15 min at 120 °C.

For *ex vivo* and *in vivo* experiments, the radiolabeled polymeric systems were freed from low molecular weight byproducts by Sephadex G-25 size exclusion chromatography (HiTrap™ Desalting Column, Sephadex G-25 Superfine, 0.9 % NaCl, flow rate: 0.5 mL/min) leading to a pure, ^{18}F-labeled polymer solution ready for subsequent experiments [23].

2.7 Tumor and animal model

For animal experiments the Walker 256 mammary carcinoma cell line was used.

Cells were grown in culture in RPMI medium supplemented with 10 mM L-glutamine and 10 % fetal calf serum (FCS) at 37 °C under a humidified 5 % CO_2 atmosphere and sub-cultivated twice per week. For tumor implantation male Sprague-Dawley rats (Charles River Wiga, Sulzfeld, Germany; body weight 188 to 387 g) housed in the animal care facility of the University of Mainz were used in this study. All experiments had previously been approved by the regional animal ethics committee and were conducted in accordance with the German Law for Animal Protection and the UKCCCR Guidelines [49]. Animals were allowed access to food and acidified water *ad libitum* before the investigation. Solid carcinomas were heterotopically induced by injection of cell suspension (0.4 mL approx. 10^4 cells/µL) subcutaneously into the dorsum of the hind foot. Tumors grew as flat, spherical segments and replaced the subcutis and corium completely. Volumes were determined by measuring the three orthogonal diameters (d) of the tumors and using an ellipsoid approximation with the formula: $V = d_1 \times d_2 \times d_3 \times \pi/6$. Tumors were used when they reached a volume of between 0.4 to 3.4 mL approx. 7 to 14 days after tumor cell inoculation.

2.8 µPET imaging

For µPET imaging, rats were anaesthetized either with pentobarbital (40 mg/kg, intraperitoneal, Narcoren, Merial, Hallbergmoos, Germany) or with isofluran (2 %). Polymers were injected via tail vein puncture.

The µPET imaging was performed on a microPET Focus 120 small animal PET (Siemens/Concorde, Knoxville, USA). During PET measurements the animals were placed in supine position and breathed room air spontaneously. Dynamic PET studies were acquired in listmode. The radiolabeled polymers were administered as a bolus injection of 0.4 - 0.7 mL simultaneously with the start of the PET scan. The mean injected activity of labeled polymers was 23.1±3.3 MBq. The PET listmode data were histogrammed into 25 frames and reconstructed using OSEM2D algorithm. Volumes-of-interests (VOIs) were defined for tumor and reference tissue (testis). The testis was used as a reference since it was in the field of view when imaging the tumors on the feet and because the tissue concentration was relatively constant between all animals on a low level. Time activity curves (TAC) were obtained with varying time frames (1.5-10 min) for a total measuring interval of 120 min. Ratios of tumor to

reference tissue were calculated from integral images between 15' and 120' after polymer injection. Finally, a whole body scan (120-135 min post injection) was performed. μPET image quantification was applied using PMOD software (PMOD Technologies Ltd.).

2.9 Biodistribution studies

In order to assess the distribution of the radiolabeled polymers in different organs of the animals, the polymer (concentration of 1 mg in 1 mL sodium chloride solution) was injected i.v. in anaesthetized tumor-bearing rats via the tail vein with a mean activity of 14.0±1.4 MBq. After 120 or 240 min, the animals were sacrificed and different organ (kidney, liver, lung, spleen, heart, skeletal muscle, small intestine, testis, blood) and tumor samples were taken. The tissue samples were weighed and minced. Finally, the ^{18}F-activity in the organs was measured in a γ-counter.

2.10 Statistical analysis

Results are expressed as means±SEM. Differences between groups were assessed by the two-tailed Wilcoxon test for paired samples and by multi-factorial ANOVA. The significance level was set at α=5% for all comparisons.

3. Results and Discussion

3.1 Synthetic concept of PEG based copolymer structures

The aim of the present study was focused on the impact of molecular weight and hydrophilicity of non-linear PEG based random copolymers on tumor uptake as well as organ distribution *in vivo*. Former studies in our groups already demonstrated the successful combination of the controlled radical polymerization technique RAFT [28, 29] with reactive ester chemistry [41, 42] to create well-defined and narrowly distributed HPMA based polymer architectures [25, 43]. Furthermore, radioactive labeling of these compounds could be established by means of the positron-emitters As-72/74 [24] or F-18 [23]. The latter enabled the precise monitoring of the polymeric nanocarrier systems in the living organism thus revealing the tremendous effect of polymer architecture as well as molecular weight on organ distribution and blood circulation properties *in vivo* [25]. Taking these results into consideration, the herein presented study concentrates on the replacement of the hydrophilic HPMA segment toward hydroxy-triethyleneglycol methacrylamide (HTEGMA) via the reactive ester approach and subsequent visualization of the pharmacokinetic profile of HTEGMA-LMA random copolymers by

means of Positron Emission Tomography (PET) as well as *ex vivo* biodistribution studies.

Overall, four different random copolymer structures were synthesized: two HTEGMA-LMA as well as two HPMA-LMA random copolymers. Each pair was exhibiting molecular weights below and above the renal threshold (limit of kidney filtration of HPMA homopolymers > 40 kDa [50]; PEG ~ 40-60 kDa [11]).

Exemplary, the synthetic route of PEG-modified random copolymers is depicted in Figure 1, based on the reactive ester precursor polymers **P1*-R** / **P2*-R** and their polymeranalogous reaction to the final polymer structures **P1*** / **P2***. Furthermore, the radioactive labeling procedure of the polymers via [^{18}F]FETos is additionally shown.

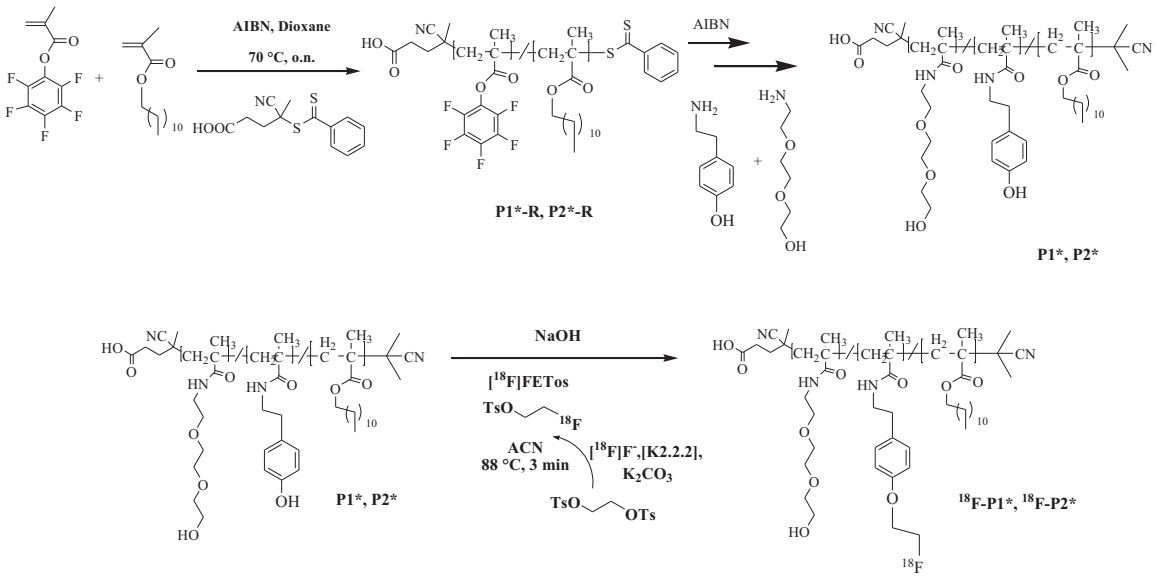

Figure 1**: Synthetic route of reactive ester precursor polymers (**P1*-R** and **P2*-R**), polymeranalogous reaction to **P1 and **P2*** as well as ^{18}F-radiolabeling to obtain final polymers **^{18}F-P1*** and **^{18}F-P2***. Exemplarily shown for HTEGMA-ran-LMA copolymers.*

Starting from the reactive ester monomer pentafluorophenyl methacrylate (PFPMA) and by simultaneous addition of lauryl methacrylate, reactive ester precursor systems **P1*-R** - **P4*-R** were synthesized [25, 41-43], possessing the advantage of being well-soluble and - due to their hydrophobic nature - inhibiting aggregate formation. This is of major importance regarding their characterization by means of gel permeation chromatography and ^{1}H-NMR spectroscopy. Furthermore it facilitates the application of the same polymeric precursor, as shown for **P2*-R** (= **P4*-R**) and thus enabling a direct correlation between the different final polymer structures. To avoid side reactions during postpolymerization modification, dithioester end groups were cleaved by an excess of 2,2'-azoisobutyronitrile, a method previously described by Perrier et al. [45].

The reactive ester precursor polymers were afterwards functionalized via polymeranalogous reaction of primary amines. To enable radioactive labeling for *in vivo* studies, a tyramine moiety (incorporation efficiency of 2 - 4 %) was introduced and subsequently either [2-(2-aminoethoxy)ethoxy]ethanol or 2-hydroxypropylamine were added to result in the polymeric structures **P1*** to **P4***. Complete conversion of the reactive ester side group was determined by ^{19}F-NMR spectroscopy. Analytical data of reactive ester precursor polymers as well as final structures are summarized in Table 1.

According to the data listed in Table 1, well-defined and narrowly distributed polymer systems could be synthesized via the RAFT polymerization technique (PDI from 1.24 – 1.41). Incorporation of lauryl methacrylate as hydrophobic segment could be achieved with a predominant efficiency of 25 %. Molecular weights (M_n) were ranging between 11000 g/mol for the smallest compound and 53000 g/mol for the highest molecular weight random copolymer **P2*** hence indicating molecular weights below and above the renal threshold. Hydrodynamic radii were determined by applying Fluorescence Correlation Spectroscopy (FCS) in isotonic sodium chloride solution. Relating to the HTEGMA-*ran*-LMA copolymers, hydrodynamic radii of 3.5 nm for the low molecular weight random copolymer **P1*** and 5.5 nm for the higher molecular weight counterpart **P2*** could be detected. These findings can be presumably explained by intrachain micellation [51].

Table 1**: Analytical data of reactive ester random copolymers (**P1*-R** to **P4*-R**) as well as final polymeric structures **P1*- P4*

Notation	Polymeric structure	Monomer ratio	M_n [g/mol]	M_w [g/mol]	PDI[b]	R_h[nm][e]	RCY [%]
P1*-R	PFPMA-*ran*-LMA copolymer	80:20[a]	24000[b]	30000[b]	1.24	n.d.	-
P2*-R	PFPMA-*ran*-LMA copolymer	80:20[a]	57000[b]	80000[b]	1.41	n.d.	-
P3*-R	PFPMA-*ran*-LMA copolymer	80:20[a]	17000[b]	21000[b]	1.26	n.d.	-
P4*-R (=P2*-R)	PFPMA-*ran*-LMA copolymer	80:20[a]	57000[b]	80000[b]	1.41	n.d.	-
P1*	HTEGMA-*ran*-LMA copolymer	75:25[c]	22000[d]	27000[d]	1.24	3.5	15±5
P2*	HTEGMA-*ran*-LMA copolymer	75:25[c]	53000[d]	74000[d]	1.41	5.5	20±8
P3*	HPMA-*ran*-LMA copolymer	82:18[c]	11000[d]	14000[d]	1.26	33.4	26 ±1
P4*	HPMA-*ran*-LMA copolymer	75:25[c]	39000[d]	55000[d]	1.41	39.9	10 ±2

*[a] = Calculated monomer ratio; [b] = Determination by GPC in THF as solvent; [c] = Monomer ratio determined by ^{1}H-NMR spectroscopy after polymeranalogous reaction with 2-hydroxypropylamine; [d] = Calculated from the molecular weight of the reactive ester polymers **P1*-R** –**P4*-R** as determined by GPC in THF as solvent; [e] = Hydrodynamic radii determined by Fluorescence Correlation Spectroscopy (FCS)*

Since these polymers exhibit a random distribution of hydrophilic and hydrophobic fragments all over the macromolecule, they belong to the class of amphiphilic polymers and thus possess a strong tendency to self-assemble in aqueous environments. On closer examination, their synthetic route implies the creation of so called "polysoaps", furthermore assured by the appropriate length of the hydrophobic lauryl methacrylate chains (minimal length of C_8 seems to be required for polysoap formation) [52]. These macro-molecular architectures are expected to consist out of a dense hydrophobic core as inner region as well as a surrounding hydrophilic corona. The assembly of the intrachain micelles induces the formation of hydrophilic loops which are anchored to the surface of the hydrophobic core [51]. Due to this process, dense micellar structures in aqueous media can be created, supporting the obtained results for HTEGMA-*ran*-LMA copolymers.

In contrast, the less hydrophilic HPMA segment induces the creation of explicitly larger superstructures,

assuming to be so called "compound micelles" [53] and stay in accordance with former observations in our group [25, 43]. The low molecular weight HPMA-*ran*-LMA copolymer **P3*** possessed a hydrodynamic radius of 33 nm and **P4*** an R_h of around 40 nm.

3.1 Radioactive labeling by means of [^{18}F]fluoroethylation

To study the *in vivo* characteristics of different polymer structures, the positron emitter fluorine-18 ($t_{1/2}$ = 110 min) was introduced via a prosthetic labeling procedure using [^{18}F]FETos. Non-invasive small animal PET imaging as well as quantitative *ex vivo* biodistribution measurements were carried out to gain deepening knowledge about structure-property relationships of the differing polymer architectures in the living organism. In contrast to commonly applied SPECT radioisotopes such as the γ-emitters ^{99m}Tc ($t_{1/2}$ = 6.0 h), ^{111}In ($t_{1/2}$ = 67.2 h) or ^{123}I ($t_{1/2}$ = 13.2 h), Positron Emission Tomography profits from higher sensitivity and spatial resolution. Radioactive labeling was accomplished by means of [^{18}F]fluoro-ethylation, a method already established for diverse HPMA based architectures [23, 25]. Decay-corrected radiochemical yields (RCYs) were determined by size exclusion chromatography and are listed in Table 1.

3.2 Organ distribution

To study the impact of the hydrophilic group – HTEGMA *vs.* HPMA – and resulting superstructure formation on the body distribution of amphiphilic random copolymers, quantification of the recovered dose of ^{18}F-labeled polymers was accomplished in selected organs (kidney, liver, spleen, heart, lung, blood, muscle, small intestine and testis) 2 and 4 hours after i.v. administration. Biodistribution data of the four different polymers are depicted in Figure 2A-F as well as Table 3.

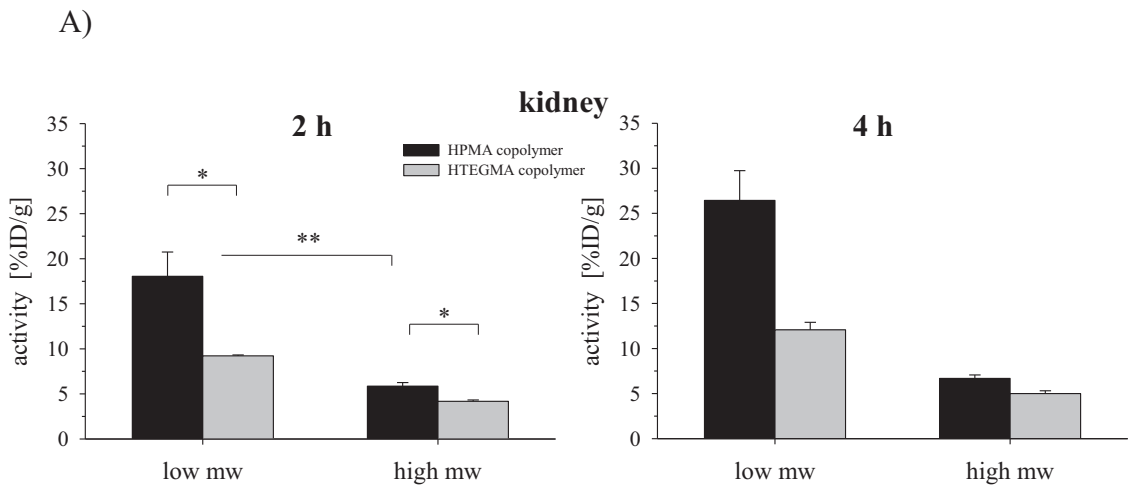

***Figure 2A**: Biodistribution data of HPMA and HTEGMA based random copolymers with low and high molecular weight in kidneys 2 and 4 hours p.i.* n=3-6, *(*) p<0.05, (**) p<0.01*

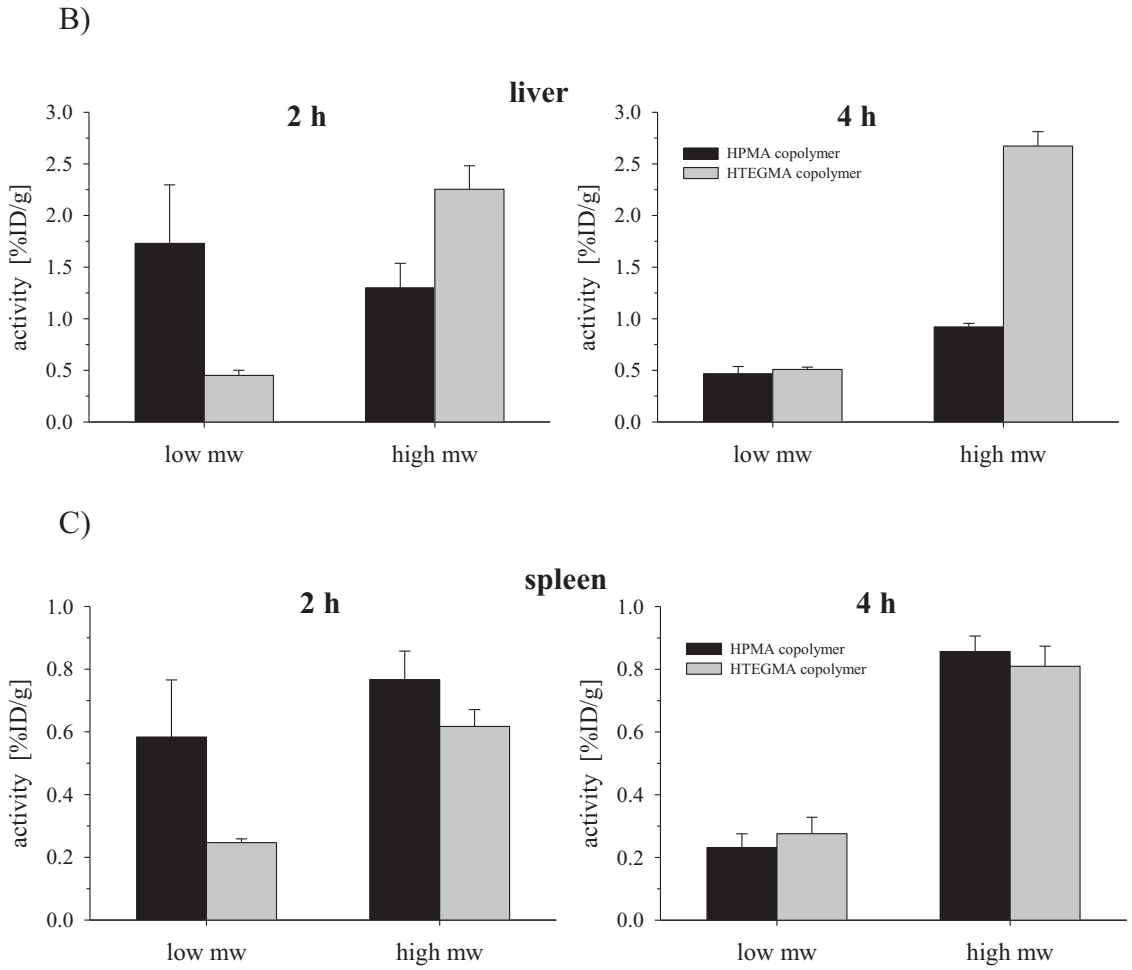

***Figure 2B/C**: Biodistribution data of HPMA and HTEGMA based random and copolymers with low and high molecular weight in liver (2B) and spleen (2C) 2 and 4 h p.i.*

As clearly seen, there is a major influence of the respective polymer moiety on the organ accumulation pattern *in vivo*. Regarding time-dependent kidney uptake, the low molecular weight HPMA based random copolymer exhibits highest values 2 and 4 hours p.i. (18.06±2.68 and 26.44±3.30 % ID/g tissue) thus indicating fast renal clearance of these compounds. Lowest kidney uptake can be detected for HTEGMA-*ran*-LMA copolymer (M_w = 74000 g/mol) possessing a molecular weight above the threshold of kidney filtration [11] and hence other excretion pathways become more important. The statistical analysis (ANOVA) revealed the both molecular size (p= 0.0002) and PEGylation (p= 0.0261) had a significant impact on kidney uptake.

In terms of hepatic and spleenic uptake, an inverted accumulation pattern of the varying polymer structures can be observed. Since the high molecular weight random HTEGMA copolymer is only poorly filtered by the kidneys, these polymers can be eliminated by the liver (via bile) or by phagocytosis by mononuclear cells (e.g. in liver or spleen). After 2 hours of i.v. administration, 2.25±0.23 % ID/g of the large HTEGMA polymer can be found in the liver, still increasing over time (4 h = 2.67±0.14 % ID/g tissue). In comparison, the large HPMA based random copolymer (also exhibiting a molecular weight above the renal threshold) shows distinct lower spleen and liver accumulation (Fig. 2B/C). Both low molecular weight counterparts were found in the liver to lower levels.

Similar uptake characteristics can be obtained for the spleen (see Fig. 2C). In general, all polymer systems are just accumulating to a small extent with highest values for high molecular weight HPMA-*ran*-LMA copolymer (4 h = 0.86±0.05 % ID/g) and HTEGMA-*ran*-LMA copolymer (4 h = 0.81±0.06 % ID/g). These results stay in good correspondence to the already observed polymer trend in liver enrichment since both organs – liver and spleen – are belonging to the mononuclear phagocyte system and thus hepatic as well as spleenic macrophages are responsible for the opsonization of polymeric nanoparticles [54].

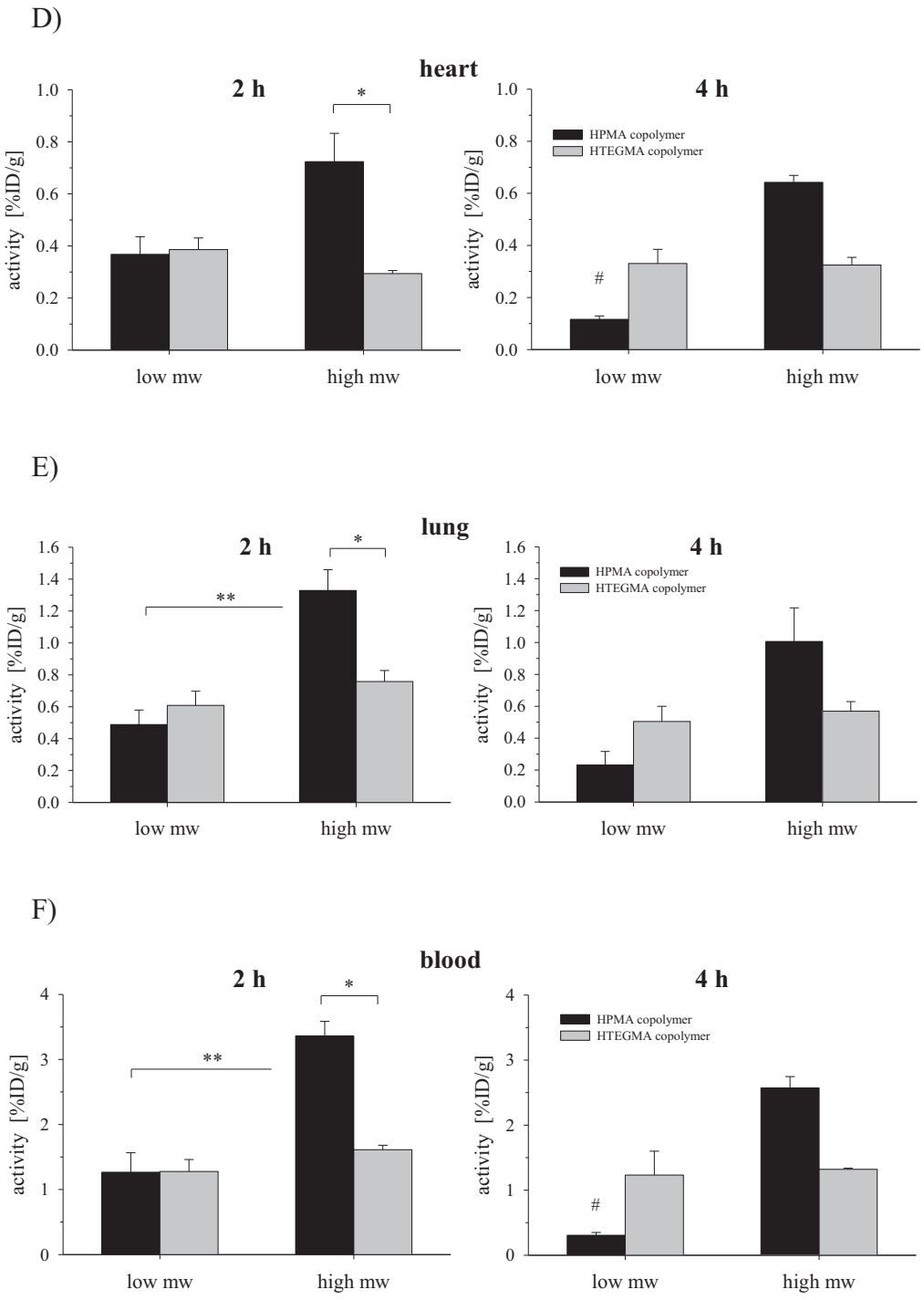

Figure 2D-F: *Biodistribution data of HPMA and HTEGMA based random copolymers with low and high molecular weight in heart (2D), lung (2E) and blood (2F) 2 and 4 h p.i. n=3-6, (*) p<0.05, (**) p<0.01, (#) p<0.05 2 h vs. 4 h*

Most likely attributed to the accumulation properties of the varying polymer architectures in kidney, liver and spleen, significant differences in the blood pool were determined (Fig. 2F). ANOVA analysis showed that molecular size ($p= 0.0004$) as well as PEGylation ($p= 0.0268$) had a statistically significant impact on the blood level of the polymers. The highest blood retention was achieved for the high molecular weight HPMA based random polymer, showing a slow decrease over time (2 h = 3.36±0.22 *vs.* 4 h = 2.57±0.18 % ID/g tissue) but still being nearly two times higher than its HTEGMA counterpart (2 h = 1.61±0.07 % ID/g tissue and 4 h = 1.32±0.02 % ID/g tissue). These findings are probably related to the increased clearance rate of the high molecular weight HTEGMA based random copolymer by liver or spleen (e.g. by phagocytosis) thereby reducing its presence in the blood stream (see Fig. 2B). In comparison, its HPMA based complement exhibits overall low excretion characteristics demonstrated by the combination of low renal filtration, hepatic as well as spleenic uptake (Figure 2A-C). The low molecular weight HTEGMA-*ran*-LMA copolymer **P1*** is presenting similar blood levels than **P2*** over time (4 h = 1.23±0.5 % ID/g tissue), presumably attributed to its medium but constant renal excretion. In this regard, a study of Hawker et al. [21] has to be mentioned, focusing on the effect of different PEG lengths (1.1, 2 and 5 kDa respectively) on the biodistribution of PMMA-PEGMA core-shell nanoparticles *in vivo*. They investigated that an increase in PEG chain lengths also resulted in an enhanced blood circulation thus assuming that the HTEGMA fragment in the present study is too short to effectively prolonging blood residence time. Besides, the small HPMA-*ran*-LMA copolymer was the one showing lowest blood pool concentration, being almost completely cleared from the blood stream within 4 hours (0.31±0.04 % ID/g tissue). This observation can be explained by its fast elimination via the kidneys and subsequent urine excretion. In addition, highly blood supplied organs such as heart (Fig. 2D) and lung (Fig. 2E) are directly reflecting the polymer trend in blood concentration, possessing highest levels for HPMA-*ran*-LMA copolymer and lowest amounts for its low molecular weight analog. A general overview of the obtained polymer concentrations in the investigated organs 2 and 4 hours p.i. are summarized in Table 2.

***Table 2**: Polymer uptake in different organs expressed by the fraction of the injected dose (ID) of the polymer per gram tissue 2 and 4 h after i.v. injection. n=3-6.*

2 h p.i.	**polymer concentration [%ID/g tissue]**			
polymer	**HTEGMA**	**HTEGMA**	**HPMA**	**HPMA**
Molecular weight	**low Mw**	**high Mw**	**low Mw**	**high Mw**
lung	0.61±0.09	0.76±0.07	0.49±0.09	1.33±0.13
liver	0.45±0.05	2.25±0.23	1.73±0.57	1.30±0.24
spleen	0.25±0.01	0.62±0.05	0.58±0.18	0.77±0.09
kidney	9.23±0.09	4.18±0.15	18.06±2.68	5.86±0.40
muscle	0.07±0.01	0.05±0.01	0.11±0.02	0.16±0.05
heart	0.39±0.04	0.29±0.01	0.37±0.07	0.72±0.11
blood	1.28±0.18	1.61±0.07	1.27±0.30	3.36±0.22
small intestine	0.21±0.01	0.25±0.04	0.29±0.10	0.46±0.11
testis	0.17±0.01	0.08±0.01	0.15±0.01	0.18±0.02

4 h p.i.	**polymer concentration [%ID/g tissue]**			
polymer	**HTEGMA**	**HTEGMA**	**HPMA**	**HPMA**
Molecular weight	**low Mw**	**high Mw**	**low Mw**	**high Mw**
lung	0.51±0.10	0.57±0.06	0.23±0.15	1.01±0.21
liver	0.51±0.02	2.67±0.14	0.47±0.07	0.92±0.04
spleen	0.28±0.05	0.81±0.06	0.23±0.04	0.86±0.05
kidney	12.07±0.84	5.00±0.31	26.44±3.30	6.68±0.39
muscle	0.08±0.01	0.05±0.01	0.05±0.00	0.09±0.00
heart	0.33±0.05	0.32±0.03	0.12±0.01	0.64±0.03
blood	1.23±0.37	1.32±0.02	0.31±0.04	2.57±0.18
small intestine	0.17±0.06	0.27±0.03	0.13±0.00	0.33±0.01
testis	0.18±0.04	0.10±0.00	0.09±0.01	0.16±0.01

3.3 Tumor accumulation

To study the influence of the hydrophilic group on tumor uptake *in vivo*, the Walker 256 mammary carcinoma model was applied in male Sprague Dawley rats. Quantitative biodistribution studies were carried out 2 and 4 hours after administration of the random copolymer structures. Polymer dependent tumor accumulation is presented in Figure 2G.

In direct comparison, the high molecular weight HPMA based random copolymer is the polymer structure with highest levels in the tumor region, staying constant over time (2 h = 0.63±0.02 and 4 h = 0.64±0.03 % ID/g tissue). This result can be correlated to its slow uptake in the kidneys, liver and spleen as well as resulting prolonged blood circulation properties. Noteworthy, even though the small HTEGMA-*ran*-LMA copolymer showed explicitly lower values in the blood pool over time, only marginal lower concentrations in the tumor were detected (2 h = 0.60±0.02 % ID/g tissue and 4 h = 0.56±0.04 % ID/g tissue) when compared to the high molecular weight HPMA based random polymer. This observation indicates that tumor retention is not only dependent on a concentration-dependent passive diffusion between the blood compartment and the tumor tissue but furthermore influenced by polymer size and architecture. In contrast, the high molecular weight HTEGMA as well as the low molecular weight HPMA random copolymer are accumulating in the tumor to very low levels (Fig. 2G), thereby being nearly two times less present in the tumor region than the aforementioned polymer structures. These findings are probably attributed to the fast hepatic uptake of the large HTEGMA-*ran*-LMA copolymer as well as the enhanced elimination of the small HPMA-*ran*-LMA copolymer via the kidneys (Figures 2A and 2B). Both are subjected to fast blood clearance which results in low tumor accumulation. In conclusion, HPMA based random copolymer systems showed a direct correlation between blood retention and resulting tumor uptake. However, the findings in the presented studies reveal that enhanced blood residence time is not the only parameter inducing increased tumor accumulation, as observed for the low molecular weight HTEGMA-*ran*-LMA copolymer. Here, polymer size as well as overall architecture is considered to possess a major influence, too. This aspect has to be evaluated in more detail in further studies.

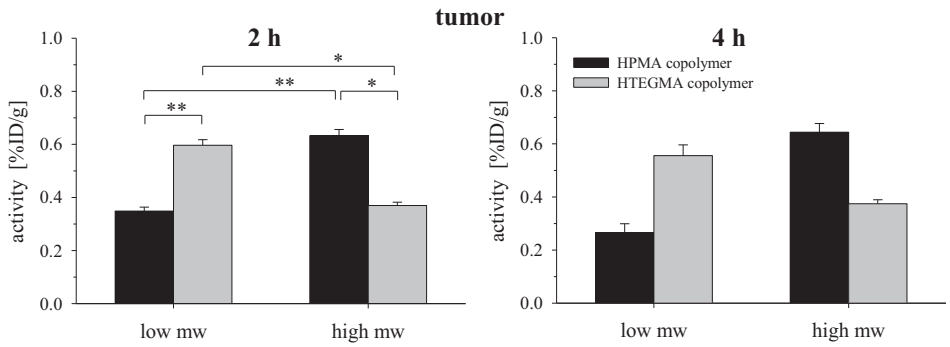

***Figure 2G**: Tumor accumulation of HPMA and HTEGMA random copolymers with low and high molecular weight in Walker 256 mammary carcinoma 2 and 4 h p.i. n=4-6, (*) p<0.05, (**) p<0.01*

3.4 MicroPET imaging in Walker 256 mammary carcinoma bearing rats

Besides a quantitative determination of organ accumulation of the herein presented polymer structures by means of *ex vivo* biodistribution studies, further *in vivo* monitoring via static and dynamic μPET imaging was accomplished. The obtained whole-body microPET images (Figure 3) stay in good accordance to the achieved biodistribution data (Figure 2A-F). The low molecular weight HTEGMA-*ran*-LMA copolymer **P1*** showed major renal clearance via kidneys and bladder, as also indicated by its biodistribution pattern (Figure 2A). In comparison, its high molecular weight counterpart **P2*** displays slight renal clearance but furthermore enhanced liver accumulation as well as blood retention – visualized by the aorta. The prolonged blood circulation times detected for HPMA-*ran*-LMA copolymer **P4*** *ex vivo* are also clearly visible by its whole-body scan. Additionally highly blood supplied organs (i.e. heart and lung) and renal excretion properties are monitored, too. Based on the quantitative findings of tumor accumulation for the varying polymer structures, their polymer specific tumor uptake in the Walker 256 carcinoma was additionally investigated using dynamic microPET imaging over a time course of 2 hours post injection. In this regard, coronal slices of summed μPET images through the tumors (which were implanted at the hind foot dorsum) were studied (Fig. 4). As clearly visible, the low molecular weight HTEGMA-*ran*-LMA copolymer (**P1***) and the high molecular weight HPMA-*ran*-LMA copolymer (**P4***) were accumulated pronouncedly in the tumor, a trend which is in good accordance to the invasive *ex vivo* biodistribution experiments.

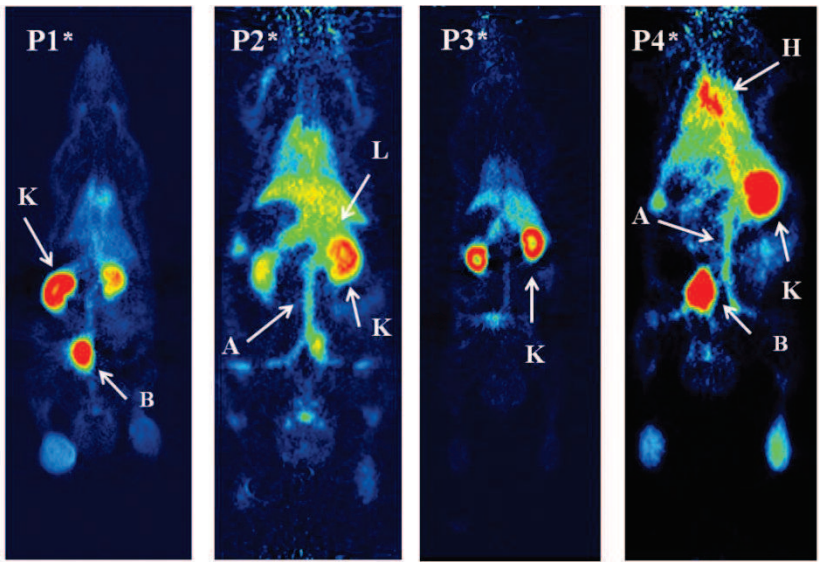

Figure 3: *Whole body µPET image sections obtained 120-135 min post injection of low (**P1***) and high (**P2***) molecular weight HTEGMA as well as low (**P3***) and high (**P4***) molecular weight HPMA random copolymers. A= aorta; B = bladder; H= heart; K = kidney; L = liver.*

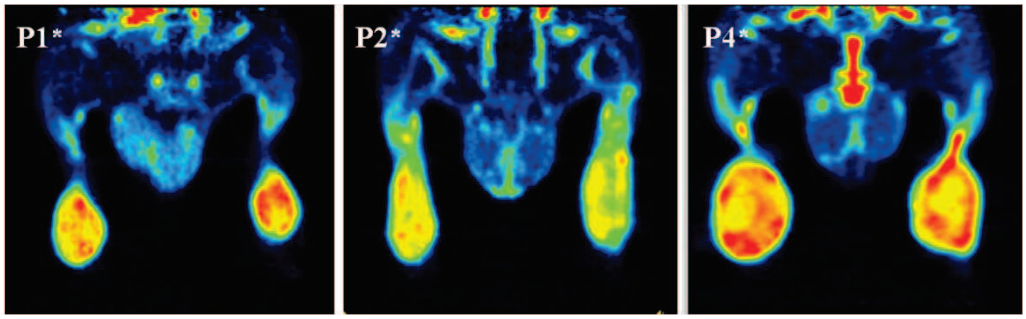

Figure 4: *Examples of coronal microPET image sections of Walker 256 tumors 60-120 min after injection of the low (**P1***) and high (**P2***) HTEGMA based random copolymers as well as the high molecular weight HPMA-ran-LMA copolymer (**P4***). The uptake of the low molecular weight HPMA based random copolymer (**P3***) was not determined in PET images in Walker 256 tumors.*

4. Conclusion

The present study clearly underlines the potential of non-linear PEG analogs in the field of polymer therapeutics. In our approach, we exploited a combination of RAFT polymerization technique with reactive ester chemistry to create methacrylamide based PEG-like structures with lauryl methacrylate as hydrophobic moiety. Random copolymers with molecular weights below and above the renal threshold of poly(ethylene glycol) were synthesized

and by introducing the short-lived radionuclide fluorine-18, subsequent monitoring via Positron Emission Tomography enabled their precise tracking *in vivo*. Their pharmacokinetic pattern – organ distribution as well as tumor accumulation – was compared to HPMA-*ran*-LMA analogs and revealed that molecular weight had a major impact on the biodistribution characteristics. The high molecular weight HTEGMA based random copolymer was presumably directly taken up by the MPS thus exhibiting comparatively low tumor uptake. In contrast, its low molecular weight HTEGMA counterpart showed pronounced renal clearance combined with nearly two-fold higher tumor accumulation in the Walker 256 mammary carcinoma. These findings were in accordance to the high M_w HPMA based polymer structure which exhibited a concurrent tumor concentration. Despite these promising results, there is still the necessity of improving the plasma-half life of the presented non-linear PEG based copolymer systems regarding their application in anticancer therapy. In this respect, the elongation of the methacrylamide based PEG side chains might be a suitable approach for future studies.

5. Acknowledgement

The authors would like to thank Barbara Biesalski, Nicole Bausbacher and Bengü Yilmaz for their support during animal studies and following interpretation. We also want to thank the Max Planck Graduate Center (MPGC, M. Allmeroth) as well as the Graduate School Materials Science in Mainz (Excellence Initiative, DFG/GSC 266, D. Moderegger) for financial support. In addition the authors are very thankful for financial support of the DFG (Rösch: RO 985/30-1; Thews: TH 482/4-1, Zentel: ZE 230/21-1) and SAMT Initiative Mainz.

6. References

1. R. Duncan, *Nat Rev Drug Discov*, 2003, **2**, 347-360.
2. J. Kopecek, P. Kopecková, T. Minko and Z.-R. Lu, *European Journal of Pharmaceutics and Biopharmaceutics*, 2000, **50**, 61-81.
3. K. Kataoka, A. Harada and Y. Nagasaki, *Advanced Drug Delivery Reviews*, 2001, **47**, 113-131.
4. G. Gaucher, M.-H. Dufresne, V. P. Sant, N. Kang, D. Maysinger and J.-C. Leroux, *Journal of Controlled Release*, 2005, **109**, 169-188.
5. F. Greco and M. J. Vicent, *Advanced Drug Delivery Reviews*, 2009, **61**, 1203-1213.

6. R. Duncan and M. J. Vicent, *Advanced Drug Delivery Reviews*, 2010, **62**, 272-282.
7. R. B. Greenwald, Y. H. Choe, J. McGuire and C. D. Conover, *Advanced Drug Delivery Reviews*, 2003, **55**, 217-250.
8. Y. Matsumura and H. Maeda, *Cancer Research*, 1986, **46**, 6387-6392.
9. J. Fang, H. Nakamura and H. Maeda, *Advanced Drug Delivery Reviews*, 2011, **63**, 136-151.
10. R. Duncan, *Nat Rev Cancer*, 2006, **6**, 688-701.
11. G. Pasut and F. M. Veronese, *Progress in Polymer Science*, 2007, **32**, 933-961.
12. G. Pasut and F. M. Veronese, *Advanced Drug Delivery Reviews*, 2009, **61**, 1177-1188.
13. T. Lammers, V. Subr, K. Ulbrich, W. E. Hennink, G. Storm and F. Kiessling, *Nano Today*, 2010, **5**, 197-212.
14. T. Lammers, *Advanced Drug Delivery Reviews*, 2010, **62**, 203-230.
15. A. Mitra, A. Nan, H. Ghandehari, E. McNeil, J. Mulholland and B. Line, *Pharmaceutical Research*, 2004, **21**, 1153-1159.
16. Y. Zhang, Y. Sun, X. Xu, X. Zhang, H. Zhu, L. Huang, Y. Qi and Y.-M. Shen, *Journal of Medicinal Chemistry*, 2010, **53**, 3262-3272.
17. B. Hoang, H. Lee, R. M. Reilly and C. Allen, *Molecular Pharmaceutics*, 2009, **6**, 581-592.
18. M. Kissel, P. Peschke, V. Subr, K. Ulbrich, A. Strunz, R. Kühnlein, J. Debus and E. Friedrich, *European Journal of Nuclear Medicine and Molecular Imaging*, 2002, **29**, 1055-1062.
19. Z.-R. Lu, *Advanced Drug Delivery Reviews*, 2010, **62**, 246-257.
20. X. Sun, R. Rossin, J. L. Turner, M. L. Becker, M. J. Joralemon, M. J. Welch and K. L. Wooley, *Biomacromolecules*, 2005, **6**, 2541-2554.
21. E. D. Pressly, R. Rossin, A. Hagooly, K.-i. Fukukawa, B. W. Messmore, M. J. Welch, K. L. Wooley, M. S. Lamm, R. A. Hule, D. J. Pochan and C. J. Hawker, *Biomacromolecules*, 2007, **8**, 3126-3134.
22. K.-i. Fukukawa, R. Rossin, A. Hagooly, E. D. Pressly, J. N. Hunt, B. W. Messmore, K. L. Wooley, M. J. Welch and C. J. Hawker, *Biomacromolecules*, 2008, **9**, 1329-1339.
23. M. M. Herth, M. Barz, D. Moderegger, M. Allmeroth, M. Jahn, O. Thews, R. Zentel and F. Rösch, *Biomacromolecules*, 2009, **10**, 1697-1703.
24. M. M. Herth, M. Barz, M. Jahn, R. Zentel and F. Rösch, *Bioorganic & Medicinal Chemistry Letters*, 2010, **20**, 5454-5458.
25. M. Allmeroth, D. Moderegger, B. Biesalski, K. Koynov, F. Rösch, O. Thews and R. Zentel, *Biomacromolecules*, 2011 **12**, 2841-2849.
26. M. Barz, R. Luxenhofer, R. Zentel and M. J. Vicent, *Polymer Chemistry*, 2011, **2**, 1900-1918.
27. K. Matyjaszewski and J. Xia, *Chemical Reviews*, 2001, **101**, 2921-2990.
28. J. Chiefari, Y. K. Chong, F. Ercole, J. Krstina, J. Jeffery, T. P. T. Le, R. T. A. Mayadunne, G. F. Meijs, C. L. Moad,

G. Moad, E. Rizzardo and S. H. Thang, *Macromolecules*, 1998, **31**, 5559-5562.

29. G. Moad, E. Rizzardo and S. H. Thang, *Australian Journal of Chemistry*, 2009, **62**, 1402-1472.
30. J.-F. Lutz, *Journal of Polymer Science Part A: Polymer Chemistry*, 2008, **46**, 3459-3470.
31. S.-i. Yamamoto, J. Pietrasik and K. Matyjaszewski, *Macromolecules*, 2007, **40**, 9348-9353.
32. M. M. Ali and H. D. H. Stöver, *Macromolecules*, 2004, **37**, 5219-5227.
33. D. Zhang, C. Macias and C. Ortiz, *Macromolecules*, 2005, **38**, 2530-2534.
34. S. J. Holder, N. A. A. Rossi, C.-T. Yeoh, G. G. Durand, M. J. Boerakker and N. A. J. M. Sommerdijk, *Journal of Materials Chemistry*, 2003, **13**, 2771-2778.
35. S. b. Garnier and A. Laschewsky, *Macromolecules*, 2005, **38**, 7580-7592.
36. M. Mertoglu, S. b. Garnier, A. Laschewsky, K. Skrabania and J. Storsberg, *Polymer*, 2005, **46**, 7726-7740.
37. K. Skrabania, J. Kristen, A. Laschewsky, Ö. Akdemir, A. Hoth and J.-F. Lutz, *Langmuir*, 2007, **23**, 84-93.
38. P. J. Roth, F. D. Jochum, R. Zentel and P. Theato, *Biomacromolecules*, 2009, **11**, 238-244.
39. J.-F. Lutz, J. Andrieu, S. Üzgün, C. Rudolph and S. Agarwal, *Macromolecules*, 2007, **40**, 8540-8543.
40. M. I. Gibson, E. Fröhlich and H.-A. Klok, *Journal of Polymer Science Part A: Polymer Chemistry*, 2009, **47**, 4332-4345.
41. M. Eberhardt, R. Mruk, R. Zentel and P. Théato, *European Polymer Journal*, 2005, **41**, 1569-1575.
42. P. Theato, *Journal of Polymer Science Part A: Polymer Chemistry*, 2008, **46**, 6677-6687.
43. M. Barz, R. Luxenhofer, R. Zentel and A. V. Kabanov, *Biomaterials*, 2009, **30**, 5682-5690.
44. E. R. G. Moad, S. H. Thang, *Aust. J. Chem.*, 2005, **58**, 379-410.
45. S. b. Perrier, P. Takolpuckdee and C. A. Mars, *Macromolecules*, 2005, **38**, 2033-2036.
46. L. Lebeau, P. Oudet and C. Mioskowski, *Helvetica Chimica Acta*, 1991, **74**, 1697-1706.
47. R. E. Rigler, E.S., *Springer Verlag* New York 2001.
48. A. Bauman, M. Piel, R. Schirrmacher and F. Rösch, *Tetrahedron Letters*, 2003, **44**, 9165-9167.
49. P. Workman, E. O. Aboagye, F. Balkwill, A. Balmain, G. Bruder, D. J. Chaplin, J. A. Double, J. Everitt, D. A. H. Farningham, M. J. Glennie, L. R. Kelland, V. Robinson, I. J. Stratford, G. M. Tozer, S. Watson, S. R. Wedge and S. A. Eccles, *Br J Cancer*, 2010, **102**, 1555-1577.
50. L. W. Seymour, R. Duncan, J. Strohalm and J. Kopeček, *Journal of Biomedical Materials Research*, 1987, **21**, 1341-1358.
51. O. V. Borisov and A. Halperin, *Current Opinion in Colloid & Interface Science*, 1998, **3**, 415-421.
52. A. Laschewsky, in *Polysoaps / Stabilizers / Nitrogen-15 NMR*, Springer Berlin Heidelberg, 1995, pp. 1-86.

53. K. Yu and A. Eisenberg, *Macromolecules*, 1998, **31**, 3509-3518.

54. G. Storm, S. O. Belliot, T. Daemen and D. D. Lasic, *Advanced Drug Delivery Reviews*, 1995, **17**, 31-48.

6. List of publications

(1) *"Radioactive labeling of Defined HPMA-Based polymeric Structures Using [^{18}F]FETos for In Vivo Imaging by Positron Emission Tomography"*
[redacted], **Mareli Allmeroth**, [redacted], *Biomacromolecules, **2009**, 10, 1697-1703*

(2) *"HPMA Based Amphiphilic Copolymers Mediate Central Nervous Effect of Domperidone"*
[redacted], **Mareli Allmeroth**, [redacted], *Macromolecular Rapid Communications, **2011**,* 32 (9-10), 712-717

(3) *"Modifying the Body Distribution of HPMA-Based Copolymers by Molecular Weight and Aggregate Formation"*
Mareli Allmeroth*, [redacted], *Biomacromolecules,* **2011**, 12, 2841-2849
* [redacted]

(4) *"How structure is influencing the biodistribution in vivo: The impact of aggregate formation and molecular weight of HPMA based copolymers"*
Mareli Allmeroth, [redacted], *ACS preprints, **2012***

(5) *"Structure and size of HPMA-based polymers decide on tumor accumulation but the tumor model makes a difference: A quantitative in vivo PET study"*
Mareli Allmeroth*, [redacted] *Angewandte Chemie,* in preparation
* [redacted]

(6) "PEGylation of HPMA-based block copolymers enhances tumor accumulation in vivo: A quantitative study using radiolabeling and Positron Emission Tomography"

Mareli Allmeroth*, [redacted]

Journal of Controlled Release, in preparation

* [redacted]

(7) "Comparative study on short and long term distribution of HPMA-ran-LMA copolymers in vivo by means of ^{18}F and ^{131}I-labeling revealing tumor retention over time"

[redacted], **Mareli Allmeroth**, [redacted], *Macromolecular Rapid Communications,* in preparation

(8) "In vivo monitoring of non-linear PEG based copolymers by means of Positron Emission Tomography: The influence of molecular weight on their pharmacokinetic profile"

Mareli Allmeroth, [redacted],

Manuscript in preparation

(9) "Fluorine-18 labeling approach for HPMA-based polymers via click chemistry"

[redacted], **Mareli Allmeroth**, [redacted], Manuscript in preparation

7. Acknowledgement

This thesis could not have been realized without many people standing by my side in a number of ways during the time as a PhD student. To all of you I owe my gratitude and thanks.

First of all it is an honor for me to thank [redacted], who has offered the chance to join his working group for the diploma as well as for the doctoral thesis. He has made it possible to work interdisciplinary, a field, I've been strongly interested in after my studies of biomedical chemistry. Thank you for your insightful comments on how to do research, for your advice and patience. Numerous suggestions, helpful discussions and valuable ideas accompanied my studies and enriched the project. As you gave me the opportunity to participate in international conferences and enabled the foreign research visit in Valencia I could practice a useful exchange of experiences.

I would like to show my deep gratitude to [redacted], my medical cooperation partner, who supported and encouraged me from the initial to the final level of the PhD thesis. You were always there when problems and issues occurred. Without your assistance and instructive insights into interesting aspects of medical research the project would not have been possible. I am grateful for a wonderful collaboration.

Furthermore it is a pleasure to mention [redacted]. Providing his competence and help to [redacted] and me, he facilitated the completion of our interdisciplinary project in any respect.

I am heartily thankful to my collaboration partner from nuclear chemistry, [redacted]. I know that cooperation can sometimes be challenging and stressful but with you it was exceptional. We were an excellent team and I can say that I found a new friend, too. Especially the last months have created a strong bond between us. I will miss our daily Skype conferences. All the best for your future!

I am indebted to all of my other collaboration partners who have considerably contributed to the variety of aspects in this work: [redacted], [redacted], [redacted], [redacted] and [redacted] (Universitätsmedizin Mainz). Their

guidance regarding animal studies and a lot of exhilarating time in between will be unforgettable. It was very pleasant to work with all of you.

Furthermore I appreciate the efforts of [redacted] and [redacted] (MPI-P) for training me on the FCS setup and using their equipment whenever I needed to. You helped me to interpret the obtained results and inspired me with fruitful discussions.

I would like to acknowledge [redacted] (Universitätsmedizin Halle) for his support regarding cellular uptake studies of the polymer systems *in vitro*.

Furthermore I hold [redacted] in high esteem. You gave me the chance to visit your laboratory during a foreign research visit. I learned a lot in terms of cellular culturing and really appreciated your encouraging meetings. In this regard, I would like to thank particularly [redacted]. She cared for my research project with enthusiasm and always had a sympathetic ear when I had to overcome setbacks. Your group is awesome; I really enjoyed working in such a kind sense of community.

Advice given by [redacted] and [redacted] (MPI-P) has been a great help during ring tensiometry measurements. [redacted] (Institute of Physical Chemistry) also fits in this circle. She provided me with valuable results about dynamic light scattering of my polymer samples. Furthermore I would like to thank my collaboration partners [redacted] (Institute of Immunology, Uniklinik Mainz) as well as [redacted] and [redacted] (Institute of Nuclear Chemistry).

Special thanks go to [redacted] and all of her help and patience synthesizing the polymeric precursors and final compounds.

I can't thank [redacted] enough. Apart of being a reliable colleague with excellent work morale she has been a very close friend since the beginning of our studies. We were gaining so many experiences together during our scholarship and common time at Cornell, in India and a lot of conferences in the USA. Having you as office / hood neighbor has been the best thing ever.

Grateful thanks are extended to [redacted], [redacted] and [redacted] for offering additional and useful stimuli during their internship in our group.

All the present and former members of the [redacted] and [redacted] group have been keeping my progress on schedule with an enriching working atmosphere. Further thanks to all the members of the MPGC program - especially [redacted] and [redacted] who shared some memorable days in Sasbachwalden and [redacted] for our weekly tennis games. I would like to thank [redacted] and [redacted] having a great time together – not only in the lab – as well as the whole "Bio-fraction" of the [redacted] group for all the memories regarding conferences, group meetings etc. Thanks to [redacted] for her advices concerning my research visit in Halle and all of her encouraging words during writing. Further thanks to [redacted] who always helped me out with computer problems.

Earnest thankfulness to [redacted]. You did a commendable job by measuring probably hundreds of my polymers via 19 F-spectroscopy.

Thanks to the Max Planck Graduate Center (MPGC) for financial support.

Finally I wish to thank gratefully my parents, my boyfriend [redacted] and my grandmother for your constructive recommendations and understanding. You didn't stop giving me love and care throughout the studies and the doctoral thesis. And not forgetting [redacted] and [redacted], my lovable friends forever, who boosted me morally in long discussions to remind that there is also life outside polymer chemistry.

And of course thanks to every single person who somehow became part of this thesis.